The Synthesis, ^{1}H-NMR Properties and Photochromism of Cyclopent[e]dimethyldihydropyrene Anion and its Metal Complexes

by

Wei Fan

BSc, University of Science and Technology of China, China, 1993
MSc, Nanyang Technological University, Singapore, 2000

A Dissertation Submitted in Partial Fulfillment of the
Requirements for the Degree of

DOCTOR OF PHILOSOPHY

in the Department of Chemistry

The Synthesis, ^{1}H-NMR Properties and Photochromism of Cyclopent[e]dimethyldihydropyrene Anion and its Metal Complexes

by

Wei Fan

BSc, University of Science and Technology of China, China, 1993
MSc, Nanyang Technological University, Singapore, 2000

Supervisory Committee

Dr. Reginald H. Mitchell, (Department of Chemistry)
Supervisor

Dr. David J. Berg, (Department of Chemistry)
Co-Supervisor

Dr. Natia L. Frank, (Department of Chemistry)
Departmental Member

Dr. Christopher Upton, (Department of Biochemistry)
Outside Member

Dr. Vance Williams, (Department of Chemistry, Simon Fraser University)
External Examiner

Supervisory Committee

Dr. Reginald H. Mitchell, (Department of Chemistry)
Supervisor

Dr. David J. Berg, (Department of Chemistry)
Co-Supervisor

Dr. Natia L. Frank, (Department of Chemistry)
Departmental Member

Dr. Christopher Upton, (Department of Biochemistry)
Outside Member

Dr. Vance Williams, (Department of Chemistry, Simon Fraser University)
External Examiner

ABSTRACT

The synthesis of the cyclopentadiene-fused dimethyldihydropyrene, CpDHP(H) **44**, from DHP **31** was achieved in a seven-step synthesis in an overall yield of 7%. Deprotonation of **44** gave the Cp anion fused CpDHP anion **28**. The photochromic properties of **28** were studied. It is found that **28** is photochromic and its behavior is intermediate between the parent DHP **31** and the benzannelated DHP **36**. The ^{1}H-NMR data of **28** were also analyzed and showed that the Cp anion has similar bond fixing effect on the DHP ring as benzene does, but to a lesser extent.

The complexation of anion **28** to various metal centers has been investigated. While the reactions of **28** with $Re(CO)_5Br$, $(Cp^*RuCl_2)_n$ and $FeCl_2$ yielded $(CpDHP)Re(CO)_3$ **51**, $Cp^*Ru(CpDHP)$ **52** and $(CpDHP)_2Fe$ **54** respectively, the reactions with Mn, Y, Yb(III) or Zr precursors either gave the starting materials back or resulted in the decomposition of **28** to unidentified products. Reaction of the protonated form CpDHP(H) **44** with $Yb[N(SiMe_3)_2](thf)_2$ afforded $Yb(CpDHP)_2(thf)_2$ **57**.

The photochromic properties of the metal complexes obtained have been studied. Compounds **51** and **52** are found to be photochromic, but **54** and **57** are not. The reason for the shut-down of the photochromism in **54** and **57** is still not known. Study of the photochromism of **51** and **52** found that complexation to a Re and Ru center improved the photoopening process from partial opening of **28** to complete opening of **51** and **52**, but did not change the relative opening and closing rates substantially. The thermal return reactions, on the other hand, have been slowed down substantially after complexation to metal centers.

The diamagnetic susceptibility, χ, of the metal containing moieties Cp*Ru, $Re(CO)_3$ and (CpDHP)Fe were calculated. Analysis of the NMR data of the metal complexes showed that the metal complexes have more bond fixing ability than benzene and the relative bond fixing ability order was CpRuCp* > CpFe(CpDHP) > $CpRe(CO)_3$ > Benzene-$Cr(CO)_3$ > benzene.

The X-ray structures of **51**, **52** and **57** were also analyzed and all three complexes were found to be η^5-coordinated. The structure data confirmed the bond fixing abilities of the metal complexes and showed that no significant geometry changes occurred during complexation.

Table of Contents

Chapter Two Syntheses and Characterization

Chapter Three Results and Discussion

References

Appendices

List of Tables

List of Figures

List of Schemes

List of Abbreviations

Ar	arene/aryl
DHP	dimethyldihydropyrene
CPD	metacyclophanediene
δ	chemical shift in ppm from standard
Φ	quantum yield
h	hour
min	minute
HRMS	high resolution mass spectrum
LSIMS	liquid secondary ion mass spectrometry
RBFA	relative Bond fixing ability
n-BuLi	n-butyllithium
t-Bu	t-Butyl
^{13}C-NMR	carbon-13 nuclear magnetic resonance
decomp.	decomposition
EtOH	ethanol
^{1}H-NMR	proton magnetic resonance
IR	infrared spectrum
Me	methyl
mp	melting point
EI-MS	electron impact mass spectrum
br	broad

s	singlet
d	doublet
t	triplet
q	quartet
dd	doublet of doublets
dt	doublet of triplets
m	multiplet
ppm	parts of per million
THF	tetrahydrofuran
d_8-THF	tetrahydrofuran-d8
UV-vis	ultraviolet visible
VT	variable temperature
CI	chemical ionization
Cp	cyclopentadienyl
Cp*	pentamethylcyclopentadienyl

List of Numbered Compounds

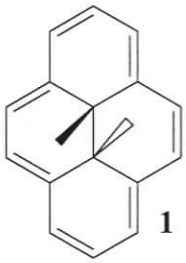
1


2


3


4a


4b

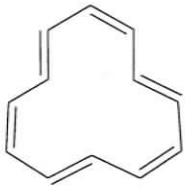
5

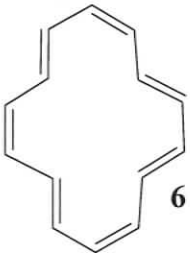
6

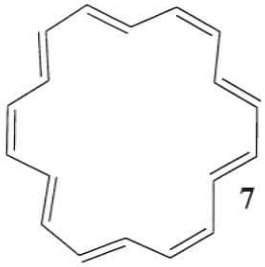
7

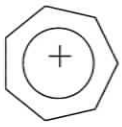
8


9

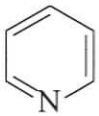

10

11

12

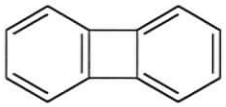
13

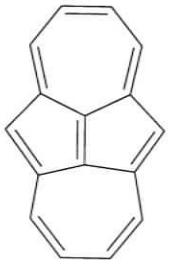
14

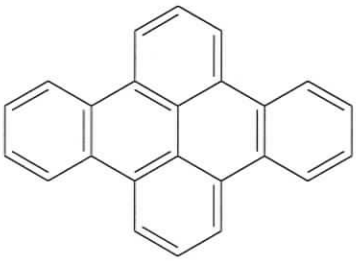
15

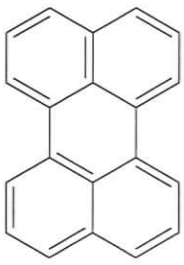
16

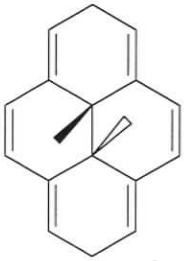
17

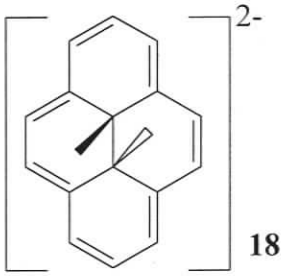

18

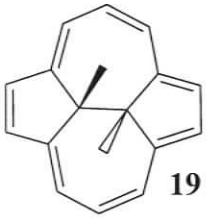

19

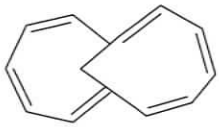

20

21

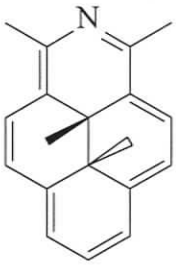

22

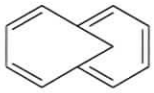

23

24

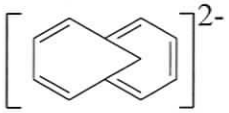

25

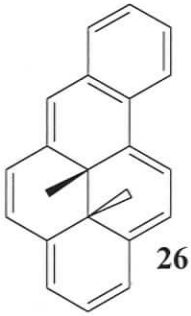

26

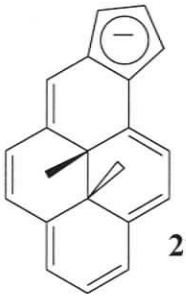

27

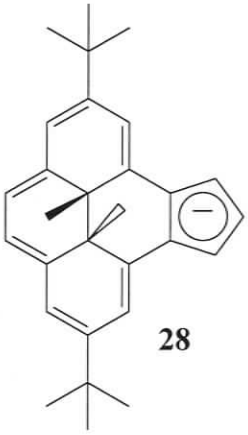

28

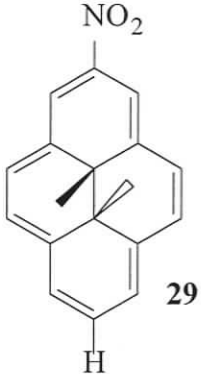

29

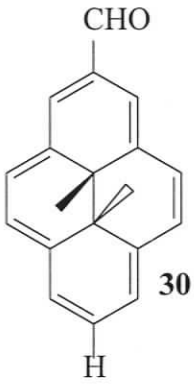

30

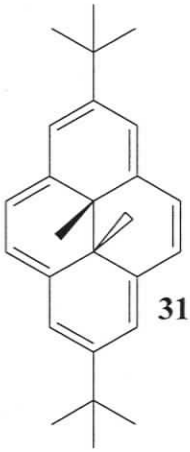

31

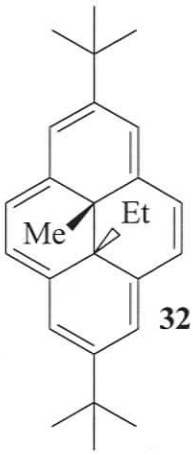

32

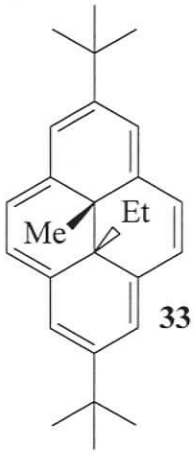

33

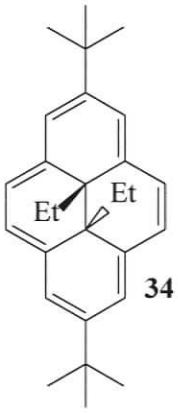

34

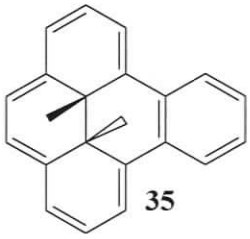

35

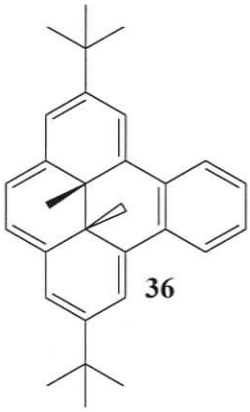

36

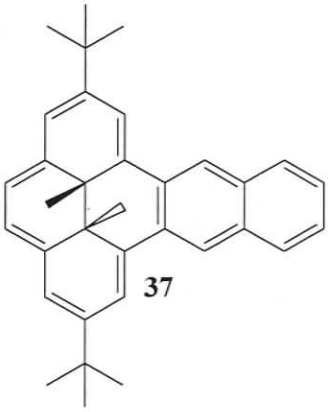

37

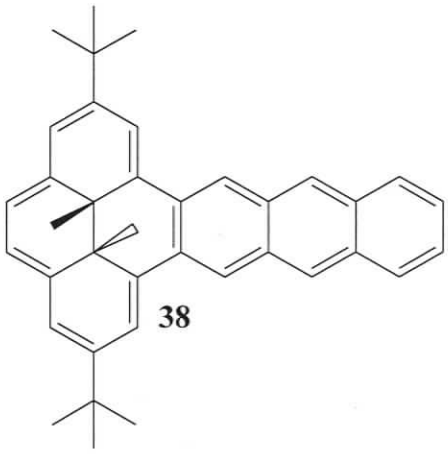

38

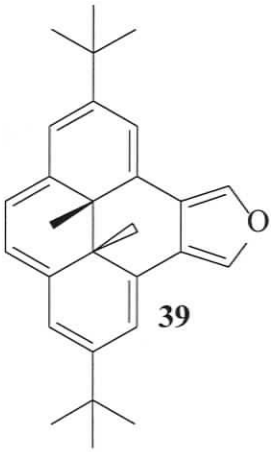

39

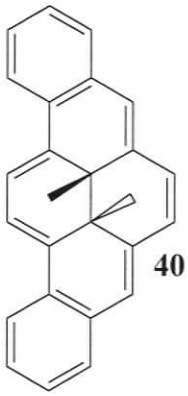

40

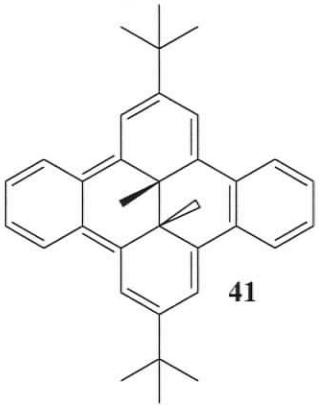

41

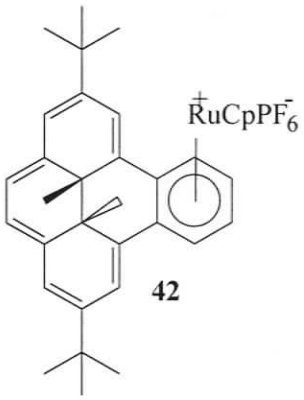

42

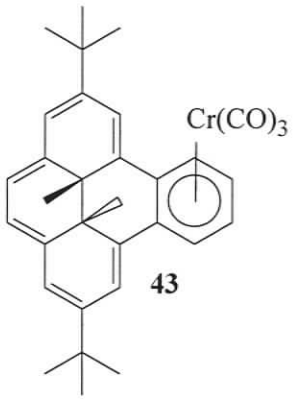

43

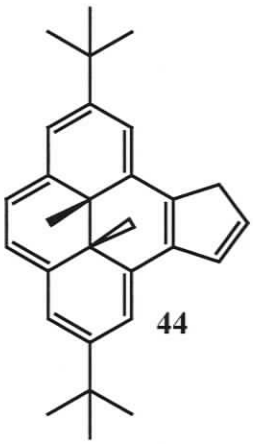

44

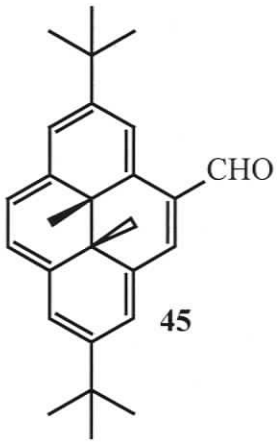

45

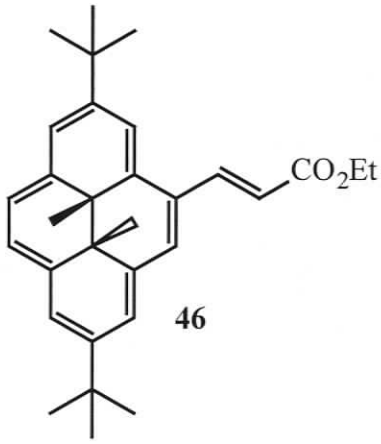

46

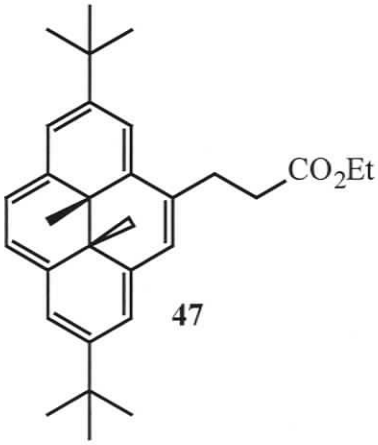

47

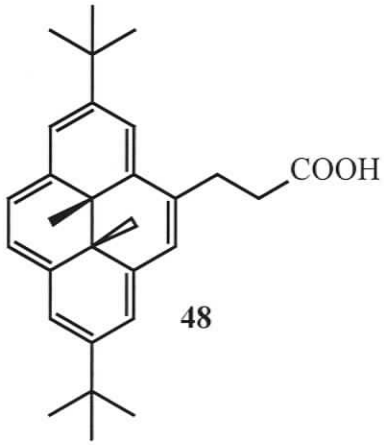

48

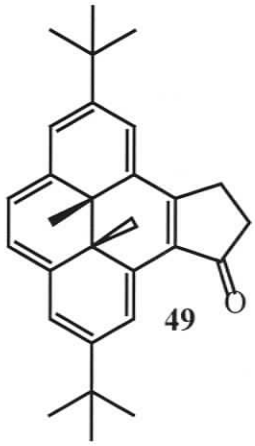

49

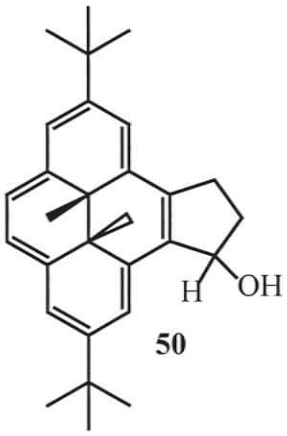

50

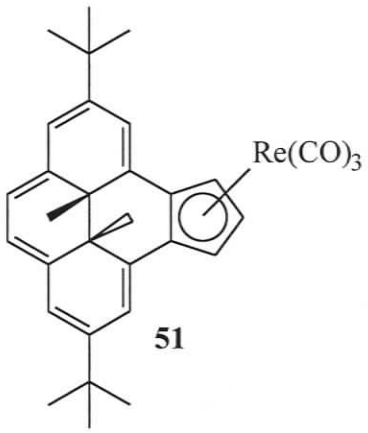

51

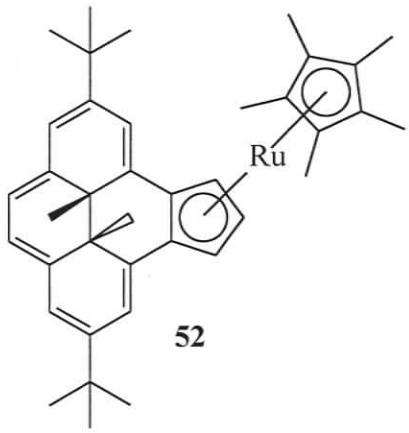

52

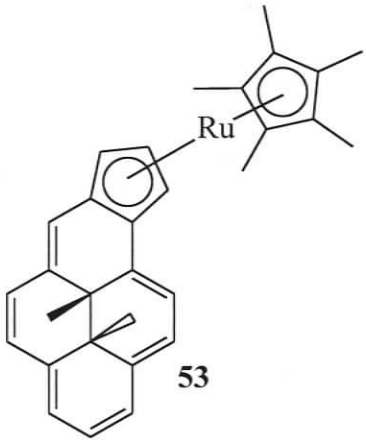

53

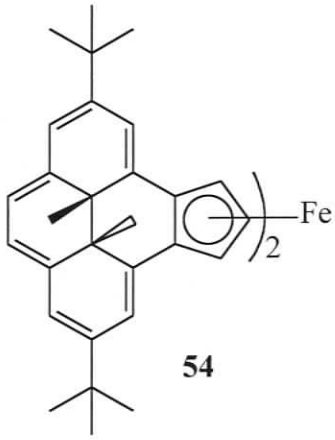

54

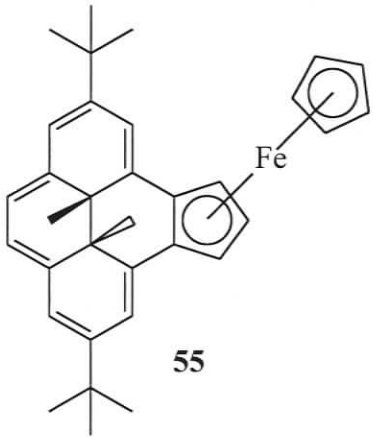

55

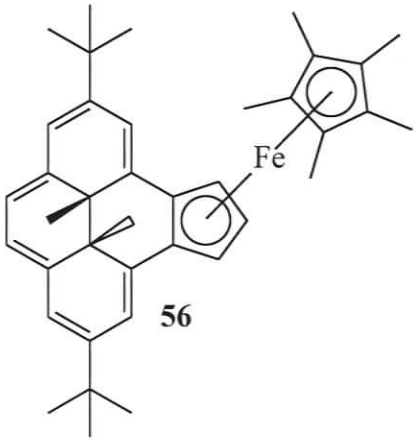

56

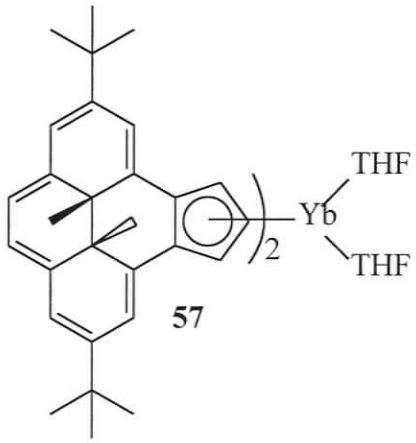

57

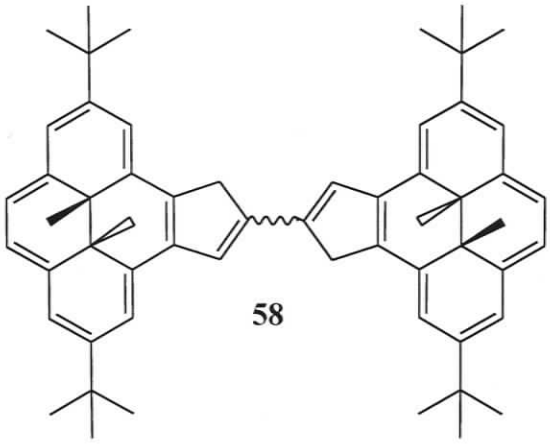

58

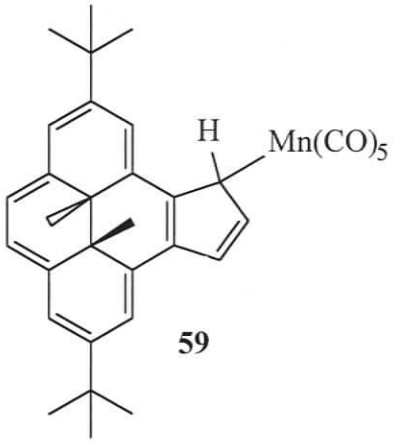

59

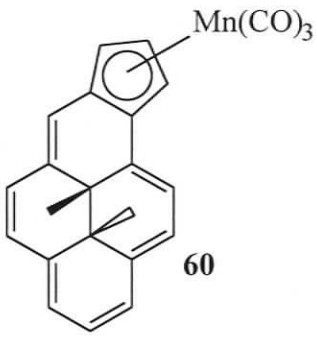

60

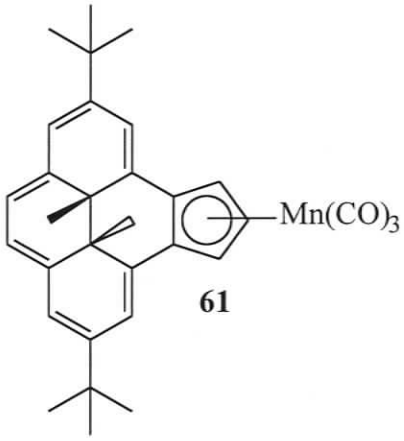

61

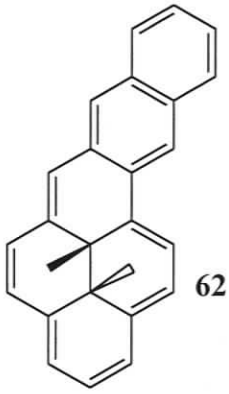

62

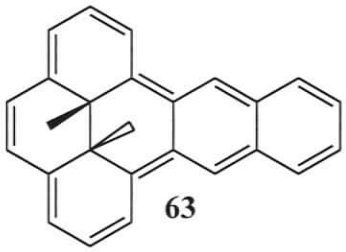

63

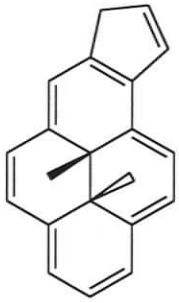

64

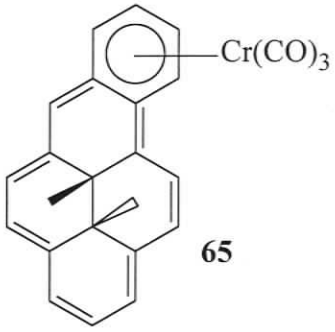

65

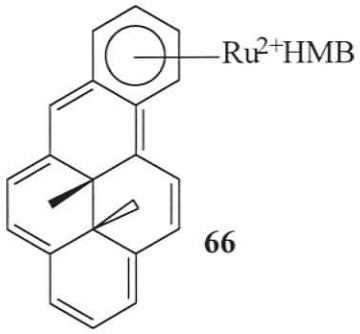

66

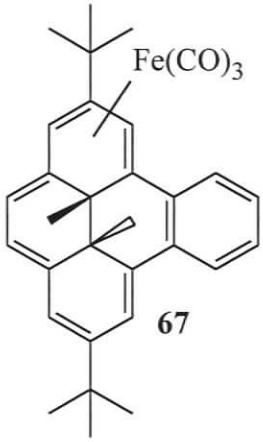

67

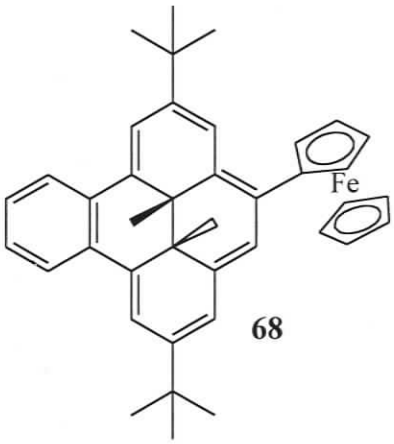

68

Acknowledgements

The author wishes to express her most sincere gratitude and deep appreciation to Dr. R. H. Mitchell and Dr. D. J. Berg for their constant guidance, help and encouragement during the course of this work.

The author also would like to thank Mrs. Christine Greenwood for recording many NMR spectra, and Dr. David McGillivray for mass spectrometric analysis.

Financial support from the University of Victoria and from NSERC is gratefully acknowledged.

To

my husband

Rui Zhang

&

my daughters

Sasa and Rose

Chapter One

Introduction

1.1 Dihydropyrenes

The Mitchell group has studied the properties of the dihydropyrenes for the last three decades. **DHP**, **1** (**Scheme 1.1**), is a fully delocalized molecule, having almost equal bond lengths, and thus like benzene has a strong ring current. Because DHP has internal methyl groups, the strength of the ring current can be probed using NMR spectroscopy, and as such the chemical shifts of the methyl groups provide a measuring stick for what is otherwise a rather poorly defined property – aromaticity. As well, the DHP molecule is photochromic; that is, irradiation of green **1** with visible light partially converts it to colorless **1'** and on irradiation of **1'** with UV light, it reverts to **1**. So dihydropyrenes have two particularly important properties that relate to aromaticity and photochromism and thus these topics will be introduced first.

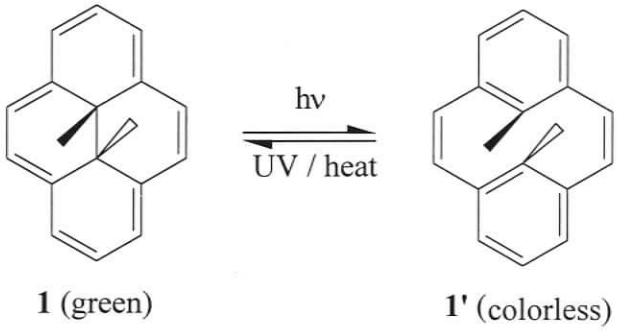

1 (green) **1'** (colorless)

Scheme 1.1. Isomerization between the closed dimethyldihydropyrene (DHP, **1**) and the open metacyclophanediene (CPD, **1'**).

1.2 Aromaticity

1.2.1 Aromaticity and the criteria for aromaticity

The discovery of benzene by Faraday[1] in 1825 opened a field of enquiry now known as aromaticity. Although more than one hundred and seventy five years have

passed, the criterion for aromaticity is still one area in physical organic chemistry which has not been fully defined. As a colloquial usage, aromaticity is typically taken to mean benzene-like. Most chemists have a feel for benzene; typically it shows low reactivity and undergoes substitution rather than addition reactions, that are normally expected for unsaturated hydrocarbons.

Although many attempts have been made to bridge theory and experiment to explain the unusual properties and stability of benzene, it was not until 1931 that the first real bridge was formulated. On the basis of molecular orbital theory, Hückel[2] extended the concept of aromaticity beyond the aromatic sextet by introducing his famous rule, which states that *planar monocyclic completely delocalized conjugated hydrocarbons will be aromatic when the ring contains 4n + 2 π-electrons*. In contrast, some of the 4n electron homologues display destabilization, great reactivity, π bond localization, and have thus become known as antiaromatics.

At the time when Hückel introduced the rule, there were only two neutral species to which it could be applied: benzene, [6]annulene, **2,** and cyclooctatetraene, [8]annulene, **3**. The rule thus initiated a systematic search for higher homologues of benzene, leading to an enormous contribution to the growth of synthetic as well as theoretical organic chemistry. Annulenes **4-7** are examples of such homologues.

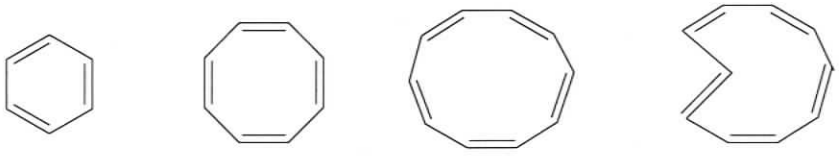

2 **3** **4a** **4b**

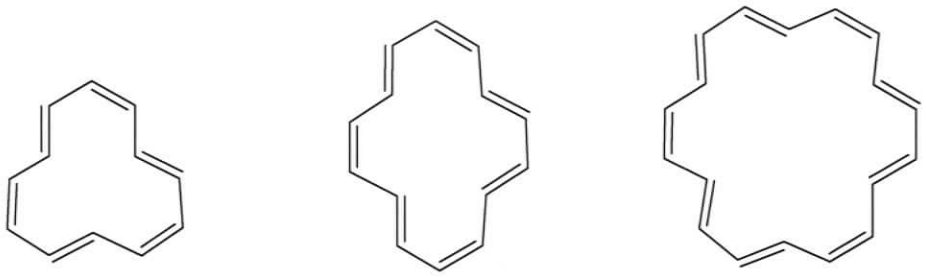

5 **6** **7**

Another important contribution of Hückel's aromaticity rule is the prediction of a new and stable class of compounds, namely the charged annulenes. It predicted cycloheptatrienyl cation, $C_7H_7^+$, **8**, to be a stable charged aromatic. The cation was prepared as far back as 1891 by Merling[3], but in the absence of theoretical support, its structure was not verified. The first reported synthesis of the cation was carried out by Doering and Knox in 1954.[4] Their studies of this 6π-[7]annulene cation proved the above prediction.

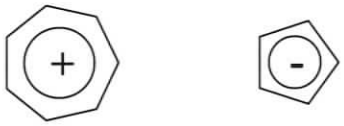

8 **9**

Studies of the isoelectronic negatively charged species, cyclopentadienide, **9,** date back to 1900.[5] This 6π-[5]annulene is also aromatic by Hückel's definition. An extensive number of charged monocyclic and polycyclic compounds are now known, these have been reviewed by a number of authors.[6,7]

Modification of Hückel's rule by Streitweiser[8] helped explain properties of conjugated heterocycles. Systems such as **10-12** are thus also called aromatic.

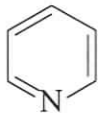

10

11

12

Another important extension to Hückel's rule is Randic's circuit theory[9,10] for polycyclic conjugated systems. This theory states that regardless of the total π-electron count, systems with only 4n + 2 electron conjugated circuits are aromatic, while those with only 4n electron circuits are antiaromatic. Systems (biphenylene, **13,** for example) which possess both 4n + 2 and 4n conjugated circuits are either aromatic or antiaromatic depending on which type of circuit prevails. Systems such as **14-16** thus could be included in the aromatic family under the above modification of the definition of aromaticity.

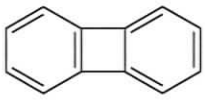

13

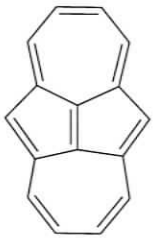

14

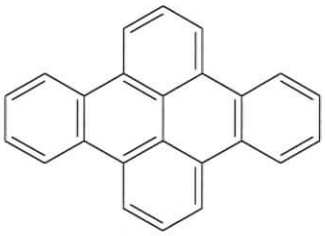

15

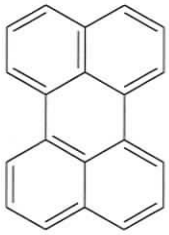

16

Despite the fact that the concept of aromaticity could not be described by a single definition, it is still important to define certain criteria for aromaticity, which should not only be able to judge whether a given compound is aromatic but also make it possible to measure the degree of aromaticity. The most widely held criteria are based on chemical, energetic, structural, or magnetic properties.

Chemically, aromatic compounds generally favor electrophilic substitution reactions over addition reactions. Some aromatic compounds such as phenanthrene, however, do undergo addition reactions. Therefore caution is required in application of the chemical criterion.

The delocalization of π-electrons lowers the energy content of the aromatic molecule relative to the hypothetical bond-localized structure. A theoretical parameter, called resonance energy, has thus been suggested as a suitable criterion for determining the aromaticity of a compound. Unfortunately, the value of resonance energy depends on the reference system chosen. Under this criterion, some compounds can be either aromatic or non-aromatic based on results using different methods and different reference systems.

The structural criterion refers to the C-C bond lengths in the compound. Applied to annulenes, aromatic systems should have equal bond lengths, whereas nonaromatic or antiaromatic ones should have significant bond alternation. Obviously, this method can not be easily applied to heterocyclic or polycyclic systems because of their lower symmetry. Moreover, X-ray data are needed for this method, and for many compounds this is not easy to obtain. Even after the data are acquired, packing forces in the crystals are another factor that might lead to bond alternation.

Perhaps the most popular aromaticity criterion that is appealing to the experimental chemist, uses ^{1}H NMR spectroscopy. An aromatic compound is characterized by its ability to sustain an induced diamagnetic ring current. As a result of the ring current, the protons inside and outside the ring would experience a secondary field against or parallel to the external applied magnetic field, which would change the

chemical shifts of those protons, and thus indicate the degree of the aromaticity of the compound. In the case of antiaromatic systems, a paramagnetic ring current is generated and has the opposite effect. We will discuss this more in the next section.

It turns out that none of the criteria mentioned above can exclusively be counted on to classify aromaticity completely, and none when violated, are good enough to discount the property. Instead, it is better to use two or more criteria when assessing aromaticity.

1.2.2 NMR spectroscopy and aromaticity

The "ring current theory" was first proposed by Pauling[11] in 1936. In macroscopic systems, current flow is induced in a cyclic conductor moving in a magnetic field to produce an opposing magnetic field. This classical model has been co-opted for use as a molecular model[12] in the ring current theory. At the molecular level, the applied magnetic field (B_0) is said to induce a ring current in an aromatic molecule, such that the magnetic field produced by the molecule opposes the applied field felt by the molecule at its center. The internal protons of an aromatic compound are thus strongly shielded compared to the analogous alkene, and resonate at higher field in an NMR spectrometer. On the other hand, outside the ring, the induced magnetic field augments the applied field. The external protons of an aromatic molecule are thus strongly deshielded compared to the analogous alkene, and therefore resonate at lower field. This is depicted for benzene in Figure 1.

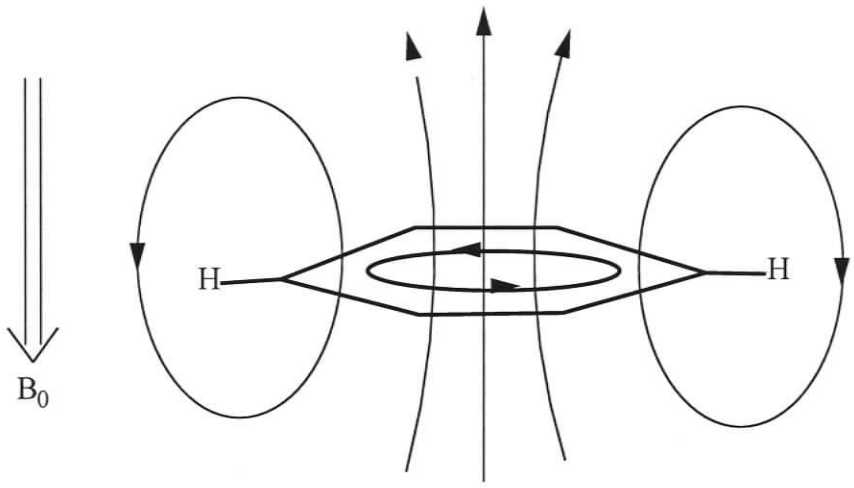

Figure 1.1 The induced magnetic field in aromatic compounds.

There is no proof that ring currents exist at the molecular level. The ring current theory is, however, used widely to explain the chemical shifts of annulenes. The ring current in $4n + 2$ π electron systems is termed diatropic, while in $4n$ π systems, a paramagnetic ring current is said to be induced, which has the opposite effect. Such systems are called paratropic.

The above model has been supported by a large amount of ^1H NMR data of annulenes. An interesting example is the bridged [14]annulene, the dimethyldihydropyrene **1**.[13] This system has an NMR spectrum with aromatic protons deshielded at δ 8.67 to 7.98, and internal methyl protons shielded at δ –4.25. The latter are shielded some 5.2 ppm from those of the non-delocalized model **17**.[14] On the other hand, the corresponding paratropic system **18** shows a very strong paratropic ring current effect with the paramagnetically deshielded internal methyl proton resonance at δ 21 and the external proton resonances shielded to δ –3.2 to –4.0[15]. More examples are shown below. Their proton chemical shifts are shown in **Table 1.1**.

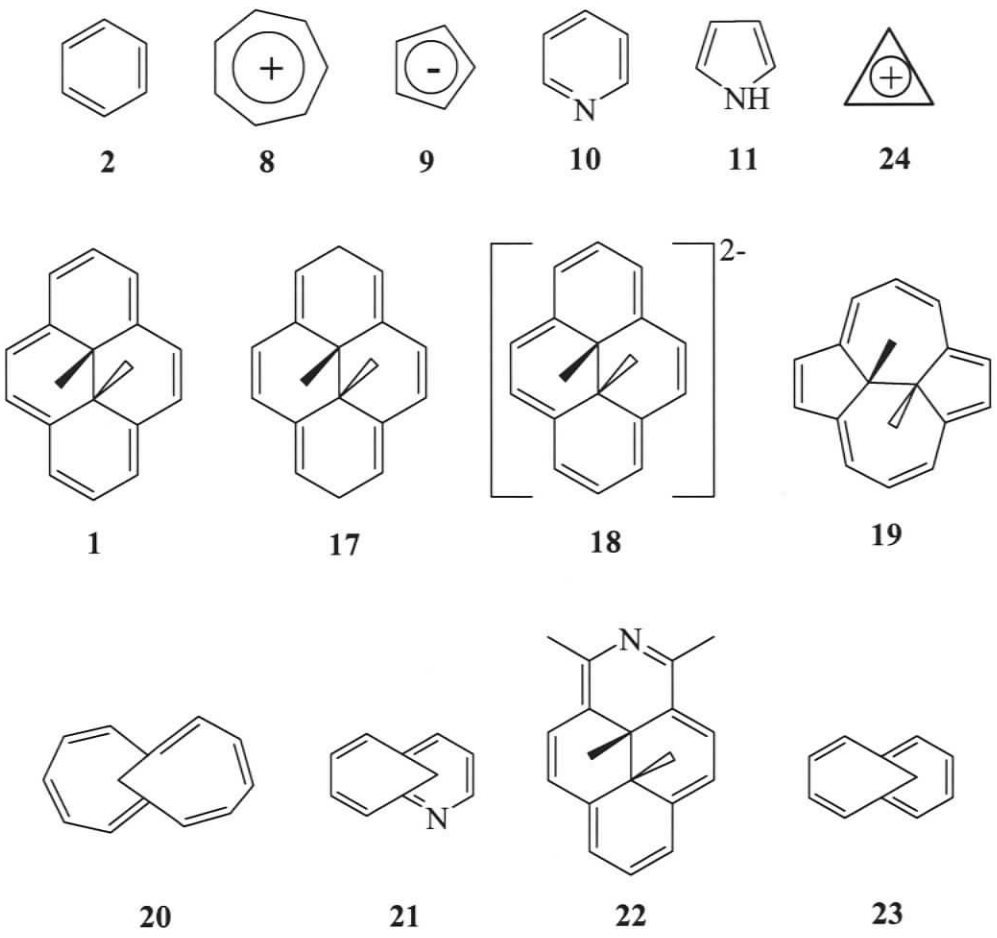

2 **8** **9** **10** **11** **24**

1 **17** **18** **19**

20 **21** **22** **23**

Archetypal benzene **2** has its proton NMR resonance at δ 7.27, 1.5 ppm downfield of typical olefins. This serves as a benchmark, implying that an additional deshielding effect is operative in benzene, the ring current. However, some recent papers dispute this.[22] Some bridged large annulenes have near planar peripheries, with near optimal π overlap, and thus induce strong magnetic shielding. Compounds **1** and **19** are such examples. The internal methyl protons of **1** and **19** resonate at δ –4.25 and δ –4.53 respectively, similarly shielded by ~ 5ppm from those of the non-delocalized model **17**.

Table 1.1. Proton NMR shifts (δ) of illustrative π systems (in ppm)

Compound	π electrons	δ outer protons	δ inner protons	reference
2	6	7.27		16
8	6	9.20		17
9	6	5.60		17
10	6	8.50-7.46		18
11	6	7.70-6.05		18
1	14	8.67-7.98	-4.25	14
18	16	-3.19 to -3.96	21.00	15
19	14	8.77-8.04	-4.53	19
20	12	5.50-5.20	6.06	20
21	10	8.23 - 6.50	0.65 to -0.40	28
22	14	9.50 - 8.70	-3.75 & -3.80	29
23	10	7.27 - 6.95	-0.52	27
24	2	11.10		21

Paratropic ring current effects are illustrated in **18** and **20**. Nearly planar **20** shows a bridge methano proton resonance at δ 6.06, strongly deshielded from typical allylic methylene signals ~ δ 2. The more rigid planar paratropic system **18** shows a very strongly deshielded internal methyl proton resonance at δ 21.

Heterocycles exhibit additional effects on proton chemical shift. Pyridine **10** displays proton signals at δ 8.5-7.46, downfield of those of pyrrole **11**, at δ 7.7-6.05. Pyridine is more aromatic/delocalized than pyrrole. Pyridine behaves more like an

electron poor deactivated aromatic (downfield shift) while pyrrole behaves more as an activated, electron rich (upfield shift) aromatic. Differences are also seen in polarization. Pyridine is polarized toward nitrogen, while pyrrole is polarized away from nitrogen. The chemical shift differences have been attributed to the dipole differences. Additional influences of hetero substitution may be seen in **21** and **22**, compared to **23** and **1**. In charged annulenes e.g. compounds **8**, **9**, **24**, besides the effect of ring current, the local electron density also affects the chemical shift, which will be discussed in the next section.

Caution is required when assigning aromaticity based on NMR chemical shifts, as the shielding or deshielding of protons by the ring current is not the only influence. Several other factors affect chemical shift too. These are shown in the following equation.

$$\sigma = \sigma^{RC} + \sigma^{LA} + \sigma_{\mu}{}^{0} + \sigma_{v}{}^{q}$$

Where

σ = the total chemical shift

σ^{RC} = shift due to ring current

σ^{LA} = shift due to local anisotropy

$\sigma_{\mu}{}^{0}$ = zero of chemical shift scale

$\sigma_{v}{}^{q}$ = shift due to excess π electron density

Moreover, besides the factors mentioned above, it should also be kept in mind that some metal hydrides and some organometallic compounds show great upfield proton resonances, while protons that are acidic or on carbonyls are quite deshielded.

Therefore, an ideal probe molecule to gauge aromaticity should have all the other factors, except for the ring current effect, constant or negligible. As we will see later in this chapter the bridged [14]annulene, dimethyldihydropyrene **1**, is such a molecule.

1.2.3 NMR spectroscopy in charged annulenes

π-Conjugated anions and cations represent an important branch of chemistry in that their study allows linking between theory and experiment, and are therefore of interest to the spectroscopist as well as the theoretical and synthetic chemist. In accordance with Hückel's rule, charged conjugated systems with 4n + 2 π-electrons are aromatic and those with 4n π-electrons are antiaromatic. These are manifested in their NMR spectra as shielding or deshielding effects of the chemical shifts by diatropic or paratropic ring currents.

In charged annulenes, however, besides the effect of ring current, the local electron density also affects the chemical shift. Thus in the tropylium cation **8,** the reduced charge density causes deshielding which acts in concert with the aromatic deshielding, resulting in a strong downfield shift to δ 9.2. Moreover, the cyclopropenium cation, **24**, shows an even stronger cation effect than **8** and has a proton resonance at δ 11.1. On the other hand, the anionic cyclopentadienide, **9,** shows an opposing effect of charge on the ring current. The increased charge density shields **9**, almost perfectly offsetting the aromatic deshielding, to result in a peak at δ 5.6.

Chemical shift–electron density correlations were first introduced by Schneider.[23] They allow an estimate of experimental charge densities by using ^{1}H or ^{13}C NMR parameters. For each negative or positive charge introduced in the conjugated species,

an overall change of approximately 10.7 ppm of proton chemical shift is incorporated to account for that charge.[6a, 24] In the case of carbon, an overall charge correction of approximately 200 ppm is incorporated.[6b, 25] In its proton NMR spectrum, anion **9** shows a singlet at δ 5.6 while cation **8** exhibits a signal at δ 9.2. The chemical shift is in reasonable agreement for a system with a diamagnetic ring current of a comparable magnitude to that of benzene, having one fifth (in the case of **9**) or one seventh (in the case of **8**) unit charge at each carbon atom.[23b, 24] The ^{13}C spectra for **9** and **8** are singlets at 156.1 and 102.8, respectively. After the charge correction, these shifts are comparable to that of benzene (δ 128.8).

Compounds **8** and **9** are examples of small symmetric charged annulenes, where the charge distribution is uniform. In larger charged annulenes, however, the charge is not distributed evenly. Therefore, the local π-charge density in these systems is the main factor influencing the individual ^{13}C chemical shifts[6b] and care must be exercised when interpreting chemical shift changes. In negatively charged annulenes, charge alternation may result.[6f] A representative example is that of dianion **25**, where the carbons 1 and 6 appear at 163.7 ppm. In the parent compound **23**, they appear at 114.6 ppm. The significant desheilding in the paratropic species is attributed to development of positive charge at these two carbons.[26]

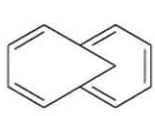

23

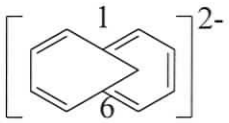

25

In principle, it should be possible to convert a neutral 4n + 2 annulene into a charged 4n system by adding or subtracting 2 electrons and vice versa. This change in

total π-electrons should lead to opposite ring currents in the neutral and charged annulenes and should be manifested in the changes of chemical shifts. An example is that of the ethano-bridged [14]annulene, **1**. The internal methyl protons of the aromatic compound appear at δ –4.25, shielded some 5.2 ppm from those of the non-delocalized model **17**.[14] On the other hand, the corresponding paratropic system **18**, a result of adding two electrons to **1**, exihibits a very strong paratropic ring current effect with the internal methyl proton resonance at δ 21, about 20 ppm downfield from the model **17**.[15]

1.2.4 Estimation of relative aromaticity – the Mitchell Method

The reason that aromaticity continues to be one of the most controversial concepts for nearly two centuries is that it is difficult to measure. This is especially true for methods that try to relate some calculated or derived quantity to that which would be obtained for a hypothetical reference structure. A case in point is resonance energy estimates derived from heats of hydrogenation where the reference structure for benzene is cyclohexatriene, usually assumed to be equivalent to three cyclohexenes. What the appropriate reference structures are, for example, for the cyclopentadienide anion **9** or ferrocene (both considered aromatic molecules) is far from obvious.

Probably a much more useful approach to estimating aromaticity is to compare the effect that the system under study has on a probe with the effect that a benzene ring has on the same probe. The advantage is that no hypothetical or reference or calculated structure was involved, the comparisons are to be made directly to the prototype aromatic, benzene.

NMR spectroscopy is one of the easiest experiment methods to characterize molecules, and is the most frequently used tool to decide whether or not a molecule is

aromatic. Extensive work from our group has shown that this tool can be used quantitatively to estimate the relative aromaticity of annulenes. The idea is to fuse an annulene to a probe aromatic molecule. The relative contributions of the ring currents of the annelated fragments to the overall ring current pattern of the fused system depends on the resonance energies of the fragments.[30, 31] Thus the fused benzenoid aromatics could be used to calibrate the effects on the probe and provide a scale relative to the effect of benzene. The chosen probe molecule is *trans*-10b,10c-dimethyldihydropyrene, **1**. It is a rigid, planar molecule,[32] with the internal methyl groups placed above and below the plane, almost over the center of the molecule, such that they are close to the center of the strongly shielding zone of the ring current. The methyl protons appear at δ –4.25, some 5.22 ppm shielded from those of the non-cyclically conjugated model **17**.[33] This chemical shift is affected little (usually < 0.3 ppm) by a variety of substituents,[33] including phenyl (δ(Me) –4.03 and –4.00),[34] but is dramatically affected by fusion of a benzene ring, e.g. in **26** δ(Me) = -1.62, a shift of 2.63 ppm, a reduction in the ring current of 50% (2.63/5.22). Most importantly, the through space deshielding of the internal methyl protons by the fused benzene ring is small (<0.1 ppm),[35] and the geometry of the molecule is not changed on fusion and thus the reduction in ring current is caused almost entirely by the change in delocalization in the macrocyclic ([14]annulene) ring.[32a]

Studies on a series of [a] and [e]-annelated derivatives of **1** have shown that the chemical shift of the internal methyl protons correlates with the degree of bond alternation around the macrocyclic [14]annulene ring as measured by $^{3}J_{H,H}$ coupling constants. Linear correlations are observed between the chemical shifts of the internal methyl protons and the more distant nonsterically affected external ring protons. Both of

these shifts thus mostly depend on the ring current, and hence, both can be used to estimate the aromaticity of the fused ring relative to a benzene ring. Good correlations are also found between the measured aromaticity and Dewar resonance energies[36] for the fused ring. Thus, by using the simple aromatic compound benzene as calibrant, a simple experimental method, which only involves measurement of chemical shift, has been found to measure the aromaticity of fused systems relative to benzene. That is the essence of the Mitchell method of estimating aromaticity.

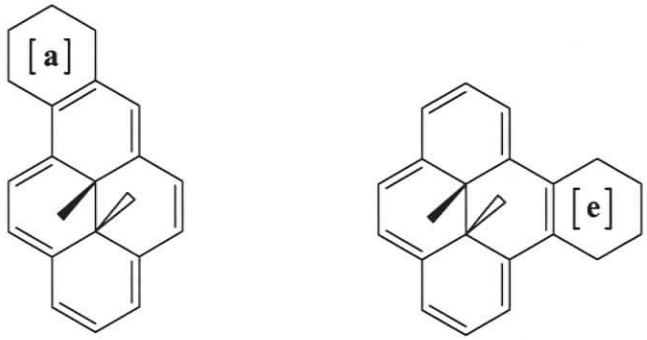

Positions and labels for [a] and [e] fused DHP

As the ethano-bridged [14]annulene **1** proves to be an excellent probe for studies of annelation as well as anisotropy effects for neutral aromatics,[32] it would be interesting to see if it is suitable for studies of fused charged systems, although in a charged species the effect of the charge will have to be considered. The cyclopent[a]dihydropyrene **27** was thus synthesized by Mitchell.[37] It is found that it has 53% of the effective bond-fixing ability of benzene fused to the same system. In terms of benzene resonance energy units, cyclopentadienyl anion **9** has an effective experimental resonance energy of 0.53.

Metallocenes are classified as 3-dimensional aromatic compounds.[39,40] Therefore, their fusion to another aromatic moiety should affect their aromaticity.

Studies on metal complexes of the anion **27**[38] showed that metallocenes are more bond-fixing than benzene. Other metal complexed annelated systems gave similar results.[41]

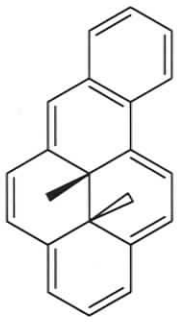

26

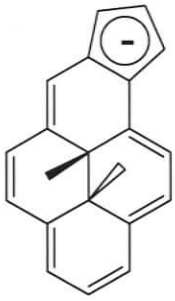

27

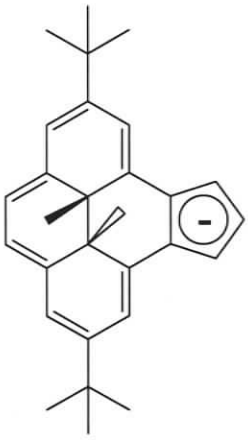

28

Theoretically, the generality of results obtained in cyclopent[a]dihydropyrene systems above, should extend to the [e]-fused DHP systems. Impetus to explore the cyclopent[e]dimethyldihydropyrene system **28** actually derives from a second intriguing behaviour displayed by DHPs; they are photochromic. This thesis in part presents results in both the investigation of aromaticity in **28** and its metal complexes, and the photochromism of such systems.

1.3 Photochromism

1.3.1 A short history of photochromism

Photochromism, although not called that at the time, is associated with reversible, light-induced photochemical processes that result in a color change, and was first observed by Fritzsche[42a] in 1867. He noticed the bleaching of an orange-colored solution of tetracene in the daylight and the regeneration of the color in the dark. Later, ter Meer[42b] saw a similar phenomenon with potassium salts of dinitroethane. Another

early contribution to the field of photochromism was published by Phipson,[42c] who noted that a painted gatepost appeared black all day and white all night. In 1899, Markwald[42d] coined the term *phototropy* to explain the reversible process in which a solid changes color when exposed to visible light and reverts to its original color in the dark. Since then, interest in photochromism has been continuous but limited until the 1940-1960 period, which saw an increase in mechanistic and synthetic studies. Scientists then found that the phenomenon includes other states of matter and that exciting radiation need not be limited to the visible region of the spectrum. In 1950, Hirshberg[42e] suggested using the term "photochromism" to describe the phenomenon. This term is composed of two parts: *photo* (light) and *chrom* (color), and is the name used today.

Photochromism expanded during the 1960s in parallel with the development of physical methods and organic synthesis. Photochromic glasses became available at that time and further stimulated research. However, it appeared that the photodegradation of the known families of organic photochromes limited their potential for applications.[43] A revival of activity started in the 1980s, essentially because of the development of fatigue-resistant spirooxazine and chromene derivatives. They triggered the fabrication and commercial application of photochromic ophthalmic lenses. Since then, new photochromic systems have been discovered and other commercial systems have been developed.

1.3.2 The current definition of photochromism

In IUPAC terminology, photochromism is: A photoinduced transformation of a molecular structure (e.g. of a solution), photochemically or thermally reversible, that

produces a spectral change, typically, but not necessarily, of visible color.[44] It usually involves two states, A and B (**Scheme 1.2**). The thermodynamically stable form A is transformed by irradiation into form B. The back reaction can occur thermally (*photochromism of type T*) or photochemically (*photochromism of type P*) or both. Usually the thermodynamically stable form A is colorless or pale yellow and form B is colored. This phenomenon is referred to as *positive photochromism*; the reverse where the colored form B is the more stable one is known as *negative* or *inverse photochromism*.

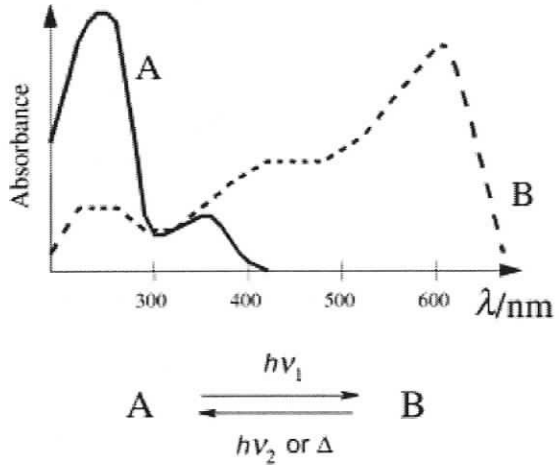

Scheme 1.2. The two states of a photochromic compound.

1.3.3 Types of organic photochromic compounds

There are many types of organic photochromic compounds. Examples are spiropyrans, spirooxazines, fulgides, diarylethenes, azo compounds, chromenes, polycyclic aromatic compounds, anils and polycyclic quinones. However, despite the favorable situation provided by recent progress of optical memory and switch technologies, organic photochromic compounds still await practical applications. The

limitation is due to lack of suitable compounds which meet the following technical requirements for the optoelectronic devices: 1) thermal stability of both isomers, 2) fatigue resistance, 3) nondestructive readout ability, 4) high efficiency of photoreactions (large quantum yields and large molar absorption coefficients), 5) high speed of photoreactions, 6) sensitivity at diode laser wavelengths, and so on. The main problems are that most organic photochromic compounds are thermally reversible and most exhibit significant photodegradation after a few switching cycles. Currently the most promising results come from fulgides and diarylethenes. Both of them can be thermally irreversible; for some of the diarylethenes with heterocyclic aryl groups, the coloration / decoloration cycle could be repeated more than 10^4 times without losing photochromic performance.

The most prevalent organic photochromic systems involve unimolecular reactions; other systems undergo bimolecular photocycloaddition reactions. The unimolecular reactions include cis-trans isomerization, electrocyclization, intramolecular hydrogen transfer and intramolecular group transfer reactions. Each of these reactions will be illustrated below using organic photochromic compounds as examples.

1.3.3.1 Cis-trans isomerization

Cis-trans isomerizations occur in stilbenes,[45] azo compounds **(Scheme 1.3)**,[46] and as well in some photochromic biological receptors that are part of living systems.[47]

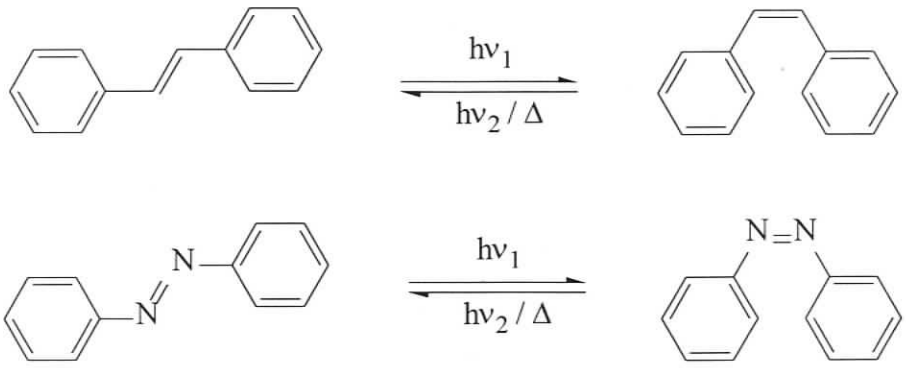

Scheme 1.3. The cis-trans isomerization for stilbene and azo-benzene.

1.3.3.2 Electrocyclization

Typical examples of organic photochromic compounds, which undergo electrocyclization, include stilbene (the prototype diarylethene), diarylethenes, fulgides, spiropyrans and spirooxazine. Besides cis-trans photoisomerization, *cis*-stilbene also undergoes a photocyclization to produce dihydrophenanthrene.[48] The diydrophenanthrene returns to stilbene in the dark in a deaerated solution. In the presence of air however, the dihydrophenanthrene irreversibly converts to phenanthrene by the hydrogen-elimination reaction with oxygen, as shown in **Scheme 1.4**. When the 2- and 6-positions of the above phenyl rings were substituted with methyl groups, the elimination reaction was suppressed and the compound underwent a reversible photocyclization reaction, that is, a photochromic reaction, even in the presence of oxygen. The lifetime of the colored dihydro-type isomer of 2,3-dimesityl-2-butene was, however, very short ($t_{1/2}$ = 1.5 min at 20 °C).[49] Such a thermally unstable photochromic system is not useful for practical uses.

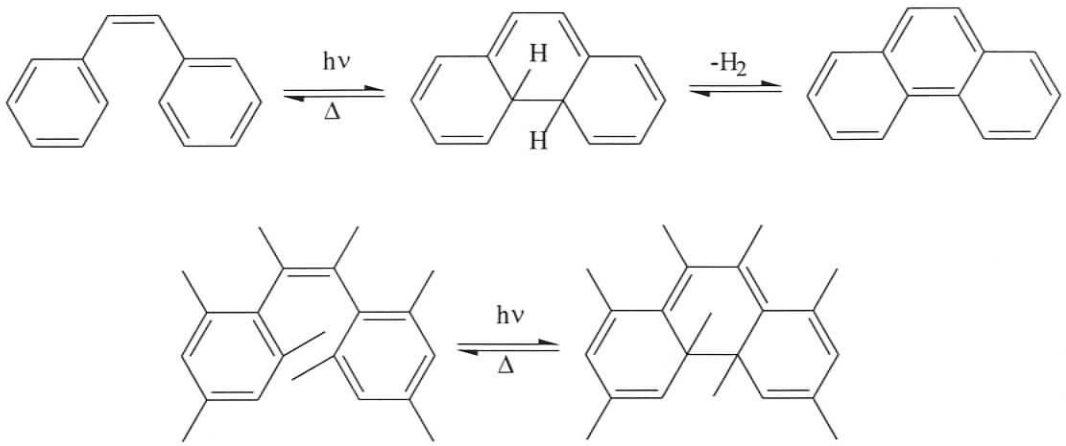

Scheme 1.4. Examples of stilbenes showing the isomerization between open and closed isomers

In the course of searching for thermally irreversible stilbene-like photochromic compounds, series of diarylethenes were developed. In 1988, Irie[49] reported the first thermally irreversible diarylethenes, in which thiophene rings replaced the phenyl rings in stilbenes (**Scheme 1.5**). Since then, various diarylethenes with different aryl groups, ethane links and suitable substitutions have been synthesized.[50]

Fulgides also undergo electrocyclization. The name "fulgides" (from the latin *fulgere*, to glisten) was given by their first investigator, Stobbe, because they were isolated as fine glittering crystals.[51] They can be described as derivatives of dialkylidenesuccinic anhydride **(Scheme 1.6)**. Upon UV irradiation, the open (E, colorless) form can undergo one of two main processes: isomerization to the colored closed form or E-Z isomerization. Visible irradiation results only in conversion of the closed form into the open E isomer. In order to exhibit photochromism fulgides require at least one aryl group on one of the methylene carbons. Initially only thermally reversible fulgides were known. Thermally irreversible ones were developed in 1981.[52a]

Since then, most of the other properties required for practical uses have been largely improved.[52b]

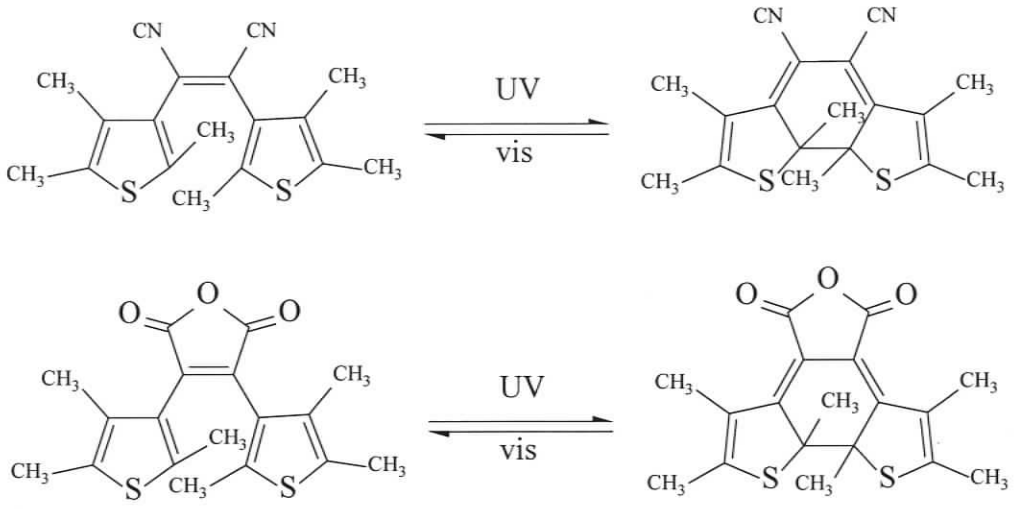

Scheme 1.5. Examples of diarylethene showing the interconversion between open and closed isomers.

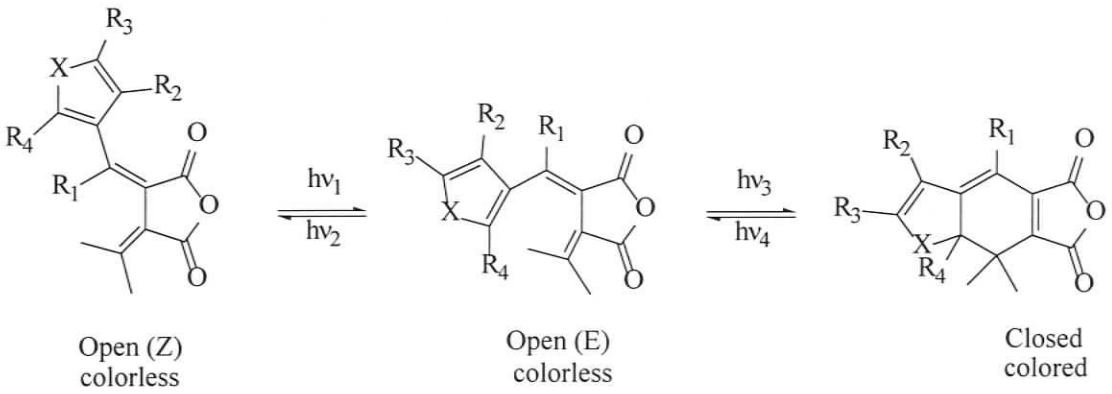

Scheme 1.6. Examples of fulgides structure showing E,Z and open-closed isomerizations.

Spiropyrans[53] also undergo a 6π - electrocyclization when switching between the two photochromic states **(Scheme 1.7)**. The closed forms are usually nice crystalline

colorless or pale yellow solids. Solutions are colorless or weakly colored, and upon irradiation with UV light develop color or become more intensely colored. The colored solution fades thermally to their original state. The open structure is essentially that of a merocyanine dye, which has a very strong tendency to associate into aggregates with a stack–like arrangement of the merocyanine molecules.[53a] The tendency for aggregation is so strong that the aggregates are formed on irradiation of a spiropyran in a methacrylate polymer and even on swelling of the polymer film in a solvent.[53a]

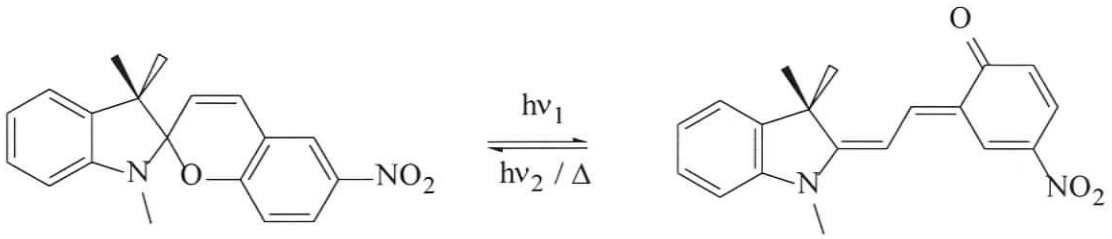

Closed form Open form (Merocyanine)

Scheme 1.7. Examples of spiropyrans structure showing interconversion between open and closed isomers.

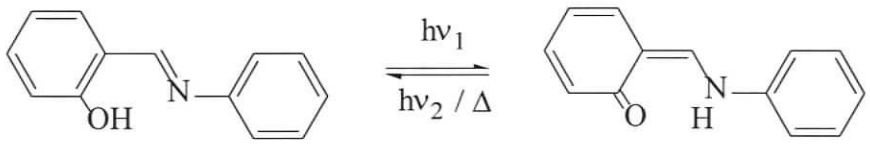

Scheme 1.8. Example showing intramolecular hydrogen transfer between two isomers.

1.3.3.3 Intramolecular hydrogen transfer

Intramolecular hydrogen transfer is found in anils and related compounds. One example is shown below (**Scheme 1.8**).[54] The mechanism was thought to involve a six-membered ring transition state in which a hydrogen transfers to form a colored quinoid

structure. The photo generated colors fade fast with warming, so photochemical studies have been done mostly at low temperature.

1.3.3.4 Intramolecular group transfers

Intramolecular group transfers operate in polycyclic quinones (periaryloxyparaquinones). An example is shown in **Scheme 1.9**.[55]

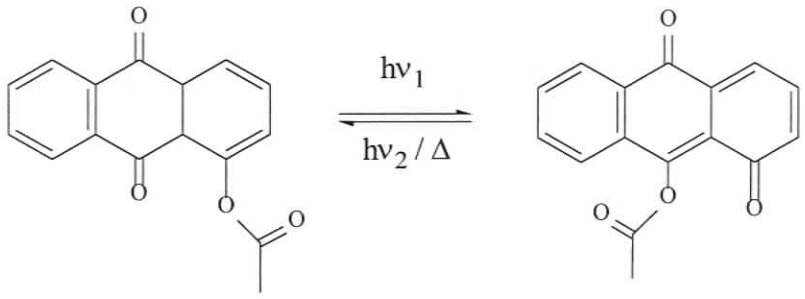

Scheme 1.9. Example showing intramolecular group transfers between two isomers.

1.3.3.5 Cycloadditions

Cycloadditions are found in (2 + 2) cycloadditions based on valence isomerizations.[56a] (4 + 4) Cycloadditions are found mainly in polycyclic aromatic hydrocarbons, for example, the photochemical dimerization of anthracene.[56b] (4 + 2) Cycloadditions are found, for example, in additions of singlet oxygen to aromatic compounds **(Scheme 1.10)**.[55]

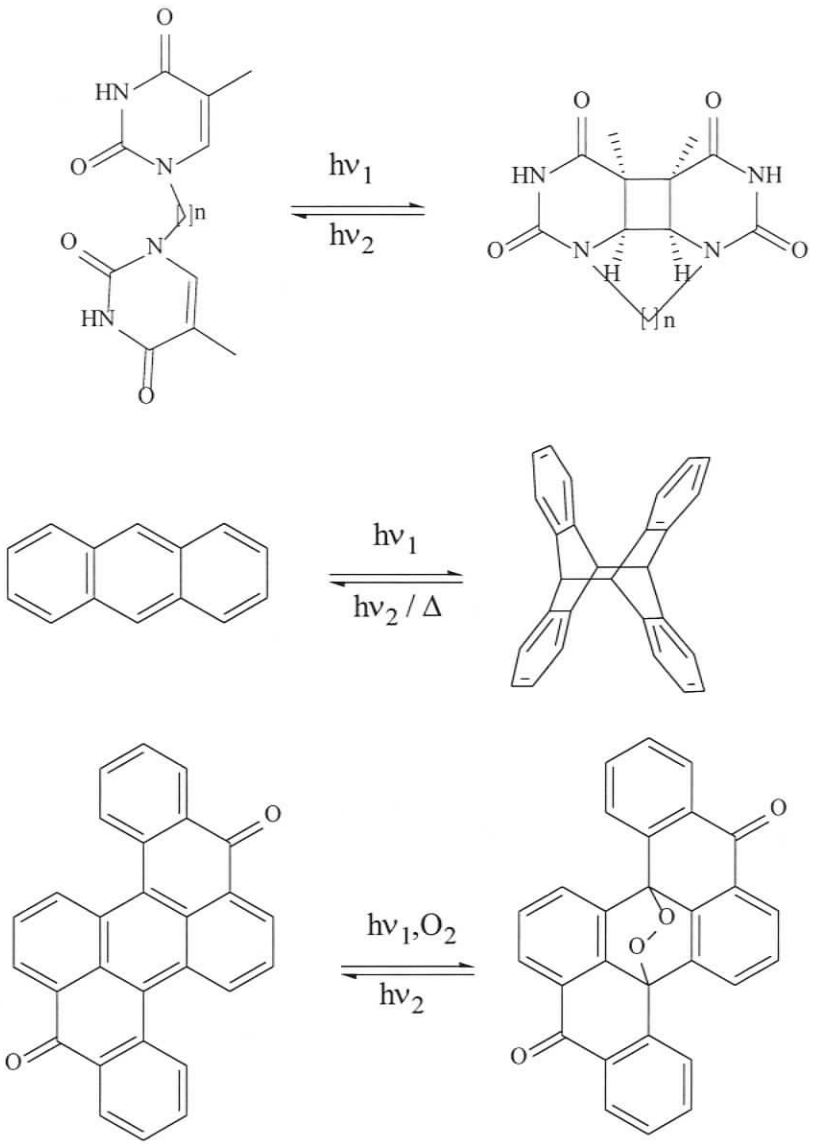

Scheme 1.10. Photochromic examples showing cycloaddition reactions.

1.3.4 Photochromism of dimethyldihydropyrene (DHP) compounds

Dimethyldihydropyrenes are in fact 1,2-diarylethenes, where a second ethene group tethers the *meta*-positions of the two aryl-groups. They have a huge advantage relative to *cis*-stilbene in that they cannot undergo dehydrogenation or E/Z-isomerization. As well, they are rare examples of negative photochromes, where the closed DHP form is the colored stable state, and the open metacyclophanediene (CPD) form is the colorless, thermally unstable state.

The green DHP **1** has a rigidly planar extended π-system and has absorptions out to 600nm. The colorless cyclophanediene (CPD) form **1'** is a stepped molecule which is also rigid but has the olefinic bridges almost at right angles to the benzene rings and thus only shows benzenoid absorption with an extended tail.[57] The effective size of the π-system thus changes from 14π in **1** to 6π in **1'**. In general, irradiation of DHP **1** and its derivatives with visible light converts it to the CPD form **1'**, while irradiation of **1'** with UV light converts **1'** back to **1**.

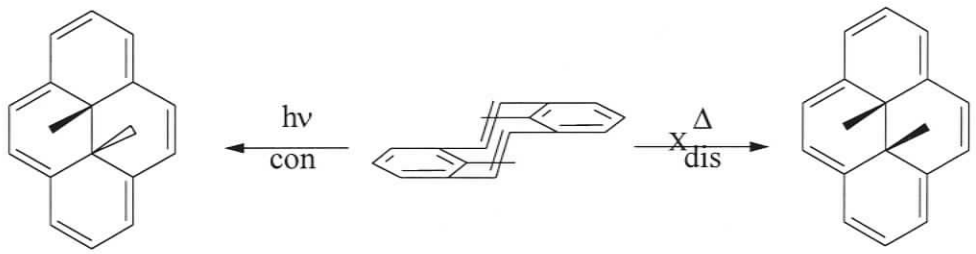

trans-**1** **1'** cis-**1**

Scheme 1.11. Possible Woodward-Hoffmann allowed processes involving the conrotatory photochemical ring closure of *trans*-CPD to *trans*-DHP and disrotatory thermal ring closure of *trans*-CPD to *cis*-DHP.

The isomerization between DHP and CPD is classified as a 6π-electrocyclization.[57] According to the Woodward-Hoffmann rules, if this reaction is concerted, it is allowed in a conrotatory fashion photochemically but forbidden thermally. The thermal reaction would have to be disrotatory to be allowed but this would give the *cis*-dimethyldihydropyrene and is not energetically favorable since the internal methyl groups can not pass through the ring **(Scheme 1.11)**. The thermal return in fact occurs to give the *trans*-DHP and implies that either the thermal return is not concerted or the Woodward-Hoffmann rules are not applicable.

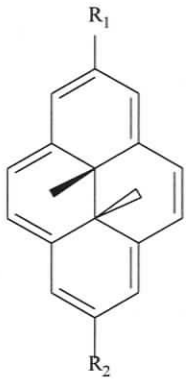

29 $R_1 = NO_2$, $R_2 = H$
30 $R_1 = CHO$, $R_2 = H$
31 $R_1 = R_2 = t$ -butyl

The reversible valence isomerization between **1** and **1'** has been observed and studied for several dozen simple substituents, where the internal alkyl groups are methyl or ethyl and are *trans* to each other.[58] However, it has not been observed in any *cis*-dimethyldihydropyrenes. The quantum yield for the UV closing of **1'** to **1** was high and not changed much by substitution, while that of the bleaching reaction by visible light, **1** to **1',** was low and is affected by substitution.[59] It appears that substitution with electron withdrawing groups at the 2-position increases the photo opening quantum yield, while electron donating groups at the 2,7-position decreases it. For example, the parent DHP **1** has a ring opening quantum yield of 0.006[59a] (previously reported as 0.02[58b]), while the

nitro and formyl substituted compounds **29, 30** have much higher quantum yields of 0.3-0.4 and the 2,7-di-*t*-butyl substituted DHP **31** shows a lower quantum yield of 0.0015 for ring opening.[58]

Table 1.2 Rate data (*k*) and activation energies (E_a) for the thermal reaction of 1' to 1 and substituted derivatives[58b, 60]

Compound	k (30 °C) [min^{-1}]	E_a [$kcal.mol^{-1}$]
DHP, **1**	0.0010	23.0
2-formyl-**1**, **30**	0.052	20.5
2-nitro-**1**, **29**	0.069	19.7
4-carboxy-**1**	0.00053	22.5
4-bromo-**1**	0.00058	25.2
1,3,6,8-tetramethyl-**1**	0.00095	24.5
2,7-di-tert-butyl-**1**, **31**	0.0008	21.8
4-nitro-2,7-di-tert-butyl-**1**	0.0018 (40 °C)	23.7

The difference in enthalpy between the DHP isomer and CPD isomer does not vary much with substituent.[58] However, the activation barrier, and hence the rate of the thermal return reaction is affected by substituents. Relevant data for some examples are shown in **Table 1.2**. It appears that an electron-withdrawing group at the 2-position speeds up the thermal return, while electron-donating groups such as methyl and t-butyl slow it down. Thus the nitro and formyl substituted compounds **29**, **30** showed higher thermal return rates (0.069, 0.052 min^{-1} at 30 °C respectively), while the 2,7-di-*tert*-butyl

substituted compound **31** showed a slower one (0.0008 min^{-1} at 30 °C) than that (0.0010 min^{-1} at 30 °C) of the parent **1**. Tashiro et al[60] have shown that when *tert*-butyl groups are in the 2,7-positions, other substituents do not affect the rate much.

Increasing the size of the alkyl substituents within the cavity of the π-electron cloud has little effect on the quantum yield of opening but actually increases the rates of thermal return.[58b, 60] For example, the thermal return rate for the photoisomers of **32**, **33**, **34** are 0.0044, 0.0047 and 0.012 min^{-1} at 40 °C. This increase possibly stems from increased repulsion between the larger alkyl group and the stepped CPD benzene rings. This is relieved slightly in the DHP form, where the internal groups project away from the plane of the molecule. However, the thermal stability of systems with larger alkyl groups within the π electron cavity decreases. Larger alkyl groups migrate to the periphery more readily to give a structure which is no longer a dihydropyrene.

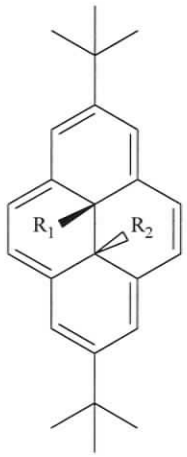

32 $R_1 = CH_3$, $R_2 = C_2H_5$
33 $R_1 = CH_3$, $R_2 = CH_2Br$
34 $R_1 = R_2 = C_2H_5$

Annelation of the DHP/CPD nucleus can also have a large effect on the ring opening quantum yields and the thermal return rates. When benzenoid systems are fused to dihydropyrenes, the extended π-system continues to be approximately planar and the principle absorptions are red shifted. In their open CPD forms however, the staircase

geometry interrupts the π-system, and benzenoid absorption persists. Benzenoid annelation of dihydropyrenes thus modifies the properties of the switch but does not change its nature.[61]

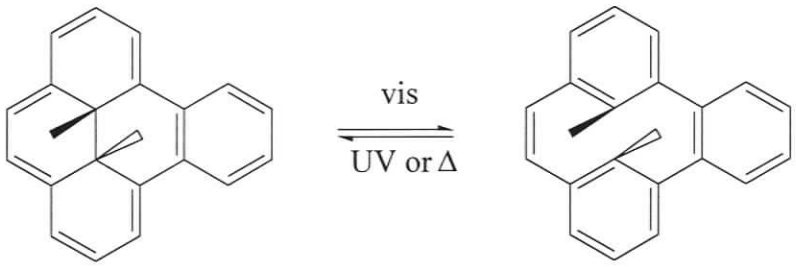

35 **35'**

Scheme 1.12. Isomerization between benzo[e]annelated system **35** to **35'**.

The disadvantages (i.e. low opening quantum yield and fast thermal return) of the parent system **1** are much reduced in the benzo[e]annelated system **35** to **35' (Scheme 1.12)**. First, the E_{act} for the thermal return reaction of **35'** to **35** is higher by 2 kcal/mol (25 kcal/mol) compared to that of the parent **1'** to **1**, with the half-life of **35'** extended to about a week at room temperature in solution.[62] Secondly, compound **35** is readily and quantitatively converted to **35'** by irradiation with visible light at room temperature. Irradiation with UV light then quantitatively converts **35'** back to **35**. This is important, because many photochromic systems give photo stationary states and complete conversion from one isomer to the other is not possible. Quantum yield studies[58] on the 2,7-di-*t*-butyl substituted analogue **36,** showed that the ring opening quantum yield (Φ = 0.042) increased about 30 times compared to the non-annelated system **31** (Φ = 0.0015). Moreover, its thermal return rate at 46 °C is about three times slower than that of **31**[63] **(Scheme 1.13)**.

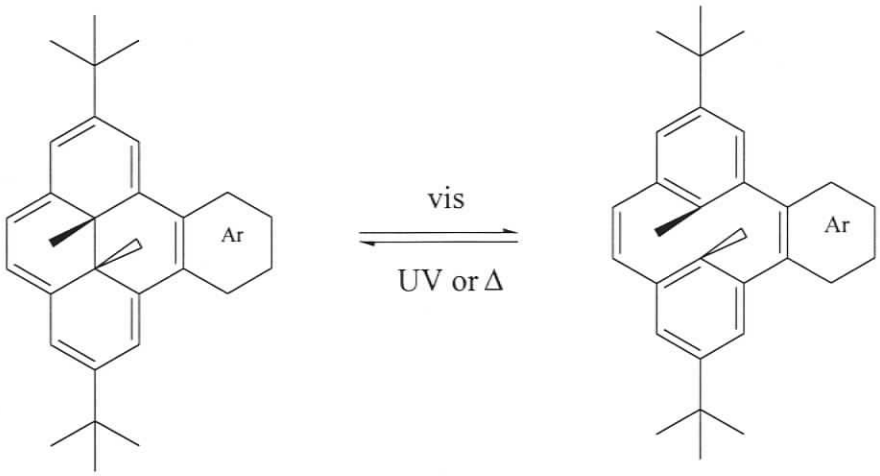

31 Ar = absent **31'**

36 Ar = **36'**

37 Ar = **37'**

38 Ar = **38'**

Scheme 1.13. Isomerizations between [e]-annelated 2,7-di-*t*-butyldimethyldihydropyrenes.

The naphtho analogue **37** bleached to **37'** even faster than **36** did to **36'**; however, bleaching of the anthro analogue **38** was slower than that of **36**. The major difference between these three analogues was in the thermal return reactions. The thermal return of **38'** to **38** is approximately 3 to 4 times faster than that of **37'** to **37**, which is 4 times

faster than that of **36'** to **36**, which is 3 times slower than the non-annelated **31'** to **31**. **Table 1.3** shows the relevant data.

Table 1.3 Half-lives ($\tau_{1/2}$, h, 46 °C) and energies of activation (E_{act}, kcal/mol) for the thermal return reactions shown in Scheme 12.[63]

Reaction	$\tau_{1/2}$	E_{act}
31' to **31**	1.88	23.0
36' to **36**	5.75	24.5
37' to **37**	1.15	22.1
38' to **38**	0.33	19.1

It is worth mentioning that at this point the furan annelated analogue **39** has the slowest thermal return rate so far, 0.000183 min^{-1} at 46 °C.[63, 64] Unfortunately this compound is not stable. Although **39** opens readily and cleanly with visible light, photoclosing with UV light causes decomposition, and as well, it is air sensitive.

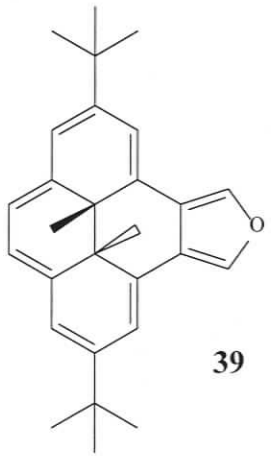

39

Fusion in the [a] position of DHPs gives very different results:[65] the thermal return reaction of CPD **26'** to DHP **26** is very rapid, such that visible light irradiation of **26** under ambient conditions permits no buildup of the CPD **26'**. Initial laser flash studies suggest that CPD **26'** does form, but rapidly reverts to **26**. Indeed, none of the [a] fused benzannulenes that we have made[32a, 61] allow useful amounts of the CPD isomer to be observed.

The possible reason for the rapid thermal return of [a]-fused systems comes from the large energy difference between the DHP and CPD isomers. AM1 calculations[61, 65] showed that the differences in the heat of formation, ΔH_f(CPD-DHP), are small for the [e]-annelated systems (ΔH_f = 0-1.5 kcal/mol) while they are all large for the [a]-annelated compounds (ΔH_f = 10-14 kcal/mol). For example, for the benzo[e]pair **35'/35** ΔH_f = 1.1 kcal/mol but for the benzo[a]pair **26'/26**, ΔH_f is 10.6 kcal/mol. Clearly in terms of energy, **26'** has more to gain in converting to **26**, than does the [e] series compound **35'** in converting to **35**.

For a practical application, a photoswitch should have no thermal return reaction and should photoopen and close fast. Thus the best "switch" so far in the dihydropyrene series is the benzannelated switch **36/36'**. It has a reasonably slow thermal return yet relatively good photoopening and closing properties. Systems with two or more DHP units in one molecule have also been synthesized.[63, 66, 67] Most of them contain **36** as a building block.

Bis annelated systems show different effects. Dibenzo derivative **40** does not photo bleach significantly, [61, 62, 68] while the [e,l]-dibenzo system **41'** actually has the CPD form as the thermally stable form[69] (**Scheme 1.14**). The green [e,l]-

dibenzodihydropyrene **41** is obtained on irradiation of **41'** at low temperatures. The thermal opening reaction is fast, 0.256 min^{-1} at –10 °C. AM1 calculations show a ΔH_f for (**41-41'**) of 18 kcal/mol, and presumably most of this difference is because of the greater degree of resonance stabilization in four benzene rings compared to that in the dihydropyrene system **41**.

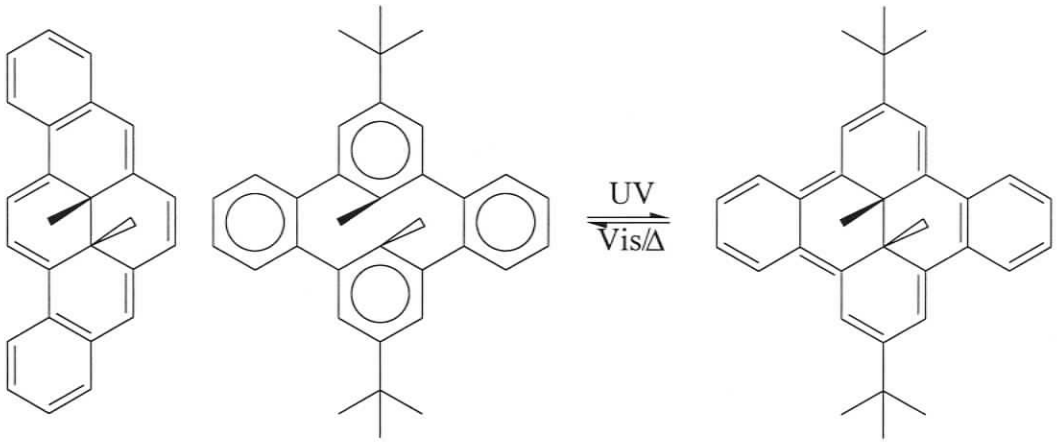

40 **41'** **41**

Scheme 1.14. Bis annelated DHP systems **40** and **41**.

Although many substituted or annelated DHP derivatives have been synthesized and been found to be photochromic, organometallic derivatives of these molecules are rare and show erratic photochromic properties. At the start of our work only one photochromic example was known, CpRu-benzodimethyldihydropyrene **42/42'**[70] (**Scheme 1.15**).

Compound **42** was synthesized from benzodihydropyrene **36** and $[CpRu(CH_3CN)_3]PF_6$ as dark purple plum-colored crystals. On irradiation of a deep purple acetone solution of complex **42** with visible light, the sample bleached to very pale violet, forming the cyclophanediene complex **42'**. Studies on the comparison of the

photoopening and closing with the benzo parent **36** showed that under the same conditions of ample light flux, complex **42** was found to photo-open at ~30% of the rate of **36**, which suggested that complexation slowed the photo-opening rate by three times. There was however no noticeable difference between the photoclosing rates of **42'** and **36'**. This is consistent with the non-complexed analyses, in which the quantum yields of the closing reaction are considerably higher than the opening reaction and are not much affected by changes to the molecule. For the thermal return reaction, compound **42'** showed an E_{act} of 23.0 kcal/mol with a $\tau_{1/2}$ = 2.2 h at 46 °C. For the parent benzo system **36'** $\tau_{1/2}$ = 5.75 h, and so complexation increased the thermal return rate by about 2.6 times.

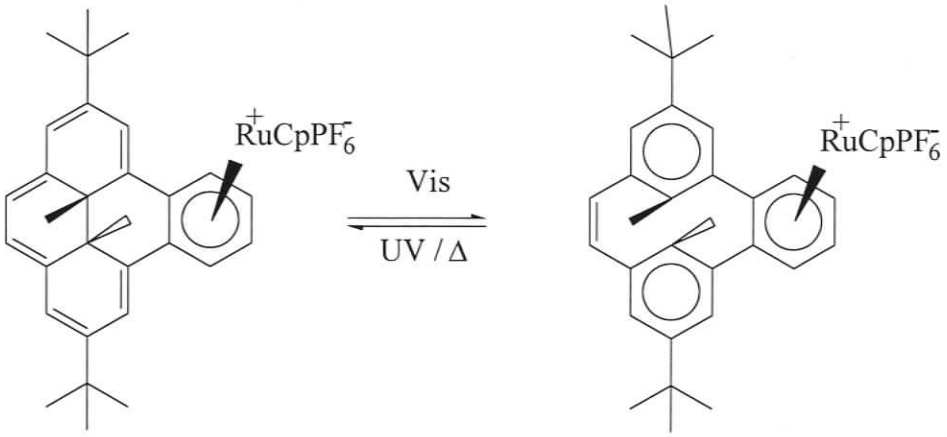

42 **42'**

Scheme 1.15. Isomerization between **42** to **42'**.

Another interesting property of compound **42** is that when the parent **36** was complexed to the metal moiety, compound **42** became electrochromic. Electrochemical reduction of the open form **42'** converts it to the closed form **42**. Thus the ring-opening

reaction only proceeds photochemically, but the ring closing reaction can be achieved photochemically, thermally, or electrochemically.

Although the Ru complex **42** is photochromic, to our surprise, the tricarbonylchromium complex **43**, was not. We were unsure whether this lack of photochromism was unique to the chromium compound, or whether there were any other reasons. To explore more organometallic examples, we decided to synthesize compound **28** and its metal complexes. This thesis in part thus presents the photochromism of these systems.

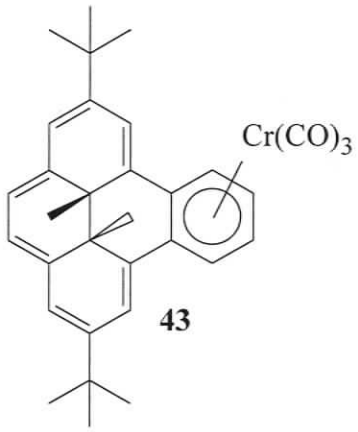

43

1.4 Indenyl metal complexes

The anion **28** is similar to an indenyl anion in which the cyclopentadienyl is fused to a dihydropyrene instead of benzene. We thought it would be interesting to see if it behaves similarly to indenyl anion when complexed to metal centers. Thus some background on indenyl metal complexes is given below.

The indenyl anion, $C_9H_7^-$, belongs to the series of six π-electron ligands, also including cyclopentadienyl anion, $C_5H_5^-$, and tris(pyrazolyl)borate, $RB(p_z)_3^-$, which form one of the most important ligand classes in organometallic chemistry. Although the

indenyl anion ligand can be simply envisioned as a benzannulated relative of the cyclopentadienyl moiety, the transition metal complexes derived from the former commonly exhibit significantly different reactivities from those of the latter. In general, the complexes $IndML_n$ (Ind = indenyl anion, radical and their substituted derivatives) undergo exchange of the ligands L at faster rates in comparison to $CpML_n$ (Cp = cyclopentadienyl anion, radical and their substituted derivatives). This rate enhancement is now called the "indenyl effect". Kinetic studies show that in associative substitution, the process proceeds through initial formation of an unsaturated η^3-indenyl complex to which the entering ligand is bonded. The higher reactivity has been attributed to the special ability of the indenyl group to undergo a slippage from η^5 to η^3 coordination which is favored by the generation of the full aromaticity of the fused benzene ring.[71-73] In the case of dissociative substitutions, the faster rates were attributed to the stabilization of the electronically and coordinatively unsaturated intermediates as a result of the interaction of the benzo ring of the indenyl ligand with the metal center.[74] Thus the presence of the benzo ring facilitates the flexible hapticity of indenyl ligands which, in turn, helps stabilize the transition states (or intermediates) of various reactions.

1.4.1 Measuring indenyl hapticity

Given the influence of metal-indenyl bonding modes on the reactivities of indenyl complexes, a discussion of indenyl hapticity in terms of a number of structural parameters is important. Both the arene ring and the five-member ring in indenyl can coordinate to metal centers. However, only the complexation through the five-member ring is relevant to us, and so only this will be discussed here.

In principle, the indenyl ligand can coordinate in a perfect η^5 mode, where all the five M-C bonds have the same length. However, experimentally a pure η^5 coordination is never observed: a slightly distorted mode, where the two M-C bonds to the hinge carbon atoms (3a, 7a) are longer than the other three M-C bonds (to 1, 2, 3) is always observed as depicted in **Scheme 1.16**. The η^3 and η^1 coordination modes and the numbering of the carbon atoms are also represented. The η^5-C_9H_7 bonding mode is the most common one as in the case for Cp complexes.[75] The η^3 and η^1 modes are less common,[76, 77]

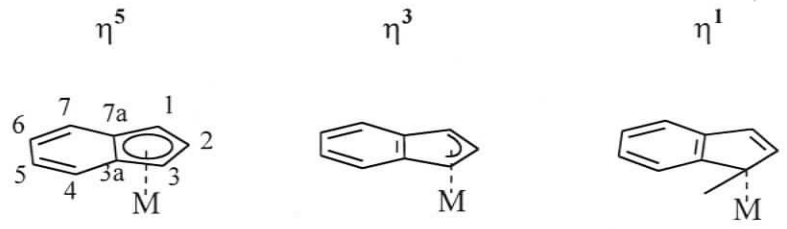

Scheme 1.16. Coordination modes of an indenyl ligand.

Several parameters can be used to describe the indenyl coordination. For comparison of solid state structures, the most straightforward ones are the slip parameter and the folding angle (**Scheme 1.17**).[78] The difference between M-C distances determines the extent of the slippage of the indenyl ligand away from an idealized pentahapto coordination. Thus the slip parameter (Δ) is defined as the difference between the average distance from the metal center to the hinge carbon atoms, C(3a) and C(7a), and the average distance from the metal to the adjacent carbon atoms, C(1) and C(3). The folding angle (FA) defined as the angle between the planes of carbons C(1),

C(2), C(3) and C(1), C(3), C(3a), C(7a). Some authors also refer to the hinge angle (HA), defined as the angle made by the planes of the five member ring C(1), C(2), C(3), C(3a), C(7a) and the six member ring C(3a), C(4), C(5), C(6), C(7), C(7a) (**Scheme 1.17**).[79] The distinction between FA and HA is that the first gives the bending along the C(1)-C(3) line, while the second describes the bending at the C(3a)-C(7a) ring junction.

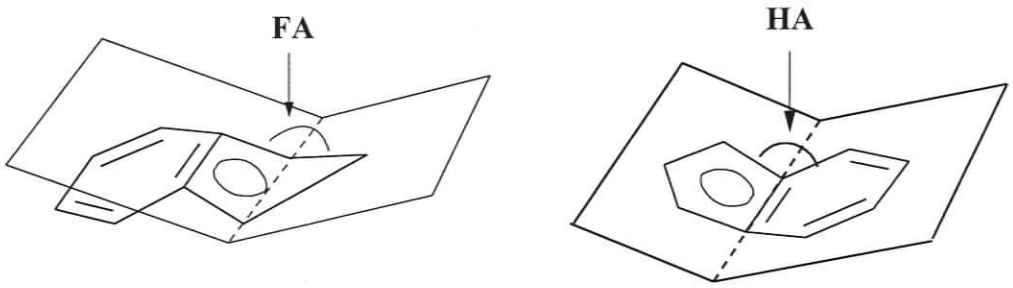

Scheme 1.17. Folding angle (FA) and hinge angle (HA) in indenyl metal complexes.

In general, the larger the Δ, FA and HA values, for a given compound, the more extensive is the slippage away from a pentahapto coordination. Thus a nearly perfect η^5 coordination is reported for $FeInd_2$ with Δ = 0.05 Å and FA = 2.6°.[80] On the other hand, the complex $[PPN][FeInd(CO)_3]$ which shows Δ = 0.75 Å and FA = 22° is considered to be a true η^3 complex.[81] Most other complexes show distortion in-between the η^5 and η^3 binding.[82]

Additional distortion parameters are necessary for bis(indenyl)metal complexes to show the conformational preference of the two indenyl ligands. For simple sandwich type complexes, $MInd_2$, the conformation adopted by the two indenyl rings can be described by the rotation angle (RA), defined as the dihedral angle between the planes of M, C(2), midpoint of the C(3a)-C(7a) ring junction and M, C(2)', midpoint of the C(3a)'-

C(7a)' ring junction (**Scheme 1.18**). A rotation angle of 0° indicates a completely eclipsed geometry, whereas an angle of 180° corresponds to the fully staggered arrangement of the two ligands. Conformations in between these two arrangements have also been found. Thus an eclipsed conformation is found in complex $RuInd_2$ (RA = 0.196°),[82] while a staggered structure is observed in complex $NiInd_2$ (RA = 175°).[73]

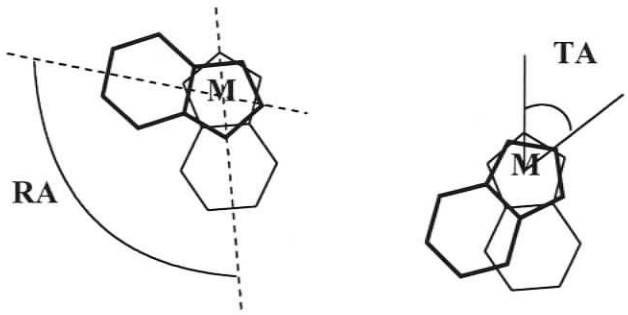

Scheme 1.18. Rotation angle and torsion angle in bis(indenyl) metal complexes.

Alternatively, the torsion angle (TA) defined as C(2)-Cp_{cent}-Cp'_{cent}-C(2)' and shown in **Scheme 1.18**, where Cp_{cent} and Cp'_{cent} are, respectively, the centroids of the pentagonal rings of the two indenyl ligands, also gives the relative orientation of the two indenyl ligands. In the case of $MInd_2$ systems, where the two indenyl ligands are nearly parallel, TA reflects only the degree of staggering, and RA and TA only show slight differences. However, when the two indenyl rings are not parallel, as in the bent metallocenes $MInd_2LL'$, TA reflects both the degree of ring staggering and the angle between rings. Therefore, for bent bis(indenyl) compounds the RA and TA parameters can be significantly different. For example, the complex $ZrInd_2(CO)_2$ has RA = 34.9°

while TA is only 3.6°.[83] On the other hand, the complex $YbInd_2\{MeO(CH_2)_2OMe\}$ shows little difference between RA (31.6°) and TA (39.9°).[83]

The indenyl hapticity in solution is also of interest and can be estimated from NMR data. It was Kohler[84] who first proposed a method for extracting metal-indenyl bonding information based on an analysis of the ^{13}C-NMR data. This method was based on the observation that the ^{13}C-NMR chemical shifts of C(3a) and C(7a) (the ring junction carbon atoms of indene) move upfield upon coordination to metals. By examining the magnitude of this shift for various complexes, Kohler noted a correlation between the indenyl ligand's (presumed) degree of hapticity in a given complex and the extent of the observed shift. For instance, the ^{13}C chemical shift for C(3a/7a) for $FeInd_2$, which was presumed to have η^5-Ind ligands, showed an upfield shift of ca. 60 ppm in comparison to the average value in indene; the corresponding values for $[CoInd_2]^+$ and $NiInd_2$ were ca. 45 and 10 ppm, respectively, reflecting the anticipated reduction in the hapticity of the indenyl ligands on going from Fe to Co to Ni.

A variant of Kohler's NMR method measures the difference between indenyl hapticities in $IndML_n$ and NaInd (as opposed to IndH). This method has been used by Baker and Marder[80,85] to demonstrate a correlation between the solid state and solution hapticity of indenyl ligands in a variety of complexes. According to this method, the magnitude of the parameter $\Delta\delta^{13}C = \delta\{C(3a/7a)$ of M-Ind$\}$-$\delta\{C(3a/7a)$ of NaInd$\}$ reflects the solution hapticity of indenyl in a given complex: larger distortions from η^5 to η^3 result in larger downfield shifts. For instance, the $\Delta\delta^{13}C$ of +3.6 ppm for $NiInd_2$ is greater than the corresponding values for the complexes $FeInd_2$ (-43.7 ppm) and $[CoInd_2]^+$ (-32.4 ppm) but less than the values in $(\eta^3$-Ind$)Ir(PMe_2Ph)_3$ (+26 ppm) and

$[(\eta^3\text{-Ind})Fe(CO)_3]^-$ (+27 ppm), which indicates the indenyl ligands are more or less pentahapto in $FeInd_2$ and$[CoInd_2]^+$, a mode between η^5 and η^3 in $NiInd_2$ and trihapto in $(\eta^3\text{-Ind})Ir(PMe_2Ph)_3$ and $[(\eta^3\text{-Ind})Fe(CO)_3]^-$. This is consistent with Marder's research[80] that the indenyl hapticity in the solid state varies from very nearly η^5 mode in $FeInd_2$ and$[CoInd_2]^+$ to an intermediate $\eta^5 \leftrightarrow \eta^3$ mode in $NiInd_2$ and to essentially trihapto in $(\eta^3\text{-Ind})Ir(PMe_2Ph)_3$ and $[(\eta^3\text{-Ind})Fe(CO)_3]^-$. In general, a $\Delta\delta^{13}C$ value in the range of –20 to –40 ppm indicates a planar η^5-indenyl, +5 to –20 ppm suggests a partially slipped η^5-indenyl and +5 to +30 ppm points to a fully η^3-indenyl ligand.[82]

1.5 Research objectives

In light of the results of previous investigators, briefly introduced above, and because of the relative accessibility of the 2,7-di-*t*-butyldimethyldihydro-pyrene **31** to us, it has become clear that a structure function study of cyclopent[e]dimethyldihydropyrene anion **28** and its metal complexes should be undertaken. The goals of this thesis research are thus:

- To synthesize cyclopent[e]dimethyldihydropyrene anion **28** and its metal complexes.
- To observe aromaticity effects of **28** and its metal complexes as displayed by the NMR probe behavior of the DHP core.
- To test the photoisomerizations and thermal return rates of **28** and its metal complexes.

Chapter Two

Syntheses And Characterization

2.1 Introduction

The most convenient route to [e]-annelated DHPs starts from **31**, as reactivity is confined to the 4 and 5 (or 9 and 10) positions because the 1,3 and 6,8 positions are sterically blocked by the 2,7-*t*-butyl groups. The synthesis of **31** itself is well established and is shown in **Scheme 2.1**.[86] This method requires formation of a cyclic thioether typically by high dilution methods. In subsequent steps, the sulphur is first extruded to form the C-C bond, and then the sulphur bearing residue is eliminated to form the C=C.

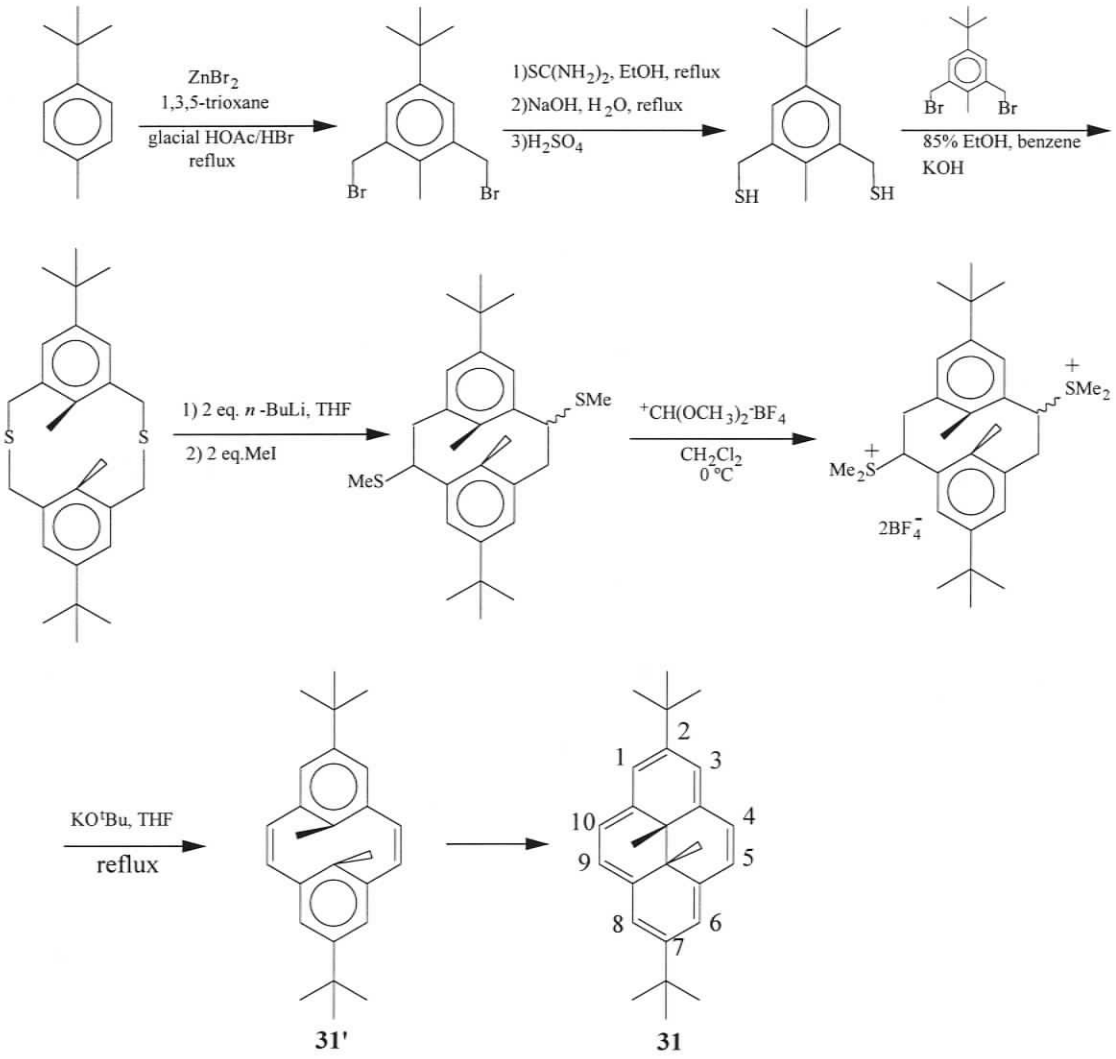

Scheme 2.1. Synthesis of 2,7-di-*t*-butyl-*trans*-10b,10c-dimethyl-10b,10c-dihydro-pyrene, **31**.[86]

Thus **31** is prepared by first synthesis of the cyclophanediene which is then valence isomerized to the dihydropyrene. The overall yield was about 25 %.

2.2 Synthesis of the DHP-fused cyclopentadiene 44

The synthesis of the cyclopentadiene-fused derivative **44** from parent **31** is shown in **Scheme 2.2**.

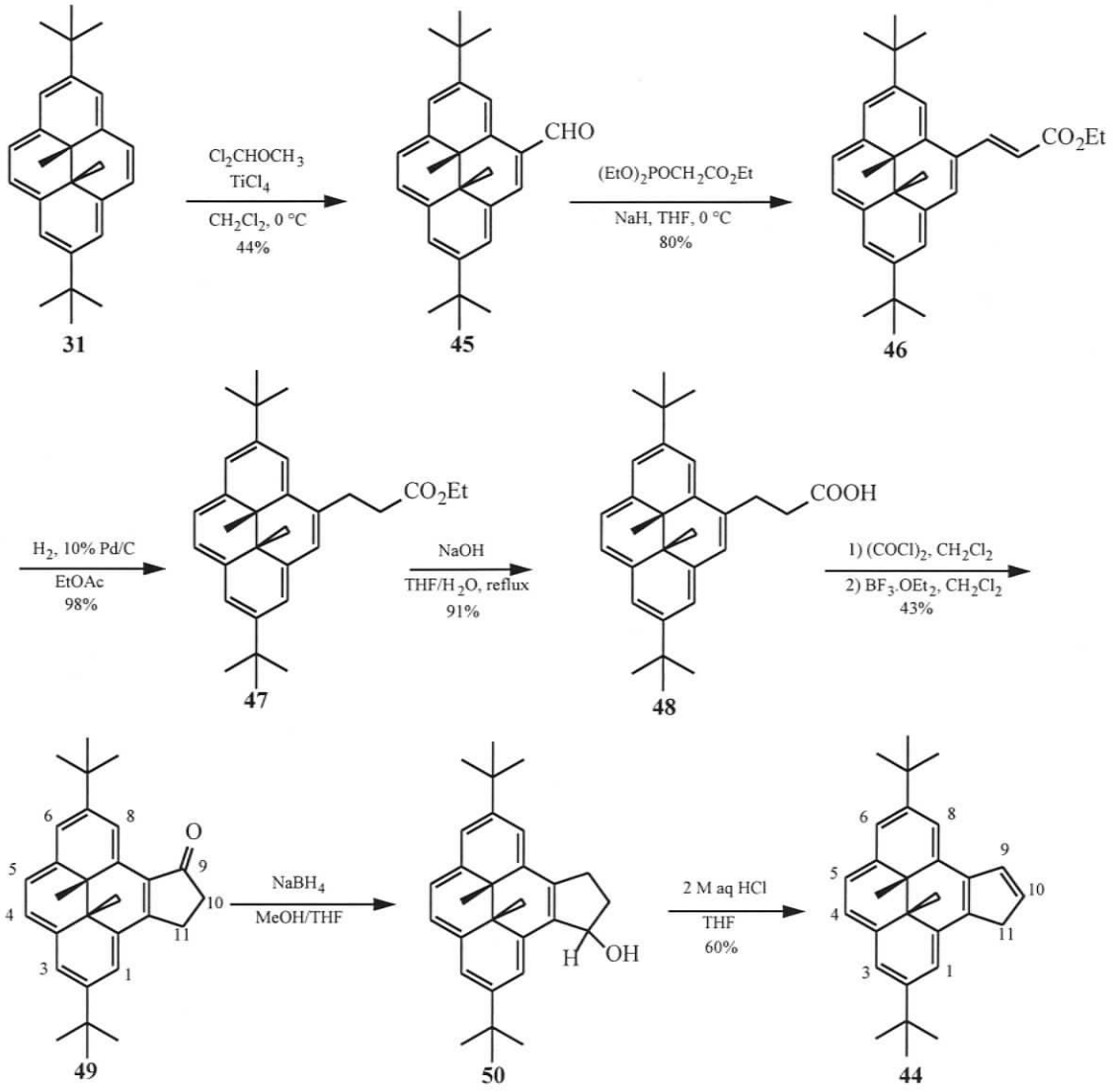

Scheme 2.2. Synthesis of the DHP-fused cyclopentadiene **44.**

2.2.1 The formylation

The aldehyde **45** was previously prepared by Miyazawa[87] in 40% yield using $SnCl_4$ as catalyst. We used $TiCl_4$ instead because we had this catalyst on hand, and obtained 44% yield, as dark brown crystals from hexane, mp 192-194 (lit.[87] mp 193-194 °C). The ^{1}H-NMR spectrum showed the internal methyl protons at δ –3.89 and –3.86. The aldehydic proton at δ 11.11 and H-3 at δ 9.80, deshielded from the other aryl protons by the C=O of the aldehyde, were consistent with reported values.[87]

2.2.2 The Wittig-Horner reaction

Chain elongation of aldehyde **45** by the Wittig-Horner reaction with triethylphosphonoacetate gave 80% of the *trans*-ester **46**. The *trans* structure was shown by the 15.6 Hz coupling constant found for the alkene hydrogens at δ 6.83 and 9.16 (and the 970 cm^{-1} IR band). The overall structure of the ester was confirmed by the ethyl protons at δ 1.41 (t) and δ 4.37 (q). The DHP internal methyl proton, as well as two *tert*-butyl proton signals were found at δ -3.79, -3.78, and δ 1.69, 1.65 respectively. The latter are more differentiated than the internal methyl protons, which is not common in DHP compounds. The ^{13}C-NMR spectrum showed all expected carbons for $C_{31}H_{38}O_2$ with the ester carbon at δ 167.9. The IR spectrum showed the conjugated ester C=O stretch at 1700 cm^{-1}. The mass spectrum (EI) gave a molecular ion at *m/z* 442 (M^+). Full characterization for all compounds is given in the experimental section. Only significant data that is used for product identification is reported here.

2.2.3 The hydrogenation and hydrolysis

Palladium-catalyzed reduction of the alkene double bond of **46** was achieved in 98% yield. The loss of conjugation changed the dark reddish brown color of **46** to green for **47**. The hydrogenation was also confirmed by ^{1}H-NMR spectroscopy by the replacement of the two doublets at δ 6.83 and 9.16 for **46** with two multiplets at δ 4.00-3.89 and δ 3.09-2.96 for **47**. The ^{13}C-NMR DEPT spectrum also showed the two saturated CH_2 groups at δ 29.4 and 37.0.

Hydrolysis of the ester **47** with NaOH in a mixed solvent of THF and water proceeded smoothly and gave the green acid **48** in 91% yield. The success of the hydrolysis was clearly shown in the ^{1}H-NMR spectrum by the disappearance of the triplet and quartet for the ester ethyl group. The acid proton showed a weak and broad signal at δ 11.5-10.0. As well, in the IR spectrum a strong and broad absorption at 3300-2600 cm^{-1} and a strong absorption at 1706 cm^{-1} confirmed the presence of a saturated carboxylic acid.

2.2.4 The cyclization

The acid **48** was converted in a one pot procedure, first to the acid chloride with oxalyl chloride, which was then directly cyclized with BF_3 etherate to yield the dark red ketone **49** in 43% yield (65% based on returned acid **48**). The overall structure of **49** was confirmed by a high resolution MS with a molecular ion at *m/z* 398, and by the change in IR spectrum which now showed a ketone C=O stretch at 1681 cm^{-1}. The ^{1}H-NMR spectrum showed the internal methyl protons at δ -3.71 and -3.74, and the two sets of *t*-butyl protons at δ 1.67 and 1.68. The protons on the 5-membered ring were more

complex. The H-11 protons which appeared at δ 3.97 and 3.87 are both split by the other H-11 proton and the two H-10 protons into two triplet of doublets. The two H-10 protons appear as a triplet, and so appear to have the same chemical shift and are split by approximately equal J values to the two H-11 protons. The ^{13}C-NMR spectrum showed the expected number of peaks, with the ketone carbon at δ 208.95.

2.2.5 The reduction and elimination

When the ketone **49** was stirred at room temperature with $NaBH_4$ in MeOH/THF, it was reduced to the alcohol **50**. The alcohol **50** contains two isomers in a 1 to 1 ratio. This was confirmed by ^{1}H-NMR spectroscopy by two groups of two singlets for the internal methyl protons in the two isomers. This alcohol was not purified, but on treatment with 18% HCl, it was directly converted to the diene (CpDHP(H)) **44** in 60% yield. Diene **44** is an unstable yellowish green solid, which decomposes on a column of silica gel. Decomposition was noticed even in the glove box under argon in the solid state after a few weeks at room temperature. Since this compound is rather unstable, ketone **49** was stored and converted to **44** as needed and was quickly chromatographed immediately before use.

The ^{1}H-NMR spectrum in C_6D_6 of **44** showed H-9 at δ 7.90 split by H-10 (J = 5.6 Hz) and by the two H-11 protons (J = 2 Hz). Proton H-10 appeared at δ 6.63 split by H-9 and the two H-11 protons. In this compound, the two H-11 protons have slightly different chemical shifts at δ 4.04 and 4.09 and each splits the other with a large germinal coupling constant of 23 Hz, and is also coupled to the H-10, 9 protons. The internal methyl protons appeared at δ –3.48 and –3.51, and the *t*-butyl protons at δ 1.68 and 1.65.

The ^{13}C-NMR spectrum showed all 29 carbons expected for $C_{29}H_{34}$. The mass spectrum (EI) gave a correct molecular ion at *m/z* 382 (M^+).

2.3 Generation of cyclopent[e]dimethyldihydropyrene anion 28

For spectroscopic purposes, generation of the cyclopent[e]dimethyldihydropyrene (CpDHP) anion **28** was accomplished in deuterated THF by treatment of diene **44** with either KH or $LiCH_2SiMe_3$. There is very little difference in the proton NMR spectra obtained when either base is used, which indicates that the counter cations are bonded to the anion equally loosely in both cases. The internal methyl groups only show one singlet at δ -1.82 ppm, which is consistent with the symmetrical structure of the anion. These protons are, as expected, substantially less shielded than those of diene **44** (δ -3.9 in d_8-THF), because of the reduced ring current in the [14]annulene ring on annelation with an aromatic species. The external protons of anion **28** are affected by both the reduction in diatropicity of the [14]annulene ring and the dispersion of the negative charge, and so are substantially less deshielded (δ 7.62 – 6.87) than those of diene **44** (δ 8.81 – 8.37). This will be discussed in the next chapter.

The UV-visible spectrum of anion **28** at first sight appears actually not to be very different from that of cyclopentadiene **44**, both being dominated by the main dihydropyrene bands around 365 and 395 nm (**Figure 2.1**). Closer inspection, however, shows that the 365-nm band of **44** has moved to 350 nm in **28**, and the 350-nm band has intensified somewhat (relative to the 395-nm band) over that of the 365-nm band. In diene **44** there is very little absorption between 540 and 640 nm, while in anion **28** there

is extensive tail absorption (ε ~ 4000-800) in this region, which probably accounts for the increase in color intensity observed when **44** is converted to **28**.

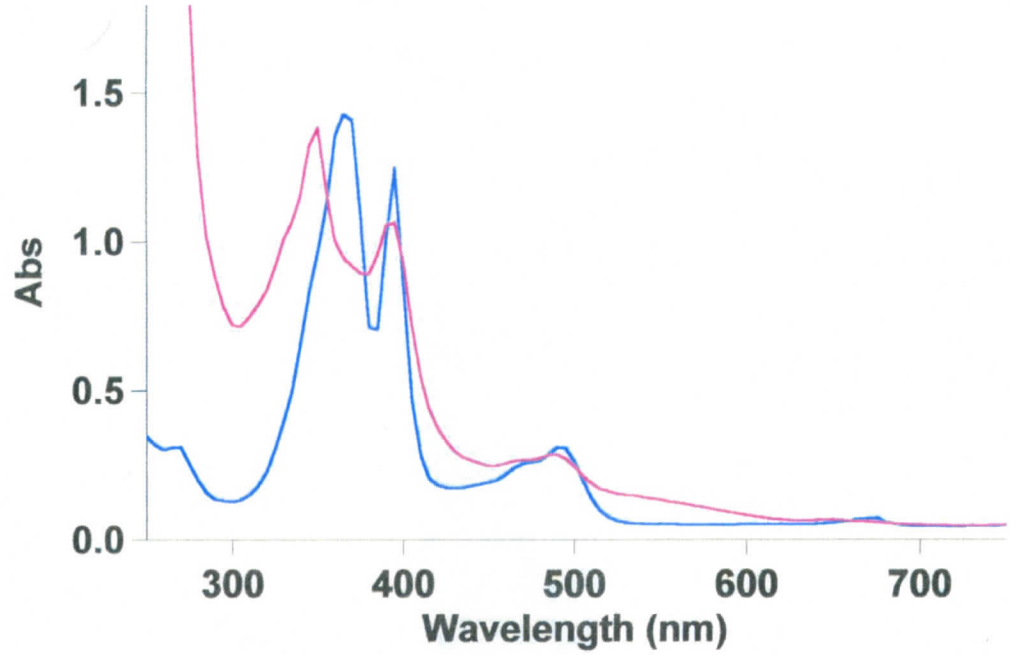

Figure 2.1. UV-vis spectra of diene **44** (blue) and anion **28** (red) in cyclohexane.

For preparative purposes, cyclopentadiene **44** was always reacted with $LiCH_2SiMe_3$ in toluene overnight at room temperature to produce a red suspension of anion **28**, which was used directly in complexation reactions with metal centers.

2.4 Synthesis of (CpDHP)Re(CO)$_3$, 51

Reaction of anion **28** with $Re(CO)_5Br$ was carried out at room temperature in toluene. After reaction overnight, $Re(CO)_3$(CpDHP) **51** and some unidentified intermediates were obtained. It was found that by keeping the reaction mixture at room temperature for a few days, all of the intermediates have been converted to **51**. Another

reaction was thus carried out in the dark at room temperature for 4 days. As a result, compound **51** was obtained as the only product.

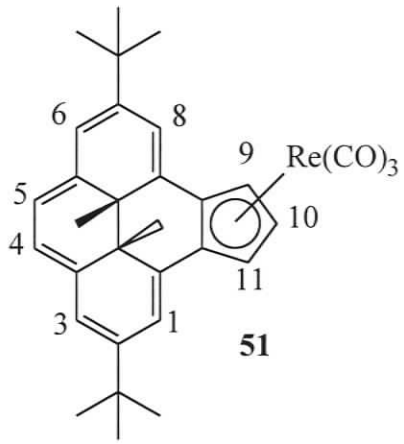

51

Characterization of **51** was accomplished by NMR, IR, MS and elemental analysis. The ^{1}H-NMR spectrum showed two signals for the internal methyl protons (δ –0.77 and –0.23 in C_6D_6) and two signals for *t*-butyl protons (δ 1.310 and 1.313), as expected because of the loss of the symmetry of the parent anion upon coordination of the rhenium tricarbonyl moiety. Moreover, the chemical shifts of the internal methyl protons moved downfield compared to the parent anion **28** (δ -1.82 in d_8-THF), which was consistent with the bond fixing ability of the metal complex and the reduction of the ring current of the DHP ring. The protons on the five-membered ring appeared in the correct region and in correct patterns for a complexed Cp according to the structure of the compound: proton H-10 (δ 4.95) was split by H-9 and H-11 in an equal J value (J = 2.9 Hz) and thus appeared as a triplet. H-9 and H-11 had the same chemical shift (δ 5.18) and each was split by H-10 to give a doublet. The ^{13}C-NMR spectrum showed all the expected carbon atoms with the CO carbons at δ 194.71. The IR spectrum showed two CO bands at 2018 and 1924 cm^{-1}. The overall structure of **51** was also confirmed by

elemental analysis and a high resolution mass spectrum with an exact mass found 652.1991 (Calculated 652.1987) for $C_{32}H_{33}O_3Re$.

2.5 Synthesis of Cp*Ru(CpDHP), 52

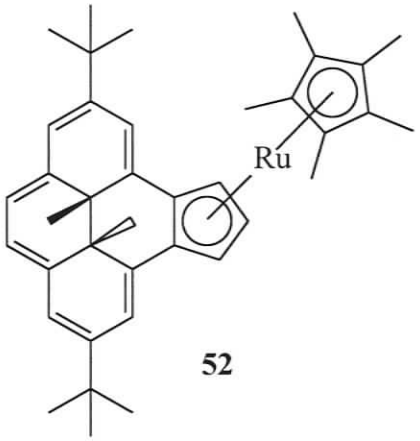

52

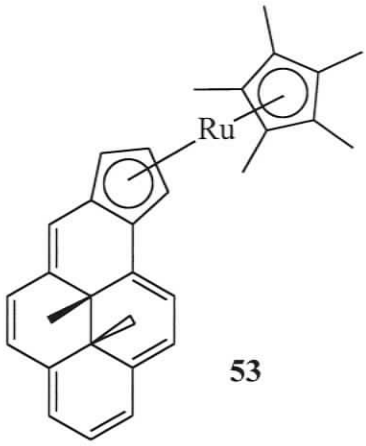

53

After the successful synthesis of the Re complex **51**, our next target was a Ru complex. The [*a*]-fused Cp*Ru(*a*-CpDHP), **53** has been made by Khalifa,[88] a previous graduate student in our group. The reagent of choice was the oligomeric species $(Cp^*RuCl_2)_n$, which is synthesized by refluxing ruthenium trichloride hydrate and pentamethylcyclopentadiene in absolute ethanol.[89-91] Reaction of [*a*]-fused CpDHP anion **27** with $(Cp^*RuCl_2)_n$ in THF yielded compound **53**. However similar reaction of anion **28** with $(Cp^*RuCl_2)_n$ failed in a mixed solvent of THF and toluene, but succeeded in pure toluene. Reactions under different conditions were carried out to optimize the synthesis of Cp*Ru(CpDHP), **52** and are shown in **Table 2.1**. It turned out that the reaction time and ratio between CpDHP(H) and base $LiCH_2SiMe_3$ are important. The reaction is quite slow and needs 3 days for completion. Also a large excess of base is required for high yield of the product. As well, both the two-step reaction - generation of anion **28** first, then reacting it with $(Cp^*RuCl_2)_n$ - and the one-pot reaction work very well.

Though the [a]-fused **53** has two diastereomers with the RuCp* moiety sitting above or below the five-member ring, the [e]-fused complex **52** exist as a pair of enantiomers because of the symmetric structure of anion **28**.

Table 2.1. Reactions of anion 28 and $(Cp^*RuCl_2)_n$ in toluene at room temperature

CpDHP(H) : $LiCH_2SiMe_3$: $(Cp^*RuCl_2)_n$	Procedure	Reaction time	Products (yield)
1 : 1 : 1		2 hours	CpDHP(H), **52**(5%) and by-product
1 : 1 : 1	Two step	1 day	**52** (15%) and by-product
1 : 3 : 1		1 day	**52** (29%)
1 : 3 : 1	One-pot	1 day	CpDHP(H) and **52** (20%)
1 : 3 : 1		3 days	**52** (32%)

The ^{1}H-NMR spectrum of **52** showed the internal methyl protons at δ 0.09 and 0.42, and two sets of *t*-butyl protons at δ 1.33 and 1.35. Similarly to those of $(CpDHP)Re(CO)_3$, the protons on the 5-membered ring showed a triplet (δ 4.15) for H-10 and a doublet (δ 4.92) for H-9 and H-11. The methyl protons of the Cp* ring appeared at δ 1.67. The ^{13}C-NMR spectrum showed the expected number of signals for the carbon atoms. The mass spectrum also confirmed the structure with an exact mass found 618.2792 (calculated 618.2793) for $C_{39}H_{48}Ru$.

2.6 Syntheses of Iron complexes

2.6.1 Synthesis of $(CpDHP)_2Fe$, 54

No DHP-ferrocene is known and so complex **54**, $(CpDHP)_2Fe$, is an attractive target. The most widely used method for the synthesis of complexes such as **54** is to react the anion with ferrous chloride in dry THF. In the case of mixed ferrocenes, some authors mix both anions together and add to $FeCl_2$, while others add the anion sequentially. Thus, ferrocene is synthesised by reacting Cp anion with $FeCl_2$ and CpFe(Ind) (Ind = η^5-indenyl) is made by reacting the same reagent with a mixture of Cp and indenyl anions. In the second case, ferrocene is also produced.

Compound **54** can be synthesized by a two-step reaction in which the anion **28** is first formed from the diene **44**, then reacted with $FeCl_2$ in a mixed solvent of THF and toluene. Alternatively a one-pot reaction of CpDHP(H) **44** and $LiCH_2SiMe_3$ with $FeCl_2$ in THF can be used. Both reactions gave the same product. Characterization by ^{1}H-NMR spectroscopy showed that there are two isomers in about a 2 to 3 ratio. The two isomers come from different arrangement of the internal methyl groups in the two DHP rings, as shown in **Scheme 2.3**.

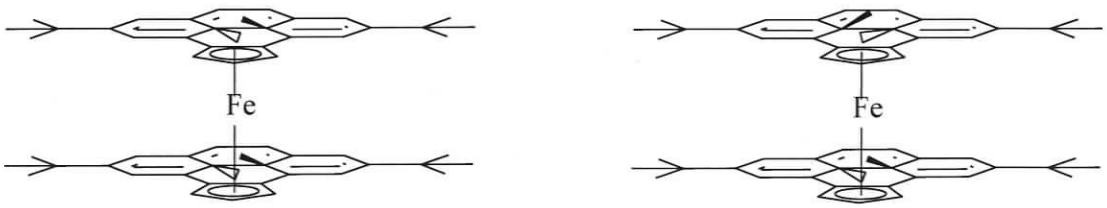

C_2(*rac*) C_s(*meso*)

Scheme 2.3 Structures of the two isomers of $(CpDHP)_2Fe$, **54.**

The ^{1}H-NMR spectrum showed four singlets for 2 pairs of internal methyl protons at –0.57 & 0.66 ppm, and -0.55 & 0.65 ppm each with an integration ratio of 3 : 2. The peaks at δ –0.57 and –0.55 are assigned to the methyl groups pointing away from the iron center, while the signal at δ 0.65 and 0.66 are assigned to the methyl groups pointing toward the metal center.[38] Similarly the *t*-butyl groups appear as 2 pairs of 2 singlets each at δ 1.29 and 1.35, and δ 1.340 and 1.342. As expected, two sets of protons on the Cp rings with an integration ratio of 3 : 2 were seen. Each H-10 is coupled to the corresponding H-9 and H-11 with the same coupling constant (J = 2.4 Hz) and appears as a triplet at δ 3.78 for the minor isomer and δ 4.02 for the major isomer. At the same time each H-9 and H-11 are coupled to the corresponding H-10 and they are both split by each other, so each of them appears as a doublet of doublets. For the aromatic protons, it is interesting to see that the protons, H-1 and H-8, which are closer to the iron center, have greater chemical shift difference in the major isomer (δ 7.03 and 7.31) than in the minor isomer (δ 7.19 and 7.28). On the other hand, the protons H-3,6 and H-4,5, farther away from the iron center, have very similar chemical shifts in both of the isomers and overlap to give multiplets. Actually this is also true for the internal methyl protons and the t-butyl protons, which are more differentiated in the major isomer than in the minor isomer. These observations suggest that the major isomer might be the meso and the minor one the rac. The ^{13}C-NMR showed the expected number of carbon atoms for each isomer. The overall structure of the product (mixed isomers) is also confirmed by high resolution mass spectrum with an exact mass found 818.4509 (calculated 818.4513) for $C_{58}H_{66}Fe$.

Compound **54** is not very stable. It decomposes in air at room temperature in a few days. Attempts were thus made to synthesize the mixed metallocenes CpFe(CpDHP) **55** and Cp*Fe(CpDHP) **56**.

2.6.2 Attempted syntheses of CpFe(CpDHP) 55 and Cp*Fe(CpDHP) 56

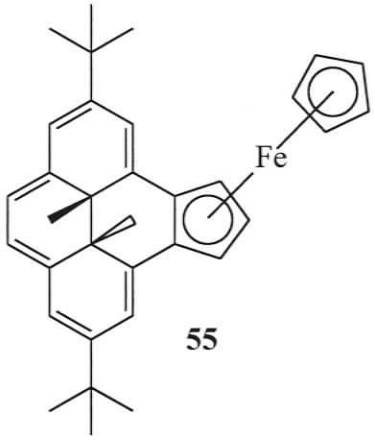

55

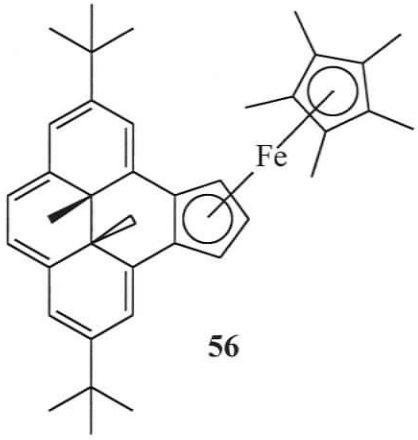

56

The first reaction tried between the Cp anion and anion **28** with $FeCl_2$ resulted in the formation of three compounds: Ferrocene, $(CpDHP)_2Fe$ **54** and the mixed ferrocene **55**. The ^{1}H-NMR spectrum of **55** (**Figure 2.2**) showed two internal methyl signals at about 0.0 and 0.8 ppm. The Cp protons are at about 3.8 ppm. The ratio of the integrations of the two internal methyl groups and Cp protons is 3:3:5, which determines the ratio of Cp ring and CpDHP ring to be 1 to 1, and thus confirmed the structure of **55**. The three protons on the 5 member ring of CpDHP have a similar pattern and chemical shifts to those in $(CpDHP)_2Fe$ **54.** Protons H-9 and H-11 (see **Scheme 2.2**) appear as two doublet of doublets at about 4.9 and 5.0 ppm and H-10 shows as a triplet at about 4.1 ppm. However, the yield of **55** was very low and the reaction was not repeatable. We couldn't get enough for full characterization. We thus searched for an alternative route, using a Cp or Cp* transfer reagent.

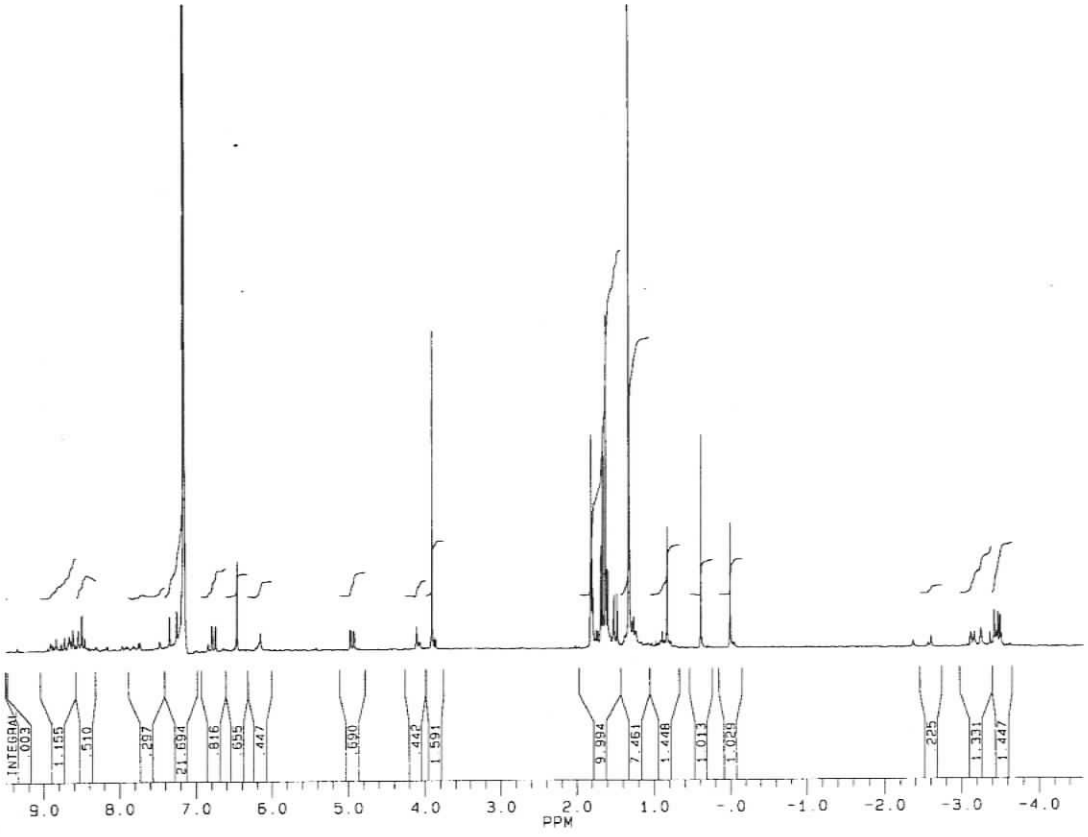

Figure 2.2 ^{1}H-NMR spectrum of CpFe(CpDHP) **55** in C_6D_6.

We tried $CpFe(CO)_2I$ (FpI) first. Unfortunately treatment of anion **28** with FpI in toluene resulted in the decomposition of the starting materials. Change of solvent from toluene to THF did not help.

Cp*Fe(acac) has been used as a Cp*Fe transfer reagent for a long time to generate mixed metallocenes in reasonably good yields.[92] In the case of the pentamethyl substituted ferrocene, the yield was 86%. The reagent Cp*Fe(acac) was thus prepared as described by Manriquez[92] using NaCp* and $Fe(acac)_2$ and used *in situ*. However, treatment of Cp*Fe(acac) with one equivalent of anion **28** failed to yield the target

compound **56**. Instead a small amount of $(CpDHP)_2Fe$ **54** was obtained. Interestingly direct reaction of $Fe(acac)_2$ with anion **28** in toluene resulted in the decomposition of the starting materials. Thus so far we have been unable to make a mixed ferrocene of type **55** or **56**.

2.7 Syntheses of Yb complexes

2.7.1 Synthesis of $Yb(CpDHP)_2(THF)_2$ 57

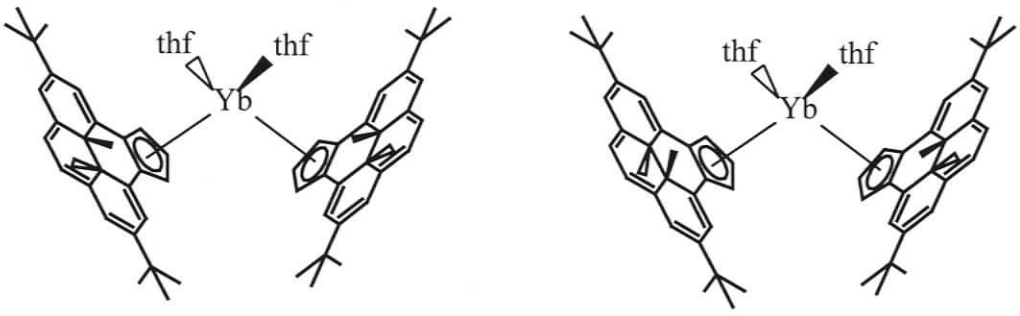

C_s(meso) C_2(*rac*)

Scheme 2.4 Structures of the two isomers of $Yb(CpDHP)_2(THF)_2$, **57**.

$Yb(CpDHP)_2(THF)_2$ **57**, was synthesized by the reaction of CpDHP(H) **44** with $Yb[N(SiMe_3)_2]_2(THF)_2$. Crystallization from hexane afforded the complex in 30% yield. The deep reddish brown compound is soluble in THF, benzene, toluene and hexane, but is air- and moisture-sensitive. The structure of the complex was determined by X-ray crystallography (See Section 3.2.5.3).

The product was isolated as a mixture of two isomers, due to the different arrangement of internal methyl groups in the two DHP rings (**Scheme 2.4**), similar to $Fe(CpDHP)_2$ **54**. The ^{1}H-NMR spectrum showed three singlets for the internal methyl protons at -1.56, -1.52 and -1.07 ppm with an integration ratio of 3 : 3 : 6. The peaks at

δ –1.56 and –1.52 are assigned to the methyl groups pointing away from the metal centers, while the signal at δ –1.07 is assigned to the methyl groups pointing toward the metal centers.[38] The chemical shifts for the inner methyls from the two isomers are accidentally the same. From the ratio of the outer methyls, the ratio of the two isomers is determined to be approximately 1 to 1. Similar to $Fe(CpDHP)_2$ **54**, the *t*-butyl groups appear as four singlets at δ 1.38, 1.49, 1.50 and 1.61. For the Cp ring, the two H-10 protons from the two isomers have similar chemical shifts and overlap to form a multiplet between δ 5.71 and 5.73. On the other hand, the two pairs of H-9 and H-11 protons (see **Scheme 2.2**) from the two isomers appear as doublets or broad singlets at δ 6.61 and 6.94, and δ 6.72 and 6.81 respectively. It's interesting to note that H-1,8, and H-3,6 are much more differentiated in one isomer (δ 7.15 and 7.93 for H-1,8; and δ 6.98 and 7.46 for H-3,6) than in the other isomer (δ 7.69 and 7.72 for H-1,8; and δ 7.02 and 7.08 for H-3,6). The two coordinated THF molecules showed two multiplets at δ 1.70-1.74 and δ 3.55-3.59. The ^{13}C-NMR spectrum confirmed the structure by showing all expected number of carbon atoms for both isomers.

2.7.2 Attempted syntheses of a Yb(III) complex

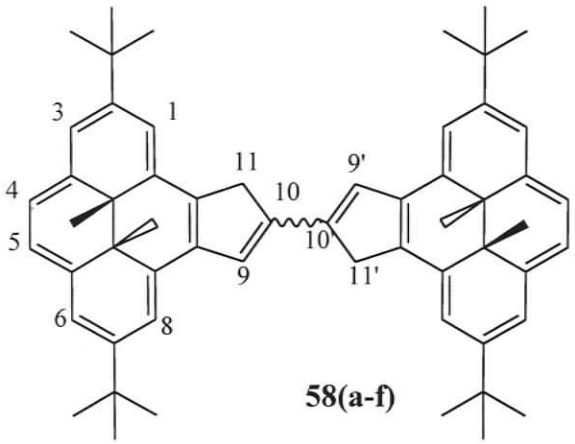

58(a-f)

a = 9,9'-bisCpDHP
b = 9,10'-bisCpDHP
c = 9,11'-bisCpDHP
d = 10,10'-bisCpDHP
e = 10,11'-bisCpDHP
f = 11,11'-bisCpDHP

Attempted oxidation of $Yb(CpDHP)_2(THF)_2$ **57** with *p*-tolyl disulfide failed and resulted in the loss of the ligand from the metal center. As soon as the *p*-tolyl disulfide was added, the solution changed from deep reddish brown to deep purple. However, it then quickly changed to greenish brown and the product isolated was just pure hydrocarbon. The mass spectrum of the product showed a weak peak at 762 (the mass for the dimer of the ligand) and a very strong peak at 381 (the mass of the ligand). The ^{1}H-NMR spectrum of this product is complicated and showed many peaks between -3 to -3.6 ppm in C_6D_6 for the internal methyl groups. Their chemical shifts indicate that the five member ring in the ligand is not coordinated to any metal center. We think that the Yb(III) compound did form as indicated by the deep purple colour,[93] but it was not stable and decomposed to a mixture of coupled bi-CpDHP isomers **58** very quickly. That the reaction of CpDHP anion **28** with $YbCl_3$ gave the same product, supported the above proposal.

2.8 Attempted synthesis of (CpDHP)Mn(CO)$_3$, 61

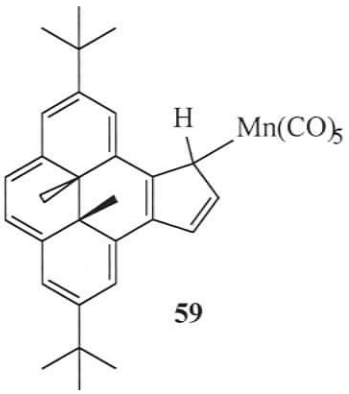

59

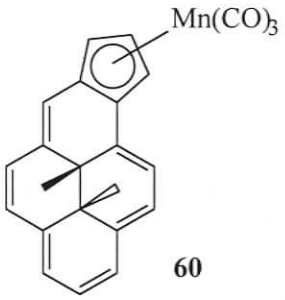

60

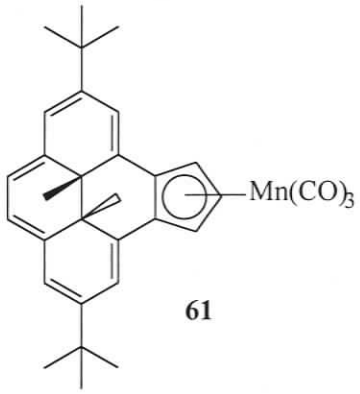

61

To our surprise, the reaction of anion **28** with $Mn(CO)_5Br$ in THF failed to produce the expected (CpDHP)$Mn(CO)_3$ **61**, but yielded the coupled bi-CpDHP **58** and $Mn_2(CO)_{10}$ instead, since the reaction of the [*a*]-fused CpDHP anion **27** with $Mn(CO)_5Br$ in THF did give the [*a*]-fused $Mn(CO)_3$(*a*-CpDHP) **60**.[88] The $Mn_2(CO)_{10}$ is very hard to get rid of. However, it has been reported that the generation of (η^5-indenyl)$Mn(CO)_3$ or (η^5-fluorenyl)$Mn(CO)_3$ by reaction with the corresponding C_9H_7Li or $C_{13}H_9Na$ with $Mn(CO)_5Br$ were in competition with the formation of biindene or bifluorene and $Mn_2(CO)_{10}$. The (η^1-fluorenyl)$Mn(CO)_5$ has been isolated as the intermediate and converted to (η^5-fluorenyl)$Mn(CO)_3$, bifluorene and $Mn_2(CO)_{10}$ or just bifluorene and $Mn_2(CO)_{10}$. We think our reaction of **28** with $Mn(CO)_5Br$ follows a similar pathway. Presumably, the intermediate (η^1-CpDHP)$Mn(CO)_5$ **59** forms first, which then decomposes to the bi-CpDHP **58** and $Mn_2(CO)_{10}$ rapidly. Similarly, reaction of [a]-fused anion **27** and $Mn(CO)_5Br$ gives the intermediate (η^1-*a*-CpDHP)$Mn(CO)_5$ first, which then converts to $Mn(CO)_3$(*a*-CpDHP) **60** rapidly. The question of why the [a]-fused η^1 intermediate decomposed to the corresponding η^5 compound but the [e]-fused did not is still a question.

2.9 Attempted synthesis of Zr complexes

Group 4 dimethylmetallocenes are catalyst precursors for the methylmetallocenium / borate catalyst systems for olefin polymerization, and they are usually prepared by methylation (with MeMgCl or MeLi) of the parent metallocene dichlorides. Our initial intent was to synthesize (CpDHP)(Cp)$ZrCl_2$ followed by methylation to give (CpDHP)(Cp)$ZrMe_2$. However, the reaction of anion **28** with $CpZrCl_3$ resulted in the decomposition of CpDHP anion. No trace of (CpDHP)(Cp)$ZrCl_2$ was detected.

Discouraged by these results, an alternative route to (CpDHP)(Cp)$ZrMe_2$ was investigated. In 2001, Balboni et al[94] reported the synthesis of bis(indenyl)dimethylzirconium, Ind_2ZrMe_2, by reacting indene with a 2-fold excess of MeLi, and then $ZrCl_4$. Using this approach, CpDHP(H) **44** was treated with a 2-fold excess of MeLi, followed by 1 equivalent of $CpZrCl_3$ and gave a red solid. The ^{1}H-NMR spectrum of this product showed that the internal methyl peaks due to the starting material had disappeared and two new peaks were seen at δ -1.2 and -0.8. These are reasonable shifts for an internal methyl proton on a coordinated CpDHP ligand. However, all the peaks on the spectrum are broad, and all attempts to recrystallize it failed.

Encouraged by the success in synthesizing $(CpDHP)_2Yb(THF)_2$ **57** by the reaction of CpDHP(H) **44** with $Yb[N(SiMe_3)_2]_2(THF)_2$. Reaction of CpDHP(H) **44** with $ZrCl_2[N(SiMe_3)_2]_2$ was carried out, in which $ZrCl_2[N(SiMe_3)_2]_2$ was prepared from $ZrCl_4$ and $NaN(SiMe_3)_2$.[95] However, no reaction was observed and the starting material was recovered.

Attemps to deprotonate neutral CpDHP(H) **44** using tetrabenzyl zirconium also failed. No reaction was observed and CpDHP(H) was recovered.

2.10 Attempted synthesis of Y complexes

2.10.1. Metathesis reactions of anion 28 with YCl_3

The metathesis reaction of $CpDHP^-Li^+$ **28** with YCl_3 went well in a NMR scale reaction. The green anion **28** was made from CpDHP(H) **44** with ca. 3 equivalents $LiCH_2SiMe_3$ in d_8-THF in a sealed NMR tube. As soon as solid YCl_3 was added, the reaction mixture went red. The ^{1}H-NMR spectrum of the resulting mixture showed that the internal methyl signal for the anion **28** disappeared, and several new peaks appeared at ~ δ 0 instead (**Figure 2.3**) . This is a reasonable shift for an internal methyl proton of a metal complex. As well, the signal due to excess $LiCH_2SiMe_3$ disappeared, which suggested that the excess $LiCH_2SiMe_3$ has reacted with the metal complex. Moreover, irradiation with > 490 nm visible light, the product changed from red to light brown and its ^{1}H-NMR spectrum changed. On the other hand, the light brown solution changed back to red when irradiation with UV light or warming up the solution in the dark; also the ^{1}H-NMR spectrum changed back, which suggested that the product is photo opening and closing. All the above evidence suggests that we have obtained a metal complex, which might be a mixture of compounds such as (CpDHP)YCl_2, (CpDHP)$Y(CH_2SiMe_3)Cl$, (CpDHP)$Y(CH_2SiMe_3)_2$, or even a dimer of these compounds.

Since the NMR scale reaction went well, we tried the reaction on a larger scale. The 1:1, 2:1 or 3:1 reaction gave similar results regardless of whether the solvent was toluene or a mixed solvent of toluene and THF. A red powder was obtained at the end

of each reaction, which was not very soluble in hexane, but was soluble in toluene. However, the solubility in toluene became less and less after each removal of solvent.

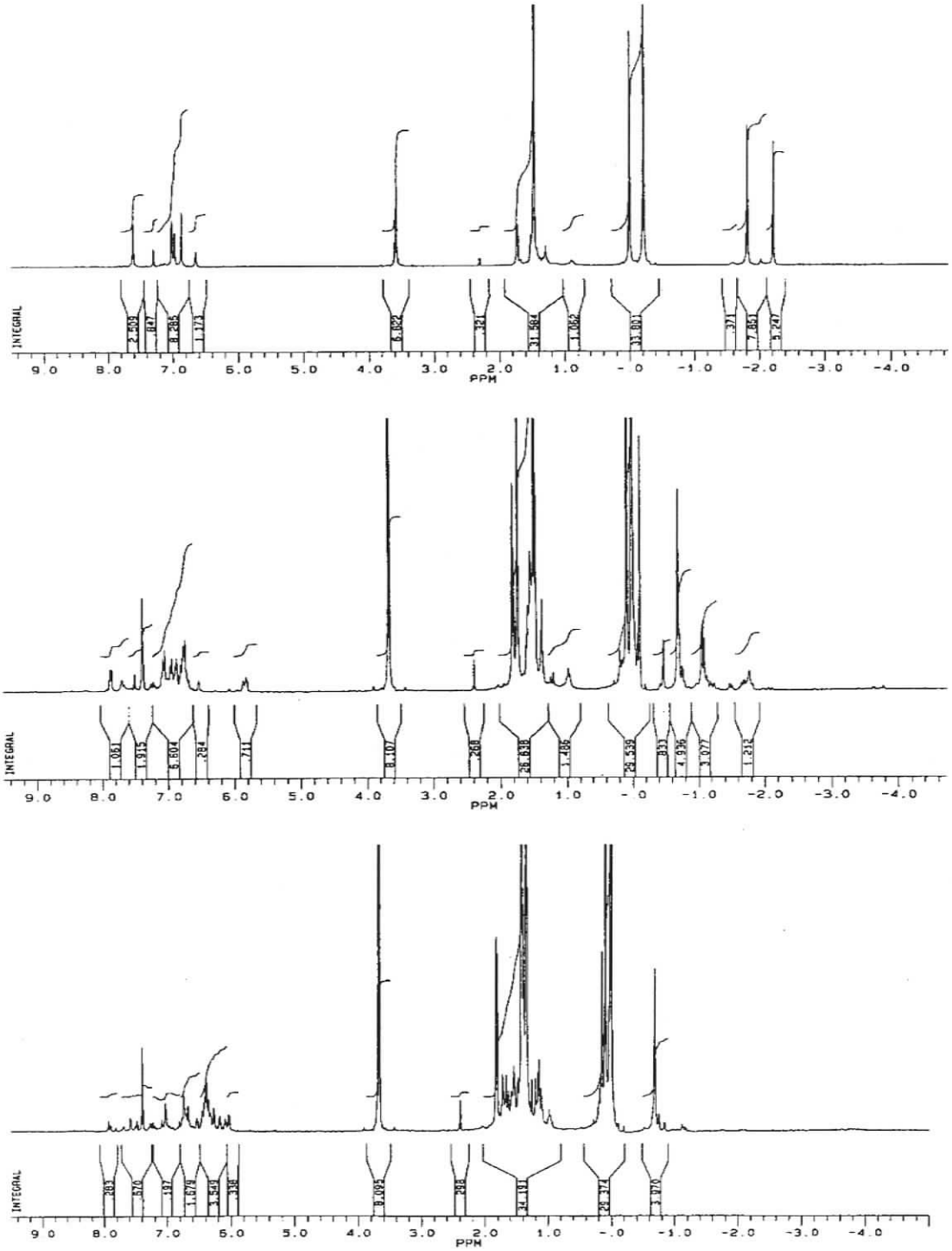

Figure 2.3. The ^{1}H-NMR spectra of anion **28** (top) and the close (middle) and open (bottom) forms of the Y products.

The ^{1}H-NMR spectrum is similar to that of the NMR scale reaction. However, all attempts to recrystallize this product failed.

2.10.2 Acid-base reaction

No reaction was found between neutral CpDHP(H) and $Y[N(HSiMe_2)_2]_3(THF)_2$ or $Y[N(SiMe_3)_2]_3$ in toluene. Starting materials were recovered.

2.11 Attempted synthesis of Ti complexes

Similar to the reaction of the Y compound, the NMR scale reaction between CpDHP anion **28** and $CpTiCl_3$ went well. The anion **28** was made in d_8-THF and was green. The $CpTiCl_3$ was added as a C_6D_6 solution, and the reaction mixture immediately turned to red. The ^{1}H-NMR spectrum indicated the formation of metal complexes.(**Figure 2.4)** Similar to the reaction of Y compound, a mixture of several compounds may be formed. However a larger scale reaction did not go well. The yield was very low and the recrystallization failed to produce clean products.

2.12 Reactions of open CpCPD anion 28' with metal complexes: $Re(CO)_5Br$, $(Cp^*RuCl_2)_n$ and $FeCl_2$

CpDHP anion **28** was made with $LiCH_2SiMe_3$ in d_8-THF in a sealed NMR tube and was exposed to visible light overnight at room temperature. The ^{1}H-NMR spectra showed that about 85% **28** has been converted to the open CpCPD form **28'**. Metal

complexes ($Re(CO)_5Br$, $(Cp^*RuCl_2)_n$ or $FeCl_2$) were then added, and the reactions were monitored by ^{1}H-NMR spectroscopy.

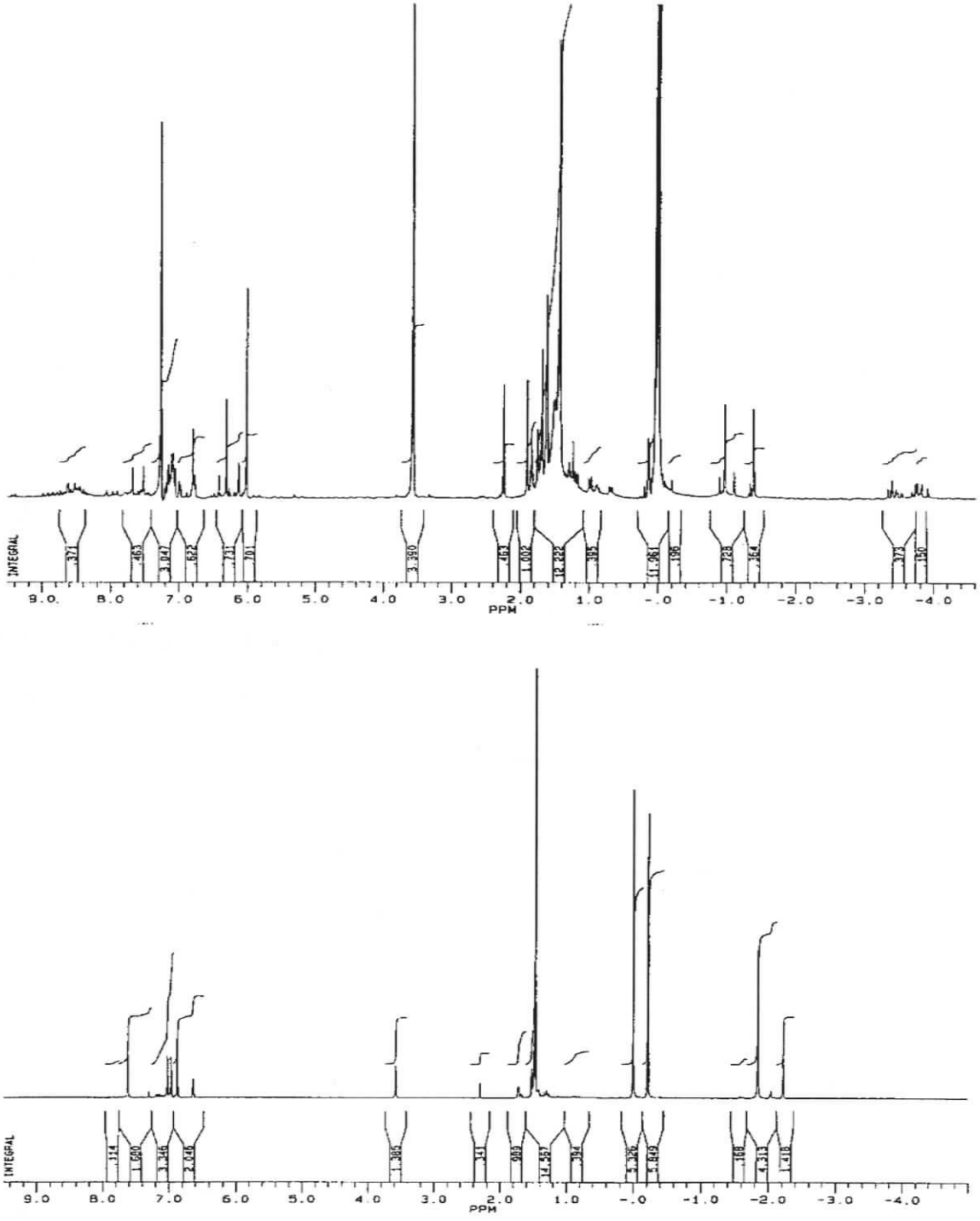

Figure 2.4. The ^{1}H-NMR spectra of anion **28** (bottom) and Ti products (top).

It is found that the reaction of **28'** with $(Cp^*RuCl_2)_n$ resulted in the formation of the open ruthenocene Cp*Ru(CpCPD) **52'**, and it gradually converted to the closed form Cp*Ru(CpDHP) **52** in the dark at room temperature.

The reaction of **28'** with $Re(CO)_5Br$, on the other hand, resulted in the conversion of **28'** to the neutral CpDHP(H) **44** and some other unidentified products. No $(CpCPD)Re(CO)_3$ **51'** or $(CpDHP)Re(CO)_3$ **51** were detected.

The reaction of **28'** with $FeCl_2$ also resulted in the decomposition of the open anion **28'** and some unidentified paramagnetic products.

Chapter Three

Results and Discussion

3.1 The properties of the anion 28

3.1.1 General

Cyclopentadienyl-fused dimethyldihydropyrene, **28**, which we will call CpDHP anion, is a charged aromatic. It is stable at room temperature under argon. The anion is soluble in THF and gives a dark green solution. However, if the anion is generated in hexane, benzene, or toluene, then a red solution is obtained rather than green, along with much red precipitate. If THF is then added, the solution immediately becomes green and the precipitate dissolves, and the same spectrum is observed as when made in THF.

3.1.2 NMR properties

3.1.2.1 ^{7}Li NMR

As we mentioned above, the CpDHP anion **28** is green in THF but red in hydrocarbon solvents. We believe that the same anion is formed in both solvents, but that it is much less soluble in the hydrocarbon solvents, where it forms red aggregates that result in a broad ^{1}H NMR spectrum. Addition of d_8-THF immediately sharpens the signals, and gives the same spectrum as that when the anion is generated in THF, suggesting that d_8-THF cleaves the aggregates and results in monomer formation. Such aggregation would be expected to affect the ^{7}Li NMR spectra when the anion is run in different solvents. Indeed in d_8-THF, the ^{7}Li NMR spectrum of the fully closed anion shows a sharp singlet at δ -1.02, while in d_6-benzene, both a broad and a sharp signal are observed. If the THF sample is exposed to room light, the singlet moves upfield towards δ -2.72. Visible light opens the CpDHP anion **28** to the cyclophanediene (CPD) anion **28′** (see below), and lithium ions would be expected to exchange between these two

species, giving a single peak. Irradiation with more intense visible light forms a photostationary state, which is about 85% CPD and 15% DHP (from the ^{1}H-NMR), and then the singlet in the ^{7}Li NMR spectrum is observed at δ -2.72. Irradiation with UV light (or more slowly thermally) closes all the CPD form to the DHP form, and moves the signal back to δ -1.0. In d_6-benzene, however, the sharp peak at δ -10.6 and the broad peak at δ 0·4 (max at δ 1.5) behave differently on irradiation. The sharp peak disappears and the broad peak maximum shifts to about δ 1.9. The peak at δ -10.6 reappears slowly thermally. In THF, the difference in Li chemical shift between the open and closed forms does not appear to be as great (~1.7 ppm), and exchange is more rapid, so that only an average signal is seen. In benzene, the sharp peak changes dramatically, suggesting that either exchange is slow (which seems unlikely) or perhaps that the open form of the anion precipitates and becomes part of the broad signal, which dissolves again as it closes thermally.

3.1.2.2 ^{1}H NMR

The ^{1}H-NMR chemical shifts for the anion **28** are listed in **Table 3.1**. The ^{1}H-NMR chemical shifts for the corresponding [a]-fused anion **27** are also included for comparison. We can draw the same conclusion we drew from **27**,[88] namely that the Cp anion in **28** behaves much like a benzene when fused to dihydropyrene and causes a reduction in ring current in the DHP ring as shown by the downfield shift of the internal methyl protons and upfield shift of the external protons compared to the precursor diene **44**. However, more detailed study on the chemical shifts of **28** and **27** shows that there are significant differences. For example, the internal methyl protons of **28** have a

Table 3.1 Comparison of ^{1}H-NMR chemical shifts (d_8-THF, δ) of 27(K^+)[88] and 28(K^+)

proton	28	proton	27
1,8	7.62	1	8.25
3,6	7.02	2	7.70
4,5	6.87	3	7.57
9	6.98	4	7.39
10	6.65	5	6.90
11	6.98	6	7.55
		7	7.61
		8	7.79
		9	7.30
		10	6.97
2,7-t-Butyl	1.48	11	6.67
Internal methyl	-1.82	Internal methyl	-2.83 and –2.88

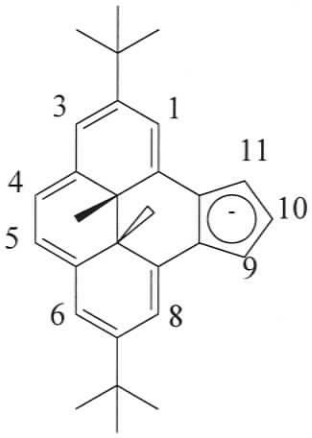

28

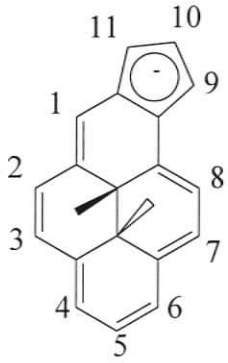

27

chemical shift of -1.82 ppm, while those of **27** are at -2.83 and -2.88 ppm, a difference of over 1 ppm. Also the aromatic protons of **28** (δ 6.87-7.62) appear at higher field than those of **27** (δ 6.90-8.25). These results are not what we expected. It has been found that in neutral DHP systems, the effect of annelation position on the chemical shifts of the internal methyl protons is small (< 0.3 ppm)[96] **(Table 3.2).** The large difference of the charged Cp-fused system is thus a surprise to us.

Table 3.2 Chemical shifts of the internal methyl protons for some dihydropyrenes.[88,96]

	[a]-2,7-H	[e]-2,7-H	[e]-2,7-Di-t-butyl
DHP	δ -4.25 (**1**)	δ -4.25 (**1**)	δ -4.06 (**31**)
benzoDHP	δ -1.62 (**26**)	δ -1.85 (**35**)	δ -1.58 (**36**)
naphthoDHP	δ -0.44 (**62**)	δ -0.74 (**63**)	δ -0.52 (**37**)
CpDHP	δ -2.85 (**27**)		δ -1.82 (**28**)
CpDHP(H)	δ -4.16 (64)		δ -3.90 (44)

As discussed in the Introduction, the geometry of the DHP is not changed on fusion of aromatic fragments. In the neutral systems, the chemical shifts of the internal methyl protons are mainly affected by the reduction in ring current caused by the change in delocalization in the [14]annulene ring in the fused systems. The through space deshielding by the fused aromatic ring is very small (<0.1 ppm).[35]

For the charged Cp system, the geometry still is not a factor on the chemical shift changes of the internal methyl protons, and the through space deshielding of the Cp ring

should be very small even though it may be larger in **28** than **27**, because the internal methyl is closer to the Cp ring center in **28** than in **27** (see arrow in **Figure 3.1**). The change of the fused ring size from six-member ring in benzoDHPs (**26** and **35**) and naphthoDHPs (**62** and **63**) to five member ring in CpDHP anions (**27** and **28**) is not a factor either, because, as we can see from **Table 3.2**, the neutral five-member ring derivatives (**64** and **44**) actually have similar chemical shifts for the internal methyl protons. We would expect the reduction in ring current to be similar in the [a] and [e]-fused anion **27** and **28** as demonstrated in the neutral systems. So the most possible reason for the large difference in the chemical shifts of the internal methyl protons in **27** and **28** would be from the through bond effect of negative charge.

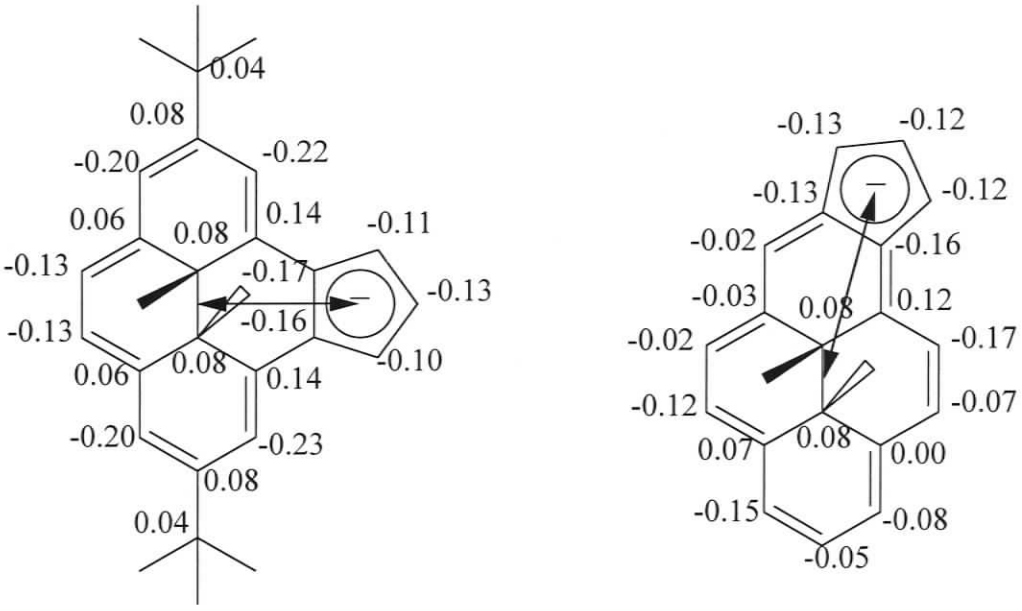

Figure 3.1. The charge distributions of **27** and **28** derived from PC model.

The only difference between **27** and **28** is the annelation position. The different annelation positions may result in different charge delocalizations. The charge

distributions of **27** and **28** were derived from PCMODEL[117] and are shown in **Figure 3.1**. Unfortunately although the charge distribution pattern on the DHP ring is different in the [a] and [e] systems, the total % between the Cp and DHP ring are actually similar, i.e. 55% of the charge is on the Cp ring and 45% is on the DHP ring, which is only slightly different from what Khalifa[88] obtained for **27,** about 40% of the charge is spread on the DHP ring. So clearly it is unlikely the difference is caused by the charge distribution. Although the difference in the chemical shifts must have an underlying cause, we have not yet determined what this is.

3.1.3 Photoswitch properties

DHP **1** and its derivatives are intensely colored compounds. They can display green, red, purple and even blue colors, depending on the visible light absorption patterns. In the UV-vis spectra, they usually show four principle absorption bands, two intense UV bands in the 300 ~ 400 nm region and two visible bands of lower intensity in the 400 ~ 800 nm region.[60] Literature[96] compounds **31** and **36** followed the general pattern with absorptions at 340 (1.1×10^5), 379 (3.8×10^4), 476 (1.1×10^4), 645 (8.1×10^2) nm and 369 (2.6×10^4), 388 (3.5×10^4), 504 (7.0×10^3), 620 (4.0×10^2) nm ($mol^{-1}.L.dm^{-1}$) respectively.

Cyclophanedienes have absorption profiles deeper in the UV, normally in the 200 ~ 320 nm region,[60] as they are derivatives of benzene, with small amounts of additional conjugation. The cyclophanedienes range from colorless to pale yellow. The literature compounds **31'** and **36'** had absorption bands at 220, 240 nm and 248 nm respectively.[96]

CpDHP anion **28** also showed the four principle absorption bands characteristic of DHPs at 350 (3.6 x 10^4), 395 (2.9 x 10^4), 490 (8.0 x 10^3), 655 (7.8 x 10^2) nm, with some red shifting from **31**, as it has greater conjugation than **31**. Irradiation of solutions of **28** with visible light caused isomerization to **28' (Scheme 3.1)**. **Figure 3.2** shows the absorption profiles of **28** and **28'**.

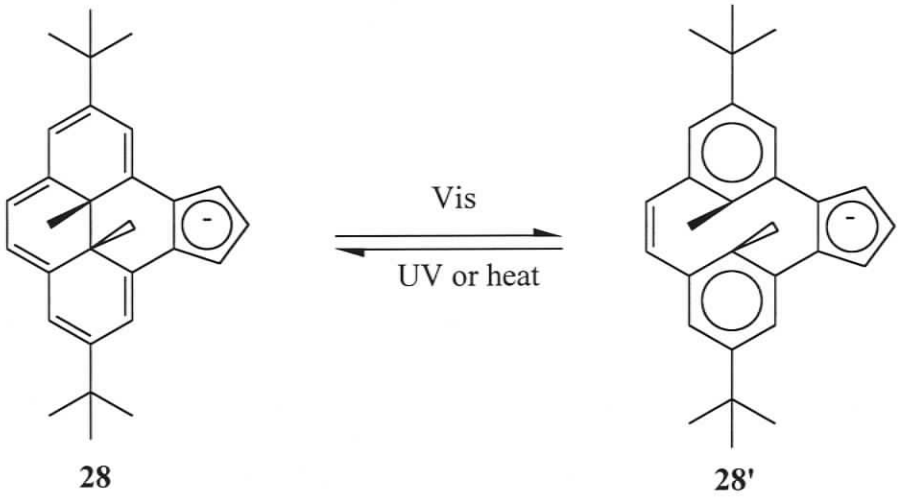

Scheme 3.1. Isomerization between isomers **28** and **28'**.

^{1}H-NMR spectroscopy also showed the conversion from **28** to **28'**. **Figure 3.3** shows the ^{1}H-NMR spectra of **28** and **28'**. Unfortunately, the conversion is not complete. Continued irradiation of **28** allows about 85% opening to **28'**, when a photostationary state appears to be reached. The chemical shifts of the open form, **28'**, are dramatically different from the closed form **28**. For example, the internal methyl protons move from δ -1.82 to δ +1.33, no longer being in the center of the large annulene ring.

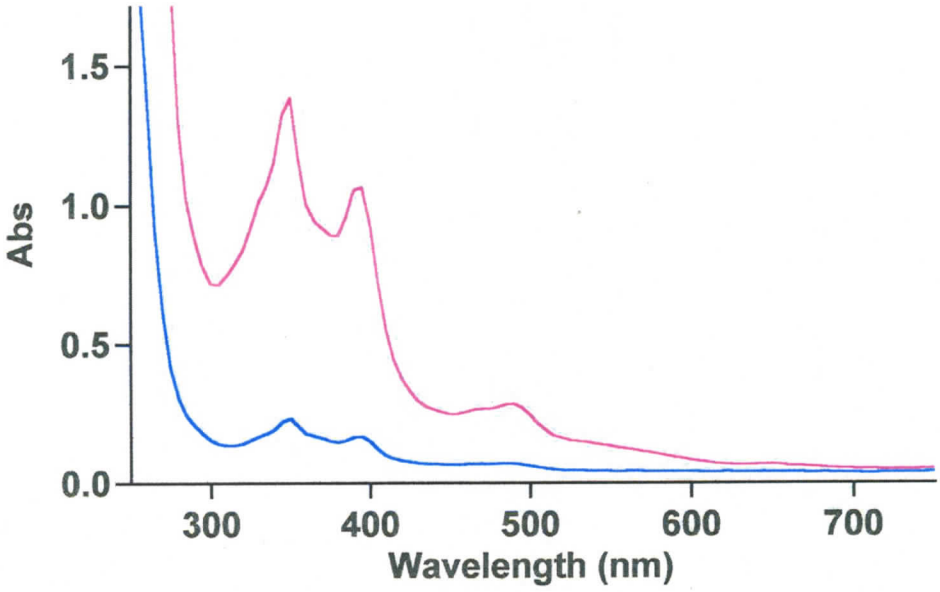

Figure 3.2. UV-Vis spectra of closed anion **28** (red) and after irradiation (blue), ~85% open anion **28'**.

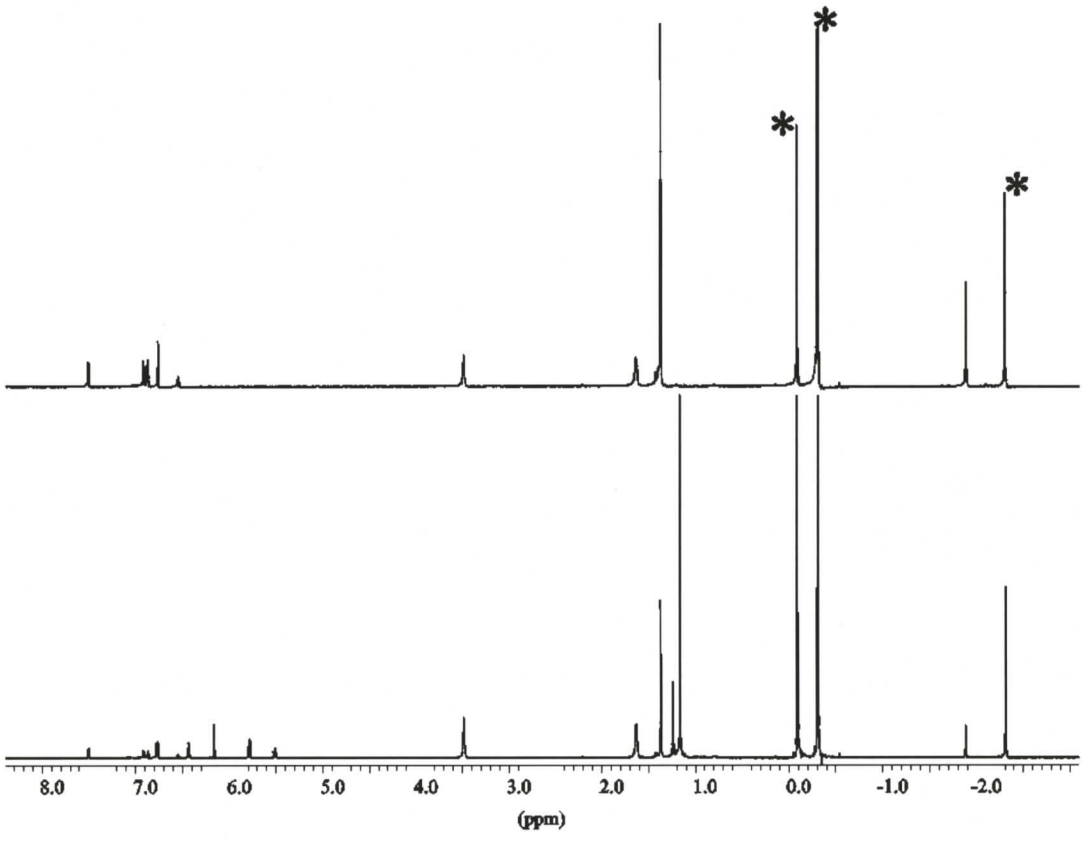

Figure 3.3. The ^{1}H-NMR spectra of the closed anion **28**(top) and after irradiation (bottom), ~85% **28'** with excess $LiCH_2SiMe_3$ (peaks with star) in d_8-THF.

The quantum yield for the visible light opening reaction of dihydropyrene (DHP) **31** to metacyclophanediene (CPD) **31′** is very low, $\Phi = 0.0015$.[59a] Benzannelation substantially increases this value by 28 times to $\Phi = 0.042$ for the reaction of **36** to **36′** reaction. We have not measured quantum yields for many of our compounds, but instead use relative opening rate compared to benzoDHP **36**.[70] Opening of the naphthannelated derivative goes faster than benzoDHP **36**.[63] If photochemically, the fused Cp anion of **28** is resembling benzene, then **28** should also photoopen faster than cyclopentadiene **44**. Indeed the latter cycloalkene-fused dihydropyrene photoopens even slower (if at all) than its parent **31**, since irradiation of a C_6D_6 solution of **44** with light of wavelength >490 nm (from a 500W Tungsten lamp with filter) for 12 h produced no changes in its ^{1}H NMR spectrum. The benzo-derivative **36**, irradiated at the same time and under the same conditions, completely opened to **36′** in 8 min. For comparison purposes, equimolar solutions of anion **28(Li$^+$)** and **36** in d_8-THF were irradiated parallel to each other with the same lamp at the same time. ^{1}H NMR spectra were recorded at intervals, so that the relative rates of opening could be determined (see **Section 5.3** for experiment and data analysis details). The photoopening of **28** to **28'** is not as fast as the benzo-derivative **36** to **36′**. The relative rate $k_{28\text{-}28'}/k_{36\text{-}36'}$ is about 0.22 (**Figure 3.4**). It is not obvious why the relative rates and quantum yields of opening in the dihydropyrenes are as low as they are,[59] and many factors may be contributing. However, fusion of an aromatic ring at the [*e*]-position does seem to increase the efficiency of the photoopening reaction. The Cp anion precursor **44** opens extremely slowly or not at all (relative to **31**), and so in the sequence no group fused, Cp anion fused, and benzene fused, the ring-opening reactivity does seem to be in an aromaticity order, with the Cp anion

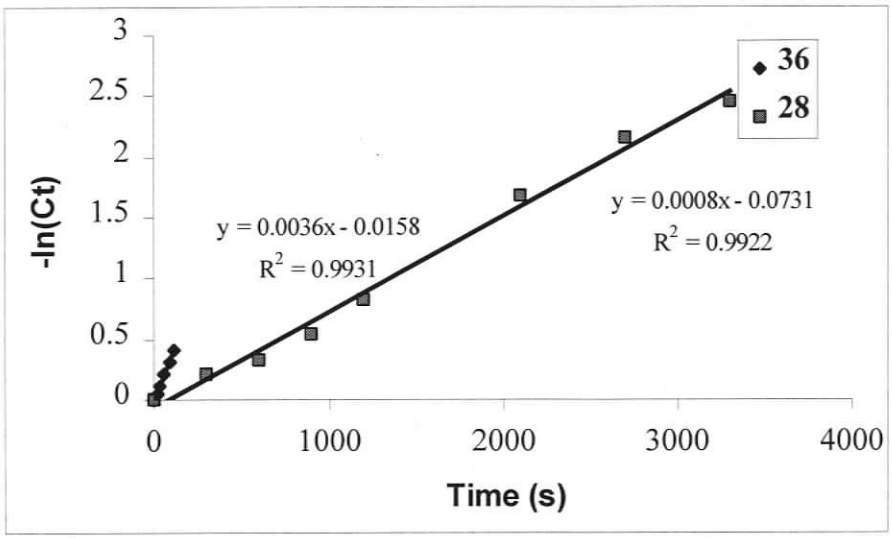

Figure 3.4. Relative rates of photoopening for **28(Li$^+$)** and **36.**

having a (reduced) benzene-like effect on the photochemical opening reaction.

The UV closing reaction, e.g. **31′** to **31**, is fast for most of the systems studied[63] (see **Section 5.3** for experiment and data analysis details). Anion **28′** is no exception. When equimolar solutions of **36′** and **28′** in d_8-THF were irradiated side by side with a

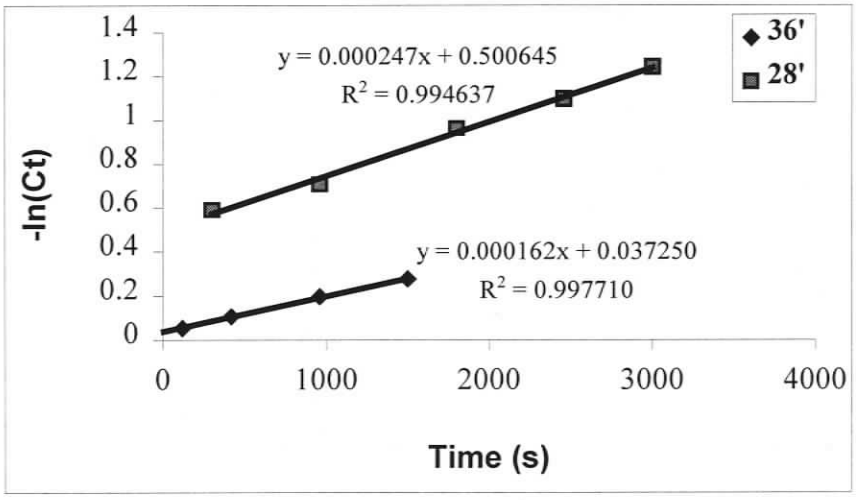

Figure 3.5. Relative rates of UV closing for **28'(K$^+$)** and **36'**.

pencil mercury lamp, anion **28′** actually closed at about 1.5 times the rate of the benzo-derivative **36′** (**Figure 3.5**).

3.1.4 Thermal return reaction

Although Woodward-Hoffmann forbidden, the closing reaction, e.g. **31′** to **31**, also occurs thermally.[63,65,97] The thermal return reaction of **28'** was studied by ^{1}H-NMR and ^{7}Li-NMR spectroscopy. The plots are given in the Appendix I.

Benzannelation substantially slows the thermal closing reaction: at 46 °C, $\tau_{1/2}$ = 1.88 h for **31′**, while for **36′** $\tau_{1/2}$ = 7.13 h. For anion **28′**, the corresponding $\tau_{1/2}$ is 2.1 h, determined from the ^{1}H NMR changes. The thermal closing can also be followed by changes in the ^{7}Li NMR spectra, where a $\tau_{1/2}$ value of 2.3 h (46 °C) was obtained, in excellent agreement with the ^{1}H-NMR derived value. The anion thus thermally closes faster than the benzo-compound **36′** but not as fast as the parent **31′**. In this case, the thermal closing rates are more affected by changes in solvation than in the purely hydrocarbon counterparts such as **31′** and **36′**. This is reflected in a larger value of $\Delta S^{\ddagger}$ for **28′** (-12±0.4 cal K^{-1} mol^{-1}, derived from both ^{1}H and ^{7}Li data) than for **36′** (+3.8 cal K^{-1} mol^{-1}) or **31′** (+4.3 cal K^{-1} mol^{-1}). We do not yet fully understand the thermal closing reaction,[63] but one of the factors that enters in to $\Delta H^{\ddagger}$ (**28**-**28′**) is the aromaticity of the [*e*]-fused ring. In comparing DHP's with different fused rings, systems in which the aromaticity (actually the bond localization energy of the fusion bond) of the fused ring is less, have a smaller ΔH_f between the open and closed forms. Here, $\Delta H^{\ddagger}$ for the closing of **28′** is smaller (20.7±0.4 kcal mol^{-1}) than that for the closing of **36′** (23.9 kcal mol^{-1}), which is consistent with the reduced aromaticity of the cyclopentadienide anion relative

to benzene.[37] However, it must be stressed that this is only one of the contributing factors,[63] since $\Delta H^{\ddagger}$ for the closing of the parent **31′** is 23.3 kcal mol^{-1}. The E_{act} value for the thermal closing reaction is also reduced. For **28′** E_{act} = 21.1±0.4 kcal mol^{-1}, and for **36′** and **31′** E_{act} = 24.9 kcal mol^{-1} and 24.0 kcal mol^{-1} respectively. Since the closing reaction breaks Woodward-Hoffmann rules, it is unlikely to be concerted, yet finding the true nature of the transition state by calculation is proving to be a substantial challenge.[98] We hope that as we acquire more data on a variety of annelated systems, we will better be able to comment on this process in the future.

At 20 °C, $\tau_{1/2}$ for the closing reaction is 46-47 h (^{1}H and ^{7}Li data), and so **28'** is thermally stable enough to be studied; for example, ^{13}C NMR data and UV data are given in Chapter 5, Experimental Section.

3.1.5. Photoswitching properties of ketone 49

While, as stated above, the quantum yield for the photoopening reaction of the parent **31** to **31**' is low, Φ = 0.0015, we have shown[59a] that for 4-acetyl-**31** the quantum yield is greater (Φ = 0.0038); likewise that for 4-acetyl-**36** (Φ = 0.095) was greater than that for **36** (Φ = 0.042).[59b] Since in ketone **49** the cyclopentanone is in essence a restricted acetyl group, we thought its photoopening would be interesting. Indeed, ketone **49** photoopens considerably faster than **31** in relative rate experiments. In fact about half as fast as **36 (Figure 3.6)**. Substitution of a carbonyl group next to the dihydropyrene ring evidently has an interesting acceleration of the photoopening reaction, which is different from that of an alkene (see below) and which we will pursue in the future. Unfortunately, when **49** is photoopened and then photoclosed with UV, some decomposition occurs, and

so not many cycles are possible. We noted above that in **44**, which has alkenyl substitution on **31**, the photoopening reaction appears to shut down completely. This effect of alkenyl substitution has been noticed in the dithenylcyclopentene photochromes,[99] but fortunately does not extend to the cyclically conjugated anion **28**.

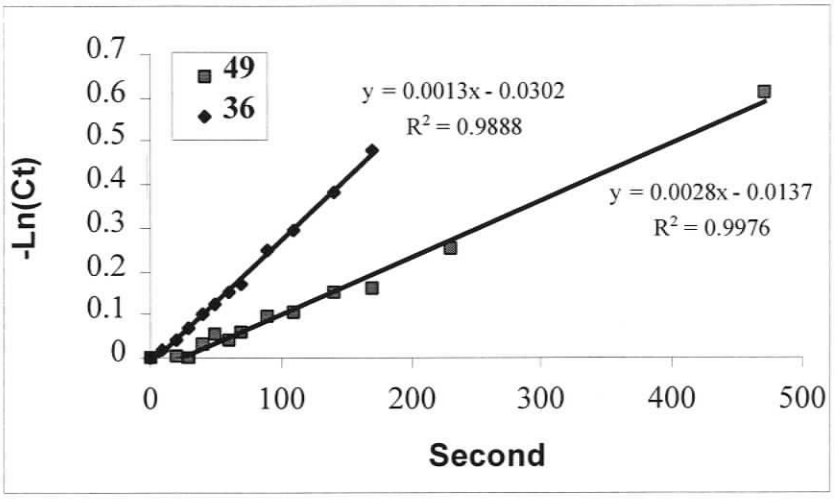

Figure 3.6. Relative rates of photoopening of **49** and **36**.

3.2 Metal complexes

3.2.1 Ring currents and relative bond fixing ability

3.2.1.1 Diamagnetic anisotropy effects

As discussed in the introduction, the chemical shift changes of the internal methyl protons of DHPs for annelated systems are mainly due to the reduction in ring currents caused by the change of delocalization of the [14] annulene ring. Thus the chemical shift changes of the internal methyl protons can be used to measure the relative bond-fixing ability of the fused systems. This is true for planar systems, where the through space anisotropic effect is small. However, for non-planar systems, such as metal complexes, the through space anisotropic effects might be larger, which would result in different

chemical shifts of the two internal methyl groups, since they have very different relative positions with respect to the metal moieties. So for metal complexes, before we can talk about their bond-fixing ability by using the chemical shifts of the internal methyl protons, the through space diamagnetic anisotropic effects have to be subtracted.

Fortunately, the elegant work of McGlinchey[100] enables us to determine the through space anisotropic effects for the metal complexes. McGlinchey has made use of the McConnell equation together with a composite geometric term for the organometallic moiety to determine χ values for several organometallic groups. The McGlinchey equation is

$$\sigma = - \chi \times 10^{36} (3\cos^2\theta - 1) / 12\pi r^3 \quad (1)$$

Where σ (ppm, + = shielding) is the chemical shift change due to the anisotropic effect; χ is the molar diamagnetic anisotropy; r is the distance from the anisotropy center to the proton and θ is the angle made by r with the central axis of the metal moiety.

To evaluate χ for a particular functional group, it is necessary to position two protons (whose chemical shifts would be identical in the absence of the anisotropic group) in different geometric positions with respect to the center of anisotropy. Thus, for two otherwise equivalent nuclei with the chemical shift difference $\Delta\delta$ and the difference in the factors Δf, where $f = (3\cos^2\theta - 1)/r^3$, the diamagnetic anisotropy can be evaluated by equation (2).

$$\chi = -12\pi \times 10^{-36} \Delta\delta / \Delta f \quad (2)$$

In general, to do so a pair of isomers of the same compound, in which a set of protons of identical chemical shifts are placed *syn* or *anti* to the metal moiety, need to be generated, provided no geometrical changes are taking place. In our DHP compounds,

such as benzoDHP **36** and anion **28**, the two internal methyls have the same chemical shift in the free ligand, but position differently relative to the metal moiety after complexation. So they provide perfect models for measuring the diamagnetic anisotropy of the metal moieties, without the need to use two isomers. The χ values for metal moieties of Cp*Ru, $Re(CO)_3$, and (CpDHP)Fe were thus determined from complexes (CpDHP)RuCp* **52**, (CpDHP)$Re(CO)_3$ **51** and $(CpDHP)_2Fe$ **54** obtained in this thesis by using equation (2). The relevant parameters were given in **Table 3.3** and the calculated χ values were shown in **Table 3.4**.

The parameters r and θ for compound **51** and **52** were obtained from X-ray data while those for **54** were obtained from a PCMODEL minimized structure, because no X-ray data were available. Whereas the values of r and θ for the ring hydrogens are unambiguous, those for the methyl groups, which can rotate, are not. The methyl protons are calculated by considering the methyl protons to be at a point at the center of the circle that they sweep out on rotation. For compound **52** and **54**, the anisotropy center was placed at the Ru and Fe atom respectively, while for compound **51**, two methods were used. One is to take the Re atom as the anisotropy center, the other one is to take the centroid of Re and the three O atoms as the center of anisotropy as shown in **Figure 3.7**. The latter method is similar to McGlinchey's "supercarbonyl" model of $Cr(CO)_3$. The center is 1.28 Å away from the Re atom.

The chemical shifts assignments are based on McGlinchey's work.[100] So the proximal methyl protons (Me_p), which are on the same side as the metal moiety, are deshielded relative to the distal methyl protons (Me_d), which are on the opposite side of the metal moiety. In the case of **54**, the chemical shifts are taken from the major isomer.

Table 3.3. Parameters for calculating χ values for metal moieties Cp*Ru, $Re(CO)_3$ and (CpDHP)Fe.

	52	**51**		**54**
		Re	Supercarbonyl	
δ_p	0.42	-0.23	-0.23	0.66
δ_d	0.09	-0.77	-0.77	-0.57
$\Delta\delta$	0.33	0.54	0.54	1.23
r_p (Å)	4.053	3.897	4.171	3.536
θ_p (°)	85.76	86.67	68.85	96.9
r_d (Å)	5.323	5.524	6.623	5.346
θ_d (°)	31.39	33.65	27.59	40.4
f_p	-0.014773697	-0.016725933	-0.008398759	-0.021639123
f_d	0.007864235	0.00640035	0.004669341	0.004842172
Δf	-0.022637932	-0.023126283	-0.0130681	-0.026481295

p = proximal, d = distal.

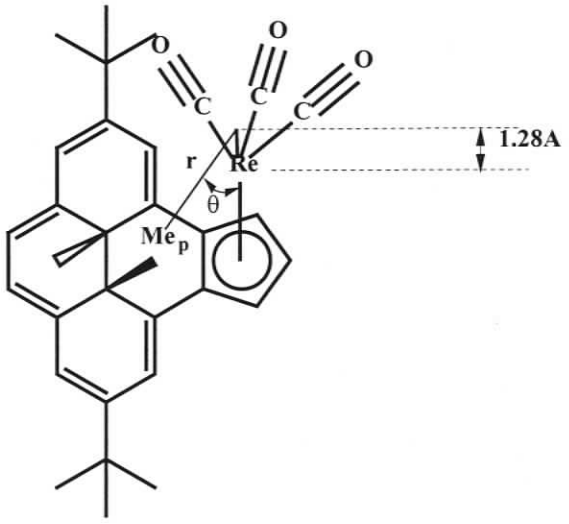

Figure 3.7. Diagram to show parameters r and θ used in equation (2).

The χ value of -549×10^{-36} m^3/molecule obtained for Cp*Ru is in good agreement with that obtained before (-478×10^{-36} m^3/molecule) from a pair of isomers of (*a*-CpDHP)RuCp* **53**,[38] which indicates that using DHP compounds for measuring the diamagnetic anisotropy of a metal moiety is reliable. The χ value (-1750×10^{-36} m^3/molecule) for a (CpDHP)Fe is very different from McGlinchey's value (-494×10^{-36} m^3/molecule) for a CpFe fragment, determined from ferrocene, which suggests that the anisotropy effect of (CpDHP)Fe is very different from that of CpFe. No literature χ value was found for a $Re(CO)_3$ fragment, so this is the first time it is reported.

Table 3.4. Experimental McGlinchey Diamagnetic Anisotropy values, χ (in units 10^{-36} m^3/molecule)

Metal fragment	Cp*Ru (**52**)	$Re(CO)_3$ (**51**)		(CpDHP)Fe (**54**)
		Re	Supercarbonyl	
χ	-549	-880	-1557	-1750

The diamagnetic anisotropy we have just obtained can be used to evaluate the anisotropy effect on the chemical shifts of the internal methyl protons and external protons on the [14]annulenes. The values of σ calculated using equation (1) for each proton in compounds **51**, **52** and **54** are given in **Table 3.5**. For the case of **51**, the χ value used is the supercarbonyl one, -1557×10^{-36} m^3/molecule, for it is closer to the physical reality of the situation; i.e., we regard each proton as experiencing the induced magnetic field attributable to three rotating carbonyl groups.

Table 3.5. Chemical shifts (δ) and Calculated shieldings (σ, ppm) for the protons of compounds **51, 52** and **54**.

proton	**51**(δ : σ)	**52** (δ : σ)	**54**[a] (σ)
Me_p	-0.23 : -0.35	0.42 : -0.22	-1.01
Me_d	-0.77 : 0.19	0.09 : 0.11	0.22
1	7.41 : 0.16	7.13 :-0.06	-0.68
3	7.003 : -0.01	6.80 : -0.02	-0.14
4	6.66 : -0.01	6.51 : -0.01	-0.11
5	6.62 : -0.02	6.50 : -0.01	-0.09
6	6.995 : -0.01	6.75 : -0.03	-0.09
8	7.35 : 0.11	7.04 : -0.14	-0.05
9	5.18 : 0.73	4.99 : 0.15	0.09
10	4.95 : 0.74	4.15 : 0.14	0.07
11	5.18 : 0.72	4.92 : 0.15	-0.09

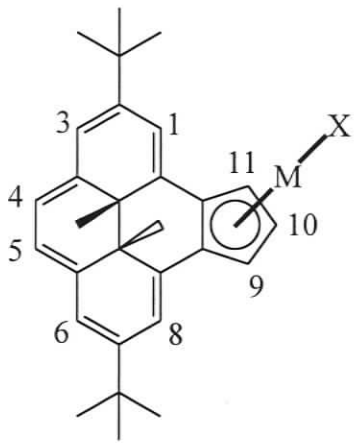

a. The chemical shifts for **54** were not shown, because the signals are overlapped with another isomer.

Clearly in compound **51** and **52**, the metal moieties do not have a large through space (anisotropy) effect on the methyl protons or indeed on any of the more distant protons (H-4,5) (**Table 3.5**). Even for the isolated protons "adjacent" to the complexed ring, σ is only calculated to be 0.16 ppm (H-1) for **51** and -0.14 ppm (H-8) for **52**. This is consistent with what we have observed before.[38] However, on comparison of the compounds (CpDHP)RuCp* **52** and (a-CpDHP)RuCp* **53**, we observe that the Cp*Ru fragment has a larger through space effect on the internal methyl protons in the [e]-

system **52** (-0.22 and 0.11 ppm) than in the [a]-system **53** (-0.07 and +0.07 ppm). Also the effects on the distant proton especially the protons "adjacent" to the complexed ring are larger in **52** than in **53** (σ < 0.03 ppm). This can be expected from the structural features of the compounds, since in the [e]-system, the internal methyls are closer to the anisotropic center than those in the [a]-system, which is manifested in the smaller r and θ values of **52** than those of **53 (Table 3.6)**.

Compared to **51**, **52** and other DHP compounds, the (CpDHP)Fe fragment in **54** has a much larger diamagnetic anisotropy effect on the internal methyl protons and the protons on the DHP ring "adjacent" to the complexed ring. This may be in part because there is a second CpDHP unit in the molecule, which has substantial through space effect. However, the shorter distance between the CpDHP unit and the Fe center should contribute to this too.

Table 3.6. Comparison of prameters r and θ for **52** and two isomers of **53**.

Parameter	**52**	**53a**	**53b**
r_p (Å)	4.053	4.278	4.755
θ_p (°)	85.76	90.2	93
r_d (Å)	5.323	6.304	5.695
θ_d (°)	31.39	41.4	38.9

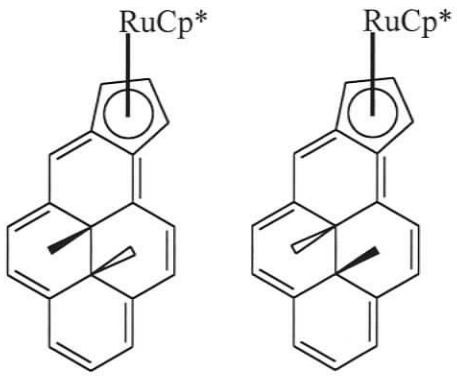

53a **53b**

In conclusion, the diamagnetic anisotropy effects on the internal methyl protons in metal complexes **51** and **52** are small and the effects on the more distant protons are

negligible. Also it is found that the effect in the [e]-system is larger than in the [a]-system. Lastly the two-DHP unit system **54** behaves differently from the one-DHP unit compounds; i.e. it has much larger through space effect on the internal methyl protons and the protons adjacent to the five-member ring.

3.2.1.2 Internal and external protons – Mitchell equation revisited

A consequence of the theoretical considerations on aromatic ring currents as discussed in the introduction would be that the different sets of chemically equivalent protons of DHP should experience different magnetic fields. This arises in part as each set of equivalent protons is a different distance from the center of the ring current induced magnetic field. Thus the changes in ring current would result in different changes in chemical shifts for the sets of chemically equivalent protons such as the internal methyl protons and the external protons. If there was no other effect operating, a linear relationship would be found between the chemical shifts of the internal methyl protons and the most distant proton, as discussed in the introduction.

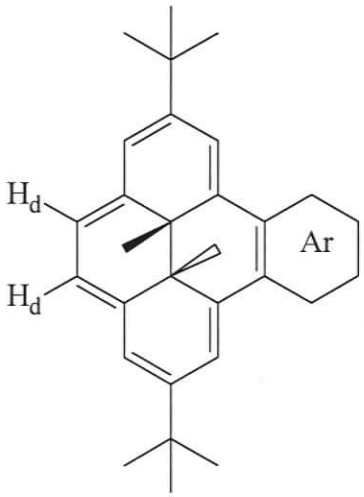

[e]-2,7-di-t-butyl compounds

The relationship between the internal methyl and the most distant external Ar-H_d proton chemical shifts for the **[e]-2,7-di-t-butyl compounds** was found to be:

$$\delta(Me) = 13.050 - 2.038\delta(H_d) \quad (R > 0.999) \qquad (3)^{64}$$

With this in hand we can test if there is any additional effect operating in the metal complexes obtained in this thesis. But before doing this, the through space anisotropies of the metal complexing fragment must be removed. With the χ values obtained above, this is now possible using

$$\delta_{calc} = \delta_{exp} + \sigma \qquad (4)$$

Where σ is the shielding (ppm) calculated using McGlinchey's equation (1) (**Table 3.5**). Calculated anisotropy-free values of δ for the internal methyl protons (Me) and the experimental δ for $H_{4,5}$ are thus shown in **Table 3.7**. Also in **Table 3.7** are shown the values of H_d calculated using equation (4).

This latter value is important in the sense that if it differs by much from the experimental value of $H_{4,5}$, an indication that a non-ring current effect is operating is obtained. As can be seen, good agreement is found for H_d and $H_{4,5}$, in support of the fact that the major change in the metal complexes is the changed ring current.

Table 3.7. Anisotropy free chemical shift vales, δ_{calc}, for use in calculating H_d.

compound	Me	H_d [calculated]	$H_{4,5}$ (found)
51	-0.58	6.69	6.66 & 6.62
52	0.20	6.31	6.51 & 6.50
54	-0.35	6.58	6.36 ~ 6.40

3.2.1.3 Relative bond fixing ability

We have concluded above that the chemical shifts of the internal methyl protons in the metal complexes are mostly dependent on changes in the ring current and then is not much affected by substituents. Thus we can use them to determine the bond fixing ability of the metal fragments relative to benzene. In its most simple form, the method of obtaining the bond fixing ability of a metal system relative to benzene would estimate the relative bond fixing ability (RBFA) as the ratio of the change in chemical shift of the internal methyl protons of DHP **1** caused by annelation with the metal system, to the chemical shift change of **1** caused by benzannelation. This is shown using the [a]-2,7-H series below, for the benzo$Cr(CO)_3$ **63**.

[a]-2,7-H series

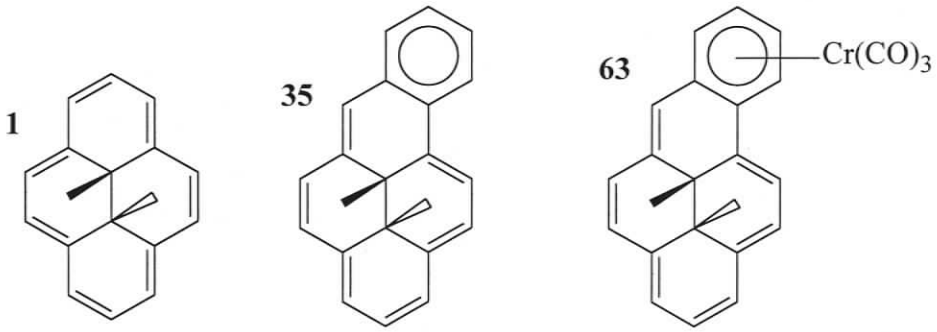

The chemical shift difference between **1** and **35** was $\Delta\delta$ = 2.63 ppm[68] while for **1** and **63** the difference was $\Delta\delta$ = -0.92-(-4.25) ppm = 3.33 ppm.[38] Thus the RBFA for the benzene-$Cr(CO)_3$ fragment would be

RBFA = 3.33 / 2.63 = 1.27

If we let $\Delta\delta$(M[a]) be the change in the chemical shift of the internal methyl protons from **1** for [a]-annelated DHP metal complexes, and if we let $\Delta\delta$(Bz[a]) be the

change in the internal methyl protons from **1** for [a]-benzoDHP **35**, then in general the relative bond fixing ability of a metal system would be given by:

$$RBFA = \Delta\delta(M[a]) / \Delta\delta(Bz[a]) = \Delta\delta(M[a]) / 2.63$$

Similarly, the relative bond fixing ability of a metal complex could be derived from [e]-annelated derivative of 2,7-di-*t*-butyl-DHP **31** by using an analogous equation.

$$RBFA = \Delta\delta(M[e]) / \Delta\delta(Bz[e]) = \Delta\delta(M[e]) / 2.48$$

The relative bond fixing ability of some metal complexes have been determined using the [a]-annelated derivatives of **1** shown below.[38] The chemical shifts of internal methyl protons, δ(Me), for related compounds and the determined RBFA are given in **Table 3.8**. The δ(Me) and the determined RBFA for the [e]-annelated metal derivatives of 2,7-di-t-butyl **31** are also shown in the same table for comparison. In **Table 3.8**, the δ(Me) are the calculated anisotropy free values by using the McGlinchey equation.

[a]-2,7-H series

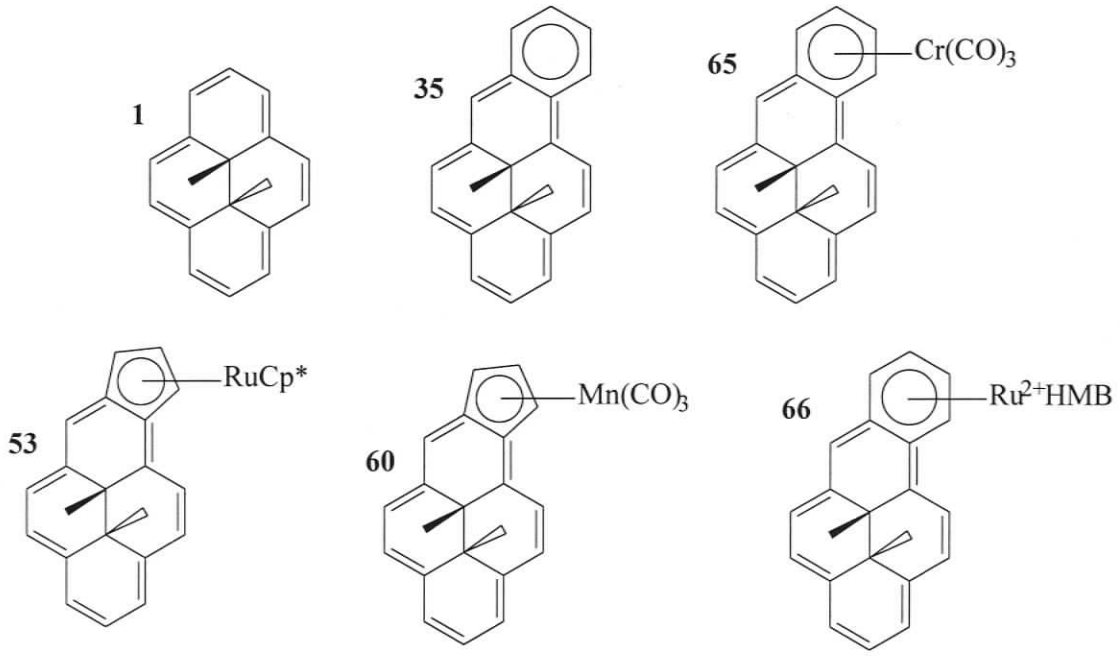

When no anisotropy free values available such as **43**, the average of the two internal methyl chemical shifts were then used. As can be seen from **Table 3.8**, the order for RBFA for the **[a]-2,7-H-series** is CpRuCp* >Benzene-Ru^{2+}HMB >$CpMn(CO)_3$ > Benzene-$Cr(CO)_3$ > benzene > Cp anion, while the order for the **[e]-2,7-di-t-butyl-series** is CpRuCp* > CpFe(CpDHP) > $CpRe(CO)_3$ > Benzene-$Cr(CO)_3$ > benzene > Cp anion. Clearly all the metal complexes have a greater bond fixing ability of the annulene ring than benzene itself. The greatest bond fixing ability was found in CpRuCp* systems and the smallest RBFA in Cp anion. Both the **[a]-2,7-H-series** and the **[e]-2,7-di-t-butyl-series** gave the same results that CpRuCp* has greater RBFA than Benzene-$Cr(CO)_3$, which then has greater RBFA than benzene itself, which in turn has greater RBFA than Cp anion. We also noted that the RBFA values derived from [a] and [e]-systems are quite different for CpRuCp* and the Cp anion, while those for Benzene-$Cr(CO)_3$ are similar. We are not sure why this is the case. One possible reason for CpRuCp* could be the solvent effect, since the chemical shifts for CpRuCp* compounds are recorded in different solvents while those for Benzene-$Cr(CO)_3$ compounds are in the same solvent. However, this is not likely to be the reason, because the chemical shifts of **27** and **28** are both recorded in d_8-THF, but the derived RBFA values for the Cp anions still have a significant difference. Another possible reason could come from the CpDHP anions (**27** and **28)**, because the measurements of the RBFAs for CpRuCp* are based on anions **27** and **28**, while that of Benzene-$Cr(CO)_3$ are based on the neutral benzoDHP **35** and **36**. As we have discussed previously, the internal methyl chemical shifts for **27** and **28** are different, maybe the same reason (unfortunately we still don't know) is working in the metal complexes too.

Table 3.8. δ(Me) (in $CDCl_3$) and RBFA for annelated DHP metal complexes.

Fused	[a]-2,7-H-series[38]			[e]-2,7-di-t-butyl-series		
fragment	Compd	δ(Me)	RBFA	Compd	δ(Me)	RBFA
-	**1**	-4.25	-	**31**	-4.06	-
benzene	**35**	-1.62	1.00	**36**	-1.58	1.00
Cp anion	**27**	-2.85[c]	0.53	**28**	-1.82[c]	0.90
Benzene-$Cr(CO)_3$	**65**	-0.92	1.27	**43**	-1.03[101]	1.22
CpRuCp*	**53**	-0.62	1.38	**52**	0.2[b]	1.65
$CpMn(CO)_3$	**60**	-0.76	1.33			
Benzene-Ru^{2+}HMB	**66**	-0.72[a]	1.34			
$CpRe(CO)_3$				**51**	-0.58[b]	1.40
CpFe(CpDHP)				**54**	-0.35[b]	1.50

a. in CD_3CN; b. in C_6D_6; c. d_8-THF; HMB = hexamethylbenzene

3.2.2 Photoswitch properties

As reviewed in the Introduction, although the effects of substitution and annelation on the photoswitching properties of DHP derivatives have been extensively studied, the study of organometallic derivatives of DHP as photoswitches has just started. At the beginning of this work, there were only two organometallic benzoDHP derivatives, [CpRu(benzoDHP)]PF_6 **42** and (benzoDHP)$Cr(CO)_3$ **43** known. Interestingly, **42** is photochromic and **43** is not. One of the purposes of obtaining a series of organometallic derivatives of CpDHP anion **28** was thus to examine the effects of

metal complexation on the photoisomerization and the properties of the photoisomers of the members of the series.

As we discussed earlier, arene annelation has a large effect on the photoswitching properties of DHP derivatives, and the benzene annelated derivative **36** has the best photoswitching properties in the DHP series so far. When irradiated with visible light, it opens readily and quantitatively to the colorless CPD form **36'**. Irradiation of **36'** by UV light then quickly and quantitatively causes reversion to the red DHP form **36**. The thermal return half-life of **36'** is over a week at room temperature, which is sufficient to do many kinds of studies. This compound is thus an excellent standard for studying the rates of photoisomerization of other DHP derivatives, and is used as a reference to compare the photo opening and closing of the photochromic compounds in this thesis.

3.2.2.1 General Aspects

Because the anion **28** is very air sensitive, its photoswitching properties are better followed in a sealed NMR tube. The metal complexes, on the other hand, are stable in air compared to the anion **28**, so their photo openings and closings were followed by UV-vis spectra because it's a faster and more convenient method than NMR spectroscopy. The samples were prepared in cyclohexane in equal molarity with standard compound **36** in quartz UV cells. The solutions were bubbled with argon for 30 min and the cells were sealed with parafilm. For the photo openings, the UV cells of the sample and the standard **36** were placed side by side and irradiated with visible light using a 490 nm cut-off filter. A 500 W tungsten lamp served as a visible light source. An electrical fan was used to cool the samples. UV-vis spectra were taken at various time intervals.

For the photo closings, the solutions of the samples and the standard **36** were first irradiated by visible light to the corresponding open CPD forms. Their reversion to the DHP form by UV light (a 254 nm mercury pen light) was thus monitored by UV-vis spectroscopy at various time intervals.

The data were plotted assuming first order reaction kinetics. Linear curve fitting was done in an MS Excel spreadsheet. Wang[102] has shown that by varying the concentration of the sample by ~ 3 times, and the distance between the lamp and the sample by ~ 3 times the maximum variation of the opening rate is only 7%.

3.2.2.2 (CpDHP)Re(CO)$_3$, 51

The coordination of the CpDHP anion **28** to a Re metal center changed the absorption pattern of the anion **28 (Figure 3.8)**. Compound (CpDHP)Re(CO)$_3$ **51** showed three principle absorption bands at 358 (2.4 x 10^4), 373 (2.6 x 10^4), 482 (7.2 x 10^3) nm with an additional UV band at 305 (1.7 x 10^4). Instead of two visible bands for most DHP compounds, **51** has only one visible band. Compared to the parent CpDHP anion **28**, the 655 nm visible band has disappeared. The visible absorption at 482 nm is responsible for the red color of the compound.

Complexation to a Re(CO)$_3$ moiety improved the photo switching properties of the anion **28**. Compound **51** undergoes complete reversible photoisomerization, compared to the partial photoopening of anion **28**. When a solution of **51** was irradiated with visible light ($\lambda > 490$ nm), the red solution was bleached to very light brown and **51** was converted to **51'** (**Scheme 3.2**). The UV-vis spectra of the open and closed form are shown in **Figure 3.8**.

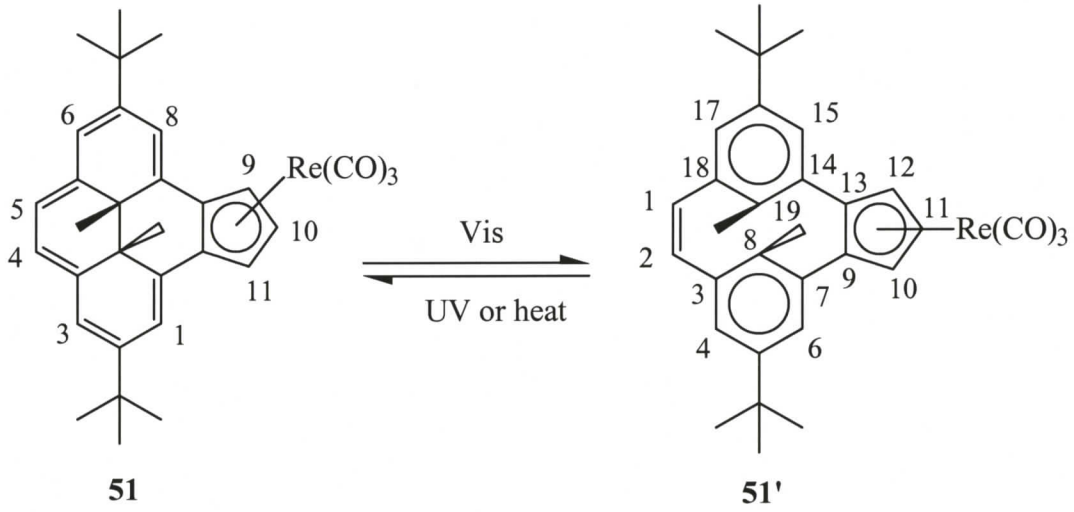

51 **51'**

Scheme 3.2. Isomerization between isomers **51** and **51'**.

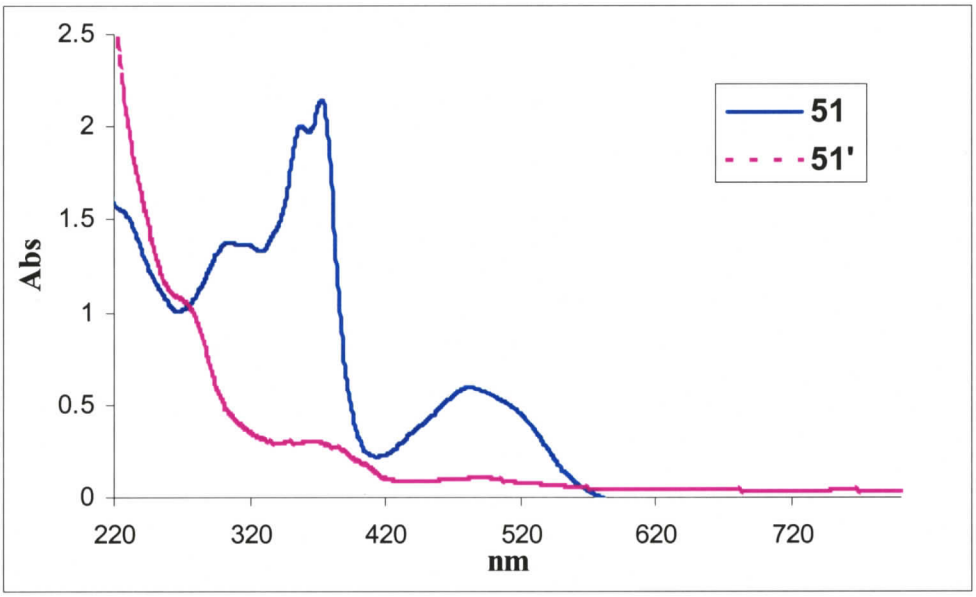

Figure 3.8. The UV-vis spectra of isomers **51** and **51'**.

^{1}H-NMR spectroscopy also showed the conversion from **51** to **51'**. **Figure 3.9** shows the ^{1}H-NMR spectra of **51** and **51'**. We can see from the spectra, the conversion was virtually complete. When **51** is converted to **51'**, the chemical shifts of the internal

methyl protons move from δ -0.77 and -0.23 to δ +1.56 and + 1.14, no longer being in the center of the large annulene ring. The number of signals for the protons on the Cp ring change from two to three. Protons H-9 and H-11 for **51** have the same chemical shift, but the corresponding protons H-10 and H-12 for **51'** do not.

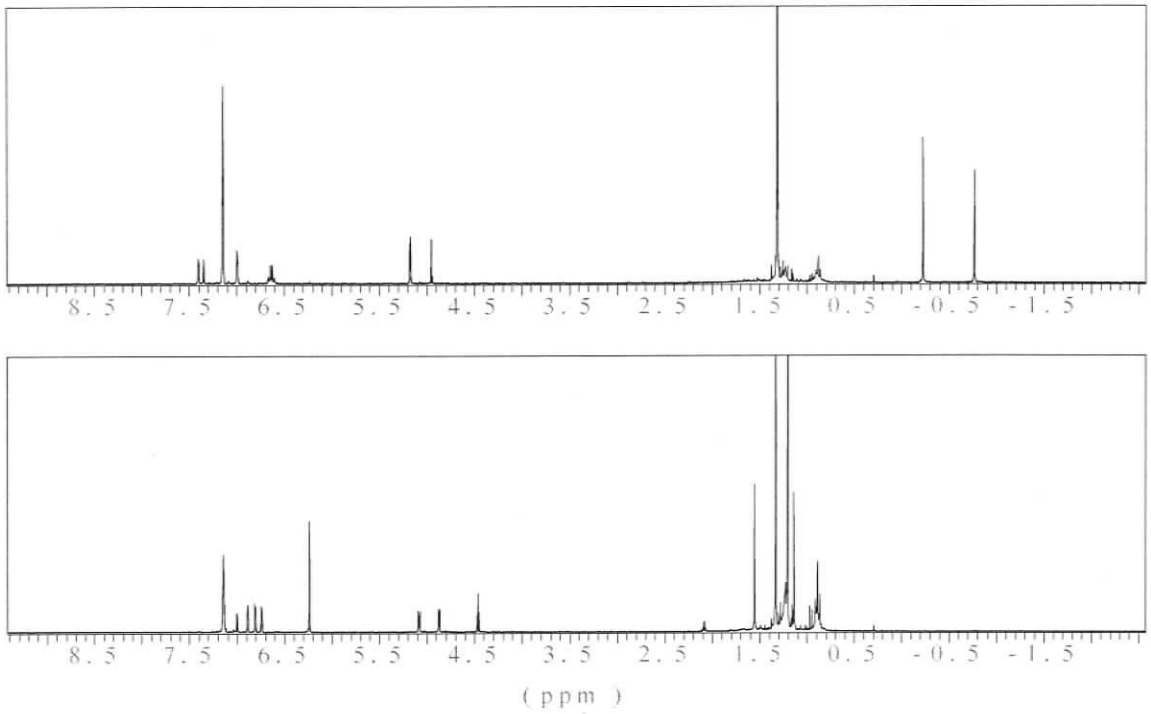

Figure 3.9. The ^{1}H-NMR spectra of isomers **51** (top) and **51'** (bottom) in C_6D_6.

For the purposes of the NMR study, d_6-benzene NMR solutions of 5 to 10 mg of **51**, chilled by ice water and irradiated with visible light ($\lambda > 490$ nm) from a 500 W tungsten lamp, resulted in virtually complete conversion of **51** to **51'** in about 30 min. The return reaction of **51'** to **51** occurred on irradiation with 350 nm or 254 nm UV light. Return of **51'** to **51** was also effected by warming in solution. Thermal return reactions for the compounds studied are discussed further below.

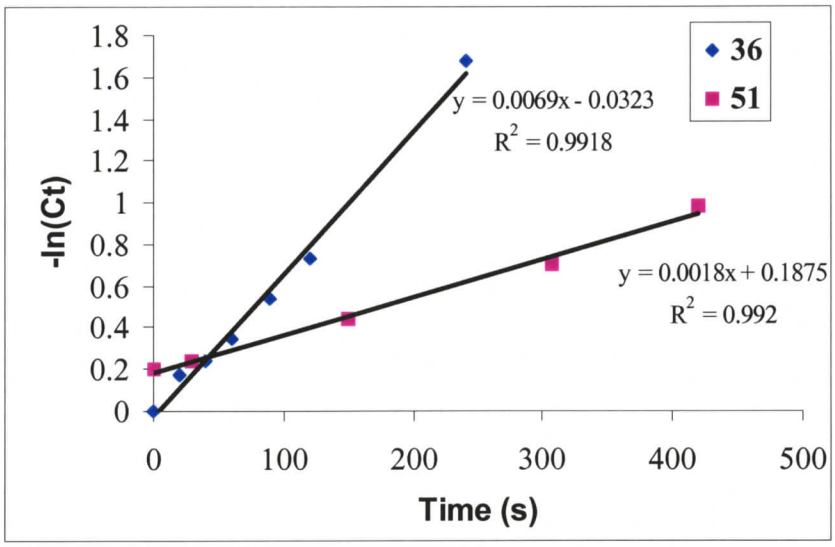

Figure 3.10. Relative rates of visible opening of **51** and **36**.

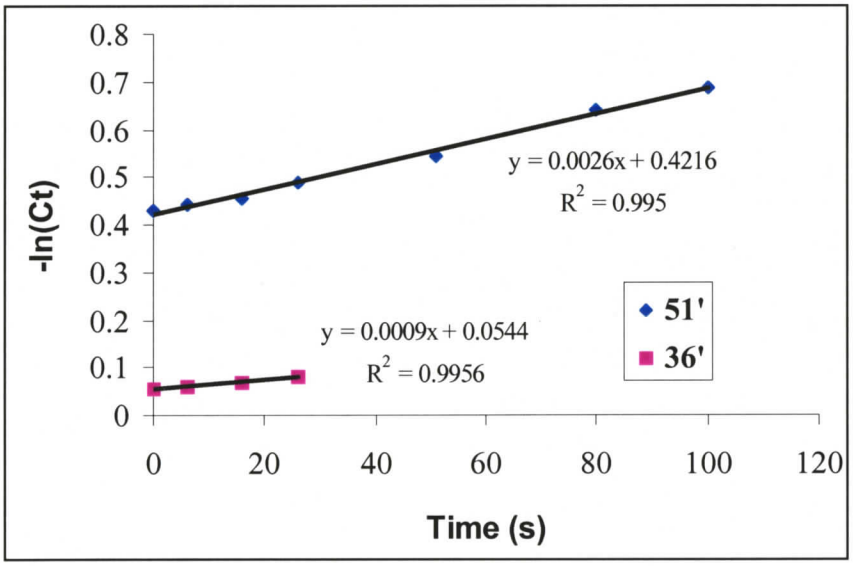

Figure 3.11. Relative rates of UV closing of **51'** and **36'**.

The relative rate studies (see **Section 5.3** for experiment details) showed that compound **51** photoopens about 4 times slower than benzoDHP **36**, and about 2 times faster than CpDHP anion **28 (Figure 3.10)**. The UV closing reaction, e.g. **51′** to **51**, is

fast as expected, although it photocloses 3 times slower than benzoDHP **36**, and about 5 times slower than the parent CpDHP anion **28 (Figure 3.11)**.

Thus compared to the CpDHP anion **28**, the complexation to the Re metal center improved the photoopening process from partial opening to complete opening and increased the opening rate, but slowed the UV closing reaction.

3.2.2.3 (CpDHP)RuCp, 52*

Different from the Re compound **51**, the Ru compound (CpDHP)RuCp* **52** followed the normal pattern for DHPs, showing intense UV-visible absorptions, which run into a strong visible band extending from 470 to 620 nm. Three UV-visible absorption bands were found at 370, 401 and 492 nm. Molar absorption coefficients were respectively 2.7 x 10^5, 2.3 x 10^5 and 5.5 x 10^4 L $mol^{-1}cm^{-1}$, which are one order of magnitude larger than those of (CpDHP)$Re(CO)_3$ **51** and the anion **28**. Two additional UV bands also occurred at 267 and 300 nm with same molar absorption coefficients of 1.7 x 10^5 dm^3 $mol^{-1}cm^{-1}$.

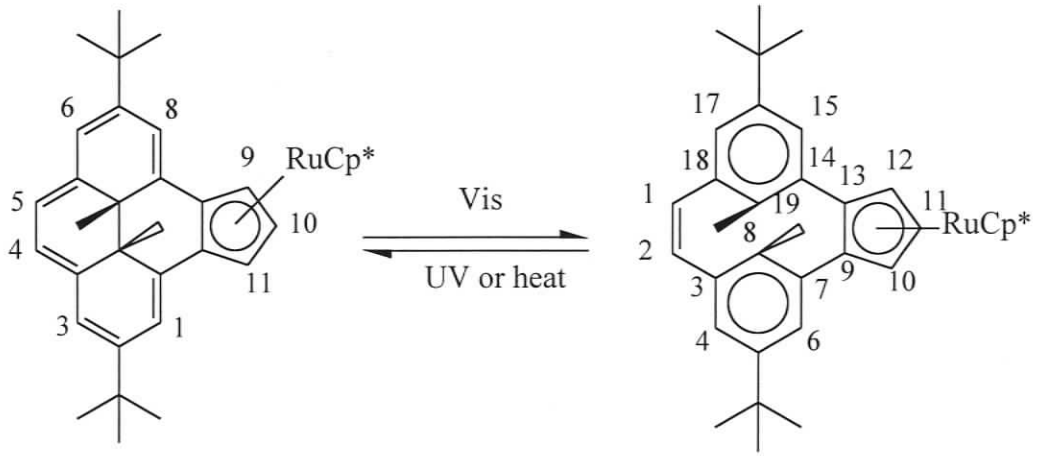

52 **52'**

Scheme 3.3. Isomerization between isomers **52** and **52'**.

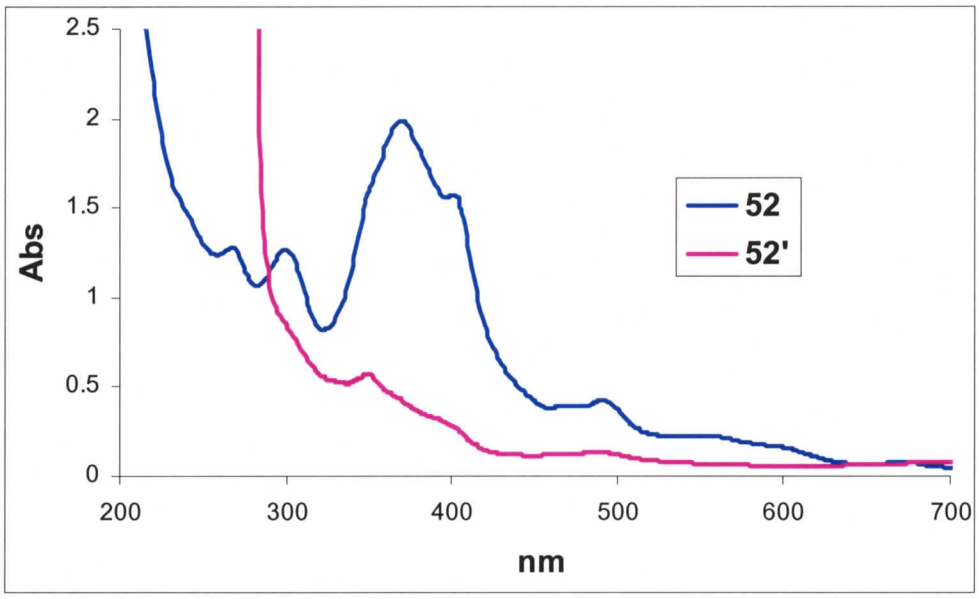

Figure 3.12. The UV-vis spectra of isomers **52** and **52'**.

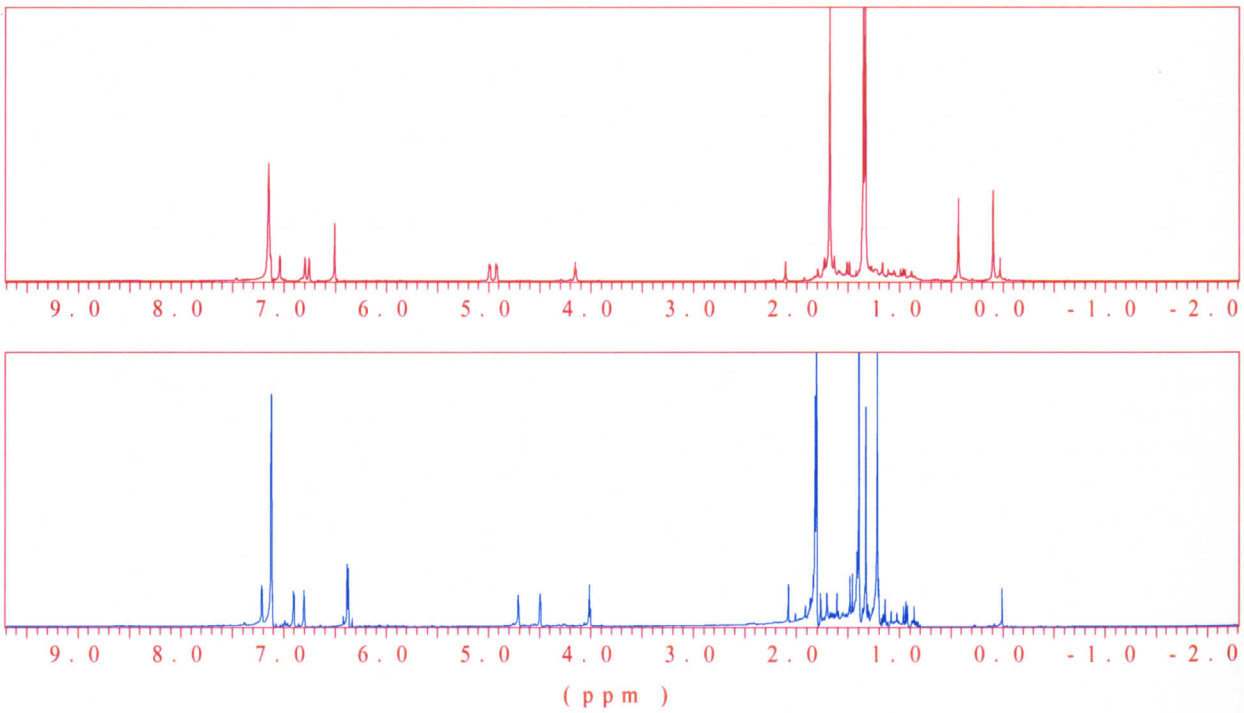

Figure 3.13. The ^{1}H-NMR spectra of isomers **52** (top) and **52'** (bottom) in C_6D_6.

Similar to (CpDHP)Re(CO)$_3$ **51, 52** undergoes complete reversible photoisomerization. Irradiation of a solution of **52** with visible light ($\lambda > 490$ nm) converted it to the open form **52'** and irradiation of **52'** with UV light closed it back to **52** (**Scheme 3.3**). The open and closed UV-vis and ^{1}H-NMR spectra are shown in **Figures 3.12** and **3.13**.

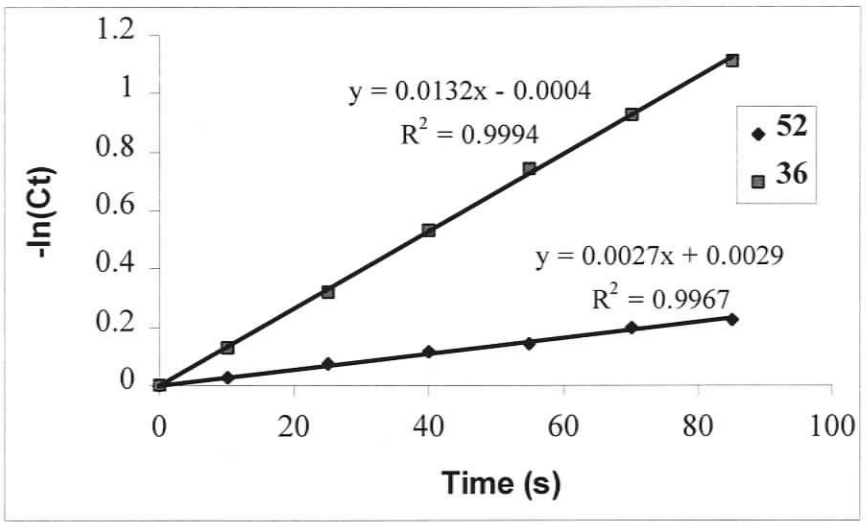

Figure 3.14. Relative rates of visible opening of **52** and **36**.

Similar to (CpDHP)Re(CO)$_3$ **51**, in their ^{1}H-NMR spectra, the chemical shifts of the internal methyl protons of **52** at δ 0.42 and 0.09 on irradiation moved downfield to δ 1.84 and 1.34 for **52'**, because the protons are no longer in the center of the large aromatic ring. Also the chemical shifts for H-10 and H-12 for **52'** are not the same, while the corresponding H-9 and H-11 for **52** do have the same chemical shifts.

The relative rate studies showed that compound **52** photoopens about 5 times slower than benzoDHP **36**, similar to that of CpDHP anion **28 (Figure 3.14)**; and it

photocloses at about 1.4 times faster than benzoDHP **36**, similar to that of the parent CpDHP anion **28 (Figure 3.15)**. Thus the complexation to the Ru metal center improved the photochromic property of the parent anion **28** in terms of the extent of the interconversion, but did not change the opening and closing rates much.

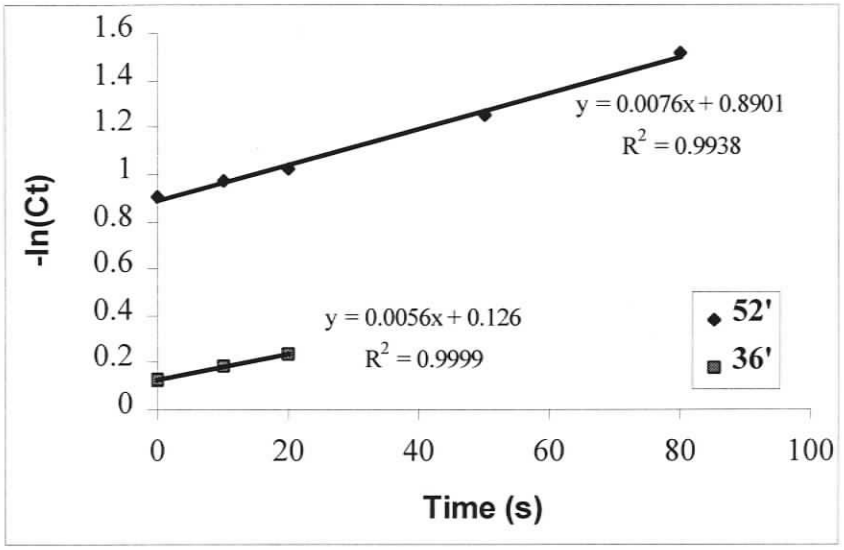

Figure 3.15. Relative rates of UV closing of **52'** and **36'**.

3.2.3 Thermal return reactions

An ideal photoswitch should have both the photoisomers stable, with no thermal interconversions. However, that is not the case for many photochromic compounds, where the thermodynamically less stable photoisomer isomerizes to the more stable one thermally. The DHP systems do this. DHP is the more stable form and so the less stable open CPD form reverts to the DHP form thermally.

As discussed earlier in **Section 1.3.4**, both simple substitution and annelation affect the thermal return rates of DHP systems. An electron-withdrawing group at the 2-

position seems to speed up thermal return, while an electron-donating group slows it down. Annelation of a benzene ring in the [e]-position substantially slows down the thermal return reaction from a half-life at 46 °C of 1.88 h for **31** to 7.13 h for **36**.[103] Annelation by a Cp anion also slows down the thermal return. The half-life at 46 °C for **28** is 2.1 h. We thus determined how complexation to metal centers affected the thermal return reactions of the DHP systems and the results obtained are presented here.

The thermal return reaction for **52** was studied using both ^{1}H-NMR spectroscopy and UV-vis spectra. The E_{act} values derived are similar, 23.4 kcal/mol from ^{1}H-NMR method and 24.0 kcal/mol from UV-vis spectra respectively. The deviation is only 0.6 kcal/mol, which is consistent with typical errors. Thus the reaction for **51** was only followed by UV-vis spectroscopy. For the UV-vis method, the photobleached sample in toluene was held at a fixed temperature and its absorption was monitored at the maximum absorption at 503 nm for **51** and 492 nm for **52**. For the ^{1}H-NMR method, the photobleached **52** in C_6D_6 was also held at a fixed temperature and ^{1}H-NMR spectra were recorded at various time intervals. Each thermal reaction was followed at a minimum of four different temperatures.

The thermal return reaction followed first order kinetics. The plots for the rates and all other thermal data are given in Appendix A and the kinetic data at 46 °C are presented in **Table 3.9**. The data for the parent anion **28**, $[(BenzoDHP)RuCp]^+PF_6^-$ **42** and BenzoDHP **36** are also listed for comparison. The E_{act} value for **52** was taken as the average value of the NMR and UV method as 23.6 kcal/mol.

Table 3.9. Thermal return rates, half-lives $\tau_{1/2}$ and activation energies ΔE_{act} at 46 °C.

Reaction	Rate (min^{-1})	$\tau_{1/2}$ (h)	ΔE_{act} (± 0.6 kcal/mol)
28' to **28**	0.0057	2.2	21.1
51' to **51**	0.00098	11.8	24.9
52' to **52**	0.0011	10.4	23.6
42' to **42**[70]	0.0053	2.2	23.0
36' to **36**[103]	0.0016	7.1	24.6

From **Table 3.9**, we can see that Re compound **51'** and Ru compound **52'** have much slower thermal return rates than **28'** or **36'**. The activation energy has increased by 3 to 4 kcal/mol from that of the anion **28'**, 21.1 kcal/mol to 23.6 kcal/mol for **52'** and 24.9 kcal.mol for **51'.** The half-life has been extended from 2.2 h for the parent anion **28'** to 10.4 h for **52'** and 11.8 h for **51'**. Both of these are even longer than that of our standard, benzoDHP **36'**. We also note that the activation energy of **52'** is less than the standard **36**, but its half life is longer. It is not apparent why that is the case. It is possible that the pre-exponential factors for such compounds are different. Contrast the benzoDHP compound **42**, where the complexation to a metal center speeds up the thermal return, with the anion **28,** where complexation to metal centers substantially slows down the thermal return.

3.2.4 Complete shut-down of the photochromism of $(CpDHP)_2Fe$ 54 and $(CpDHP)_2Yb(THF)_2$ 57

The structures of the metal complexes discussed in this section are shown in **Scheme 3.4**. The complexes $(CpDHP)_2Fe$ **54** and $(CpDHP)_2Yb(THF)_2$ **57** are not photochromic, which means that when a sample of solution of **54** or **57** was irradiated with visible light ($\lambda > 490$ nm), neither the UV-vis nor ^{1}H-NMR spectra changed. This is different from (CpDHP)Re(CO)$_3$ **51** and Cp*Ru(CpDHP) **52**.

Lack of photochromic behavior was seen before in the compound (BenzoDHP)Cr(CO)$_3$ **43** (discussed in **Section 1.3.4)**. This has also been observed recently in other metal complexes such as (BenzoDHP)Fe(CO)$_3$ **67,** in which the Fe(CO)$_3$ was coordinated directly to the DHP ring not the benzene ring.[104] It's also interesting to note that with a attachment of a ferrocenyl substituent to a DHP system, **68** shuts down the photochromism of that compound too.[103]

Although we are not sure what has caused the shut-down of the photochromism of the metal complexes, we note that so far, except for the lanthanide complex **57**, none of the first row transition metal complexes (Fe, Cr) are photochromic, while all the second and third row transition metal complexes (Re and Ru) undergo reversible photoisomerization as seen in **42**, **51** and **52**.

We also note that all the iron compounds that we have made are not photochromic, no matter whether the iron center is coordinated at the Cp ring (**54**), the DHP ring(**67**) or even just an substituent (**68**). All the Ru complexes that we have made are photochromic, no matter whether the ligand is anionic (**52**) or neutral (**42**), or whether the final complex is neutral (**52**) or ionic (**42**). This may suggest that the photochromism

Complexes that are not photochromic.

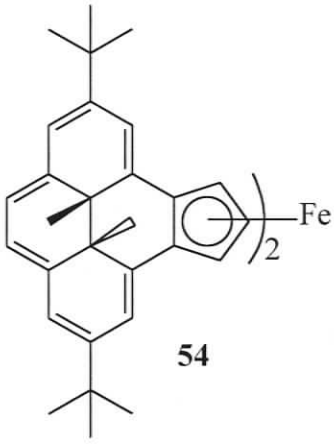

54

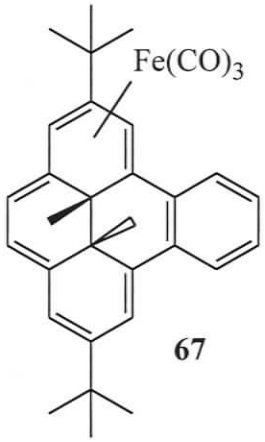

67

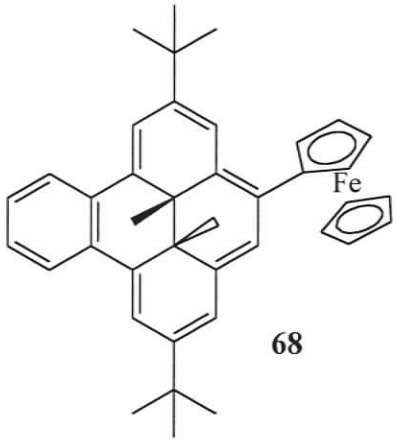

68

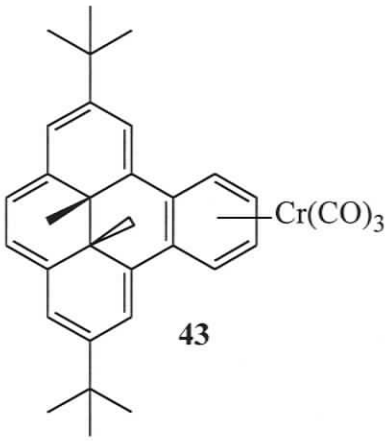

43

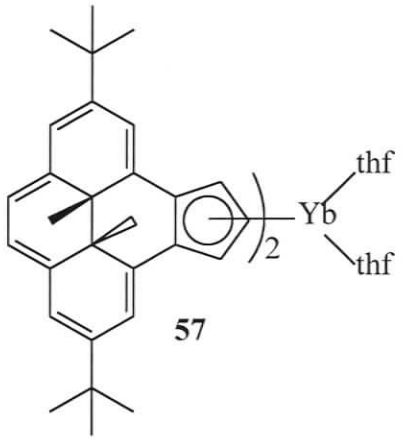

57

Complexes that are photochromic.

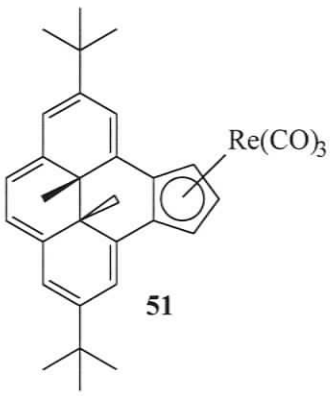

51

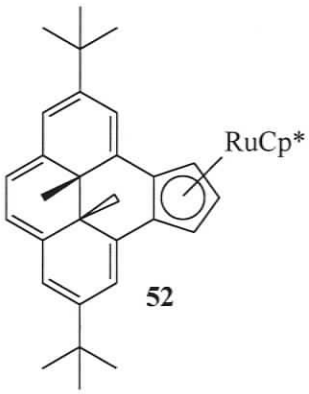

52

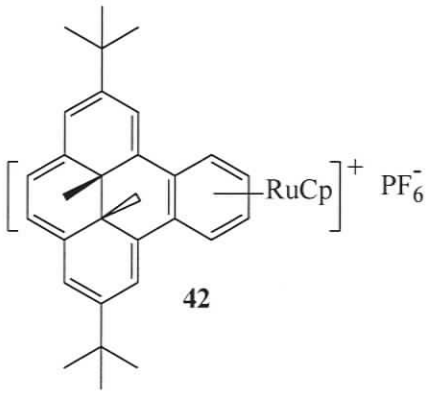

42

Scheme 3.4. Metal complexes of DHP systems.

of metal complexes is related to the individual metal center. Maybe some metal complexes can undergo electron or charge transfer between the metal center and the DHP ligand, which absorbs the energy of the photon and thus stops the photoisomerization process. Perhaps those that are photochromic do not or can not do this. This is supported by the fact that $YbCp^*_2(THF)_2$ complexes are highly colored due to metal to ligand charge transfer (MLCT) bands and it is simply possible that energy is absorbed by these processes. The same is true for ferrocene as well, for it absorbs in the same region (440 nm) as $(CpDHP)_2Fe$ **54** (a band at 410 nm with shoulder tailed to 800 nm). However, The $Cr(CO)_3$ complex **43** does not really support this since the Yb and Fe complexes are colored and benzene-$Cr(CO)_3$ is not very colored.

3.2.5 X-ray structures

3.2.5.1 (CpDHP)Re(CO)$_3$, 51

The molecular structure of **51** is shown in **Figure 3.16**. The crystallographic data are summarized in **Table 3.10** and selected bond length and bond angles are shown in **Table 3.11**. Compound **51** has the appearance of a normal Cp half-sandwich transition metal complex. The average (O)C-Re-C(O) bond angle (90.2°) is not significantly different from the ideal octahedral angle of 90°, or that found in the η^5-fluorenyl complex $(\eta^5\text{-}C_{13}H_9)Re(CO)_3$ (90.5°)[106] and the indenyl complexes $[\eta^5\text{-}1\text{-}(C_6F_5)C_9H_6]Re(CO)_3$ (89.1°)[107] and $\{\mu\text{-}(\eta^5\text{-}C_9H_6)C_2H_4(\eta^5\text{-}C_9H_6)\}[Re(CO)_3]_2$ (90.2 and 90.9°).[108] The Cp π-plane and the plane defined by the three carbon atoms of the CO ligands have a dihedral angle of 2.7°, indicating no significant distortion from the usual octahedral geometry. The middle CO is slightly twisted away from the middle carbon C(6) of the Cp ring with

a torsion angle C(2)-Re(1)-CpDHP$_{cent}$-C(6) of 9.4°. The average Re-C-O angle of 176.7° is normal.

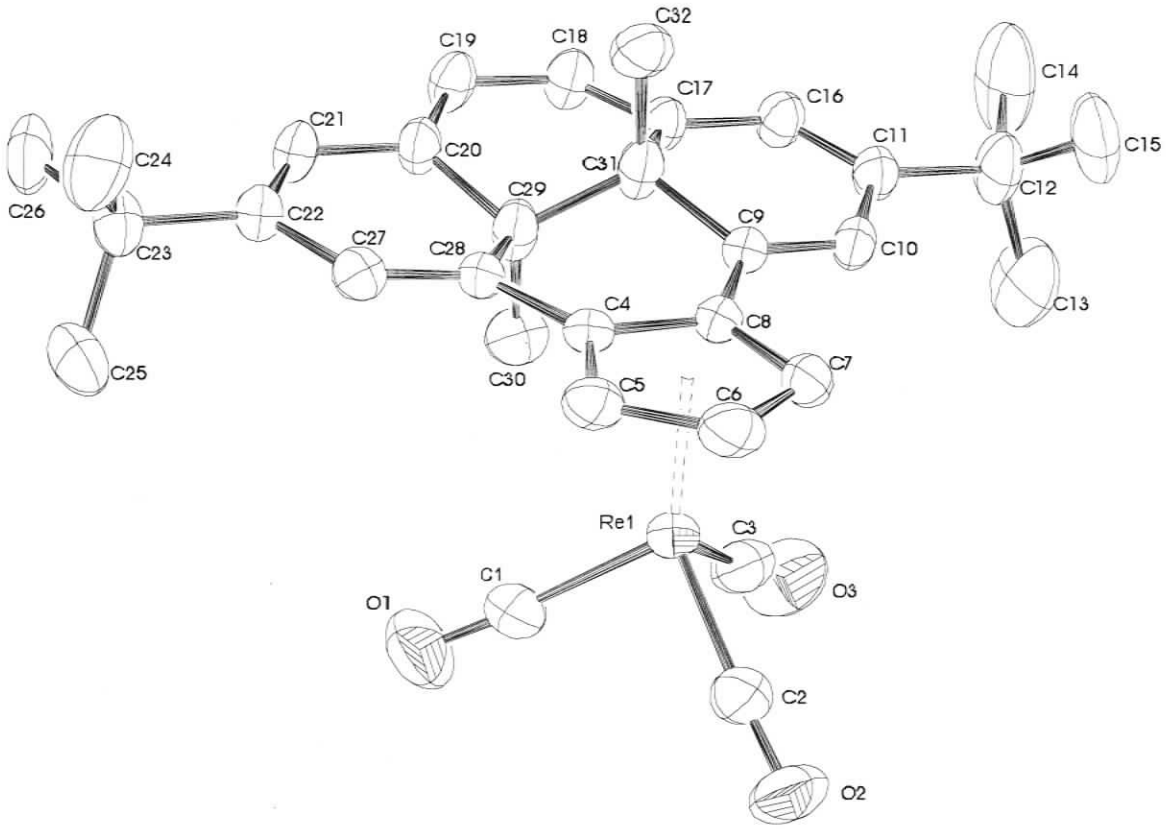

Figure 3.16. ORTEP-3[105] diagram (thermal ellipsoid 50% probability) of compound **51**. Hydrogen atoms are eliminated for clarity.

The η^5-binding of the Cp ring of the CpDHP ligand is confirmed by the Re-C bond lengths (2.265(4)-2.371(3) Å), which are similar to the values for (η^5-$C_{13}H_9$)Re(CO)$_3$ (2.288(4)-2.369(4) Å)[106] and indenyl complexes (2.287(5)-2.379(4) Å).[107,108] The Re-C distances to the Cp ring carbons show a typical pattern of longer distances to the ring fusion carbons (average 2.364 Å) than to the three "allylic" carbons

(average 2.278 Å). Here the Re center slips toward the C(6)-C(7) bond, presumably avoid steric interaction with the internal methyl carbon C(30). The small slip distortion value (see **Section 1.4**) (Δ = 0.086 Å) is slightly larger than the values found for the fluorenyl complex (η^5-$C_{13}H_9$)Re(CO)$_3$ (Δ = 0.072 Å)[1] and indenyl complexes (Δ = 0.047 ~ 0.072 Å).[107,108]

Table 3.10. Crystallographic data for 51.

formula	$ReO_3C_{32}H_{33}$
fw (g/mol)	651.78
crystal size, mm	0.42 x 0.52 x 0.54
a, Å	9.880(3)
b, Å	10.150(3)
c, Å	14.041(4)
α, deg	93.395(5)
β, deg	97.609(4)
γ, deg	96.004(5)
V, Å^3	1384.1(6)
cell detn, refls	800
d(calcd), g cm^{-3}	1.56
space group	P-1
Z	2
F000	648
λ, Å	0.71073
temp, K	228
linear abs coeff, mm^{-1}	4.42
R for merge	0.015
refls in refinement I>2.0σ(I)	4380
R1, wR2	0.023, 0.057
R1 for I>0.0σ(I)	0.027

The five carbon atoms of the five-membered ring are almost planar, with the largest deviation from the least squares plane being 0.016 Å for C(6). The five-membered ring is slightly folded away from the DHP ring with a folding angle (see

Section 1.4) of 9.0°. The hinge angle (see **Section 1.4**) is slightly smaller and is found to be 7.0°.

The 14 DHP peripheral carbon atoms are almost planar, with the largest deviation found to be 0.068 Å. The two bridge carbons, C(29) and C(31), are +0.324 Å and -0.395 Å out of the plane respectively. The two internal methyl carbons, on the other hand, are +1.89 Å and -1.94 Å above and under the plane respectively and they are 3.93 Å away from each other. These values are all similar to the values found for other DHP compounds.[32b,103] The non-bonded distances between the Re center and the two internal methyl carbons are 3.87 Å (Re(1)···C(30)) and 5.31 Å (Re(1)···C(32)) respectively. Comparison of the bond lengths in **51** with those of benzoDHP **36**, shows slightly greater average bond length alternation ($\Delta\Sigma$) around the [14]-DHP ring in **51** (0.077 Å) versus **36** (0.071 Å),[103] where $\Delta\Sigma$ = average long bond (Å) -average short bond (Å), which is consistent with the NMR ring current observations.

There are no exceptionally close contacts in the molecule. The closest distance between the carbonyls and the t-butyl methyl carbons is 4.65 Å, which is found between O(3) and C(13). The presence of two t-butyl groups does not disturb the planarity of the DHP periphery significantly. The dihedral angle between the least square planes that include the t-butyl carbons [defined by C(10), C(11), C(12), C(16); C(21), C(22), C(23), C(27)] and the DHP ring are only 2.2° and 1.7°. Similar to other DHP compounds,[32b,103] the t-butyl groups adopt a conformation in which one carbon atom of the methyl groups almost eclipses an adjacent aromatic C-C bond with torsion angles for C(21)-C(22)-C(23)-C(26) and C(14)-C(12)-C(11)-C(16) of 1.7° and 11.0°.

Table 3.11. Selected bond lengths (Å) and bond angles (degrees) for 51.

Re(1)-C(6)	2.265(4)	C(9)-C(10)	1.336(5)
Re(1)-C(7)	2.279(4)	C(10)-C(11)	1.458(5)
Re(1)-C(5)	2.289(4)	C(11)-C(16)	1.359(5)
Re(1)-C(8)	2.357(3)	C(16)-C(17)	1.424(5)
Re(1)-C(4)	2.371(3)	C(17)-C(18)	1.362(5)
C(4)-C(8)	1.434(5)	C(18)-C(19)	1.423(5)
C(4)-C(5)	1.448(5)	C(19)-C(20)	1.351(5)
C(4)-C(28)	1.452(5)	C(20)-C(21)	1.429(5)
C(5)-C(6)	1.412(5)	C(21)-C(22)	1.361(5)
C(6)-C(7)	1.410(6)	C(22)-C(27)	1.447(5)
C(7)-C(8)	1.438(5)	C(27)-C(28)	1.337(5)
C(8)-C(9)	1.449(5)		

C(2)-Re(1)-C(3)	88.12(18)	O(3)-C(3)-Re(1)	176.7(4)
C(2)-Re(1)-C(1)	91.27(18)	O(2)-C(2)-Re(1)	177.1(4)
C(3)-Re(1)-C(1)	91.2(2)	O(1)-C(1)-Re(1)	176.3(4)

3.2.5.2 (CpDHP)RuCp, 52*

The structure of **52** was determined by single crystal X-ray diffraction analysis. **Figure 3.17** shows an ORTEP-3 drawing of **52**. The crystal data are given in **Table 3.12**. **Table 3.13** lists selected bond lengths. As can be seen in **Figure 3.16**, the two five-membered cyclopentadienyl units are very nearly eclipsed (twist 8.0°), consistent with other ruthenocene structures.[109] The two five-membered rings are essentially planar, with the largest deviation of 0.007 Å for the Cp* ring and 0.014 Å for the five-membered ring of the CpDHP ligand, respectively. The methyl groups of the Cp* ring are bent out of the plane by 2.9°. These two five-membered rings are slightly tilted with the wide mouth open towards the DHP ring. The dihedral angle between the five-membered ring planes is 8.6° and the Centroid-Ru-Centroid angle is 174.7°. Such a configuration is undoubtedly due to steric interactions between the methyl groups of the

Cp* ring and the proximal internal methyl group, as the distance of C(2)···C(37) is only 3.72 Å.

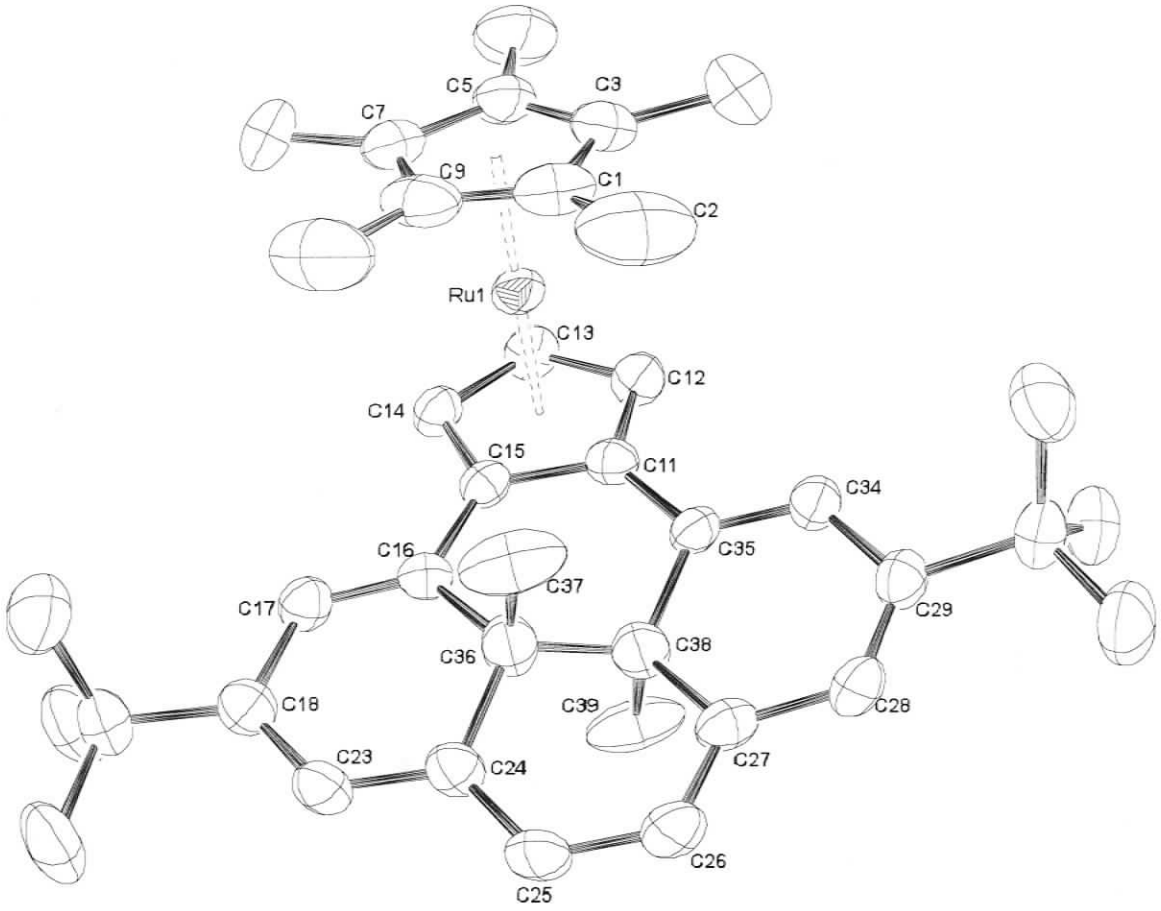

Figure 3.17. ORTEP-3[105] diagram (thermal ellipsoid 50% probability) of compound **52**. Hydrogen atoms are eliminated for clarity.

The ruthenium atom is not spaced evenly between the two five-membered rings. It resides 1.805 Å from the centroid of the Cp* ring and 1.830 Å from the centroid of the five-membered ring of the CpDHP moiety. Studies of a series of ruthenocenes showed that generally the ruthenium resides closer to the more electron-withdrawing cyclopentadienyl moiety than to the more electron-donating cyclopentadienyl derivative.[109c] So the fact that the ruthenium in **52** is 0.025 Å closer to the Cp* ring than

to the CpDHP five-membered ring may suggest that the electron density on the CpDHP five-membered ring is greater than that of Cp*. On the other hand, the IR spectrum of (CpDHP)$Re(CO)_3$ **51** showed that its highest CO stretch is at 2018 cm^{-1}, similar to that of Cp*$Re(CO)_3$ (2017 cm^{-1}),[110] which suggests that the donating ability of CpDHP is similar to Cp*. In other words, the electron density on the five-membered ring of CpDHP is similar to that of Cp*, which we believe is more likely.

Table 3.12. Crystallographic data for 52.

formula	$RuC_{39}H_{48}$
fw (g/mol)	617.84
crystal size, mm	0.10 x 0.24 x 0.42
cystal color	red
crystal mount	on glass fiber covered with epoxy
a, Å	12.817(2)
b, Å	17.769(3)
c, Å	29.094(5)
V, $Å^3$	6626.0(19)
cell detn, refls	516
d(calcd), g cm^{-3}	1.24
space group	Pbca
Z	8
F000	2608
λ, Å	0.71073
temp, K	223
linear abs coeff, mm^{-1}	0.50
R for merge	0.094
R1, wR2	0.041, 0.088
R1 for I>0.0σ(I)	0.098
GOF	0.94

Similar to complex **51**, there was a slight slippage of CpDHP ligand toward η^3-bonding in **52**. The slip parameter (Δ = 0.064 Å) is small for **52** and similar to that of **51** (Δ = 0.086 Å). However, the five-membered ring in **52** is more folded away from the

DHP ring than in **51**. The folding angle is found to be 14.7°, compare to 9.0° in **51**. The hinge angle is almost the same as the folding angle and found to be 13.2° (7.0° in **51**). Another difference between **51** and **52** is that the peripheral DHP carbon atoms in **52** deviate more from planarity than those in **51**. The largest deviation was found to be 0.194 Å for **52**, and only 0.068 Å in **51**.

A comparison of the bond lengths of **52** to those of benzoDHP **36** shows that **52** ($\Delta\Sigma$ = 0.070 Å) has similar bond alternation in the DHP ring to that of **36** ($\Delta\Sigma$ = 0.071 Å)[5] and slightly less than that of **51** ($\Delta\Sigma$ = 0.077 Å), and hence the bond localizing ability of the Ru-Cp* fragment of **52** is similar to that of the benzene in **36** and somewhat less than the $Re(CO)_3$ fragment of **51**. Lastly the non-bonded distances between the Ru center and the two internal methyl carbons are 4.00 Å (Ru(1)···C(37)) and 5.12 Å (Ru(1) ···C(39)), similar to the distances between Re and the two internal methyl carbons (3.87 and 5.31 Å) in **51**.

Table 3.13. Selected bond lengths (Å) for 52.

Ru(1)-C(13)	2.158(4)	C(14)-C(15)	1.435(5)
Ru(1)-C(5)	2.160(4)	C(15)-C(16)	1.453(5)
Ru(1)-C(7)	2.163(4)	C(16)-C(17)	1.346(5)
Ru(1)-C(3)	2.168(5)	C(17)-C(18)	1.450(5)
Ru(1)-C(12)	2.176(4)	C(18)-C(23)	1.355(6)
Ru(1)-C(14)	2.177(4)	C(23)-C(24)	1.414(5)
Ru(1)-C(9)	2.186(5)	C(24)-C(25)	1.370(6)
Ru(1)-C(1)	2.191(5)	C(24)-C(36)	1.515(6)
Ru(1)-C(11)	2.221(4)	C(25)-C(26)	1.418(6)
Ru(1)-C(15)	2.247(4)	C(26)-C(27)	1.363(5)
C(11)-C(15)	1.431(5)	C(27)-C(28)	1.423(6)
C(11)-C(12)	1.437(5)	C(28)-C(29)	1.354(6)
C(11)-C(35)	1.451(5)	C(29)-C(34)	1.445(5)
C(12)-C(13)	1.416(5)	C(34)-C(35)	1.344(5)
C(13)-C(14)	1.422(5)		

3.2.5.3 $Yb(CpDHP)_2(THF)_2$, 57

An ORTEP-3 diagram of the structure is shown in **Figure 3.18**. The crystal data and selected bond lengths and bond angles are given in **Table 3.14** and **3.15**, respectively.

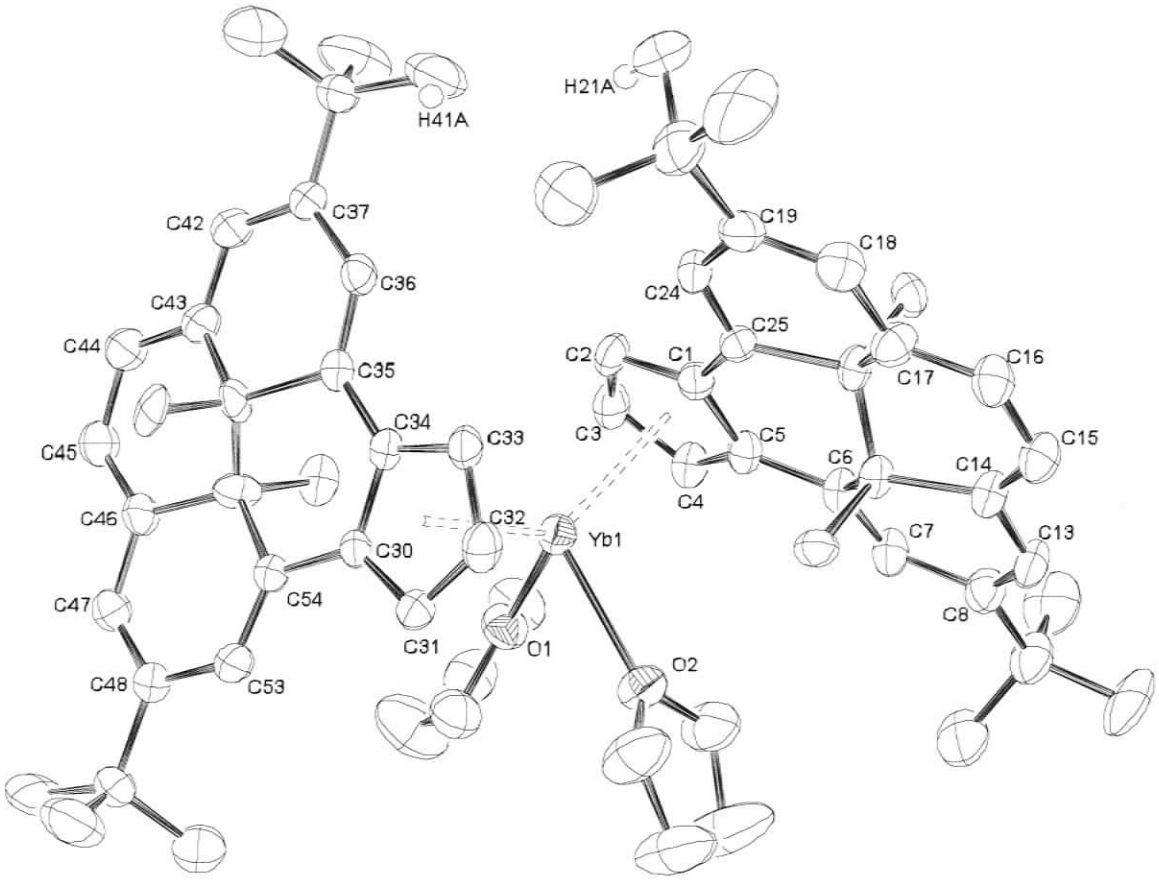

Figure 3.18. ORTEP-3[105] diagram (thermal ellipsoid 50% probability) of compound **57**. Selected hydrogen atoms are shown in calculated positions.

Because of the different arrangements of the internal methyls, **57** is chiral and exists as a *meso* form with C_i symmetry (RS) and a racemic form with C_2 symmetry (RR/SS). However, in the crystal structure, the molecule itself has no symmetry. The internal methyls are disordered, and only one contributor is shown in **Figure 3.18**.

Complex **57** is an eight-coordinate complex having a bent sandwich structure. The two CpDHP groups are bonded to the central Yb in η^5 fashions. The CpDHP moieties are essentially planar with the fold angles being only 6.7° and 7.3° respectively for the two five-membered rings. The two five-membered rings are staggered with a torsion angle C(3)-$CpDHP_{Cent}$-$CpDHP_{Cent}$-C(32) of 167.8°. Overall, the structure closely resembles the distorted-tetrahedral coordination geometry of the corresponding indenyl $Yb(C_9H_7)_2(THF)_2$[111] and fluorenyl $Yb(C_{13}H_9)_2(THF)_2$ complexes.[112]

The $CpDHP_{Cent}$-Yb-$CpDHP_{Cent}$ angle of 130.6° is larger than those in the complexes $Yb(C_9H_7)_2(THF)_2$ (128.6°)[111] and $Yb(C_{13}H_9)_2(THF)_2$ (124.87° and 125.58°),[112] obviously due to the greater steric demand of the CpDHP groups. The closest non-bonding C···C distance between the two CpDHP groups is 3.90 Å, from the distance of between two methyl carbons of the t-butyl groups (C(21)···C(41)). The closest H···H distance is found to be only 2.66 Å from the distance of H21A-H41A. The CpDHP groups show restricted rotation about the Yb-$CpDHP_{cent}$ axis in the variable temperature ^{1}H-NMR spectra, consistent with significant steric crowding. The O-Yb-O angle of 79.5° is compressed in **57** compared with those found for $Yb(C_9H_7)_2(THF)_2$ (82.3°) and $Yb(C_{13}H_9)_2(THF)_2$ (78.4 and 81.4°), again illustrating the crowded coordination sphere of the metal.

The two CpDHP groups are bonded to the central Yb in a typical partially slipped η^5 to η^3 fashion. The dihedral angle of the two five-membered rings is 53.2°. The distances of Yb-$CpDHP_{Cent}$ are 2.493 and 2.505 Å, slightly larger than the values for $Yb(C_9H_7)_2(THF)_2$ (2.440 and 2.449 Å), but similar to the values for $Yb(C_{13}H_9)_2(THF)_2$ (2.503 and 2.518 Å). The Yb-C distances range from 2.691(4)- 2.872(4) Å. The slip

parameters (Δ = 0.171 and 0.172 Å) are much larger than those of complex **51** and **52**, but are smaller than those in $Yb(C_{13}H_9)_2(THF)_2$ ((Δ = 0.25 and 0.38 Å).[9]

Table 3.14. Crystallographic data for 57.

formula	$YbO_2C_{72}H_{96}$
fw (g/mol)	116.53
crystal size, mm	0.23 x 0.33 x 0.36
cystal color	black
a, Å	19.010(3)
b, Å	15.518(2)
c, Å	22.079(3)
β, deg	109.142(3)
V, $Å^3$	6153.1(16)
cell detn, refls	303
d(calcd), g cm^{-3}	1.26
space group	$P2_1/n$
Z	4
F000	2456
λ, Å	0.71073
temp, K	223
linear abs coeff, mm^{-1}	1.56
R for merge	0.042
R1, wR2	0.035, 0.071
R1 for I>0.0σ(I)	0.064
GOF	0.92

The Yb-O distances of 2.432(3)-2.441(3) Å are slightly larger than those of $Yb(C_{13}H_9)_2(THF)_2$ (2.389-2.409 Å), but still in the Yb^{+2}-O^{thf} distances range of 2.34-2.46 Å for the known ytterbocene(+2) mono- and bis(tetrahydrofuranates).[113] The distances between the Yb and the closer internal methyl carbons (3.904-3.978 Å) and between the Yb and the farther internal methyl carbons (5.743-5.794 Å) are larger than those in **51** (3.871 Å and 5.303 Å), but not as large as in **52** (4.004 Å and 5.121 Å).

The average bond alternations ($\Delta\Sigma$) around the two [14]-DHP rings are 0.064 and 0.066 Å, slightly smaller than those of **51** ($\Delta\Sigma$ = 0.077 Å) and **52** ($\Delta\Sigma$ = 0.070 Å).

Table 3.15. Selected bond lengths (Å) and bond angles (degrees) for 57.

Yb(1)-O(1)	2.432(3)	C(16)-C(17)	1.358(5)
Yb(1)-O(2)	2.441(3)	C(17)-C(18)	1.430(5)
Yb(1)-C(32)	2.691(4)	C(18)-C(19)	1.358(5)
Yb(1)-C(33)	2.692(4)	C(19)-C(24)	1.446(6)
Yb(1)-C(3)	2.700(4)	C(24)-C(25)	1.353(5)
Yb(1)-C(2)	2.701(4)	C(30)-C(34)	1.431(5)
Yb(1)-C(31)	2.776(4)	C(30)-C(54)	1.446(5)
Yb(1)-C(4)	2.789(4)	C(34)-C(35)	1.440(5)
Yb(1)-C(34)	2.811(4)	C(35)-C(36)	1.353(5)
Yb(1)-C(1)	2.825(4)	C(36)-C(37)	1.436(5)
Yb(1)-C(30)	2.862(4)	C(37)-C(42)	1.364(6)
Yb(1)-C(5)	2.872(4)	C(42)-C(43)	1.413(5)
C(1)-C(25)	1.434(5)	C(43)-C(44)	1.363(5)
C(1)-C(5)	1.438(5)	C(44)-C(45)	1.420(6)
C(5)-C(6)	1.442(5)	C(45)-C(46)	1.354(5)
C(6)-C(7)	1.353(5)	C(45)-C(46)	1.354(5)
C(7)-C(8)	1.435(6)	C(46)-C(47)	1.430(5)
C(8)-C(13)	1.355(6)	C(47)-C(48)	1.354(5)
C(13)-C(14)	1.415(6)	C(48)-C(53)	1.444(5)
C(14)-C(15)	1.360(6)	C(53)-C(54)	1.353(5)
C(15)-C(16)	1.419(6)		
O(1)-Yb(1)-O(2)	79.47(10)		

3.2.6 Measuring the hapticity of CPDHP anion 28

As shown above from the X-ray structures, the CPDHP anion **28** behaves similarly to the indenyl anion in the solid state when coordinated to a metal center, since it shows ring slippage away from an ideal pentahapto coordination. We think it thus would be interesting to see if the CPDHP anion **28** also behaves similarly to the indenyl anion in solution, in terms of coordination modes.

As discussed in the Introduction, the indenyl hapticity in solution can be estimated from ^{13}C NMR data. The parameter $\Delta\delta^{13}C = \delta\{C(3a/7a)$ of M-Ind$\}-\delta\{C(3a/7a)$ of NaInd$\}$ reflects the solution hapticity of indenyl in a given complex: larger distortions from η^5 to η^3 result in larger downfield shifts. Where $\delta\{C(3a/7a)$ of M-Ind$\}$and $\delta\{C(3a/7a)$ of NaInd$\}$ were the ^{13}C-NMR chemical shifts of the ring junction carbon atoms C(3a) and C(7a) of indenyl in metal complexes IndMLn and NaInd respectively. $\Delta\delta^{13}C$ was the difference of these chemical shifts.

The parameter $\Delta\delta^{13}C$ can be derived for CPDHP complexes by using the analogous equation: $\Delta\delta^{13}C = \delta\{C(11a/11f)$ of M-CPDHP$\}-\delta\{C(11a/11f)$ of LiCPDHP$\}$. Thus the average ^{13}C NMR chemical shifts for the ring junction carbon atoms C(11a) and C(11f) for CPDHP anion **28**, metal complexes **51**, **52**, **54** and **57** and the corresponding $\Delta\delta^{13}C$ are listed in **Table 3.16**. The slip parameter Δ from X-ray structures for **51**, **52** and **57** are also listed for comparison.

Table 3.16 The average ^{13}C-NMR chemical shifts (δ) of C(11a) and C(11f) and the corresponding $\Delta\delta^{13}C$ in **28**, **51**, **52**, **54, 57** and the slip parameters (Δ) for **52**, **54** and **57.**

Compound	δ(ppm)	$\Delta\delta^{13}C$(ppm)	Δ(Å)
28	122.53	-	-
51	104.16	-18.37	0.086
52	87.08	-35.47	0.064
54	83.68 & 82.98[a]	-38.85 & -39.55	-
57	122.19 & 121.91[a]	-0.34 & -0.62	0.172

a. Values from two isomers

We can see from **Table 3.16,** that the smallest upfield shift from anion **28** was observed in the Yb complex **57** followed by the Re complex **51** and the Ru complex **52.** The iron complex **54** has the largest upfield shift from anion **28**. If CPDHP anion **28** behaves similarly as indenyl anion in solution, this would mean that the distortions from η^5 to η^3 coordination mode would follow the order of : **57 > 51 > 52 > 54**. This is actually the distortion order observed in the solid state (**Table 3.16**), where the slip parameter Δ follow the order of : **57 > 51 > 52**. Thus we found that the CPDHP anion **28** behaves similarly to the indenyl anion when coordinated to metal centers in terms of coordination modes and hapticity both in solution and in solid state.

Chapter Four

Conclusions

The synthesis of cyclopentadiene-fused dimethyldihydropyrene, CpDHP(H) **44**, from DHP **31** was achieved in a seven-step synthesis in an overall yield of 7%. Deprotonation of **44** gave the Cp anion fused DHP (CpDHP anion) **28**. Anion **28** is photochromic and its photoswitching behavior is intermediate between the no aromatic fused parent DHP 31 and the benzannelated DHP 36. Analysis of the ^{1}H-NMR data showed that the Cp anion has similar bond fixing effect on the DHP ring as benzene does, but to a lesser extent.

While the reactions of **28** with $Re(CO)_5Br$, $(Cp^*RuCl_2)_n$ and $FeCl_2$, yielded $(CpDHP)Re(CO)_3$ **51**, $Cp^*Ru(CpDHP)$ **52** and $(CpDHP)_2Fe$ **54** respectively, the reactions with Mn, Y, Yb(III) or Zr compounds either returned the starting materials, caused decomposition of **28** or gave unidentified products. Reaction of the protonated form CpDHP(H) **44** with $Yb[N(SiMe_3)_2](thf)_2$ afforded $Yb(CpDHP)_2(thf)_2$ **57**.

The metal complexes **51** and **52** are photochromic, but **54** and **57** are not. The reason for the shut-down of the photochromism in **54** and **57** is still not known. Study of the photochromism of **51** and **52** found that complexation to Re and Ru center improved the photoopening process from partial opening of **28** to complete opening of **51** and **52**, but did not change the relative opening and closing rates much. The thermal return reactions, on the other hand, have been slowed down substantially after complexation to metal centers.

The diamagnetic susceptibility, χ, of metal moiety Cp^*Ru was calculated to be -549×10^{-36} m^3/molecule, in a good agreement of the value (-478×10^{-36} m^3/molecule) obtained previously. The same parameter for $Re(CO)_3$ was calculated for the first time to be -880 m^3/molecule with the center of the anisotropy located the metal atom and –1557

m^3/molecule with the "supercarbonyl" method respectively. Similarly the χ value of (CpDHP)Fe was calculated to be -1750 m^3/molecule.

Analysis of the NMR data of the metal complexes showed that the metal moieties have more bond fixing ability than benzene and the relative bond fixing ability order was CpRuCp* > CpFe(CpDHP) > $CpRe(CO)_3$ > Benzene-$Cr(CO)_3$ > benzene. Both the **[a]-2,7-H-series** and the **[e]-2,7-di-t-butyl-series** gave the same results that CpRuCp* has greater RBFA than Benzene-$Cr(CO)_3$, which in turn has greater RBFA than benzene itself.

The X-ray structures of **51**, **52** and **57** were analyzed and all three complexes were found to be η^5-coordinated. The structural data also confirmed the bond fixing abilities of the metal complexes and confirmed there are no significant geometry changes during complexation.

Chapter Five

Experimental

5.1 General Procedure and Instrumentation

The manipulations of the anion and its metal complexes were carried out under an argon atmosphere, with the rigorous exclusion of oxygen and water, using standard glovebox (Braun MB150-GH) or Schlenk techniques, except as noted in the text. Tetrahydrofuran(THF), diethyl ether, hexane and toluene were dried by distillation from sodium benzophenone ketyl under argon immediately prior to use. $LiCH_2SiMe_3$ was prepared from Li powder and Me_3SiCH_2Cl in hexane. The oligomeric $(CpRuCl_2)_n$ was synthesized by refluxing ruthenium trichloride hydrate and pentamethylcyclopentadiene in ethanol[114]. $Yb[N(SiMe_3)_2]_2(THF)_2$, $Y[N(SiMe_3)_2]_3$, $Y[N(HSiMe_2)_2]_3(THF)_2$ were prepared as reported in the literature[115]. Anhydrous metal trichlorides (Yb and Y) were prepared from the hydrated salts by prolonged reflux in neat $SOCl_2$ followed by vacuum distillation and drying at 150 °C (10^{-2} torr) for 16 to 20 h. All other chemicals were of reagent grade, unless otherwise specified.

Proton NMR spectra were recorded either on a Bruker AVANCE 500 spectrometer at 500 MHz or a Bruker AMX 360 spectrometer at 360 MHz, using the solvent residual peak for calibration. Kinetic data was obtained using a Bruker AC 300 MHz spectrometer. Carbon NMR spectra were recorded at 125.8 or 90.6 or 75.0 MHz, using the solvent peak for calibration. Where peaks within the same sample are very close in chemical shift, a third decimal place is given. ^7Li NMR spectra were recorded at 139.9 MHz. The chemical shifts are referenced to external 1M LiCl in D_2O. For the anion and its metal complexes, spectra were recorded at room temperature unless otherwise specified in C_6D_6 or C_7D_8, dried over activated 4 Å molecular sieves, or in C_4D_8O previously distilled from sodium under argon, using 5-mm tubes fitted with a

Teflon valve (Brunfeldt). All solvents were thoroughly degassed prior to use. Melting points were determined on a Reichert 7905 melting point apparatus integrated to an Omega Engineering Model 199 Chromel-alumel thermocouple. Infrared spectra, calibrated with polystyrene, were recorded as KBr disks on a Bruker IFS25 FT-IR spectrometer and only the major fingerprint bands are reported. UV-Visible spectra were recorded on a Cary 5 UV-VIS-NIR spectrometer. Mass spectra were recorded on a Finnigan 3300 gas chromatography-mass spectroscopy system using methane as a carrier gas for chemical ionization. Exact mass measurements were done on a Kratos Concept-H instrument using perfluorokerosene as the standard. X-ray crystallographic details are given in Appendix. Elemental analyses were performed by Canadian Microanalytical Services Ltd., Vancouver, B.C. All evaporations were carried out under reduced pressure on a rotary evaporator, or by using an oil pump and liquid nitrogen condenser. SiGel refers to Merck silica gel, 60-200 mesh and was deactivated by 5% (by weight) water. NMR assignments were made on the basis of 2D COSY/NOESY experiments for ^{1}H and HETCORR/HMQCB experiments for ^{13}C. H-1,2 means H-1 and H-2; H-1/2 means H-1 or H-2. Expanded data sets were used to obtain coupling constant data.

5.2 Syntheses

2,7-Di-*tert*-butyl-4-formyl-*trans*-10b,10c-dimethyl-10b,10c-dihydropyrene (45)

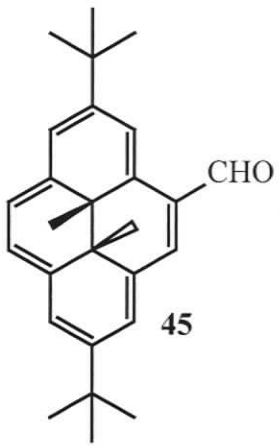

45

This is a modified procedure of Miyazawa[116] suitable for a larger scale. $TiCl_4$ (12.00 mL. 100 mmol) was added with stirring under N_2 to a solution of dihydropyrene **31** (6.88 g, 20.0 mmol) and Cl_2CHOCH_3 (2.40 mL, 28.0 mmol) in CH_2Cl_2 (650 mL) at 0 °C. The resulting red-brown solution then was stirred at 20 °C for 5 h, and then added slowly to ice-water (700 mL). The aqueous layer was extracted with CH_2Cl_2 (500 mL) and then the combined organic layers were washed with water, dried ($MgSO_4$), and evaporated. The resulting brown solid was chromatographed over silica gel. Unchanged green **31** (3.45 g, 10.0 mmol, 50%) was eluted first with hexanes. Then hexanes-CH_2Cl_2 (1:1) eluted the product **45** (3.24 g, 44%) as dark brown crystals, mp 192-194 °C (lit.[3] mp 193-194 °C), identical with an authentic sample.

Ethyl 3-[4'-(2',7'-di-*tert*-butyl-*trans*-10b',10c'-dimethyl-10b',10c'-dihydropyrenyl)]-propenoate (46)

Triethyl phosphonoacetate [$(EtO)_2POCH_2CO_2Et$] (8.90 mL, 45 mmol) was added to a stirred suspension of 60% NaH (4.32 g, 180 mmol) in dry THF (450 mL) under N_2 at 0 °C. After 1 h, a solution of aldehyde **45** (5.58 g, 15.0 mmol) in dry THF (500 mL) was added dropwise, and then the mixture was allowed to stir without further cooling for

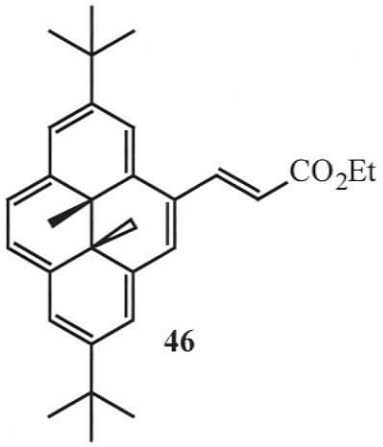

46

an additional hour. Saturated NH_4Cl solution (500 mL) was then added, and the solution was extracted with CH_2Cl_2 (4 × 500 mL). The combined organic extracts were washed well with water, dried, and evaporated to a dark brown solid. This was chromatographed over silica gel, with hexane-CH_2Cl_2 (1:3) as eluant to yield 5.3 g (80%) of ester **46** as dark reddish brown crystals from MeOH, mp 165-166 °C. ^{1}H NMR (360 MHz, $CDCl_3$) δ 9.16 (d, J = 15.6 Hz, 1H, H-3), 8.89 (s, 1H, H-3'), 8.69 (s, 1H, H-5'), 8.483 (s, 1H, H-1'), 8.475 (s, 1H, H-6'/8'), 8.46 (s, 1H, H-8'/6'). 8.42 (AB, J = 8.2 Hz, 1H, H-9'), 8.38 (AB, 1H, H-10'), 6.83 (d, J = 15.6 Hz, 1H, H-2), 4.37 (q, J = 7.1 Hz, 2H, -OC*H*$_2$CH$_3$), 1.69 and 1.65 (s, 9H each, *t*-Bu), 1.41 (t, J = 7.1 Hz, 3H, OCH$_2$C*H*$_3$), -3.777 and -3.786 (s, 3H each, CH$_3$-10c',10b'); ^{13}C NMR (90.6 MHz, $CDCl_3$) δ 167.92 (C-1), 147.73/146.47 (C-2'/7'), 141.55 (C-3), 138.94/137.12/136.88/136.46 (C-3a'/5a'/10a'/10d'), 124.73 (C-9'/10'), 124.64 (C-4'), 123.87 (C-10'/9'), 122.32/121.70/121.55 (C-1'/6'/8'), 119.73 (C-5'), 117.02 (C-2), 115.93 (C-3'), 60.33, 36.43/35.88 (*C*(CH$_3$)$_3$), 31.84/31.75 (C(*C*H$_3$)$_3$, 31.45 (C-10b'), 29.87 (C-10c'), 15.34/15.21 (10b',10c'-*C*H$_3$), 14.49; IR (KBr) ν 1700, 1608, 1286, 1169, 1158, 1034, 970, 886, 867, 674, 660 cm^{-1}; HRMS *m/z* calcd for $C_{31}H_{38}O_2$ 442.2872, found 442.2874. Anal. Calcd: C, 84.12; H, 8.65. Found: C, 83.83; H, 8.79.

Ethyl 3-[4'-(2',7'-di-*tert*-butyl-*trans*-10b',10c'-dimethyl-10b',10c'-dihydropyrenyl)]-propanoate (47)

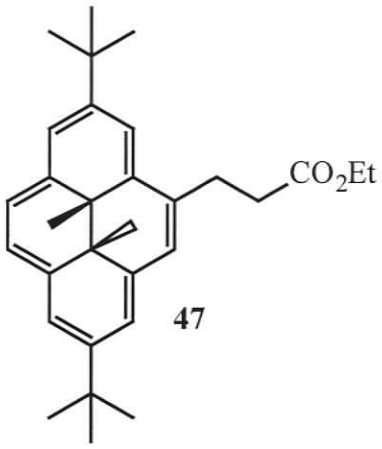

47

Palladium on activated charcoal (300 mg, 10%) was added to the unsaturated ester **46** (3.98 g, 9.00 mmol) in EtOAc (500 mL) and then the mixture was stirred under H_2 (1 atm) at 20 °C for 3 h, during which time the mixture turned green. The catalyst was removed on Celite, which was washed with CH_2Cl_2 (3 × 75 mL), and then the combined solutions were evaporated to give a green residue. This was chromatographed over silica gel with hexane-CH_2Cl_2 as eluant to yield 3.92 g (98%) of the saturated ester **47** as a green oily solid. This could not be crystallized satisfactorily, though by ^{1}H NMR it was sufficiently pure to be used directly in the next step. ^{1}H NMR (500 MHz, $CDCl_3$) δ 8.66 (s, 1H), 8.47 (s, 1H), 8.44 (s, 1H), 8.43 (s, 1H), 8.364 (AB, J = 8 Hz, 1H), 8.359 (AB, 1H), 8.34 (s, 1H), 4.08 (t, J = 7 Hz, 2H), 3.93 (q, J = 7 Hz, 2H), 2.96 (t, J = 7 Hz, 2H), 1.68 and 1.65 (s, 9H each), 1.14 (t, J = 7 Hz, 3H), -3.97 and -4.02 (s, 3H each); ^{13}C NMR (125.8 MHz, $CDCl_3$) δ 173.72, 145.99, 145.00, 137.13, 137.07, 136.92, 132.86, 132.02, 124.64, 123.01, 122.61, 120.85, 120.54, 120.49, 117.10, 60.59, 37.02, 36.33, 36.13, 32.25, 32.13, 30.13, 29.95, 29.43, 14.81, 14.61, 14.39; HRMS *m/z* calcd for $C_{31}H_{40}O_2$ 444.3028, found 444.3029.

3-[4'-(2',7'-Di-*tert*-butyl-*trans*-10b',10c'-dimethyl-10b',10c'-dihydropyrenyl)]-propanoic acid (48)

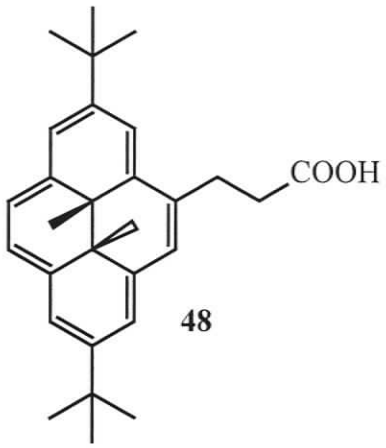

48

The crude saturated ester **47** from above (3.52 g, 7.92 mmol) in THF (400 mL) was mixed with 2 M NaOH (740 mL) and refluxed for 16 h under argon. The solution was cooled and then neutralized with 2 M HCl (740 mL) and then was extracted with CH_2Cl_2. The combined organic extracts were washed, dried, and evaporated to a green residue. This was chromatographed over silica gel with CH_2Cl_2 as eluant to yield 3.0 g (91%) of the acid **48** as a green solid by evaporation from CH_2Cl_2, mp 161-162 °C. ^{1}H NMR (500 MHz, $CDCl_3$) δ 11.5-10.0 (v br s, 1H, -COOH), 8.66 (s, 1H), 8.48 (s, 1H), 8.45 (s, 1H), 8.44 (s, 1H), 8.373 (AB, J = 8.7 Hz, 1H), 8.369 (AB, 1H), 8.35 (s, 1H), 4.00-3.89 (m, 2H), 3.09-2.96 (m, 2H), 1.66 and 1.68 (s, 9H each), -3.96 and -4.01 (s, 3H each); ^{13}C NMR (125.8 MHz, $CDCl_3$) δ 178.20, 146.06, 145.08, 137.11, 137.09, 136.95, 132.83, 131.50, 124.48, 123.35, 123.09, 122.70, 120.91, 120.62, 117.01, 36.44, 36.36 (C-2), 36.14, 32.25/32.13 ($C(CH_3)_3$), 30.15/29.94 (C-10b,c), 29.02 (C-3), 14.84, 14.64; IR (KBr) ν 3300-2600 (br, -COOH), 1706, 883, 668 cm^{-1}; HRMS *m/z* calcd for $C_{29}H_{36}O_2$ 416.2715, found 416.2710. Anal. Calcd: C, 83.61; H, 8.71. Found: C, 83.55; H, 8.77.

2,7-Di-*tert*-butyl-*trans*-11c,11d-dimethyl-9,10,11c,11d-tetrahydro-11-oxo-11H-cyclopenta[*e*]pyrene (49)

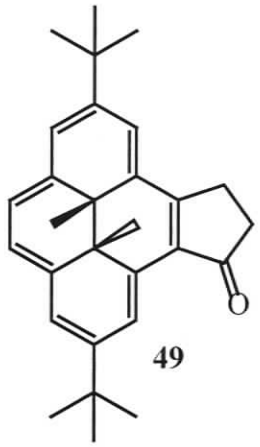

49

Oxalyl chloride (5.27 mL, 60 mmol) was added at 20 °C under argon with stirring to a solution of acid **48** (5.00 g, 12 mmol) in dry CH_2Cl_2 (700 mL). After the solution was stirred for 6 h, the solvent was evaporated (under vacuum) and the green residue was pumped upon for an additional 30 min to remove all chlorinating reagent. The oily residue was then redissolved in dry CH_2Cl_2 (1 L) and $BF_3{\cdot}OEt_2$ (3.05 mL, 24 mmol) was added, and the mixture was stirred at 20 ° C for 12 h. Ice-water was then added and the organic extracts were washed, dried, and evaporated to a reddish brown solid. This was chromatographed on silica gel with hexane-CH_2Cl_2 (1:1) to elute 2.06 g (43%, 65% based on returned acid) of the dark red ketone **49**. Elution with CH_2Cl_2 then eluted returned acid **48** (1.66 g, 33%). Ketone **49** as crystallized by evaporation of a hexane-CH_2Cl_2 solution had mp 185-187 ° C. ^{1}H NMR (500 MHz, $CDCl_3$) δ 9.84 (s, 1H, H-1), 8.72 (d, J = 1.0 Hz, 1H, H-8), 8.50 (s, 1H, H-6), 8.40 (s, 1H, H-3), 8.35 (AB, J = 7.26 Hz, 1H, H-5), 8.25 (AB, 1H, H-4), 3.97 and 3.87 (each dt, J = 17.2, 5.9 Hz, 2H, H-9), 3.10 (~t, J = 6 Hz, 2H, H-10), 1.677 and 1.669 (s, 9H each, 2,7-C(CH_3)$_3$), -3.71 and -3.74 (s, 3H each, 11c,d-CH_3); ^{13}C NMR (125.8 MHz, $CDCl_3$) δ 208.95 (C-11), 150.47 (C-2), 149.26 (C-11f), 144.55 (C-7), 139.73 (C-3a), 136.31 (C-5a), 133.02 (C-11b), 130.49 (C-11e), 125.98 (C-11a), 125.05 (C-5), 124.04 (C-6), 122.45 (C-4), 120.85 (C-8), 120.63 (C-3), 119.09 (C-1), 37.52 (C-10), 36.47 (2-*C*(CH$_3$)$_3$), 35.95 (7-*C*(CH$_3$)$_3$), 31.93 (2-C(*C*H$_3$)$_3$), 31.78 (7-C(*C*H$_3$)$_3$), 31.33 (C-11c), 30.44 (C-11d), 24.66 (C-9), 15.40 (11c-

CH_3), 14.77 (11d-CH_3); IR (KBr) ν1681, 1462, 1261, 1211, 883 cm^{-1}; UV-vis (cyclohexane) λ_{max} (ε_{max}) nm 340 (32 000), 365 (32 000), 400 (39 000), 485 (6400), 510 (7100), 605 (1300), 670 (4400); HRMS *m/z* calcd for $C_{29}H_{34}O$ 398.2610, found 398.2612. Anal. Calcd: C, 87.39; H, 8.60. Found: C, 87.44; H, 8.58.

2,7-Di-*tert*-butyl-*trans*-11c,11d-dimethyl-11c,11d-dihydro-9*H*-cyclopenta[*e*]pyrene (44)

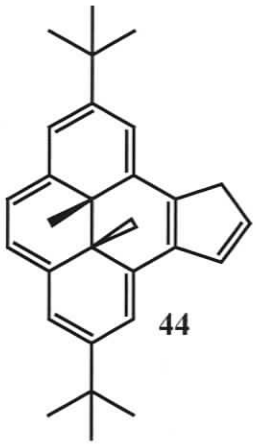

$NaBH_4$ (200 mg, 5.26 mmol) was added to a stirred solution of ketone **49** (180 mg, 0.45 mmol) in MeOH-THF (1:1, 180 mL) under argon at 20 °C and stirring was continued for 2 h, when the solution had become green. Ice-water was then added, followed by CH_2Cl_2. The organic extracts were washed, dried, and evaporated to alcohol **50** as a green solid. This was dissolved in degassed THF (30 mL), and under argon, degassed aq HCl (2 M, 30 mL) was added with stirring at 20 °C. The mixture was stirred for 1 h and then ice-water and CH_2Cl_2 were added. The organic extracts were washed, dried, and evaporated and the green residue was flash chromatographed over silica gel under argon with hexanes as eluant and on evaporation gave 150 mg (88%) of yellow-green cyclopentadiene **44**, mp ~184 °C dec. This compound is not very stable, especially in chlorinated solvents, and is best generated from ketone **49** as required. ^1H NMR (500 MHz, C_6D_6) δ 8.89 (d, *J* = 1.0 Hz, 1H, H-1), 8.71 (d, *J* = 1.2 Hz, 1H, H-8), 8.60 (s, 1H, H-3), 8.59 (s, 1H, H-6), 8.45 and 8.43 (AB, *J* = 7.7 Hz, 2H, H-4/5), 7.90 (dt, *J* = 5.6, 1.9 Hz, 1H, H-11), 6.63 (dt, *J* = 5.6, 2.1 Hz, 1H, H-10), 4.04 and 4.09 (dt, *J* = 23, 2 Hz, 2H,

H-9), 1.68 (s, 9H, 7-C(CH_3)$_3$), 1.65 (s, 9H, 2-C(CH_3)$_3$), -3.48 (s, 3H, 11c-CH_3), -3.51 (s, 3H, 11d-CH_3); ^{13}C NMR (125.8 MHz, C_6D_6) δ 145.21 (C-7), 144.47 (C-2), 139.03 (C-11a), 137.36 (C-5a), 136.65 (C-11f), 136.61 (C-3a), 133.53 (C-10), 131.85 (C-11), 131.27 (C-11e), 129.40 (C-11b), 123.64 (C-4), 123.03 (C-5), 121.24 (C-3), 120.60 (C-6), 117.54 (C-1), 116.37 (C-8), 38.82 (C-9), 36.09 (7-C(CH_3)$_3$), 36.05 (2-C(CH_3)$_3$), 32.15 (7-C(CH_3)$_3$), 32.08 (2-C(CH_3)$_3$), 31.46 (C-11c), 31.40 (C-11d), 15.44 (11c-CH_3), 15.13 (11d-CH_3); IR (KBr) ν3030, 883, 867, 730, 690, 668, 634 cm^{-1}; UV-vis (cyclohexane) λ_{max} (ε_{max}) nm 365 (41 000), 395 (36 000), 470 (7500), 490 (9000), 675 (1300) [note: in THF the last two maxima shift to 495 and 670 nm]; HRMS *m/z* calcd for $C_{29}H_{34}$ 382.2660, found 382.2665. Anal. Calcd: C, 91.04; H, 8.96. Found: C, 90.79; H, 9.21.

Generation of lithium [or potassium] cyclopentadienide 28

Diene **44** (5 mg, 0.013 mmol) was dissolved in d_8-THF (0.6 mL) in a sealable NMR tube under nitrogen. $LiCH_2SiMe_3$ (1.3 mg, 0.014 mmol) [or KH (~0.6 mg, 0.014 mmol)] was added at 20 °C, and the tube was sealed and shaken. The anion **28** formed immediately as a dark green solution. ^{1}H NMR (500 MHz, d_8-THF) δ 7.62 (d, J = 1.5 Hz, 2H, H-1,8), 7.02 (d, J = 1.5 Hz, 2H, H-3,6), 6.98 (d, J = 3.4 Hz, 2H, H-9,11), 6.87 (s, 2H, H-4,5), 6.65 (t, J = 3.4 Hz, 1H, H-10), 1.48 (s, 18H, 2,7-C(CH_3)$_3$), -1.82 (s, 6H, 11c,d-CH_3); ^{13}C NMR (90.6 MHz, d_8-THF) δ 143.94 (C-2,7), 138.73 (C-11b,e), 138.38 (C-3a,5a), 122.53 (C-11a,f), 117.55 (C-4,5), 113.16 (C-3,6), 112.55 (C-10), 107.78 (C-1,8), 99.08

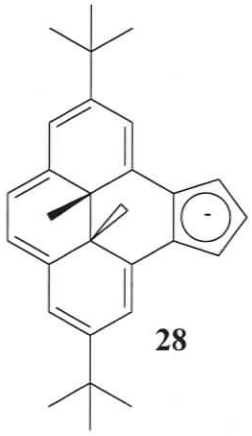

28

(C-9,11), 37.87 (C-11c,11d), 35.76 (2,7-*C*(CH_3)$_3$), 31.69 (2,7-C(*C*H_3)$_3$), 18.97 (11c,d-*C*H_3). When d_8-toluene or d_6-benzene was used as the solvent, similar proton spectra with much broader lines were observed. When d_8-THF was added, normal spectra were obtained. UV-vis (cyclohexane) λ_{max} (ε_{max}) nm 345 (35 000), 350 (36 000), 390 (28 000), 395 (29 000), 490 (8000), 655 (780) (tail absorption between 500 and 700, see **Figure 3.2**.

Photoopening of dihydropyrene anion 28 to cyclophanediene anion 28'

The NMR sample of **28** from above was placed in an ice-water bath and irradiated with a 500-W tungsten lamp with use of a 490-nm filter such that the sample was irradiated with visible light of >490 nm wavelength. After a few hours of irradiation, a photostationary state was reached, where NMR indicated about 85% of the open form, the CPD anion **28'**, had formed: ^{1}H NMR (300 MHz, d_8-THF) δ 6.88 (d, J = 2 Hz, H-6,15), 6.53 (d, J = 2 Hz, H-4,17), 6.26 (s, H-1,2), 5.88 (d, J = 4 Hz, H-10,12), 5.61 (t, J = 4 Hz, H-11), 1.33 (s, 8,19-CH_3), 1.26 (s, 2,7-C(CH_3)$_3$); ^{13}C NMR (360 MHz, d_8-THF) δ 148.65, 144.29, 139.20, 137.76, 132.54, 125.84, 124.98, 122.50, 104.25, 103.52, 34.60, 32.17, 20.85; for the UV-vis spectrum of the 85% photostationary state, see **Figure 3.2**.

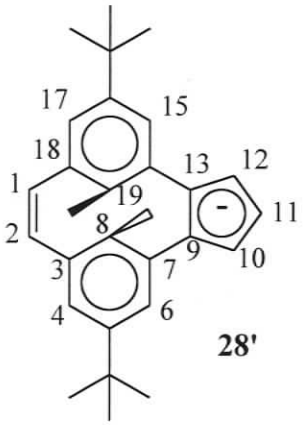

28'

[9, 10, 11, 11a, 11f- η^5]-*trans*-11c, 11d-Dimethyl-11c, 11d-dihydrocyclopent[e]-pyrene-tricarbonylrhenium(I) 51

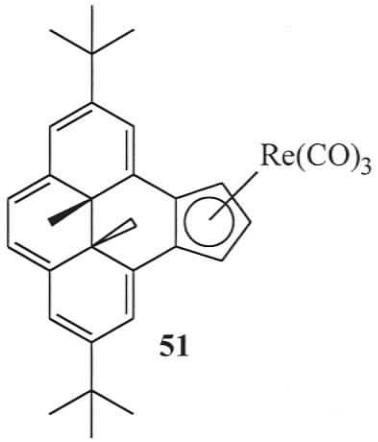

51

The anion **28** was generated by the treatment of a solution of diene **44** (69 mg, 0.18 mmol) in toluene (10 mL) with $LiCH_2SiMe_3$ (25 mg, 0.27 mmol) at room temperature overnight in the glove box. Then solid $Re(CO)_5Br$ (99mg, 0.25 mmol) was added, followed by toluene (3 mL). The resulting mixture was stirred at room temperature in the dark for 4 days. Solvent was then removed and the residue was chromatographed over deactivated neutral Al_2O_3 using hexane : CH_2Cl_2 (6 : 1) under Ar to give 60 mg (51%) of complex **51** as a bright red solid. Recrystallization from hot hexane yielded red crystals, mp 172 °C. ^{1}H NMR (500 MHz, C_6D_6) δ 7.41 and 7.35 (d, J = 1.4 Hz, 1H each, H-1/8), 7.003 and 6.995 (t, J = 1.1 Hz, 1H each, H-3/6), 6.66 and 6.62 (dAB, $J_{3,4/5,6}$ = 0.8 Hz, $J_{4,5}$ = 6.3 Hz, 2H, H-4,5), 5.18 (d, J = 2.9 Hz, 2H, H-9,11), 4.95 (t, J = 2.9 Hz, 1H, H-10), 1.313 and 1.310 (s, 9H each, 2,7-C(CH_3)$_3$), -0.23 and –0.77 (s, 3H each, 11c, d-CH_3); ^{13}C NMR (125.8 MHz, C_6D_6) δ 194.71 (Re-*C*O), 144.57 and 144.19 (C-2/7), 138.94 (C-3a, 5a), 130.15/129.81 (C-11b/11e), 122.29/121.94 (C-4/5), 120.92 (C-8/1), 120.86/120.84 (C-3/6), 119.76 (C-1/8), 104.62/103.69 (C-11a/11f), 89.78 (C-10), 72.26/70.02 (C-9/11), 38.55/38.35 (C-11c/11d), 35.11/35.03 (2,7-*C*(CH_3)$_3$), 30.12/30.09 (2,7-C(CH_3)$_3$), 25.12/18.23 (11c,d-CH_3); IR (CH_2Cl_2) ν_{CO} 2018, 1924 cm^{-1}; UV-vis (cyclohexane) λ_{max} (ε_{max}) nm 305 (1.7 x 10^5), 358 (2.4 x 10^5), 373 (2.6 x 10^5), 482 (7.2 x 10^4); HRMS *m/z*

calcd for $C_{32}H_{33}O_3Re$ 652.1987, found 652.1991. Anal. Calcd: C, 58.97; H, 5.10. Found: C, 58.75; H, 5.17.

Photoopening of the dihydropyrene tricarbonylrhenium(I) 51 to the cyclophanediene tricarbonylrhenium(I) 51'

The NMR sample of **51** from above was placed in an ice-water bath and irradiated with a 500-W tungsten lamp with use of a 490-nm filter such that the sample was irradiated with visible light of >490 nm wavelength. After ca. 30 mins of irradiation, the dihydropyrene pentamethylcyclopentadienyl-ruthenium(II) **51** was converted to the cyclophanediene pentamethylcyclopentadienylruthenium(II) **51'**: ^{1}H NMR (500 MHz, C_6D_6) δ 6.89 (d, J = 2.1 Hz, 1H, H-6/15), 6.81 (d, J = 2.1 Hz, 1H, H-4/17), 6.75 (d, J = 2.1 Hz, 1H, H-17/4), 6.23 (s, 2H, H-1,2), 5.07 and 4.85 (dd, J = 2.9 Hz, J = 1.9 Hz, 1H each, H-10/12), 4.43 (t, J = 2.9 Hz, 1H, H-11), 1.33 and 1.20 (s, 9H each, 5, 16-C(CH_3)$_3$), 1.56 and 1.14 (s, 3H each, 8,19-CH_3); One hydrogen signal (H-6 or 15) lies underneath the solvent residue peak of C_6H_6. ^{13}C NMR (125.8 MHz, C_6D_6) δ 195.02 (Re-*C*O), 139.72/139.67 (C-8/19), 138.23/137.50 (C-3/18), 132.21/132.04 (C-1/2), 131.06/130.99 (C-7/14), 129.34/126.71 (C-6/15), 124.58/123.66 (C-4/17), 118.76/107.21 (C-9/13), 81.93 (C-10/12), 81.64 (C-

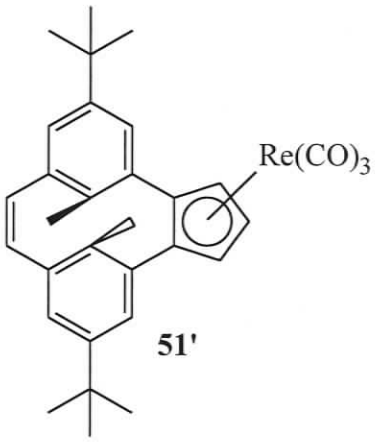

51'

11), 80.93 (C-12/10), 34.19/34.05 (5,16-*C*(CH_3)$_3$), 31.28/31.25 (5,16-C(*C*H_3)$_3$), 20.67/18.76 (8,19-*C*H_3).

[9, 10, 11, 11a, 11f- η^5]-*trans*-11c, 11d-Dimethyl-11c, 11d-dihydrocyclopent[e]pyrene -pentamethylcyclopentadienylruthenium(II) 52

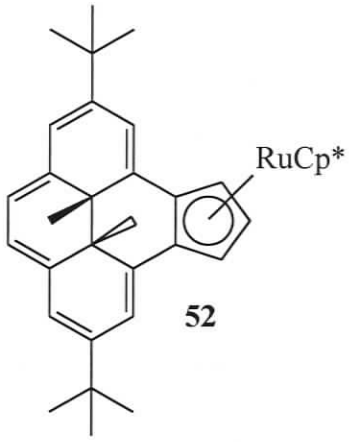

52

Method A: A solution of diene **44** (40 mg, 0.10 mmol) and $LiCH_2SiMe_3$ (38 mg, 0.40 mmol) in toluene (5 mL) was stirred at room temperature overnight in the glove box. Solid $(Cp^*RuCl_2)_n$ (46 mg, 0.15 mmol) was then added, followed by toluene (5 mL). The resulting reddish brown mixture was then stirred at room temperature in the dark overnight, and then was heated to ca. 60 °C for 2 hrs. The mixture was then filtered through Celite and the filtrate was dried under vacuum. The reddish brown residue was chromatographed over deactivated neutral alumina under Ar using hexane **:** benzene (6 **:** 1) as eluant to give 18 mg (29%) of complex **52** as a red solid.

Method B: A solution of diene **44** (38 mg, 0.10 mmol), $LiCH_2SiMe_3$ (28 mg, 0.30 mmol) and $(Cp^*RuCl_2)_n$ (34 mg, 0.11 mmol) in toluene (15 mL) was stirred at room temperature in the dark for 3 days in the glove box. The reaction mixture was then filtered through Celite, and the filtrate was dried and chromatographed over deactivated neutral alumina under Ar using hexane as eluant to give 20 mg (32%) of complex **52** as a red solid. Recrystallization from hot hexane gave red crystals, mp 182-183 °C. ^{1}H NMR (500 MHz, C_6D_6) δ 7.13 (d, J = 1.4 Hz, 1H, H-8/1), 7.04 (d, J = 1.5 Hz, 1H, H-

1/8), 6.80 (d, J = 1.3 Hz, 1H, H-3/6), 6.75 (d, J = 1.4 Hz, 1H, H-6/3), 6.51 and 6.50 (AB, J = 6.3 Hz, 2H, H-4,5), 4.99 (d, J = 2.3 Hz, 1H, H-9/11), 4.92 (d, J = 2.4 Hz, 1H, H-11/9), 4.15 (t, J = 2.4 Hz, 1H, H-10), 1.67 (s, 15H, $C_5(CH_3)_5$), 1.35 and 1.33 (s, 9H each, 2,7-$C(CH_3)_3$), 0.42 and 0.09 (s, 3H each, 11c,d-CH_3); ^{13}C NMR (125.8 MHz, C_6D_6) δ 144.85/144.51 (C-2/7), 140.26/140.19/138.39/137.95 (C-11b/11e/3a/5a), 120.81/120.57 (C-4/5), 118.26/117.87 (C-3/6), 115.77/115.41 (C-1/8), 87.47/86.69 (C-11a/11f), 84.83 (C_5Me_5), 74.77 (C-10), 71.49/67.72 (C-9/11), 40.69 (C-11c, 11d), 34.88/34.83 (2,7-$C(CH_3)_3$), 30.12/30.07 (2,7-$C(CH_3)_3$), 25.11/20.09 (11c,d-CH_3), 11.30 ($C_5(CH_3)_5$); IR (KBr) ν 3025, 2961, 2863, 1632, 1457, 1360, 1225, 1029, 869, 676 cm^{-1}; UV-vis (cyclohexane) λ_{max} (ε_{max}) nm 267 (1.7 x 10^5), 300 (1.7 x 10^5), 370 (2.7 x 10^5), 492 (5.5 x 10^4); HRMS m/z calcd for $C_{39}H_{48}Ru$ 618.2793, found 618.2792.

Photoopening of the dihydropyrene pentamethylcyclopentadienylruthenium(II) 52 to the cyclophanediene pentamethylcyclopentadienylruthenium(II) 52'

The NMR sample of **52** from above was placed in an ice-water bath and irradiated with a 500-W tungsten lamp with use of a 490-nm filter such that the sample was irradiated with visible light of >490 nm wavelength. After ca. 30 mins of irradiation, the dihydropyrene pentamethylcyclopentadienyl-ruthenium(II) **52** was converted to the cyclophanediene

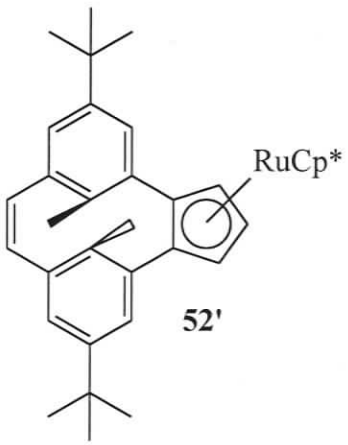

52'

pentamethylcyclopentadienylruthenium(II) **52'**: ^{1}H NMR (500 MHz, C_6D_6) δ 7.24 (d, J = 2.1 Hz, 1H, H-6/15), 7.14 (d, J = 2.2 Hz, 1H, H-15/6), 6.93 (d, J = 2.2 Hz, 1H, H-4/17), 6.83 (d, J = 2.1 Hz, 1H, H-17/4), 6.42 and 6.39 (AB, J = 11.4 Hz, 2H, H-1,2), 4.73 (dd, J = 1.1 & 2.3 Hz, 1H, H-12/10), 4.52 (dd, J = 1.1 & 2.3 Hz, 1H, H-10/12), 4.04 (t, J = 2.3 Hz, 1H, H-11), 1.83 (s, 15H, $C_5(CH_3)_5$), 1.84 and 1.34 (s, 3H each, 8, 19-CH_3), 1.42 and 1.24 (s, 9H each, 5,16-$C(CH_3)_3$); ^{13}C NMR (125.8 MHz, C_6D_6) δ 149.22/148.13 (C-5/16), 138.67/139.56 (C-8/19), 137.51/137.39 (C-3/18), 136.68/136.25 (C-7/14), 131.77/131.39 (C-1/2), 127.43/126.28 (C-6/15), 122.89/122.32 (C-4/17), 98.49/94.45 (C-9/13), 85.86 ($C_5(CH_3)_5$), 73.98 (C-10/12), 72.78 (C-11), 70.39 (C-12/10), 34.20/33.98 (5,16-$C(CH_3)_3$), 31.75/31.47 (5,16-$C(CH_3)_3$), 20.33/19.28 (8,19-CH_3), 11.83 ($C_5(CH_3)_5$).

Synthesis of [9, 10, 11, 11a, 11f-η^5]-*trans*-11c, 11d-dimethyl-11c, 11d-dihydrocyclopent[e]pyrene-ferrocene 54

Method A: A solution of the diene **44** (38 mg, 0.10 mmol) and $LiCH_2SiMe_3$ (14 mg, 0.15 mmol) in toluene (5 mL) was stirred at room temperature overnight in the glove box. Solid $FeCl_2$ (19 mg, 0.15 mmol) was then added, followed by a few drops of d_8-THF. The resulting green mixture was stirred at room temperature overnight. Then solvent was removed and the residue

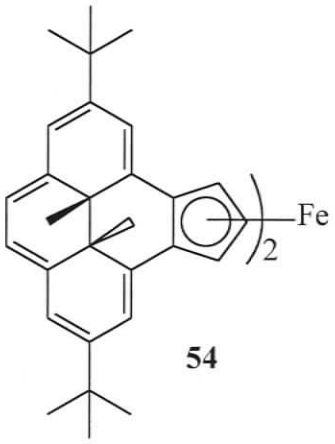

54

was taken up in hexane and filtered through Celite. The filtrate was dried and the residue was recrystallized from hot hexane to give 9 mg (22%) of the ferrocene **54** as dark brown crystals.

Method B: In a Kontes flask, a solution of the diene **44** (76 mg, 0.20 mmol), $LiCH_2SiMe_3$ (38 mg, 0.40 mmol) and $FeCl_2$ (38 mg, 0.30 mmol) in toluene (2 mL) and THF (10 mL) was stirred under Ar at room temperature overnight. Then solvent was removed and the residue was taken up in toluene and filtered through Celite in the glove box. The filtrate was dried and the residue was recrystallized from hot hexane to give 16 mg (20%) of complex **54** as dark brown crystals, mp: (decomp.) 350 °C. ^{1}H NMR (500 MHz, d_8-THF) δ 7.31 (d, J = 1.4, 1H, H-8'/1'), 7.28 (d, J = 1.4, 1H, H-8/1), 7.19 (d, J = 1.4, 1H, H-1/8), 7.03 (d, J = 1.4, 1H, H-1'/8'), 6.65~6.68 (m, 4H, H-3,6,3',6'), 6.36~6.40 (m, 4H, H-4,5,4',5'), 4.88 and 5.08 (dd, J = 2.4 & 0.8 Hz, 1H each, H-9,11), 4.78 and 5.03 (dd, J = 2.4 & 0.8 Hz, 1H each, H-9',11'), 4.02 (t, J = 2.4 Hz, 1H, H-10'), 3.78 (t, J = 2.4 Hz, 1H, H-10), 1.35/1.342/1.340/1.29 (s, 9H each, 2,7,2',7'-C(CH_3)$_3$), 0.66/0.65/-0.55/-0.57(s, 3H each, 11c,d, 11c',d'-CH_3); ^{13}C NMR (125.8 MHz, d_8-THF) δ 145.63/145.54/145.50 (C-2,7,2',7'), 141.79/141.61/141.16/140.96/139.89/ 139.52/138.83 (C-3a, 5a, 11b, 11e, 3a', 5a', 11b', 11e'), 121.65/121.58/121.56/121.52 (C-3',6',4/5,4'/5'), 119.32/119.22/119.13/119.08 (C-3,6,4/5,4'/5'), 118.72 (br,s, C-8/1, 8'/1'), 118.29 (C-1'/8'),117.98 (C-1/8), 84.03/83.32/83.15/82.81 (C-11a,f, 11a',f'), 75.10 (C-10), 74.05 (C-10'), 67.97/65.49 (C-9'/11'), 68.18/64.64 (C-9/11), 41.70/41.63/ 40.37/40.20 (C-11c,d, 11c',d'), 35.51/35.48/35.47/35.41 (2,7,2',7'-C(CH_3)$_3$), 30.54/ 30.48/30.44 (2,7,2',7'-C(CH_3)$_3$, 25.21/25.14 /20.07/20.04 (11c,d, 11c',d'-CH_3); IR (KBr) ν 3018, 2961, 2863, 1627, 1458, 1360, 1260, 1225, 1093, 1023, 879, 803, 675 cm^{-1}; UV-

vis (cyclohexane) λ_{max} (ε_{max}) nm 289 (3.80 x 10^5), 410 (4.56 x 10^5), shoulder tail to 800 nm; HRMS *m/z* calcd for $C_{58}H_{66}Fe$ 818.4513, found 818.4509.

Synthesis of Yb(CpDHP)$_2$(THF)$_2$ 57

A solution of the diene **44** (78 mg, 0.20 mmol) and Yb[N(SiMe$_3$)$_2$]$_2$(THF)$_2$ (64 mg, 0.10 mmol) in toluene (15 mL) was stirred at room temperature for 2 days in the glove box. The reaction mixture was then filtered through celite. The filtrate was dried and the residue was recrystallized from hot hexane to give 32 mg (30%) of **57** as dark red crystals. ^{1}H NMR (500 MHz, d$_8$-THF) δ 7.93 (s, 1H, H-8/1), 7.72 and 7.69 (s, 1H each, H-8',1'), 7.46 (s, 1H, H-6/3), 7.15 (s, 1H, H-1/8), 7.08 (s, 1H, H-6'/3'), 7.02 (s, 1H, H-3'/6'), 6.98 (s, 1H, H-3/6), 6.94 (br,s, 1H, H-9/11), 6.83~6.89 (m, 4H, H-4,5,4',5') 6.81 (br,s, 1H, H-9'/11'), 6.72 (br,s, 1H, H-11'/9'), 6.61 (d, J = 1.9 Hz, 1H, H-9/11), 5.73~5.71 (m, 4H, H-10, 10'), 1.61/1.50/1.49/1.38 (s, 9H each, 2,7,2',7'-C(C*H*$_3$)$_3$), -1.07 (br,s, 6H, 11c/11d, 11c'/11d'), -1.52/-1.56 (s, 3H each, 11d/11c, 11d'/11c'); ^{13}C NMR (125.8 MHz, d$_8$-THF) δ 145.35/145.11/144.86/144.72 (C-2,7,2',7'), 139.94/139.78/ 138.88/138.62 (C-3a,5a,3a',5a'), 137.43/137.15/136.92 (C-11b,11e,11b',11e'), 122.23/ 122.15/121.94/121.87 (C-11a,11f,11a',11f'), 120.13/120.02/119.98/119.90 (C-4,5,4',5'), 116.98/116.78/116.34 (C-3,6,3',6'),114.00/113.65 (C-10,10'), 112.79/112.76/112.54/ 112.37 (C-1,8,1',8'),

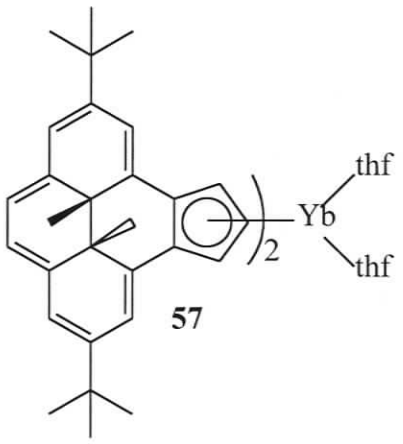

57

103.04/102.85/101.45 (C-9,11,9',11'), 68.27/66.37 (-O*C*H_2CH_2-CH_2*C*H_2-), 39.56/39.41/37.36/37.33 (C-11c,11d,11c',11d'), 36.11/35.97/35.81 (2,7,2',7'-*C*$(CH_3)_3$), 31.67/31.52/31.42/31.30 (2,7,2',7'-C(*C*$H_3)_3$, 26.43/23.56 ((-OCH_2*C*H_2*C*H_2CH_2-), 20.06/19.97/18.97/18.86 (11c, 11d, 11c',11d'-*C*H_3).

5.3 Relative rate studies

5.3.1 Photoopening

Both UV-vis and NMR spectroscopy were used for the photoisomerization experiments. For the relative rate studies, in separate NMR tubes or UV cells, the sample and standard **36** were prepared at the same concentration and in the same solvent. The NMR tubes sealed under argon and UV cells sealed with parafilm after bubbling argon through them were thus placed side by side inside a cold water jacket and irradiated at the same time with a 500-W tungsten lamp with use of a 490-nm filter (**Figure 5.1**). The tubes or cells were monitored after selected periods of time by ^{1}H NMR or UV-vis spectroscopy. The apparent relative rate constants (assuming constant and excess light flux, pseudo first order kinetics) for the photoopening reaction were obtained with use of the following equation: $-\ln(c_t) = kt + A$, where c_t is the mole fraction of the closed form at each time = closed/(closed + open), A is a constant. The plot of $-\ln(c_t)$ vs t (s) was linear and yielded apparent rate constants. The relevant data are the ratio of these constants.

5.3.2 Photoclosing

The samples above, which had been irradiated to open as far as possible, were then placed side by side in front of a pencil Hg UV lamp with a short wave filter. Their ^{1}H NMR spectra or UV-vis spectra were then monitored at selected time intervals of

irradiation. The results were plotted similarly as photoopening by using the following equation: $-\ln(c_t) = kt + A$, where c_t is the mole fraction of the **open** form at each time = open/(closed + open). The ratio of the apparent rates of photoclosing obtained for the sample and standard **36** gave the relative photoclosing rate.

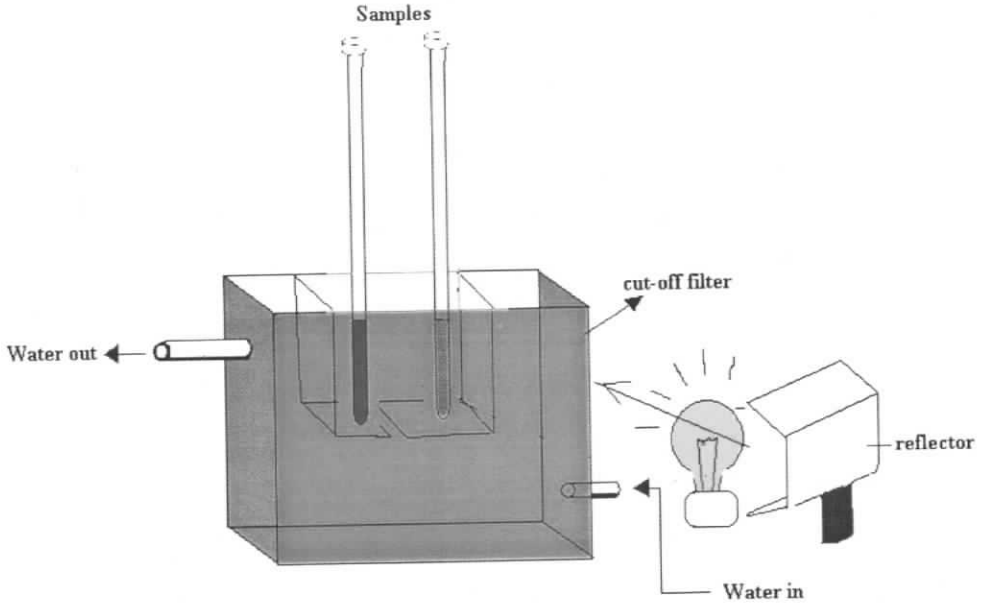

Figure 5.1. Schematic drawing of the irradiation set-up.[103]

References

1. Faraday, M. *Phil. Trans. Roy. London* **1825**, 440-466.
2. a) Hückel, E. *Z. Physik*, **1931**, *70*, 204-286. b)*ibid* **1931**, *72*, 310.
3. Merling, G. *Ber. Dtsch. Chem. Ges*. **1891**, *24*, 3108.
4. Doering, W. Von E.; Knox, L.H. *J. Am, Chem. Soc.* **1954**, *76*, 3202-3206.
5. Thiele, J. *Ber*. **1900**, *33*, 660.
6. a) Rabinovitz, M.; Willner, I. *Pure Appl. Chem*. **1980**, *52*,1575-1585. b) Mullen, K.; Huber, W.; Meul, T.; Nakagawa, M.; Iyoda, M. *J. Am. Chem. Soc.* **1982**, *104*, 5403-5411. c) Rabinovitz, M. *Acc. Chem. Res.* **1983**, *16*, 298-304. d) Prakash, G.; Rawdah, T.; Olah, G. *Angew. Chem. Int. Ed. Engl*. **1983**, *22*, 390-401. e) Mullen, K.; Meul, T.; Schade, P.; Schmickler, H.; Vogel, E. *J. Am. Chem. Soc*. **1987**, *109*, 4992-5003. f) Klabunde, K.; Mullen, K.; Vogler, H. *Tetrahedron* **1987**, *43*, 1183-1196.
7. Rabinovitz. M.; Cohen, Y. *Tetrahedron* **1988**, *44*, 6957-6994.
8. Streitweiser, A., *Molecular Orbital Theory for Organic Chemists*; John Wiley & Sons, Inc.; New York; pp 117-135, 1961.
9. Randic, M. *Chem. Phys. Lett.* **1976**, *38*, 68-70.
10. Randic,M. *J. Am. Chem. Soc*. **1977**, *99*,444-448. c) Randic, M. *Tetrahedron* **1977**, *33,* 1905-1912.
11. Pauling, L. *J. Chem. Phys*. **1936**, *4,* 673-677.
12. a) Pople, J. A. *J. Chem. Phys.* **1956**, *24*, 1111-1116. b) Haigh, C. W.; Mallion, R. B., *Progress in NMR Spectroscopy*, **1980**, *13*, 303-344.
13. Boekelheide, V.; Phillips, J. B. *Proc. Natl. Acad. Sci. U.S.A.* **1964**, *51*, 550-552.

14. Boekelheide, V.; Phillips, J. B. *J. Am. Chem. Soc.* **1967**, *89*, 1695-1704.

15. Mitchell, R. H.; Klopfenstein, C.E.; Boekelheide, V. *J. Am. Chem. Soc.* **1969**, *91*, 4931-4932.

16. Haigh, C. W.; Mallion, R.B. *Mol. Phys.* **1970,** *18*, 737-750.

17. Laszlo, P.; Stang, P. *Organic Spectroscopy: Principles and Applications* Harper & Row, New York, N.Y. 1971.

18. Pouchert, C.J.; Behnke, J., *The Aldrich Library of* ^{13}C *and* ^{1}H *FT NMR Spectra*, Ed. 1; Vol. III; Aldrich Chemical Company, Milwaukee, 1993.

19. Huber, W.; Lex, J.; Meul, T.; Mullen, K., *Angew. Chem. Int. Ed. Engl.* **1981**, *20*, 391-292.

20. Vogel, E.; Konigshofen, H.; Mullen, k.; Oth, J.F.M. *Angew. Chem. Int. Ed. Engl.* **1974**, *13*, 281-283.

21. Breslow, R.; Groves, J. *J. Am. Chem. Soc.* **1970**, *92*, 984-988.

22. a) Kovacevic, B.; Baric, D.; Maksic, Z.B. and Muller, T. *Chem. Phys. Chem.* **2004**, *5*, 1352-1364. b) Wannere, C.S. and Schleyer, P.V.R. *Org. Lett.*, **2003**, *5(5)*, 605-608.

23. a) Spiesecke, H.; Schneider, W. *J. Chem. Phys.* **1961**, *35*, 731-738. b) Spiesecke, H.; Schneider, W. *Tetrahedron Lett.* **1961**, 468-472.

24. Schaefer, T.; Schneider, W. *Can. J. Chem.* **1963**, *41*, 966-982.

25. a) Huber, W.; Mullen, K.; Wennerstrom, O. *Angew. Chem. Int. Ed. Engl.* **1980**, *19*, 624-625. b) Huber, W.; Mullen, K. *J. Chem. Soc., Chem. Commun.* **1980**, 698-700.

26. Schalmz, D.; Gunther, H. *Angew. Chem. Int. Ed. Engl.* **1988**, *27*, 1692-1693.

27. a) Vogel, E.; Boll, W.A. *Angew. Chem. Int. Ed. Engl.* **1964**, *3,* 642 –643. b) Vogel, E.; Roth, H.D. *Angew. Chem. Int. Ed. Engl.* **1964**, *3*, 228-229.

28. Schafer-Ridder, M.; Wagner, A.; Schwamborn, M.; Schreiner, H.; Devrout, E.; Vogel, E. *Angew. Chem. Int. Ed. Engl.* **1978**, *17*, 853-855.

29. Boekelheide, V.; Pepperdine, W. *J. Am. Chem. Soc.* **1970**, *92*, 3684-3688.

30. Haddon, R.C. *J. Am. Chem. Soc.* **1979**, *101*, 1722-1728.

31. a) Aihara, J. *Bull. Chem. Soc. Jpn.* **1980**, *53*, 1163-1164. b) Verbruggen, A. *Bull. Soc. Chim. Belg.* **1982**, *91*, 865-868. c) Hess, B.A. Jr.; Schaad, L.J.; Agranat, F. *J. Am. Chem. Soc.* **1978**, *100*, 5268-5271.

32. a) Mitchell, R.H.; Iyer, V.S.; Khalifa, N.; Mahadevan, R.; Venugopalan, S.; Weerawarna, S. A.; Zhou, P. *J. Am. Chem. Soc.* **1995**, *117*, 1514-1532. b) Williams, R.V.; Edwards, W.D.; Vij, A.; Tolbert, R.W.; Mitchell, R.H. *J. Org. Chem.* **1998**, *63,* 3125-3127.

33. Mitchell, R.H. *Adv. Theor. Interesting Mol.* **1989**, *1*, 135-199.

34. Mitchell, R.H.; Chaudhary, M.; Dingle, T.W.; Williams, R.V. *J. Am. Chem. Soc.* **1984**, *106*, 7776-7779.

35. Memory, J.D. *J. Magn. Reson.* **1977**, *73*, 241-244.

36. Dewar, M.J.S.; De Llano, Carlos. *J. Am. Chem. Soc.* **1969**, *91*, 789-795.

37. Mitchell, R.H.; Khalifa, N.A.; Dingle, T.W. *J. Am. Chem. Soc.* **1991**, *113*, 6696-6697.

38. Mitchell, R.H.; Chen, Y.; Khalifa, N.; Zhou, P. *J. Am. Chem. Soc.* **1998**, *120*, 1785-1794.

39. Woodward, R.B.; Rosenblum, M.; Whiting, M.C. *J. Am. Chem. Soc.* **1952**, *74*, 3458-3459.

40. Garratt, P.J. *Aromaticity*; John Wiley & Sons: New York, **1986**, p130-133.

41. Mitchell, R.H.; Chen, Y. *Tetrahedron Lett.* **1996**, *37*, 6665-6668.

42. a) Fritsche, M. *Comp. Rend.* **1867**, *69*, 1035. b)Ter Merr, E. *Ann. Chem.* **1876**, *181*, 1. c) Phipson, T.L. *Chem. News* **1881**, *43*, 283. d) Marckwald, W.Z. *Phys. Chem.* **1899**, *30*, 140. e) Hirshberg, Y. *Compt. Rend.* **1950**, *231*, 903.

43. Bertelson, R.C. *Mol. Cryst. Liq. Cryst.* **1994**, *246*, 1 (period 1955-1993).

44. IUPAC Compendium of Chemical Terminology, 2nd edition, 1997.

45. a) Henry, A. J. *J. Chem. Soc.* **1946**, 1156-1164. b) Beveridge, D.J.; Jaffe, H. H. *J. Am. Chem. Soc.* **1965**, *87*, 5340-5346. c) Dyck, R.H.; McClure, D.S. *J. Chem. Phys.* **1962**, *36*, 2326-2345. d) Muszkat, K.A.; Fischer, E. *J.Chem. Soc. (B)* **1967**, 662-678. e) Gegiou, D.; Muszkat, K.A.; Fischer, E. *J. Am. Chem. Soc.* **1968**, *90*, 3907-3918.

46. a) Balzani, V.; Scandola, F., *Supramolecular Photochemistry*, Horwood, Chichester, **1991**, chapter 7. b) Rau. H. In *Photochromism, Molecules and Systems,* (Eds.: Durr, H. and Bouas – Laurent, H.), Elsevier, Amsterdam, **1990**, chapter 4. c) Kumar, G.S.; Neckers, D.C. *Chem. Rev.* **1989**, *89*, 1915-1925.d) Shinkai, S.; Manabe, O. *Topics Curr. Chem.* **1984**, *121*, 67-104. e) Malkin, S.; Fischer, E. *J. Phys., Chem.* **1962**, *66*, 2482. f) Zimmerman, G.; Chow, L.Y.; Paik, U.J. *J. Chem. Phys.* **1958**, *80*, 3528-3531. g) Fischer, E.; Frei,Y. *J. Chem. Phys.* **1957**, *27*, 328-330.

47. *Photochromism, Molecules and Systems,* (Eds.: Durr, H. and Bouas – Laurent, H.), Elsevier, Amsterdam, **1990**, chapter 19 and 20.

48. a) Waldeck, D.H. *Chem. Rev.* **1991**, 415. b) Saltiel, J.; Sun, Y.-P. In *photochromism, Molecules and Systems,* (Eds.: Durr, H. and Bouas – Laurent, H.), Elsevier, Amsterdam, **1990**, p64. c) Mallory, F.B.; Mallory, C.W. *Org. React.* **1984**, *30*, 1.

49. Irie, M.; Mohri, M. *J. Org. Chem.* **1988**, *53*, 803-808.

50. Irie, M. *Chem, Rev.* **2000**, *100*, 1685-1716.

51. Stobbe, H. *Ber. Dtsch. Chem. Ges.* **1905**, *38*, 3673-3682.

52. a) Heller, H.G. *IEE Proc.* **1983**, *130*, Pt. I, 209-211. b) Yokoyama, Y. *Chem. Rev.* **2000**, *100*, 1717-1739.

53. a) Berkovic, G.; Krongauz, V.; Weiss, V. *Chem, Rev.* **2000**, *100*, 1741-1753. b) Bercovici, T.; Fischer, E. *J. Am. Chem. Soc.* **1964**, *86*, 5687-5688. c) Hirshberg, Y. *J. Am. Chem. Soc.*, **1956**, *78*, 2304-2312.

54. Brown, G.H. *Photochromism*, John Wiley & Sons; New York; **1971**, p98-99, p440-444, p569-578.

55. Bouas-Laurent, H.; Durr, H. *Pure Appl. Chem.* **2001**, *73*, 639-665.

56. a) Leonard, N.J.; McCredie, R.S.; Logue, M.W.; Cundall, R.L. *J. Am. Chem. Soc.* **1973**, *95*, 2320-2324. b)Woodward, R.B. and Hoffmann, R. *Angew. Chem. Int. Ed. Engl.* **1969**, *8*(11), 781-853.

57. Blattmann, H.R.; Meuche, D.; Heilbronner, E.; Molyneux, R.J.; Boekelheide, V. *J. Am. Chem. Soc.* **1965**, *87*, 130-131.

58. Blattmann, H.R.; Schmidt, W. *Tetrahedron* **1970**, *26*, 5885-5899.

59. a) Sheepwash, M.A.; Mitchell, R.H.; Bohne, C. *J. Am. Chem. Soc.* **2002**, *124*, 4693-4700. b) Sheepwash, M.A.L.; Ward, T.R.; Wang, Y.; Bandyopadhyay, S.; Mitchell, R.H.; Bohne, C. *Photochem. Photobiol. Sci.* **2003**, *2*, 104-112. c) Sheepwash, M. *PhD Thesis*; University of Victoria: Victoria, B.C. Canada, **2002**; p119.

60. Murakam, S.; Tsutsui, T.; Saito, S.; Yamato, T.; Tashiro, M. *Nippon. Kagukukai. Shi.* **1988**, 221-229.

61. Mitchell, R.H.; Iyer, V.S.; Mahadevan, R.; Venugopalan, S.; Zhou, P. *J. Org. Chem.* **1996**, *61*, 5116-5120.

62. Mitchell, R.H.; Yan, J.S.H.; Dingle, T.W. *J. Am. Chem. Soc.* **1982**, *104*, 2551-2559.

63. Mitchell, R.H.; Ward, T.R.; Chen, Y.; Wang, Y.; Weerawarna, S.A. *J. Am. Chem. Soc.*, **2003**, *125*, 2974-2988.

64. Mitchell, R.H.; Ward, T.R. *Tetrahedron* **2001**, *57*, 3689-3695.

65. Mitchell, R.H. *Eur. J. Org. Chem*. **1999**, 2695-2703.

66. Mitchell, R.H.; Ward, T.R.; Wang, Y.; Dibble, P.W. *J. Am. Chem. Soc.*, **1999**, *121*, 2601-2602.

67. Mitchell, R. H. and Bandyopadhyay, S. *Org. Lett.* **2004**, *6*(11), 1729-1732.

68. Mitchell, R.H.; Carruthers, R.J.; Mazuch, L.; Dingle, T.W. *J. Am. Chem. Soc.* **1982**, *104*, 2544-2551.

69. Mitchell, R.H.; Chen, Y.-S. *Tetrahedron Lett.* **1996**, *37*, 5239-5242.

70. Mitchell, R.H.; Brkic Z.; Sauro, V.A. and Berg, D.J. *J. Am. Chem. Soc.* **2003**, *125*, 7581-7585.

71. a) Rerek, M.E.; Ji, L.N.; Basolo, F. *J. Chem. Soc. Chem. Commun.* **1983**, 1208-1209. b) Rerek, M.E.; Basolo, F. *organometallics,* **1983**, *2*, 372-376. c) Rerek, M.E.; Basolo, F. *J. Am. Chem. Soc.*, **1984**, *106*, 5908-5912.

72. Cheong, M.; Basolo, F. *organometallics* **1988**, *7*, 2041-2044.

73. Kakkar, A.K.; Taylor, N.J.; Marder, T.B. *Inorg. Chim. Acta* **1992**, *198-200*, 219-231.

74. Zargarian, D. *Coord. Chem. Rev.* **2002**, *233-234*, 157-176.

75. Lobanova, I.A.; Zdanovich, V.I. *Russ. Chem. Rev.* **1988**, *57*, 967-?.

76. For an example, see:Gamelas, C.A.; Herdtweck, E. *Organometallics* **1999**, *18*, 506-515.

77. McGlinchey, M.J.; Stradiotto, M. *Coord. Chem. Rev.* **2001**, *219-221*, 311-378.

78. Faller, J.W.; Crabtree, R.H.; Habib, A. *Organometalics* **1985**, *4*, 929-935.

79. Trnka, T.N.; Bonanno, J.B.; Bridgewater, B.M. *Organometallics* **2001**, *20*, 3255-3264.

80. Westcott, S.A.; Kakkar, A.K.; Stringer, N. J. *J. Organomet. Chem.* **1990**, *394*, 777-794.

81. Forschner, T.C.; Cutler, A.R. *Organometallics* **1987**, *6*, 889-?.

82. Cadierno, V.; Diez, J. *Coord. Chem. Rev.* **1999**, *193-195*, 147-205.

83. Calhorda, M.J.; Felix, V.; Veiros, L.F. *Coord. Chem. Rev.* **2002**, *230*, 49-64.

84. Kohler, F.H. *Chem. Ber.* **1974**, *107*, 570.

85. Baker, R.T.; Tulip, T.H. *Organometaallics* **1986**, *5*, 839-845.

86. Tashiro, M.; Yamato, T. *J. Am. Chem. Soc.* **1982**, *104*, 3701-3707.

87. Miyazawa, A.; Yamato, T.; Tashiro, M. *J. Org. Chem.* **1991**, *56*, 1334-1337.

88. Khalifa N.A. *PhD Thesis*; University of Victoria: Victoria, B.C. Canada, **1990.**

89. Oshima, N.; Suzuki, H.; Moroka, Y. *Chem. Lett.* **1984**, 1161-1164.

90. Tilley, T.D.; Grubbs, R.H.; Bercaw, J.E. *Organometallics* **1984**, *3*, 274-278.

91. Gassman, P.G.; Winter, G.H., *J. Am. Chem. Soc.* **1988**, *110*, 6130-6135.

92. Bunel, E.E.; Valle, L.; Manriquez, J.M., *Organometallics*, **1985**, *4*, 1680-1682.

93. Berg, D.J.; Andersen, R.A.; Zalkin, A. *Organometallics* **1988**, *7*, 1858-1863.

94. Balboni, D.; Camurati, I.; Prini, G.; Resconi, L.; Galli, S.; Mercandelli, P. and Sironi, A. *Inorg. Chem.* **2001,** *40*, 6588-6597.

95. Wengrovius, J.H. and Schrock, R.R. *J. Oganomet. Chem.* **1981**, *205*, 319.

96. Ward, T.R. *PhD Thesis*, University of Victoria, Victoria, B.C. Canada, **2000**.

97. a) Schmidt, W. *Helv. Chim. Acta.* **1971**, 54, 862-868. b) Schmidt, W. *Tetrahedron, Lett.* **1972**, *12*, 581-584.

98. Dr. R.V.Williams (University of Idaho), who has considerable experience in DHP calculations is attempting to model this process.

99. Bens, A.T.; Frewert, D.; Kodatis, K.; Ktyschi, C.; Martin, H-D.; Trommsdorff, H.P. *Eur. J. Org. Chem.* **1998**, 2333-2338.

100. McGlinchey, M.J.; Burns, R.C.; Hofer R.; Top, S.; Jaouen, G. OM **1986**, *5*, 104-109.

101. Mitchell, R.H.; Brkic, Z; Berg, D.J.; Barclay, T.M. *J. Am. Chem. Soc.*, **2002**, 124, 11983-11988.

102. Wang, Y. *PhD Thesis*, University of Victoria, Victoria, B.C. Canada, **2003**; p141.

103. Bandyopadhyay, S. *PhD Thesis*, University of Victoria, Victoria, B.C. Canada, **2004**.

104. A compound made by our graduate student Mr. Rui Zhang recently.

105. ORTEP-3 for Windows: Farrugia, L.J. *J. Appl.Cryst.*, **1997**, 30, 565.

106. Mejdrich, A.L. and Hanks, T.W., *Synth. React. Inorg. Met.-org. Chem*, **1998**, 28(6), 953-973.

107. Deck, P.A.and Fronczek, F.R. O*rganometallics,* **2000**, 19, 327-333.

108. Khayatpoor, R.and Shapley, J.R. *Organometallics*, **2000**, 19, 2382-2388.

109. a) Trotter, J. *Acta Crystallogr.*, **1963**, 16, 571. b) Seiler, P.and Dunitz, J.D. *Acta Crystallogr., Sect. B: Struct. Sci*, **1980**, 36, 2946. c) Gassman, P.G. and Winter, C.H. *J. Am. Chem. Soc.*, **1988**, 110, 6130-6135. d) Yang, J.; Yin, J.; Abboud, K.A and Jones, W.M. *Organometallics*, **1994**, 13, 971-978.

110. King, R.B.and Bisnetter, M.B. *J. Organomet. Chem.* **1967**, 8, 287-297.

111. Jin, J.Z.; Jin, Z.S.; Chen, W.Q.; Zhang, Y. *Chinese J. Struct. Chem. (Jiegou Huaxue)* **1993**, 12, 241-245.

112. Trifonov, A.A.; Kirillov, E.N.; Dechert, S.; Schumann, H. and Bochkarev, M.N. *Eur.J. Inorg. Chem*, **2001**, 2509-2514.

113. Khvostov, A.V.; Bulychev, B.M.; Belsky, V.K. and Sizov, A.I. *J. Organomet. Chem.*, **1999**, 584, 164-170 and refs in.

114. a) Oshima, N.; Suzuki, H.; Moroka,Y. *Chem. Lett.* **1984**, 1161-1164. b) Tilley, T. D.; Grubbs, R.H.; Bercaw, J.E. *Organometallics* **1984**, *3*, 274-278. c) Gassman, P.G.; Winter, G.H. *J. Am. Chem. Soc*. **1988**, *110*, 6130-6135.

115. a) Tilley, T.D.; Boncella, J.M.; Berg, D.J.; Burns, C.J.; Andersen, R.A. *Inorg. Synth*. **1990**, *27*, 146. b) Aspinall, H.C.; Bradley, D.C.; Hursthouse, M.B.; Sales, K.D.; Walker, N.P.C.; Hussain, B. *J. Chem, Soc,. Dalton Trans*, **1989,** 623.

116. Miyazawa, A; Yamato, T.; Tashiro, M. *J. Org. Chem.* **1991**, *56*, 1334-1337.

117. PCMODEL V8.5, Serena Software, Box 3076, Bloomington, IN 47402-3076. The force field used is derived from MM2 force field of N. L. Allinger, with the pi-VESCF routines taken from MMP1, also by N. L. Allinger.

Appendices

Appendix A. Plots for the calculation of k, E_{act}, $\Delta H^{\#}$ and $\Delta S^{\#}$.

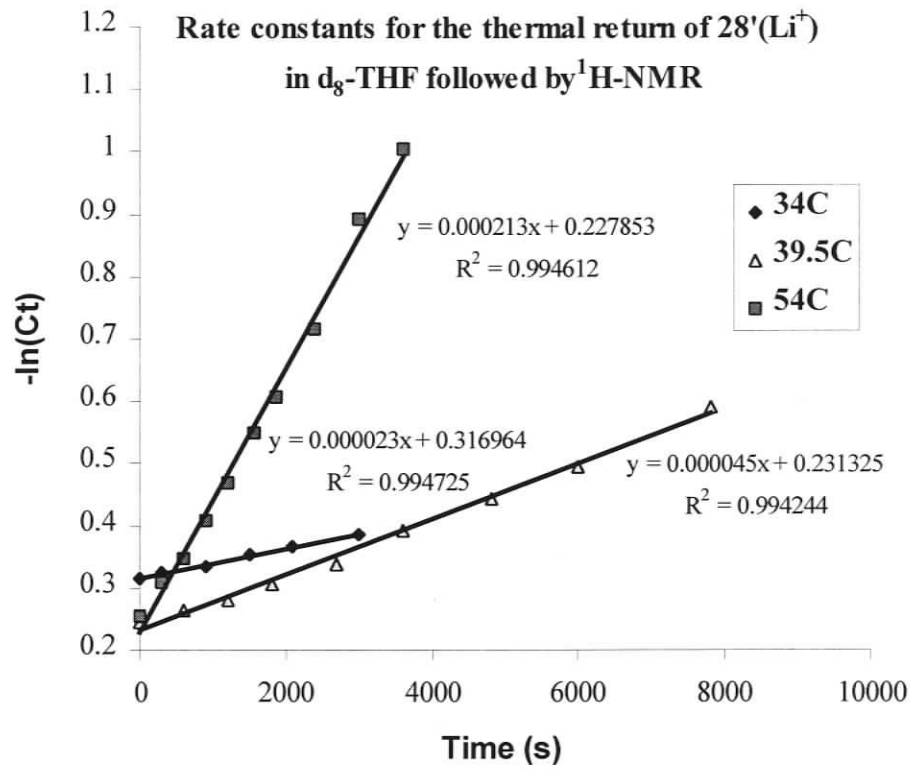

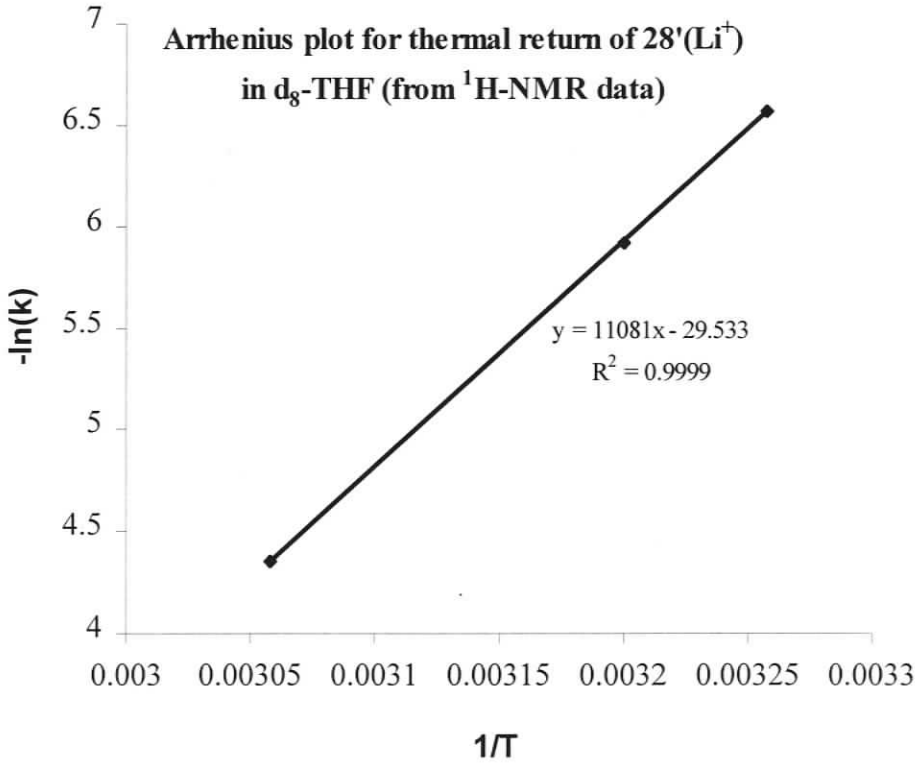

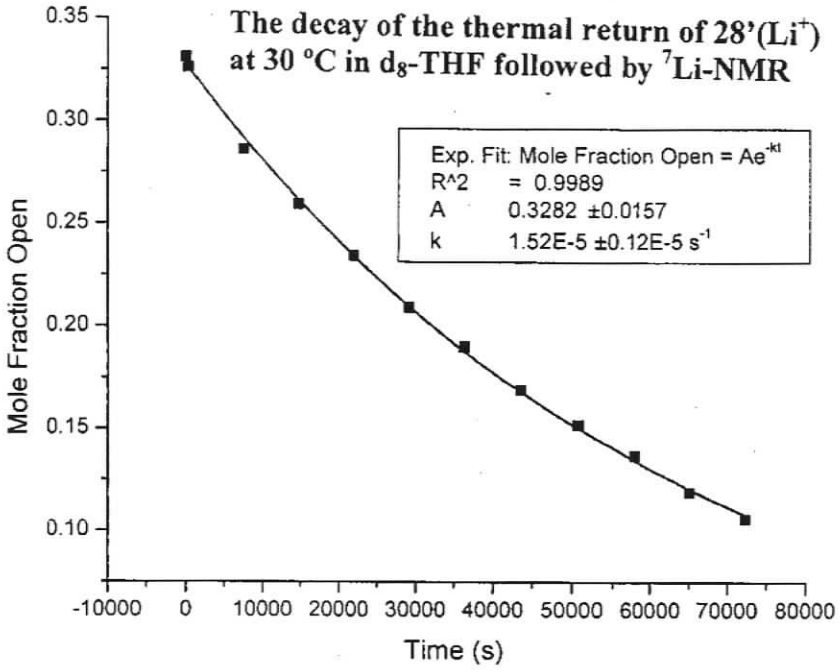
The decay of the thermal return of 28'(Li+) at 30 °C in d8-THF followed by 7Li-NMR
Exp. Fit: Mole Fraction Open = Ae^-kt
R^2 = 0.9989
A 0.3282 ±0.0157
k 1.52E-5 ±0.12E-5 s^-1
Mole Fraction Open
Time (s)
0.35
0.30
0.25
0.20
0.15
0.10
-10000
0
10000
20000
30000
40000
50000
60000
70000
80000

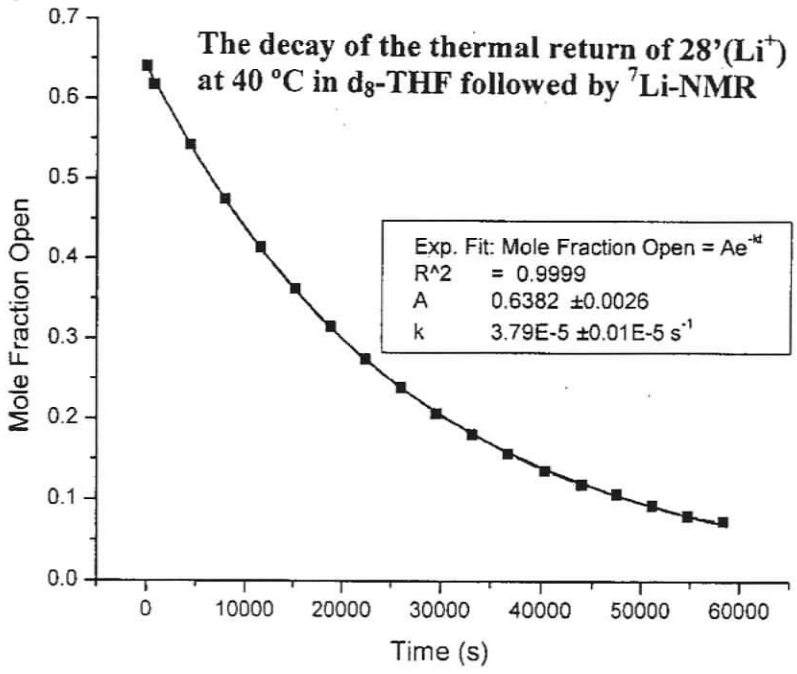
The decay of the thermal return of 28'(Li+) at 40 °C in d8-THF followed by 7Li-NMR
Exp. Fit: Mole Fraction Open = Ae^-kt
R^2 = 0.9999
A 0.6382 ±0.0026
k 3.79E-5 ±0.01E-5 s^-1
Mole Fraction Open
Time (s)
0.7
0.6
0.5
0.4
0.3
0.2
0.1
0.0
0
10000
20000
30000
40000
50000
60000

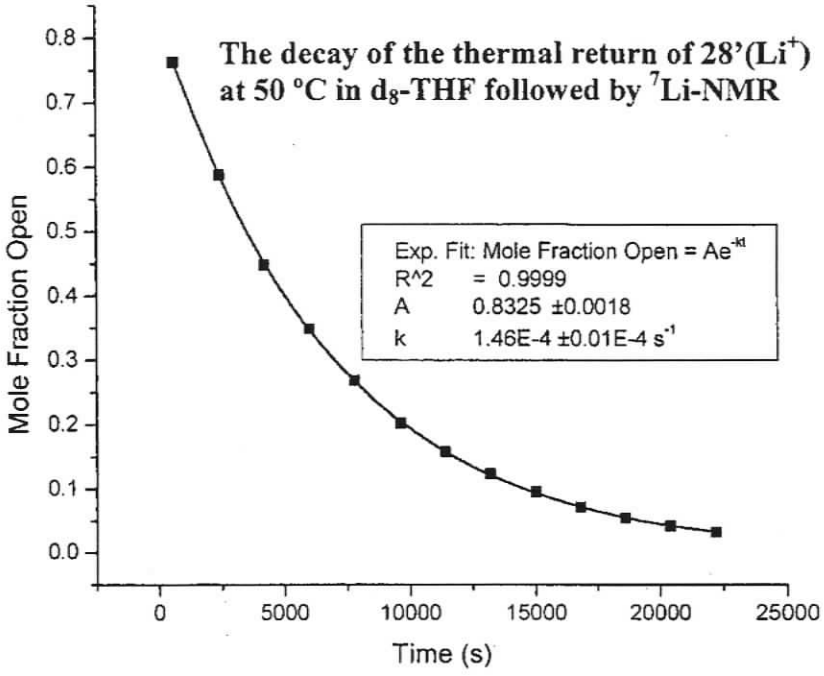
The decay of the thermal return of 28'(Li+) at 50 °C in d8-THF followed by 7Li-NMR
Exp. Fit: Mole Fraction Open = Ae-kt
R^2 = 0.9999
A 0.8325 ±0.0018
k 1.46E-4 ±0.01E-4 s-1
Mole Fraction Open
Time (s)
0.0
0.1
0.2
0.3
0.4
0.5
0.6
0.7
0.8
0
5000
10000
15000
20000
25000

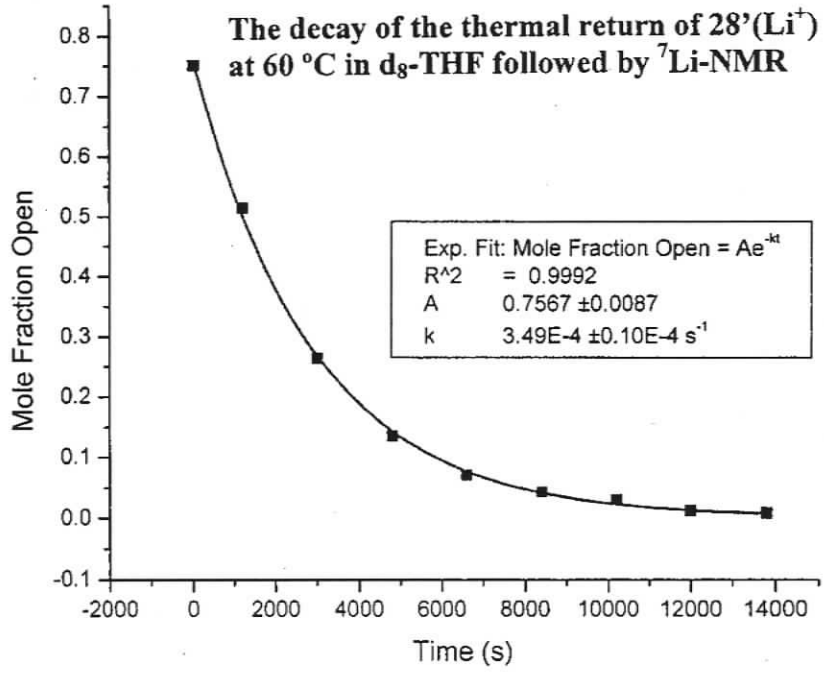
The decay of the thermal return of 28'(Li+) at 60 °C in d8-THF followed by 7Li-NMR
Exp. Fit: Mole Fraction Open = Ae-kt
R^2 = 0.9992
A 0.7567 ±0.0087
k 3.49E-4 ±0.10E-4 s-1
Mole Fraction Open
Time (s)
-0.1
0.0
0.1
0.2
0.3
0.4
0.5
0.6
0.7
0.8
-2000
0
2000
4000
6000
8000
10000
12000
14000

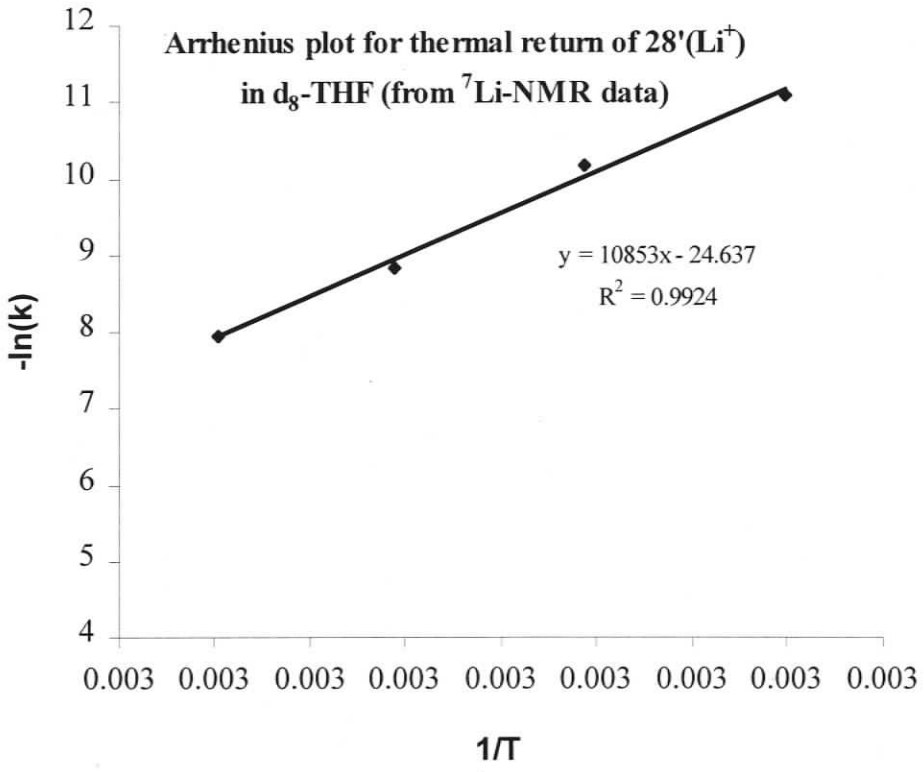
Arrhenius plot for thermal return of 28'(Li+) in d8-THF (from 7Li-NMR data)
y = 10853x - 24.637
R2 = 0.9924
-ln(k)
12
11
10
9
8
7
6
5
4
0.003 0.003 0.003 0.003 0.003 0.003 0.003 0.003 0.003
1/T

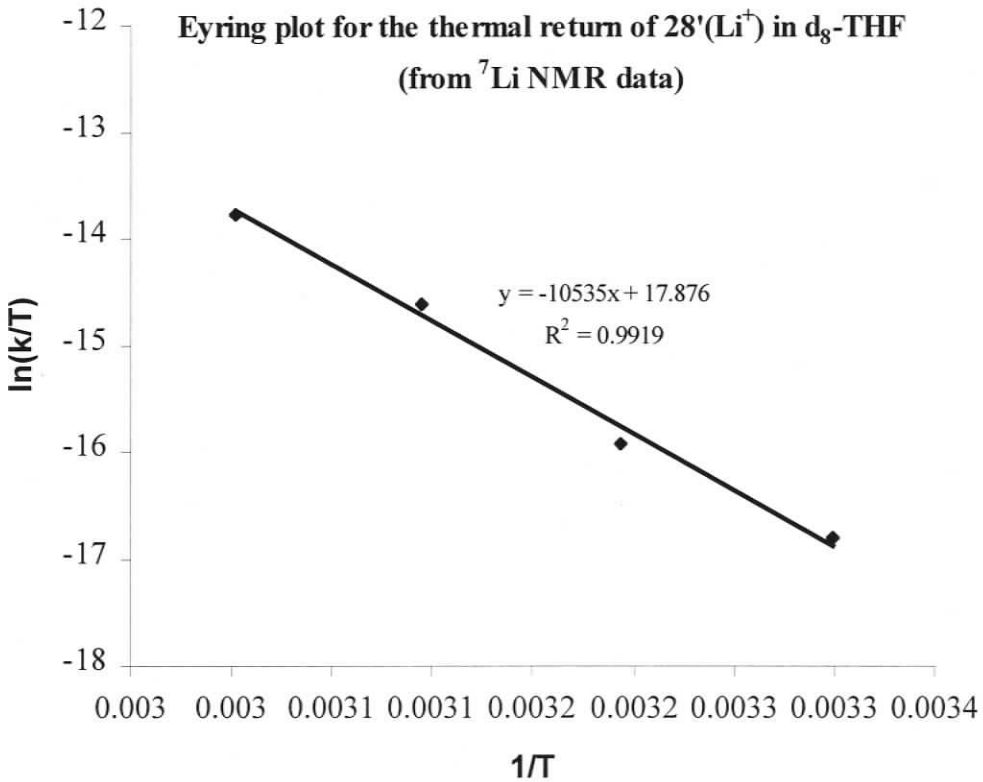
Eyring plot for the thermal return of 28'(Li+) in d8-THF (from 7Li NMR data)
y = -10535x + 17.876
R2 = 0.9919
ln(k/T)
-12
-13
-14
-15
-16
-17
-18
0.003 0.003 0.0031 0.0031 0.0032 0.0032 0.0033 0.0033 0.0034
1/T

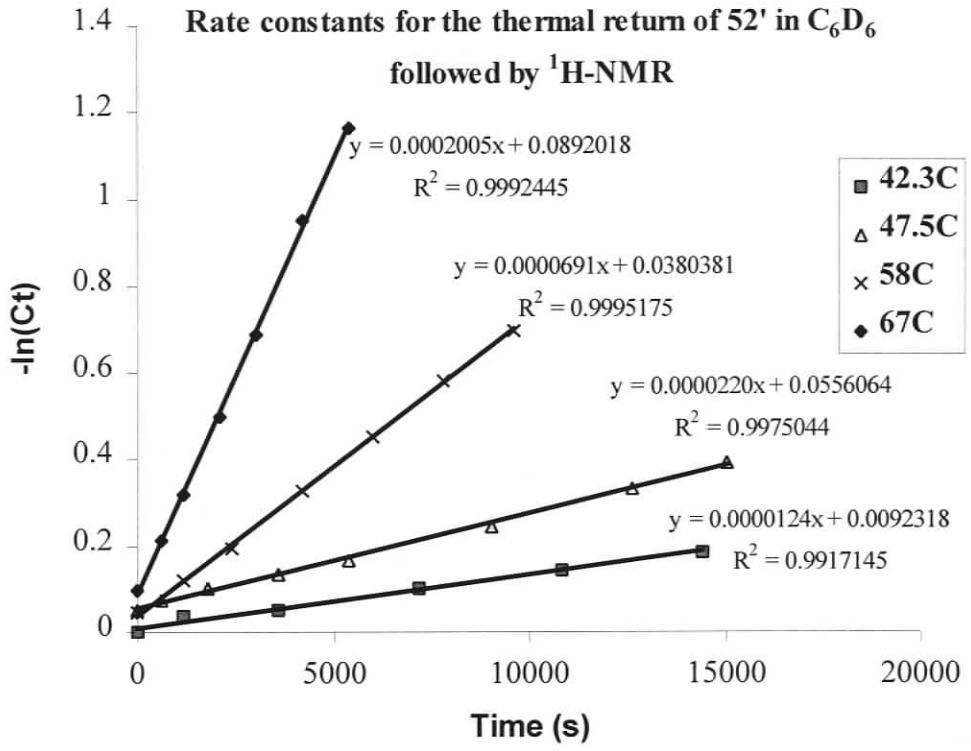
Rate constants for the thermal return of 52' in C_6D_6 followed by ^{1}H-NMR
y = 0.0002005x + 0.0892018
R^2 = 0.9992445
y = 0.0000691x + 0.0380381
R^2 = 0.9995175
y = 0.0000220x + 0.0556064
R^2 = 0.9975044
y = 0.0000124x + 0.0092318
R^2 = 0.9917145
42.3C
47.5C
58C
67C
-ln(Ct)
Time (s)
0
0.2
0.4
0.6
0.8
1
1.2
1.4
0
5000
10000
15000
20000

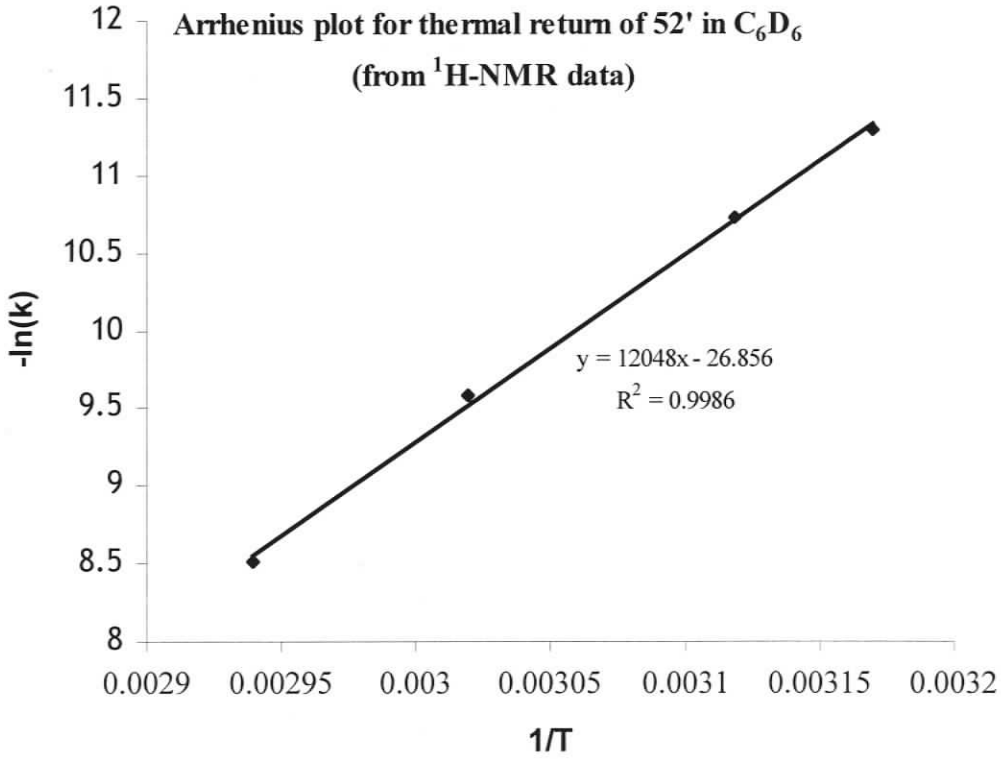
Arrhenius plot for thermal return of 52' in C_6D_6 (from ^{1}H-NMR data)
y = 12048x - 26.856
R^2 = 0.9986
-ln(k)
1/T
8
8.5
9
9.5
10
10.5
11
11.5
12
0.0029
0.00295
0.003
0.00305
0.0031
0.00315
0.0032

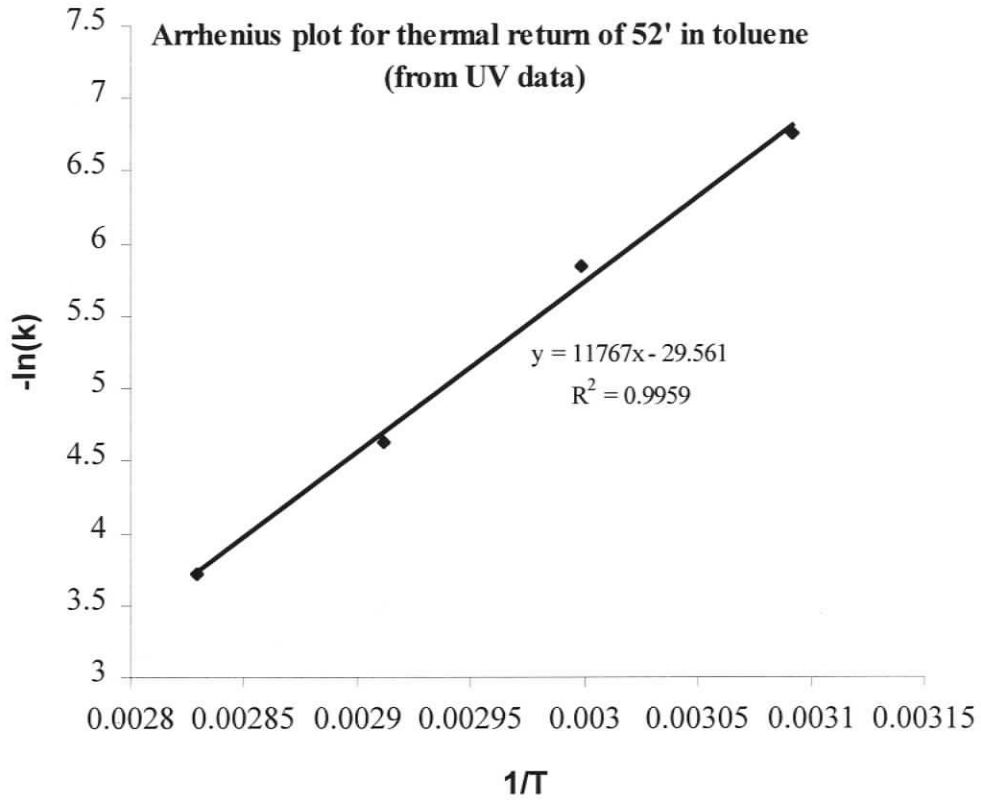
Arrhenius plot for thermal return of 52' in toluene
(from UV data)
y = 11767x - 29.561
R2 = 0.9959
-ln(k)
1/T
7.5
7
6.5
6
5.5
5
4.5
4
3.5
3
0.0028 0.00285 0.0029 0.00295 0.003 0.00305 0.0031 0.00315

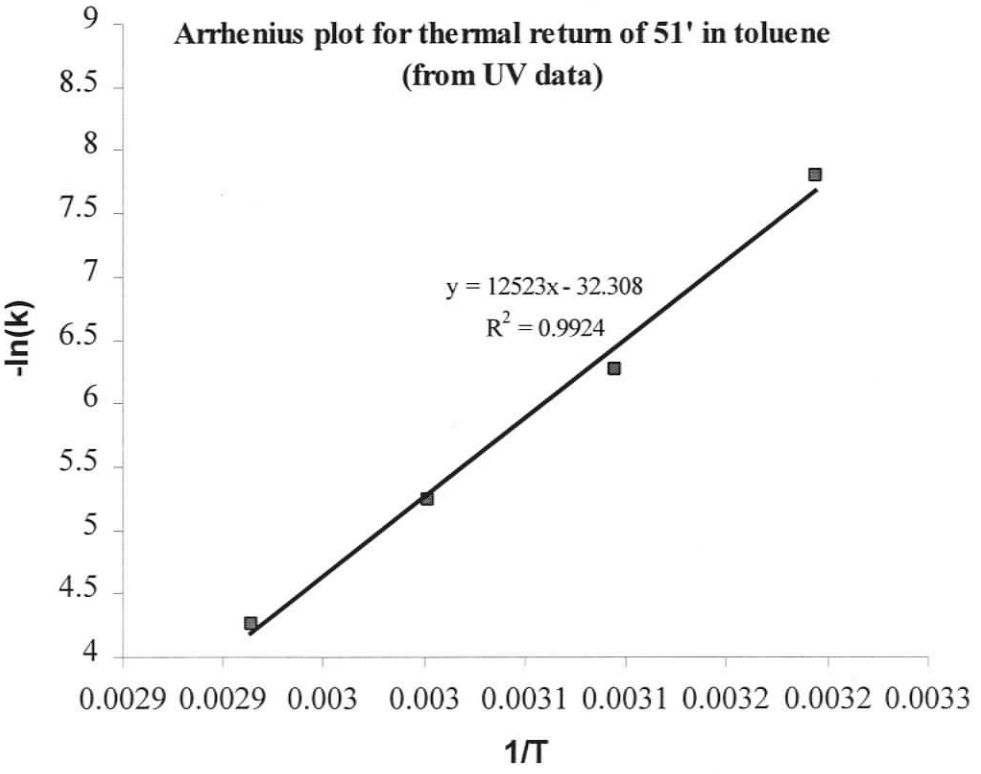
Arrhenius plot for thermal return of 51' in toluene
(from UV data)
y = 12523x - 32.308
R2 = 0.9924
-ln(k)
1/T
9
8.5
8
7.5
7
6.5
6
5.5
5
4.5
4
0.0029 0.0029 0.003 0.003 0.0031 0.0031 0.0032 0.0032 0.0033

Appendix B: X-ray crystallography data

Table B.1. Crystal, Data Collection and Refinement Parameters for **51**.

formula	$ReO_3C_{32}H_{33}$
fw (g/mol)	651.78
crystal size, mm	0.42 x 0.52 x 0.54
cystal color	red
a, Å	9.880(3)
b, Å	10.150(3)
c, Å	14.041(4)
α, deg	93.395(5)
β, deg	97.609(4)
γ, deg	96.004(5)
V, Å^3	1384.1(6)
cell detn, refls	800
d(calcd), g cm^{-3}	1.56
space group	P-1
Z	2
F000	648
radiation, λ (Å)	MoKα, graphite monochromated, 0.71073
temp, K	228
linear abs coeff, mm^{-1}	4.42
diffractometer	Smart 1000
scan technique, 2θ range, deg	omega, 4-50
crystal decay, %	0.20
absorption correction	Sadabs (empirical)
absorption range	0.83 - 1.00
refl meas / unique refls	7854 / 4778
R for merge	0.015
refls in refinement I>2.0σ(I)	4380
solution method	Shelxs-97 (Sheldrick, 1990)
parameters refined	325
R1, wR2	0.023, 0.057
R1 for I>0.0σ(I)	0.027
GOF	1.05
final diff map, e Å^{-3}	-0.67, +0.98
scattering factors	Internat.Tables for Crystallography, Vol C
H atom treatment	riding (C-H)

Table B.2. Bond Lengths [Å] and Angles [deg] for **51**.

Re(1)-C(2)	1.895(4)
Re(1)-C(3)	1.909(5)
Re(1)-C(1)	1.914(4)
Re(1)-C(6)	2.265(4)
Re(1)-C(7)	2.279(4)
Re(1)-C(5)	2.289(4)
Re(1)-C(8)	2.357(3)
Re(1)-C(4)	2.371(3)
O(1)-C(1)	1.144(5)
O(2)-C(2)	1.156(5)
O(3)-C(3)	1.146(5)
C(4)-C(8)	1.434(5)
C(4)-C(5)	1.448(5)
C(4)-C(28)	1.452(5)
C(5)-C(6)	1.412(5)
C(6)-C(7)	1.410(6)
C(7)-C(8)	1.438(5)
C(8)-C(9)	1.449(5)
C(9)-C(10)	1.336(5)
C(9)-C(31)	1.522(5)
C(10)-C(11)	1.458(5)
C(11)-C(16)	1.359(5)
C(11)-C(12)	1.521(5)
C(12)-C(15)	1.513(7)
C(12)-C(13)	1.521(8)
C(12)-C(14)	1.521(7)
C(16)-C(17)	1.424(5)
C(17)-C(18)	1.362(5)
C(17)-C(31)	1.506(5)
C(18)-C(19)	1.423(5)
C(19)-C(20)	1.351(5)
C(20)-C(21)	1.429(5)
C(20)-C(29)	1.521(5)
C(21)-C(22)	1.361(5)
C(22)-C(27)	1.447(5)
C(22)-C(23)	1.526(5)
C(23)-C(25)	1.521(7)
C(23)-C(24)	1.526(7)
C(23)-C(26)	1.535(6)
C(27)-C(28)	1.337(5)
C(28)-C(29)	1.532(5)
C(29)-C(31)	1.519(5)

C(29)-C(30)	1.568(6)
C(31)-C(32)	1.589(6)
C(2)-Re(1)-C(3)	88.12(18)
C(2)-Re(1)-C(1)	91.27(18)
C(3)-Re(1)-C(1)	91.2(2)
C(2)-Re(1)-C(6)	94.05(17)
C(3)-Re(1)-C(6)	138.30(17)
C(1)-Re(1)-C(6)	130.33(18)
C(2)-Re(1)-C(7)	107.00(16)
C(3)-Re(1)-C(7)	103.81(17)
C(1)-Re(1)-C(7)	156.50(17)
C(6)-Re(1)-C(7)	36.15(14)
C(2)-Re(1)-C(5)	115.27(16)
C(3)-Re(1)-C(5)	154.20(15)
C(1)-Re(1)-C(5)	98.62(17)
C(6)-Re(1)-C(5)	36.11(14)
C(7)-Re(1)-C(5)	60.51(14)
C(2)-Re(1)-C(8)	142.55(15)
C(3)-Re(1)-C(8)	95.07(15)
C(1)-Re(1)-C(8)	125.86(15)
C(6)-Re(1)-C(8)	59.74(13)
C(7)-Re(1)-C(8)	36.10(12)
C(5)-Re(1)-C(8)	59.92(12)
C(2)-Re(1)-C(4)	151.09(16)
C(3)-Re(1)-C(4)	119.15(15)
C(1)-Re(1)-C(4)	97.14(16)
C(6)-Re(1)-C(4)	59.69(13)
C(7)-Re(1)-C(4)	59.81(13)
C(5)-Re(1)-C(4)	36.15(12)
C(8)-Re(1)-C(4)	35.31(12)
O(1)-C(1)-Re(1)	176.3(4)
O(2)-C(2)-Re(1)	177.1(4)
O(3)-C(3)-Re(1)	176.7(4)
C(8)-C(4)-C(5)	107.3(3)
C(8)-C(4)-C(28)	122.2(3)
C(5)-C(4)-C(28)	130.4(3)
C(8)-C(4)-Re(1)	71.80(19)
C(5)-C(4)-Re(1)	68.8(2)
C(28)-C(4)-Re(1)	126.9(2)
C(6)-C(5)-C(4)	107.7(3)
C(6)-C(5)-Re(1)	71.0(2)
C(4)-C(5)-Re(1)	75.0(2)
C(7)-C(6)-C(5)	109.3(3)
C(7)-C(6)-Re(1)	72.5(2)
C(5)-C(6)-Re(1)	72.9(2)

C(6)-C(7)-C(8)	107.9(3)
C(6)-C(7)-Re(1)	71.4(2)
C(8)-C(7)-Re(1)	74.9(2)
C(4)-C(8)-C(7)	107.7(3)
C(4)-C(8)-C(9)	121.5(3)
C(7)-C(8)-C(9)	130.5(3)
C(4)-C(8)-Re(1)	72.89(19)
C(7)-C(8)-Re(1)	69.0(2)
C(9)-C(8)-Re(1)	128.2(2)
C(10)-C(9)-C(8)	124.5(3)
C(10)-C(9)-C(31)	120.0(3)
C(8)-C(9)-C(31)	114.7(3)
C(9)-C(10)-C(11)	123.5(3)
C(16)-C(11)-C(10)	117.6(3)
C(16)-C(11)-C(12)	123.9(3)
C(10)-C(11)-C(12)	118.5(3)
C(15)-C(12)-C(11)	111.1(4)
C(15)-C(12)-C(13)	108.5(5)
C(11)-C(12)-C(13)	108.3(4)
C(15)-C(12)-C(14)	108.1(5)
C(11)-C(12)-C(14)	112.1(4)
C(13)-C(12)-C(14)	108.7(6)
C(11)-C(16)-C(17)	123.4(3)
C(18)-C(17)-C(16)	123.8(3)
C(18)-C(17)-C(31)	117.3(3)
C(16)-C(17)-C(31)	118.3(3)
C(17)-C(18)-C(19)	121.5(3)
C(20)-C(19)-C(18)	122.2(3)
C(19)-C(20)-C(21)	123.8(3)
C(19)-C(20)-C(29)	116.9(3)
C(21)-C(20)-C(29)	118.8(3)
C(22)-C(21)-C(20)	122.8(3)
C(21)-C(22)-C(27)	118.5(3)
C(21)-C(22)-C(23)	123.4(3)
C(27)-C(22)-C(23)	118.1(3)
C(25)-C(23)-C(24)	110.0(4)
C(25)-C(23)-C(22)	108.9(4)
C(24)-C(23)-C(22)	109.9(4)
C(25)-C(23)-C(26)	108.0(4)
C(24)-C(23)-C(26)	107.9(4)
C(22)-C(23)-C(26)	112.0(3)
C(28)-C(27)-C(22)	123.2(3)
C(27)-C(28)-C(4)	124.3(3)
C(27)-C(28)-C(29)	120.7(3)
C(4)-C(28)-C(29)	114.8(3)
C(31)-C(29)-C(20)	109.7(3)

C(31)-C(29)-C(28)	111.6(3)
C(20)-C(29)-C(28)	111.6(3)
C(31)-C(29)-C(30)	109.4(3)
C(20)-C(29)-C(30)	106.3(3)
C(28)-C(29)-C(30)	108.1(3)
C(17)-C(31)-C(29)	110.6(3)
C(17)-C(31)-C(9)	112.8(3)
C(29)-C(31)-C(9)	111.9(3)
C(17)-C(31)-C(32)	106.1(3)
C(29)-C(31)-C(32)	109.0(3)
C(9)-C(31)-C(32)	106.1(3)

Table B.3. Atomic Coordinates [x 10^4] and Equivalent Isotropic Displacement Parameters [A^2 x 10^3] for **51**.

	x	y	z	U_{eq}
Re(1)	6673(1)	8434(1)	5673(1)	35(1)
O(1)	6376(4)	11005(3)	6836(3)	75(1)
O(2)	7126(4)	9854(3)	3868(2)	68(1)
O(3)	9784(4)	8686(4)	6253(3)	79(1)
C(1)	6525(5)	10063(4)	6391(3)	50(1)
C(2)	6960(4)	9347(4)	4566(3)	46(1)
C(3)	8619(5)	8632(4)	6034(3)	50(1)
C(4)	5274(4)	7024(3)	6527(2)	30(1)
C(5)	4486(4)	7434(4)	5673(2)	35(1)
C(6)	5017(4)	6909(4)	4864(3)	40(1)
C(7)	6156(4)	6238(4)	5179(3)	38(1)
C(8)	6317(4)	6287(3)	6214(2)	31(1)
C(9)	7226(4)	5643(3)	6888(2)	30(1)
C(10)	8270(4)	5013(4)	6654(3)	37(1)
C(11)	9119(4)	4305(4)	7333(3)	39(1)
C(12)	10226(5)	3559(5)	6964(3)	53(1)
C(13)	11344(6)	4572(7)	6711(6)	111(3)
C(14)	10868(8)	2702(8)	7713(4)	117(3)
C(15)	9649(6)	2670(6)	6068(4)	80(2)
C(16)	8898(4)	4387(4)	8268(3)	40(1)
C(17)	7861(4)	5090(4)	8606(3)	35(1)
C(18)	7694(4)	5256(4)	9552(3)	41(1)
C(19)	6615(4)	5938(4)	9847(3)	41(1)
C(20)	5820(4)	6609(4)	9233(2)	35(1)
C(21)	4714(4)	7289(4)	9499(3)	39(1)
C(22)	3870(4)	7887(4)	8854(3)	36(1)
C(23)	2694(4)	8626(4)	9130(3)	46(1)
C(24)	1327(5)	7955(6)	8596(4)	73(2)
C(25)	2927(6)	10056(5)	8867(4)	71(2)
C(26)	2612(5)	8646(5)	10215(3)	66(1)
C(27)	4064(4)	7779(4)	7850(3)	34(1)
C(28)	5096(4)	7206(3)	7534(2)	30(1)
C(29)	6258(4)	6786(4)	8246(3)	41(1)
C(30)	7472(4)	7937(4)	8394(3)	48(1)
C(31)	6767(4)	5517(4)	7875(3)	40(1)
C(32)	5534(4)	4353(4)	7738(3)	46(1)

U_{eq} is defined as one third of the trace of the orthogonalized U_{ij} tensor.

Table B.4. Anisotropic Displacement Parameters [$A^2 \times 10^3$] for **51**.

	U11	U22	U33	U23	U13	U12
Re(1)	44(1)	31(1)	34(1)	8(1)	11(1)	8(1)
O(1)	97(3)	46(2)	82(2)	-15(2)	17(2)	14(2)
O(2)	82(2)	71(2)	64(2)	38(2)	32(2)	25(2)
O(3)	47(2)	105(3)	86(3)	23(2)	7(2)	7(2)
C(1)	61(3)	36(2)	53(2)	4(2)	14(2)	4(2)
C(2)	51(2)	42(2)	50(2)	14(2)	17(2)	14(2)
C(3)	53(3)	48(2)	51(2)	15(2)	17(2)	5(2)
C(4)	33(2)	27(2)	32(2)	5(1)	7(1)	4(1)
C(5)	40(2)	32(2)	33(2)	8(1)	2(2)	6(2)
C(6)	57(2)	34(2)	29(2)	4(2)	1(2)	2(2)
C(7)	57(2)	33(2)	28(2)	4(1)	12(2)	10(2)
C(8)	40(2)	27(2)	30(2)	4(1)	11(2)	7(2)
C(9)	35(2)	29(2)	29(2)	3(1)	10(1)	5(1)
C(10)	45(2)	39(2)	31(2)	4(2)	18(2)	13(2)
C(11)	42(2)	39(2)	41(2)	5(2)	14(2)	16(2)
C(12)	50(3)	67(3)	52(2)	3(2)	19(2)	33(2)
C(13)	62(4)	119(6)	164(7)	-9(5)	67(4)	15(4)
C(14)	135(6)	168(7)	73(4)	18(4)	23(4)	125(6)
C(15)	95(4)	78(4)	76(4)	-15(3)	21(3)	49(3)
C(16)	38(2)	48(2)	38(2)	8(2)	9(2)	20(2)
C(17)	33(2)	42(2)	33(2)	5(2)	7(2)	12(2)
C(18)	40(2)	56(2)	30(2)	9(2)	6(2)	19(2)
C(19)	44(2)	55(2)	25(2)	3(2)	9(2)	12(2)
C(20)	40(2)	40(2)	30(2)	1(2)	12(2)	13(2)
C(21)	43(2)	46(2)	32(2)	-2(2)	16(2)	9(2)
C(22)	35(2)	36(2)	41(2)	0(2)	13(2)	9(2)
C(23)	41(2)	50(2)	52(2)	-1(2)	15(2)	16(2)
C(24)	39(3)	101(4)	82(4)	-5(3)	16(2)	17(3)
C(25)	87(4)	54(3)	84(4)	11(3)	32(3)	39(3)
C(26)	74(3)	76(3)	61(3)	0(2)	35(3)	34(3)
C(27)	33(2)	34(2)	38(2)	4(2)	6(2)	8(2)
C(28)	34(2)	29(2)	29(2)	3(1)	9(1)	6(1)
C(29)	45(2)	51(2)	32(2)	5(2)	13(2)	20(2)
C(30)	48(2)	47(2)	44(2)	1(2)	1(2)	-3(2)
C(31)	42(2)	53(2)	29(2)	7(2)	10(2)	22(2)
C(32)	57(3)	43(2)	38(2)	8(2)	10(2)	0(2)

The anisotropic displacement factor exponent takes the form:
$-2\pi^2[h^2 a^{*2} U11 + \ldots + 2 h k a^* U12]$

Table B.5. Hydrogen Coordinates (x 10^4) and Isotropic Displacement Parameters (A^2 x 10^3) for **51**.

	x	y	z	U(eq)
H(5A)	3655	7887	5656	42
H(6A)	4608	6936	4192	48
H(7A)	6665	5725	4764	46
H(10A)	8465	5026	6024	44
H(13A)	10951	5119	6237	166
H(13B)	12038	4118	6457	166
H(13C)	11749	5119	7279	166
H(14A)	10172	2057	7878	175
H(14B)	11275	3253	8279	175
H(14C)	11564	2254	7455	175
H(15A)	9260	3196	5579	120
H(15B)	8950	2017	6219	120
H(15C)	10372	2233	5839	120
H(16A)	9454	3961	8711	48
H(18A)	8298	4916	10015	49
H(19A)	6451	5921	10483	49
H(21A)	4565	7324	10139	47
H(24A)	1186	7055	8769	110
H(24B)	1342	7959	7914	110
H(24C)	594	8429	8770	110
H(25A)	2976	10069	8189	107
H(25B)	3773	10480	9223	107
H(25C)	2180	10523	9023	107
H(26A)	2458	7751	10397	99
H(26B)	1867	9124	10360	99
H(26C)	3458	9074	10567	99
H(27A)	3441	8125	7404	41
H(30A)	7151	8741	8623	72
H(30B)	7810	8065	7792	72
H(30C)	8199	7708	8857	72
H(32A)	5850	3545	7509	69
H(32B)	4802	4579	7278	69
H(32C)	5207	4231	8344	69

Table B.6. Crystal, Data Collection and Refinement Parameters for **52**.

formula	$RuC_{39}H_{48}$
fw (g/mol)	617.84
crystal size, mm	0.10 x 0.24 x 0.42
cystal color	red
a, Å	12.817(2)
b, Å	17.769(3)
c, Å	29.094(5)
V, Å^3	6626.0(19)
cell detn, refls	516
d(calcd), g cm^{-3}	1.24
space group	Pbca
Z	8
F000	2608
Radiation, λ (Å)	MoKα, graphite monochromated, 0.710730.71073
temp, K	223
linear abs coeff, mm^{-1}	0.50
diffractometer	Smart 1000
scan technique, 2θ range, deg	omega, 4-50
crystal decay, %	0.02
absorption correction	Sadabs (empirical)
absorption range	0.66 - 1.00
refl meas / unique refls	26250 / 5852
R for merge	0.094
refls in refinement I>2.0σ(I)	3279
solution method	Shelxs-97 (Sheldrick, 1990)
parameters refined	361
R1, wR2	0.041, 0.088
R1 for I>0.0σ(I)	0.098
GOF	0.94
final diff map, e Å^{-3}	-0.46, +0.72
scattering factors	Internat.Tables for Crystallography, Vol C
H atom treatment	riding (C-H)

Table B.7. Bond Lengths [Å] and Angles [deg] for **52**.

Ru(1)-C(13)	2.158(4)
Ru(1)-C(5)	2.160(4)
Ru(1)-C(7)	2.163(4)
Ru(1)-C(3)	2.168(5)
Ru(1)-C(12)	2.176(4)
Ru(1)-C(14)	2.177(4)
Ru(1)-C(9)	2.186(5)
Ru(1)-C(1)	2.191(5)
Ru(1)-C(11)	2.221(4)
Ru(1)-C(15)	2.247(4)
C(1)-C(9)	1.422(7)
C(1)-C(3)	1.429(6)
C(1)-C(2)	1.510(6)
C(3)-C(5)	1.416(6)
C(3)-C(4)	1.509(7)
C(5)-C(7)	1.418(6)
C(5)-C(6)	1.506(6)
C(7)-C(9)	1.437(7)
C(7)-C(8)	1.515(7)
C(9)-C(10)	1.502(6)
C(11)-C(15)	1.431(5)
C(11)-C(12)	1.437(5)
C(11)-C(35)	1.451(5)
C(12)-C(13)	1.416(5)
C(13)-C(14)	1.422(5)
C(14)-C(15)	1.435(5)
C(15)-C(16)	1.453(5)
C(16)-C(17)	1.346(5)
C(16)-C(36)	1.513(5)
C(17)-C(18)	1.450(5)
C(18)-C(23)	1.355(6)
C(18)-C(19)	1.524(6)
C(19)-C(21)	1.515(6)
C(19)-C(20)	1.522(6)
C(19)-C(22)	1.533(6)
C(23)-C(24)	1.414(5)
C(24)-C(25)	1.370(6)
C(24)-C(36)	1.515(6)
C(25)-C(26)	1.418(6)
C(26)-C(27)	1.363(5)
C(27)-C(28)	1.423(6)
C(27)-C(38)	1.533(5)

C(28)-C(29)	1.354(6)
C(29)-C(34)	1.445(5)
C(29)-C(30)	1.529(6)
C(30)-C(32)	1.523(6)
C(30)-C(33)	1.531(6)
C(30)-C(31)	1.547(6)
C(34)-C(35)	1.344(5)
C(35)-C(38)	1.515(5)
C(36)-C(38)	1.472(6)
C(36)-C(37)	1.644(6)
C(38)-C(39)	1.636(6)

C(13)-Ru(1)-C(5)	107.08(17)
C(13)-Ru(1)-C(7)	119.13(18)
C(5)-Ru(1)-C(7)	38.30(16)
C(13)-Ru(1)-C(3)	125.16(17)
C(5)-Ru(1)-C(3)	38.18(17)
C(7)-Ru(1)-C(3)	64.33(18)
C(13)-Ru(1)-C(12)	38.12(14)
C(5)-Ru(1)-C(12)	119.03(16)
C(7)-Ru(1)-C(12)	150.78(17)
C(3)-Ru(1)-C(12)	110.18(17)
C(13)-Ru(1)-C(14)	38.29(14)
C(5)-Ru(1)-C(14)	125.48(17)
C(7)-Ru(1)-C(14)	110.39(17)
C(3)-Ru(1)-C(14)	159.90(17)
C(12)-Ru(1)-C(14)	64.13(16)
C(13)-Ru(1)-C(9)	154.22(19)
C(5)-Ru(1)-C(9)	63.93(17)
C(7)-Ru(1)-C(9)	38.58(18)
C(3)-Ru(1)-C(9)	63.98(18)
C(12)-Ru(1)-C(9)	167.7(2)
C(14)-Ru(1)-C(9)	125.21(18)
C(13)-Ru(1)-C(1)	162.24(18)
C(5)-Ru(1)-C(1)	63.76(18)
C(7)-Ru(1)-C(1)	64.14(19)
C(3)-Ru(1)-C(1)	38.26(17)
C(12)-Ru(1)-C(1)	130.79(18)
C(14)-Ru(1)-C(1)	159.45(18)
C(9)-Ru(1)-C(1)	37.93(18)
C(13)-Ru(1)-C(11)	63.29(14)
C(5)-Ru(1)-C(11)	153.91(16)
C(7)-Ru(1)-C(11)	167.78(16)
C(3)-Ru(1)-C(11)	125.31(17)
C(12)-Ru(1)-C(11)	38.14(13)
C(14)-Ru(1)-C(11)	63.33(15)

C(9)-Ru(1)-C(11)	135.00(16)
C(1)-Ru(1)-C(11)	117.66(16)
C(13)-Ru(1)-C(15)	63.17(14)
C(5)-Ru(1)-C(15)	162.41(16)
C(7)-Ru(1)-C(15)	131.32(16)
C(3)-Ru(1)-C(15)	159.40(16)
C(12)-Ru(1)-C(15)	63.40(15)
C(14)-Ru(1)-C(15)	37.81(13)
C(9)-Ru(1)-C(15)	117.88(15)
C(1)-Ru(1)-C(15)	129.59(15)
C(11)-Ru(1)-C(15)	37.35(13)
C(9)-C(1)-C(3)	108.0(4)
C(9)-C(1)-C(2)	127.5(5)
C(3)-C(1)-C(2)	124.3(5)
C(9)-C(1)-Ru(1)	70.8(3)
C(3)-C(1)-Ru(1)	70.0(3)
C(2)-C(1)-Ru(1)	128.6(3)
C(5)-C(3)-C(1)	107.8(4)
C(5)-C(3)-C(4)	126.9(5)
C(1)-C(3)-C(4)	125.2(5)
C(5)-C(3)-Ru(1)	70.6(3)
C(1)-C(3)-Ru(1)	71.7(3)
C(4)-C(3)-Ru(1)	126.4(4)
C(3)-C(5)-C(7)	108.9(4)
C(3)-C(5)-C(6)	125.0(4)
C(7)-C(5)-C(6)	126.1(5)
C(3)-C(5)-Ru(1)	71.2(3)
C(7)-C(5)-Ru(1)	71.0(2)
C(6)-C(5)-Ru(1)	124.2(4)
C(5)-C(7)-C(9)	107.4(4)
C(5)-C(7)-C(8)	126.6(5)
C(9)-C(7)-C(8)	126.0(5)
C(5)-C(7)-Ru(1)	70.7(3)
C(9)-C(7)-Ru(1)	71.6(3)
C(8)-C(7)-Ru(1)	124.3(4)
C(1)-C(9)-C(7)	107.9(4)
C(1)-C(9)-C(10)	126.7(5)
C(7)-C(9)-C(10)	125.2(5)
C(1)-C(9)-Ru(1)	71.2(3)
C(7)-C(9)-Ru(1)	69.9(3)
C(10)-C(9)-Ru(1)	128.8(3)
C(15)-C(11)-C(12)	108.3(3)
C(15)-C(11)-C(35)	121.4(3)
C(12)-C(11)-C(35)	130.0(4)
C(15)-C(11)-Ru(1)	72.3(2)
C(12)-C(11)-Ru(1)	69.2(2)

C(35)-C(11)-Ru(1)	129.3(3)
C(13)-C(12)-C(11)	107.3(4)
C(13)-C(12)-Ru(1)	70.3(2)
C(11)-C(12)-Ru(1)	72.6(2)
C(12)-C(13)-C(14)	109.1(3)
C(12)-C(13)-Ru(1)	71.6(2)
C(14)-C(13)-Ru(1)	71.6(2)
C(13)-C(14)-C(15)	107.8(3)
C(13)-C(14)-Ru(1)	70.2(2)
C(15)-C(14)-Ru(1)	73.8(2)
C(11)-C(15)-C(14)	107.4(3)
C(11)-C(15)-C(16)	122.7(3)
C(14)-C(15)-C(16)	129.7(4)
C(11)-C(15)-Ru(1)	70.3(2)
C(14)-C(15)-Ru(1)	68.4(2)
C(16)-C(15)-Ru(1)	130.8(3)
C(17)-C(16)-C(15)	125.3(4)
C(17)-C(16)-C(36)	119.8(4)
C(15)-C(16)-C(36)	114.9(4)
C(16)-C(17)-C(18)	123.2(4)
C(23)-C(18)-C(17)	118.3(4)
C(23)-C(18)-C(19)	123.8(4)
C(17)-C(18)-C(19)	117.9(4)
C(21)-C(19)-C(20)	109.9(4)
C(21)-C(19)-C(18)	110.1(4)
C(20)-C(19)-C(18)	108.4(4)
C(21)-C(19)-C(22)	108.2(4)
C(20)-C(19)-C(22)	108.1(4)
C(18)-C(19)-C(22)	112.2(4)
C(18)-C(23)-C(24)	123.1(4)
C(25)-C(24)-C(23)	124.1(4)
C(25)-C(24)-C(36)	116.7(4)
C(23)-C(24)-C(36)	118.6(4)
C(24)-C(25)-C(26)	122.4(4)
C(27)-C(26)-C(25)	122.3(4)
C(26)-C(27)-C(28)	125.0(4)
C(26)-C(27)-C(38)	116.2(4)
C(28)-C(27)-C(38)	118.7(4)
C(29)-C(28)-C(27)	123.6(4)
C(28)-C(29)-C(34)	118.5(4)
C(28)-C(29)-C(30)	123.6(4)
C(34)-C(29)-C(30)	117.9(4)
C(32)-C(30)-C(29)	112.2(4)
C(32)-C(30)-C(33)	109.1(4)
C(29)-C(30)-C(33)	108.7(4)
C(32)-C(30)-C(31)	108.0(4)

C(29)-C(30)-C(31)	108.8(4)
C(33)-C(30)-C(31)	110.1(4)
C(35)-C(34)-C(29)	123.6(4)
C(34)-C(35)-C(11)	125.6(4)
C(34)-C(35)-C(38)	120.8(4)
C(11)-C(35)-C(38)	113.0(3)
C(38)-C(36)-C(16)	115.3(4)
C(38)-C(36)-C(24)	113.4(4)
C(16)-C(36)-C(24)	112.9(4)
C(38)-C(36)-C(37)	104.2(4)
C(16)-C(36)-C(37)	104.9(4)
C(24)-C(36)-C(37)	104.6(4)
C(36)-C(38)-C(35)	113.9(4)
C(36)-C(38)-C(27)	112.0(4)
C(35)-C(38)-C(27)	113.0(4)
C(36)-C(38)-C(39)	104.9(4)
C(35)-C(38)-C(39)	105.3(4)
C(27)-C(38)-C(39)	106.9(4)

Table B.8. Atomic Coordinates [x 10^4] and Equivalent Isotropic Displacement Parameters [A^2 x 10^3] for **52**.

	x	y	z	U_{eq}
Ru(1)	3174(1)	2269(1)	6142(1)	36(1)
C(1)	3320(4)	1328(3)	5659(2)	57(1)
C(2)	4119(4)	704(3)	5654(2)	96(2)
C(3)	2341(4)	1288(3)	5893(2)	53(1)
C(4)	1971(4)	631(3)	6178(2)	90(2)
C(5)	1769(3)	1945(3)	5782(2)	51(1)
C(6)	682(4)	2117(3)	5948(2)	80(2)
C(7)	2384(4)	2406(3)	5490(2)	56(1)
C(8)	2072(4)	3158(3)	5288(2)	92(2)
C(9)	3350(4)	2017(3)	5410(2)	59(2)
C(10)	4190(4)	2270(4)	5085(2)	100(2)
C(11)	4240(3)	2287(2)	6744(1)	33(1)
C(12)	3169(3)	2288(2)	6890(1)	39(1)
C(13)	2705(3)	2954(2)	6718(1)	39(1)
C(14)	3457(3)	3360(2)	6458(1)	37(1)
C(15)	4425(3)	2956(2)	6483(1)	31(1)
C(16)	5457(3)	3173(2)	6324(1)	31(1)
C(17)	5683(3)	3807(2)	6091(1)	38(1)
C(18)	6737(3)	4026(2)	5970(1)	40(1)
C(19)	6878(4)	4718(2)	5667(2)	47(1)
C(20)	6373(4)	4562(3)	5203(2)	72(2)
C(21)	6368(4)	5396(3)	5889(2)	71(2)
C(22)	8031(4)	4903(3)	5585(2)	73(2)
C(23)	7539(3)	3605(2)	6132(2)	42(1)
C(24)	7395(3)	2946(2)	6396(2)	38(1)
C(25)	8193(3)	2531(2)	6580(2)	49(1)
C(26)	8020(3)	1842(3)	6814(2)	47(1)
C(27)	7044(3)	1585(2)	6913(2)	40(1)
C(28)	6813(3)	866(2)	7103(2)	45(1)
C(29)	5831(3)	601(2)	7160(2)	40(1)
C(30)	5584(4)	-189(2)	7339(2)	47(1)
C(31)	4938(4)	-611(3)	6971(2)	65(2)
C(32)	6568(4)	-644(3)	7432(2)	70(2)
C(33)	4957(4)	-117(3)	7784(2)	61(2)
C(34)	4967(3)	1080(2)	7034(1)	37(1)
C(35)	5082(3)	1776(2)	6861(1)	33(1)
C(36)	6311(3)	2609(3)	6425(2)	52(1)
C(37)	6260(4)	2005(3)	5997(2)	71(2)
C(38)	6148(3)	2143(3)	6837(2)	55(1)
C(39)	6177(4)	2736(3)	7267(2)	70(2)

U_{eq} is defined as one third of the trace of the orthogonalized U_{ij} tensor.

Table B.9. Anisotropic Displacement Parameters [$A^2 \times 10^3$] for **52**.

	U11	U22	U33	U23	U13	U12
Ru(1)	25(1)	47(1)	35(1)	5(1)	-2(1)	-2(1)
C(1)	45(3)	69(4)	56(3)	-15(3)	-14(3)	-3(3)
C(2)	78(4)	89(5)	119(5)	-60(4)	-19(4)	14(4)
C(3)	48(3)	58(3)	52(3)	1(3)	-11(3)	-17(3)
C(4)	97(5)	66(4)	106(5)	28(4)	-29(4)	-34(3)
C(5)	34(2)	70(3)	49(3)	10(3)	-9(2)	-13(3)
C(6)	34(3)	110(5)	97(4)	9(4)	-11(3)	-10(3)
C(7)	47(3)	72(4)	48(3)	11(3)	-17(2)	-16(3)
C(8)	105(5)	96(5)	74(4)	50(4)	-42(4)	-24(4)
C(9)	48(3)	94(4)	35(3)	-14(3)	1(2)	-24(3)
C(10)	75(4)	177(6)	49(4)	-11(4)	14(3)	-48(4)
C(11)	31(2)	36(2)	31(2)	-3(2)	0(2)	-2(2)
C(12)	30(2)	50(3)	37(2)	6(2)	6(2)	3(2)
C(13)	30(2)	44(3)	42(3)	0(2)	6(2)	10(2)
C(14)	34(2)	37(3)	38(3)	5(2)	-3(2)	7(2)
C(15)	32(2)	32(2)	28(2)	-2(2)	-2(2)	5(2)
C(16)	30(2)	31(2)	30(2)	-7(2)	0(2)	2(2)
C(17)	35(2)	39(3)	40(3)	3(2)	0(2)	6(2)
C(18)	38(2)	41(3)	42(3)	-1(2)	3(2)	-1(2)
C(19)	50(3)	38(3)	53(3)	7(2)	10(3)	-2(2)
C(20)	81(4)	82(4)	54(4)	18(3)	2(3)	-2(3)
C(21)	70(4)	43(3)	101(4)	9(3)	18(3)	-1(3)
C(22)	58(3)	62(4)	100(5)	29(3)	26(3)	-8(3)
C(23)	32(2)	47(3)	46(3)	3(3)	5(2)	-7(2)
C(24)	31(2)	36(3)	48(3)	0(2)	4(2)	2(2)
C(25)	26(2)	52(3)	68(3)	6(2)	-3(2)	-2(2)
C(26)	33(3)	45(3)	64(3)	4(3)	-8(2)	10(2)
C(27)	32(2)	43(3)	45(3)	-2(2)	-6(2)	8(2)
C(28)	42(3)	39(3)	54(3)	8(2)	-10(2)	12(2)
C(29)	46(3)	32(3)	41(3)	2(2)	-3(2)	5(2)
C(30)	54(3)	40(3)	47(3)	12(2)	3(2)	9(2)
C(31)	84(4)	42(3)	68(4)	1(3)	1(3)	-6(3)
C(32)	68(4)	51(3)	92(4)	26(3)	1(3)	13(3)
C(33)	81(4)	52(3)	51(3)	17(3)	6(3)	4(3)
C(34)	34(2)	40(3)	36(3)	6(2)	0(2)	2(2)
C(35)	28(2)	38(3)	34(3)	5(2)	-4(2)	3(2)
C(36)	32(2)	50(3)	73(4)	23(3)	3(2)	3(2)
C(37)	51(3)	107(5)	55(4)	-44(3)	-7(3)	19(3)
C(38)	27(2)	53(3)	85(4)	25(3)	-5(2)	2(2)
C(39)	52(3)	95(4)	61(4)	-46(3)	-22(3)	22(3)

The anisotropic displacement factor exponent takes the form:

$-2\pi^2[h^2 a^{*2} U11 + \ldots + 2 h k a^* U12]$

Table B.10. Hydrogen Coordinates (x 10^4) and Isotropic Displacement Parameters (A^2 x 10^3) for **52**.

	x	y	z	U(eq)
H(2A)	3984	374	5400	143
H(2B)	4078	426	5936	143
H(2C)	4805	917	5623	143
H(4A)	1623	274	5983	135
H(4B)	1496	806	6409	135
H(4C)	2559	394	6322	135
H(6A)	184	1915	5736	121
H(6B)	592	2652	5970	121
H(6C)	578	1894	6245	121
H(8A)	1735	3080	4997	138
H(8B)	2683	3463	5245	138
H(8C)	1601	3409	5494	138
H(10A)	4059	2064	4785	150
H(10B)	4855	2098	5194	150
H(10C)	4192	2810	5068	150
H(12A)	2837	1917	7092	47
H(13A)	1991	3122	6782	46
H(14A)	3351	3851	6313	44
H(17A)	5136	4120	6004	45
H(20A)	5648	4446	5247	108
H(20B)	6715	4143	5059	108
H(20C)	6436	4998	5011	108
H(21A)	5642	5293	5941	107
H(21B)	6435	5824	5690	107
H(21C)	6703	5500	6177	107
H(22A)	8363	5009	5873	110
H(22B)	8084	5336	5388	110
H(22C)	8367	4482	5441	110
H(23A)	8217	3758	6065	50
H(25A)	8873	2707	6550	58
H(26A)	8593	1556	6903	57
H(28A)	7367	561	7192	54
H(31A)	5340	-658	6694	97
H(31B)	4310	-335	6908	97
H(31C)	4762	-1103	7083	97
H(32A)	6981	-393	7661	105
H(32B)	6965	-691	7154	105
H(32C)	6379	-1136	7541	105

H(33A)	5365	145	8010	92
H(33B)	4786	-610	7897	92
H(33C)	4326	158	7725	92
H(34A)	4293	897	7075	44
H(37A)	5588	1766	5994	107
H(37B)	6793	1632	6036	107
H(37C)	6367	2267	5712	107
H(39A)	5626	3097	7233	104
H(39B)	6837	2992	7271	104
H(39C)	6086	2467	7551	104

Table B.11. Crystal, Data Collection and Refinement Parameters for **57**.

formula	$YbO_2C_{72}H_{96}$
fw (g/mol)	116.53
crystal size, mm	0.23 x 0.33 x 0.36
cystal color	black
a, Å	19.010(3)
b, Å	15.518(2)
c, Å	22.079(3)
β, deg	109.142(3)
V, $Å^3$	6153.1(16)
cell detn, refls	303
d(calcd), g cm^{-3}	1.26
space group	$P2_1/n$
Z	4
F000	2456
radiation, λ (Å)	MoKα, graphite monochromated, 0.71073
temp, K	223
linear abs coeff, mm^{-1}	1.56
diffractometer	Smart 1000
scan technique, 2θ range, deg	omega, 4-50
crystal decay, %	0.02
absorption correction	Sadabs
absorption range	0.90 - 1.00
refl meas / unique refls	25292 / 10605
R for merge	0.042
refls in refinement I>2.0σ(I)	7101
solution method	Shelxs-97 (Sheldrick, 1990)
parameters refined / restraints	745 / 18
R1, wR2	0.035, 0.071
R1 for I>0.0σ(I)	0.064
GOF	0.92
final diff map, e $Å^{-3}$	-0.40, +0.82
scattering factors	Internat.Tables for Crystallography, Vol C
H atom treatment	riding (C-H)

Table B.12. Bond Lengths [Å] and Angles [deg] for **57**.

Yb(1)-O(1)	2.432(3)
Yb(1)-O(2)	2.441(3)
Yb(1)-C(32)	2.691(4)
Yb(1)-C(33)	2.692(4)
Yb(1)-C(3)	2.700(4)
Yb(1)-C(2)	2.701(4)
Yb(1)-C(31)	2.776(4)
Yb(1)-C(4)	2.789(4)
Yb(1)-C(34)	2.811(4)
Yb(1)-C(1)	2.825(4)
Yb(1)-C(30)	2.862(4)
Yb(1)-C(5)	2.872(4)
O(1)-C(59)	1.441(5)
O(1)-C(62)	1.448(5)
O(2)-C(66)	1.432(5)
O(2)-C(63)	1.437(5)
C(1)-C(2)	1.414(5)
C(1)-C(25)	1.434(5)
C(1)-C(5)	1.438(5)
C(2)-C(3)	1.398(6)
C(3)-C(4)	1.394(5)
C(4)-C(5)	1.414(5)
C(5)-C(6)	1.442(5)
C(6)-C(7)	1.353(5)
C(6)-C(282)	1.516(11)
C(6)-C(281)	1.572(12)
C(7)-C(8)	1.435(6)
C(8)-C(13)	1.355(6)
C(8)-C(9)	1.537(6)
C(9)-C(11)	1.530(6)
C(9)-C(12)	1.530(6)
C(9)-C(10)	1.531(7)
C(13)-C(14)	1.415(6)
C(14)-C(15)	1.360(6)
C(14)-C(281)	1.501(12)
C(14)-C(282)	1.563(11)
C(15)-C(16)	1.419(6)
C(16)-C(17)	1.358(5)
C(17)-C(18)	1.430(5)
C(17)-C(262)	1.502(12)
C(17)-C(261)	1.558(14)
C(18)-C(19)	1.358(5)
C(19)-C(24)	1.446(6)

C(19)-C(20)	1.529(6)
C(20)-C(23)	1.524(7)
C(20)-C(22)	1.533(6)
C(20)-C(21)	1.537(6)
C(24)-C(25)	1.353(5)
C(25)-C(262)	1.515(12)
C(25)-C(261)	1.566(14)
C(261)-C(281)	1.53(2)
C(261)-C(271)	1.57(2)
C(281)-C(291)	1.54(2)
C(262)-C(282)	1.538(19)
C(262)-C(272)	1.592(19)
C(282)-C(292)	1.60(2)
C(30)-C(31)	1.409(5)
C(30)-C(34)	1.431(5)
C(30)-C(54)	1.446(5)
C(31)-C(32)	1.400(5)
C(32)-C(33)	1.399(5)
C(33)-C(34)	1.415(5)
C(34)-C(35)	1.440(5)
C(35)-C(36)	1.353(5)
C(35)-C(571)	1.531(11)
C(35)-C(572)	1.558(17)
C(36)-C(37)	1.436(5)
C(37)-C(42)	1.364(6)
C(37)-C(38)	1.532(5)
C(38)-C(40)	1.506(6)
C(38)-C(41)	1.516(6)
C(38)-C(39)	1.546(7)
C(42)-C(43)	1.413(5)
C(43)-C(44)	1.363(5)
C(43)-C(571)	1.545(11)
C(43)-C(572)	1.560(18)
C(44)-C(45)	1.420(6)
C(45)-C(46)	1.354(5)
C(46)-C(47)	1.430(5)
C(46)-C(552)	1.506(18)
C(46)-C(551)	1.557(11)
C(47)-C(48)	1.354(5)
C(48)-C(53)	1.444(5)
C(48)-C(49)	1.549(6)
C(49)-C(52)	1.518(6)
C(49)-C(51)	1.520(7)
C(49)-C(50)	1.525(6)
C(53)-C(54)	1.353(5)
C(54)-C(551)	1.513(10)

C(54)-C(552)	1.573(17)
C(551)-C(561)	1.526(17)
C(551)-C(571)	1.587(16)
C(571)-C(581)	1.521(17)
C(552)-C(572)	1.44(3)
C(552)-C(562)	1.65(3)
C(572)-C(582)	1.63(3)
C(59)-C(60)	1.466(7)
C(60)-C(61)	1.474(7)
C(61)-C(62)	1.487(6)
C(63)-C(64)	1.456(7)
C(64)-C(65)	1.415(7)
C(65)-C(66)	1.489(7)
CS1-CS2	1.490(5)
CS2-CS3	1.483(5)
CS3-CS4	1.525(5)
CS4-CS5	1.494(5)
CS5-CS6	1.494(5)
CS7-CS8	1.498(5)
CS8-CS9	1.487(5)
CS9-CS10	1.518(5)
CS10-CS11	1.493(5)
CS11-CS12	1.501(5)

O(1)-Yb(1)-O(2)	79.47(10)
O(1)-Yb(1)-C(32)	125.83(11)
O(2)-Yb(1)-C(32)	86.21(11)
O(1)-Yb(1)-C(33)	135.83(11)
O(2)-Yb(1)-C(33)	115.20(11)
C(32)-Yb(1)-C(33)	30.12(11)
O(1)-Yb(1)-C(3)	86.34(12)
O(2)-Yb(1)-C(3)	126.44(11)
C(32)-Yb(1)-C(3)	140.10(13)
C(33)-Yb(1)-C(3)	110.79(13)
O(1)-Yb(1)-C(2)	115.15(12)
O(2)-Yb(1)-C(2)	136.51(11)
C(32)-Yb(1)-C(2)	111.00(13)
C(33)-Yb(1)-C(2)	83.58(13)
C(3)-Yb(1)-C(2)	29.99(12)
O(1)-Yb(1)-C(31)	96.38(11)
O(2)-Yb(1)-C(31)	82.43(11)
C(32)-Yb(1)-C(31)	29.63(11)
C(33)-Yb(1)-C(31)	49.39(12)
C(3)-Yb(1)-C(31)	150.82(12)
C(2)-Yb(1)-C(31)	131.60(12)
O(1)-Yb(1)-C(4)	83.10(11)

O(2)-Yb(1)-C(4)	97.32(11)
C(32)-Yb(1)-C(4)	150.87(12)
C(33)-Yb(1)-C(4)	131.13(13)
C(3)-Yb(1)-C(4)	29.37(11)
C(2)-Yb(1)-C(4)	48.86(13)
C(31)-Yb(1)-C(4)	179.46(13)
O(1)-Yb(1)-C(34)	108.46(11)
O(2)-Yb(1)-C(34)	130.47(11)
C(32)-Yb(1)-C(34)	48.69(12)
C(33)-Yb(1)-C(34)	29.69(11)
C(3)-Yb(1)-C(34)	103.05(12)
C(2)-Yb(1)-C(34)	85.68(12)
C(31)-Yb(1)-C(34)	48.51(11)
C(4)-Yb(1)-C(34)	131.80(12)
O(1)-Yb(1)-C(1)	131.04(11)
O(2)-Yb(1)-C(1)	109.43(10)
C(32)-Yb(1)-C(1)	103.03(12)
C(33)-Yb(1)-C(1)	85.34(12)
C(3)-Yb(1)-C(1)	48.80(12)
C(2)-Yb(1)-C(1)	29.54(11)
C(31)-Yb(1)-C(1)	132.05(12)
C(4)-Yb(1)-C(1)	48.48(12)
C(34)-Yb(1)-C(1)	101.08(11)
O(1)-Yb(1)-C(30)	87.56(11)
O(2)-Yb(1)-C(30)	107.80(10)
C(32)-Yb(1)-C(30)	48.06(12)
C(33)-Yb(1)-C(30)	48.65(12)
C(3)-Yb(1)-C(30)	122.98(12)
C(2)-Yb(1)-C(30)	113.31(11)
C(31)-Yb(1)-C(30)	28.89(11)
C(4)-Yb(1)-C(30)	151.10(12)
C(34)-Yb(1)-C(30)	29.20(10)
C(1)-Yb(1)-C(30)	130.03(11)
O(1)-Yb(1)-C(5)	108.51(11)
O(2)-Yb(1)-C(5)	88.57(11)
C(32)-Yb(1)-C(5)	123.15(12)
C(33)-Yb(1)-C(5)	113.06(12)
C(3)-Yb(1)-C(5)	47.98(12)
C(2)-Yb(1)-C(5)	48.28(12)
C(31)-Yb(1)-C(5)	151.51(12)
C(4)-Yb(1)-C(5)	28.87(11)
C(34)-Yb(1)-C(5)	130.03(11)
C(1)-Yb(1)-C(5)	29.23(11)
C(30)-Yb(1)-C(5)	159.19(11)
C(59)-O(1)-C(62)	108.5(3)
C(59)-O(1)-Yb(1)	122.5(3)

C(62)-O(1)-Yb(1)	129.0(3)
C(66)-O(2)-C(63)	107.3(4)
C(66)-O(2)-Yb(1)	123.0(3)
C(63)-O(2)-Yb(1)	129.8(3)
C(2)-C(1)-C(25)	131.4(4)
C(2)-C(1)-C(5)	106.5(4)
C(25)-C(1)-C(5)	122.1(4)
C(2)-C(1)-Yb(1)	70.4(2)
C(25)-C(1)-Yb(1)	121.0(3)
C(5)-C(1)-Yb(1)	77.2(2)
C(3)-C(2)-C(1)	108.7(4)
C(3)-C(2)-Yb(1)	75.0(2)
C(1)-C(2)-Yb(1)	80.1(2)
C(4)-C(3)-C(2)	108.9(4)
C(4)-C(3)-Yb(1)	78.8(2)
C(2)-C(3)-Yb(1)	75.0(2)
C(3)-C(4)-C(5)	108.0(4)
C(3)-C(4)-Yb(1)	71.8(2)
C(5)-C(4)-Yb(1)	78.8(2)
C(4)-C(5)-C(1)	107.8(4)
C(4)-C(5)-C(6)	130.4(4)
C(1)-C(5)-C(6)	121.5(4)
C(4)-C(5)-Yb(1)	72.3(2)
C(1)-C(5)-Yb(1)	73.6(2)
C(6)-C(5)-Yb(1)	124.7(3)
C(7)-C(6)-C(5)	125.3(4)
C(7)-C(6)-C(282)	118.7(5)
C(5)-C(6)-C(282)	114.1(5)
C(7)-C(6)-C(281)	116.9(5)
C(5)-C(6)-C(281)	116.1(5)
C(6)-C(7)-C(8)	124.0(4)
C(13)-C(8)-C(7)	118.5(4)
C(13)-C(8)-C(9)	123.0(4)
C(7)-C(8)-C(9)	118.5(4)
C(11)-C(9)-C(12)	107.9(4)
C(11)-C(9)-C(10)	108.2(4)
C(12)-C(9)-C(10)	109.8(4)
C(11)-C(9)-C(8)	112.1(4)
C(12)-C(9)-C(8)	110.1(4)
C(10)-C(9)-C(8)	108.7(4)
C(8)-C(13)-C(14)	123.3(4)
C(15)-C(14)-C(13)	124.4(4)
C(15)-C(14)-C(281)	116.2(6)
C(13)-C(14)-C(281)	117.5(6)
C(15)-C(14)-C(282)	115.9(5)
C(13)-C(14)-C(282)	117.8(5)

C(14)-C(15)-C(16)	122.5(4)
C(17)-C(16)-C(15)	121.4(4)
C(16)-C(17)-C(18)	123.4(4)
C(16)-C(17)-C(262)	118.9(5)
C(18)-C(17)-C(262)	116.1(6)
C(16)-C(17)-C(261)	115.5(6)
C(18)-C(17)-C(261)	119.4(6)
C(19)-C(18)-C(17)	122.8(4)
C(18)-C(19)-C(24)	118.9(4)
C(18)-C(19)-C(20)	123.4(4)
C(24)-C(19)-C(20)	117.6(4)
C(23)-C(20)-C(19)	112.0(4)
C(23)-C(20)-C(22)	110.0(5)
C(19)-C(20)-C(22)	109.9(4)
C(23)-C(20)-C(21)	106.8(4)
C(19)-C(20)-C(21)	109.1(4)
C(22)-C(20)-C(21)	109.0(4)
C(25)-C(24)-C(19)	123.5(4)
C(24)-C(25)-C(1)	125.5(4)
C(24)-C(25)-C(262)	116.8(6)
C(1)-C(25)-C(262)	116.7(5)
C(24)-C(25)-C(261)	119.6(6)
C(1)-C(25)-C(261)	112.6(6)
C(281)-C(261)-C(17)	107.6(11)
C(281)-C(261)-C(25)	112.0(11)
C(17)-C(261)-C(25)	109.0(9)
C(281)-C(261)-C(271)	114.1(17)
C(17)-C(261)-C(271)	107.8(9)
C(25)-C(261)-C(271)	106.2(9)
C(14)-C(281)-C(261)	108.2(11)
C(14)-C(281)-C(291)	110.3(8)
C(261)-C(281)-C(291)	111.5(16)
C(14)-C(281)-C(6)	111.3(8)
C(261)-C(281)-C(6)	105.2(11)
C(291)-C(281)-C(6)	110.1(8)
C(17)-C(262)-C(25)	114.9(8)
C(17)-C(262)-C(282)	108.9(10)
C(25)-C(262)-C(282)	109.3(10)
C(17)-C(262)-C(272)	109.0(8)
C(25)-C(262)-C(272)	107.1(8)
C(282)-C(262)-C(272)	107.4(14)
C(6)-C(282)-C(262)	113.6(10)
C(6)-C(282)-C(14)	111.0(8)
C(262)-C(282)-C(14)	109.2(9)
C(6)-C(282)-C(292)	108.6(8)
C(262)-C(282)-C(292)	107.0(15)

C(14)-C(282)-C(292)	107.1(7)
C(31)-C(30)-C(34)	107.9(4)
C(31)-C(30)-C(54)	130.1(4)
C(34)-C(30)-C(54)	121.7(4)
C(31)-C(30)-Yb(1)	72.1(2)
C(34)-C(30)-Yb(1)	73.4(2)
C(54)-C(30)-Yb(1)	125.8(3)
C(32)-C(31)-C(30)	107.6(4)
C(32)-C(31)-Yb(1)	71.9(2)
C(30)-C(31)-Yb(1)	79.0(2)
C(33)-C(32)-C(31)	109.5(4)
C(33)-C(32)-Yb(1)	75.0(2)
C(31)-C(32)-Yb(1)	78.5(2)
C(32)-C(33)-C(34)	107.7(4)
C(32)-C(33)-Yb(1)	74.9(2)
C(34)-C(33)-Yb(1)	79.8(2)
C(33)-C(34)-C(30)	107.4(4)
C(33)-C(34)-C(35)	130.4(4)
C(30)-C(34)-C(35)	122.1(4)
C(33)-C(34)-Yb(1)	70.5(2)
C(30)-C(34)-Yb(1)	77.4(2)
C(35)-C(34)-Yb(1)	120.4(3)
C(36)-C(35)-C(34)	125.6(4)
C(36)-C(35)-C(571)	118.1(5)
C(34)-C(35)-C(571)	115.4(5)
C(36)-C(35)-C(572)	119.0(7)
C(34)-C(35)-C(572)	112.8(7)
C(35)-C(36)-C(37)	124.0(4)
C(42)-C(37)-C(36)	118.2(4)
C(42)-C(37)-C(38)	120.6(4)
C(36)-C(37)-C(38)	121.2(4)
C(40)-C(38)-C(41)	109.3(4)
C(40)-C(38)-C(37)	110.6(4)
C(41)-C(38)-C(37)	113.3(4)
C(40)-C(38)-C(39)	108.8(4)
C(41)-C(38)-C(39)	105.9(4)
C(37)-C(38)-C(39)	108.7(4)
C(37)-C(42)-C(43)	124.0(4)
C(44)-C(43)-C(42)	124.7(4)
C(44)-C(43)-C(571)	117.5(5)
C(42)-C(43)-C(571)	116.4(5)
C(44)-C(43)-C(572)	114.8(7)
C(42)-C(43)-C(572)	118.3(7)
C(43)-C(44)-C(45)	122.0(4)
C(46)-C(45)-C(44)	121.8(4)
C(45)-C(46)-C(47)	123.5(4)

C(45)-C(46)-C(552)	115.5(7)
C(47)-C(46)-C(552)	119.6(7)
C(45)-C(46)-C(551)	117.8(5)
C(47)-C(46)-C(551)	116.7(5)
C(48)-C(47)-C(46)	122.8(4)
C(47)-C(48)-C(53)	118.8(4)
C(47)-C(48)-C(49)	123.4(4)
C(53)-C(48)-C(49)	117.7(4)
C(52)-C(49)-C(51)	108.6(4)
C(52)-C(49)-C(50)	108.3(4)
C(51)-C(49)-C(50)	110.0(4)
C(52)-C(49)-C(48)	111.8(4)
C(51)-C(49)-C(48)	108.7(4)
C(50)-C(49)-C(48)	109.4(4)
C(54)-C(53)-C(48)	123.7(4)
C(53)-C(54)-C(30)	125.3(4)
C(53)-C(54)-C(551)	117.6(5)
C(30)-C(54)-C(551)	114.4(5)
C(53)-C(54)-C(552)	119.0(7)
C(30)-C(54)-C(552)	114.8(7)
C(54)-C(551)-C(561)	108.6(7)
C(54)-C(551)-C(46)	111.6(7)
C(561)-C(551)-C(46)	107.7(7)
C(54)-C(551)-C(571)	110.2(8)
C(561)-C(551)-C(571)	112.1(11)
C(46)-C(551)-C(571)	106.7(8)
C(581)-C(571)-C(35)	109.2(7)
C(581)-C(571)-C(43)	108.9(7)
C(35)-C(571)-C(43)	112.1(7)
C(581)-C(571)-C(551)	112.4(11)
C(35)-C(571)-C(551)	107.5(8)
C(43)-C(571)-C(551)	106.8(8)
C(572)-C(552)-C(46)	112.1(16)
C(572)-C(552)-C(54)	109.8(16)
C(46)-C(552)-C(54)	111.1(11)
C(572)-C(552)-C(562)	106(2)
C(46)-C(552)-C(562)	108.9(11)
C(54)-C(552)-C(562)	108.9(12)
C(552)-C(572)-C(35)	114.4(16)
C(552)-C(572)-C(43)	109.7(16)
C(35)-C(572)-C(43)	109.8(12)
C(552)-C(572)-C(582)	106(2)
C(35)-C(572)-C(582)	107.3(12)
C(43)-C(572)-C(582)	109.3(12)
O(1)-C(59)-C(60)	105.5(4)
C(59)-C(60)-C(61)	106.4(5)

C(60)-C(61)-C(62)	104.3(5)
O(1)-C(62)-C(61)	107.5(4)
O(2)-C(63)-C(64)	107.2(5)
C(65)-C(64)-C(63)	108.2(5)
C(64)-C(65)-C(66)	107.1(5)
O(2)-C(66)-C(65)	106.9(4)
CS3-CS2-CS1	114.3(8)
CS2-CS3-CS4	106.6(7)
CS5-CS4-CS3	105.5(7)
CS6-CS5-CS4	110.6(7)
CS9-CS8-CS7	112.0(7)
CS8-CS9-CS10	108.1(7)
CS11-CS10-CS9	107.1(6)
CS10-CS11-CS12	109.4(7)

Table B.13. Atomic Coordinates [x 10^4] and Equivalent Isotropic Displacement Parameters [A^2 x 10^3] for **57**.

	x	y	z	U_{eq}
Yb(1)	-455(1)	-3920(1)	7395(1)	31(1)
O(1)	-1040(2)	-2900(2)	6542(2)	45(1)
O(2)	-868(2)	-2819(2)	7994(1)	43(1)
C(1)	-923(2)	-5557(2)	7672(2)	28(1)
C(2)	-767(2)	-5594(3)	7089(2)	34(1)
C(3)	-1315(2)	-5132(3)	6623(2)	37(1)
C(4)	-1811(2)	-4781(3)	6901(2)	35(1)
C(5)	-1584(2)	-5044(3)	7550(2)	31(1)
C(6)	-1944(2)	-4936(3)	8027(2)	32(1)
C(7)	-2585(2)	-4499(3)	7942(2)	37(1)
C(8)	-2923(2)	-4392(3)	8430(2)	40(1)
C(9)	-3653(3)	-3878(3)	8268(2)	51(1)
C(10)	-4265(3)	-4376(4)	7763(3)	74(2)
C(11)	-3902(3)	-3747(4)	8854(3)	77(2)
C(12)	-3555(3)	-2988(3)	8008(3)	84(2)
C(13)	-2590(2)	-4758(3)	9011(2)	39(1)
C(14)	-1936(2)	-5263(3)	9156(2)	36(1)
C(15)	-1616(2)	-5679(3)	9722(2)	39(1)
C(16)	-967(2)	-6193(3)	9841(2)	37(1)
C(17)	-622(2)	-6283(2)	9395(2)	36(1)
C(18)	41(2)	-6778(3)	9498(2)	39(1)
C(19)	379(2)	-6867(2)	9046(2)	36(1)
C(20)	1105(3)	-7366(3)	9159(2)	50(1)
C(21)	963(3)	-8118(3)	8681(3)	64(2)
C(22)	1698(3)	-6771(3)	9053(3)	74(2)
C(23)	1390(3)	-7756(4)	9829(3)	84(2)
C(24)	47(2)	-6462(2)	8428(2)	32(1)
C(25)	-571(2)	-5965(2)	8279(2)	27(1)
C(261)	-1093(8)	-6018(10)	8699(7)	27(3)
C(271)	-1658(9)	-6765(9)	8407(6)	35(4)
C(281)	-1459(8)	-5154(10)	8737(6)	24(3)
C(291)	-877(9)	-4444(8)	9006(5)	32(4)
C(262)	-825(7)	-5681(9)	8831(6)	34(3)
C(272)	-459(8)	-4764(7)	9060(4)	40(3)
C(282)	-1675(6)	-5556(9)	8587(5)	30(3)
C(292)	-2036(8)	-6480(8)	8361(5)	42(3)
C(30)	948(2)	-3383(2)	7307(2)	28(1)
C(31)	888(2)	-3048(3)	7881(2)	32(1)

C(32)	898(2)	-3745(3)	8287(2)	37(1)
C(33)	935(2)	-4516(3)	7970(2)	32(1)
C(34)	976(2)	-4302(3)	7359(2)	27(1)
C(35)	1069(2)	-4845(2)	6862(2)	28(1)
C(36)	1125(2)	-5714(2)	6885(2)	31(1)
C(37)	1233(2)	-6233(2)	6384(2)	34(1)
C(38)	1270(3)	-7217(3)	6433(2)	40(1)
C(39)	713(3)	-7603(3)	5816(3)	80(2)
C(40)	2041(3)	-7532(3)	6498(3)	90(2)
C(41)	1044(3)	-7567(3)	6983(3)	78(2)
C(42)	1318(3)	-5823(3)	5865(2)	40(1)
C(43)	1292(2)	-4919(3)	5785(2)	36(1)
C(44)	1403(2)	-4498(3)	5282(2)	40(1)
C(45)	1372(2)	-3586(3)	5230(2)	40(1)
C(46)	1278(2)	-3081(3)	5697(2)	34(1)
C(47)	1285(2)	-2160(3)	5679(2)	38(1)
C(48)	1223(2)	-1665(3)	6164(2)	34(1)
C(49)	1299(3)	-671(3)	6180(2)	44(1)
C(50)	601(3)	-268(3)	6257(3)	73(2)
C(51)	1979(3)	-420(3)	6741(3)	69(2)
C(52)	1392(3)	-323(3)	5568(3)	69(2)
C(53)	1101(2)	-2080(2)	6707(2)	33(1)
C(54)	1060(2)	-2944(2)	6768(2)	31(1)
C(551)	1377(7)	-3504(6)	6360(5)	24(2)
C(561)	2210(5)	-3619(7)	6705(5)	30(2)
C(571)	950(7)	-4400(6)	6217(5)	26(3)
C(581)	120(5)	-4292(8)	5871(4)	33(3)
C(552)	987(14)	-3533(10)	6170(9)	33(4)
C(562)	98(7)	-3770(15)	5814(6)	37(5)
C(572)	1356(14)	-4342(11)	6379(9)	35(5)
C(582)	2230(8)	-4112(15)	6747(8)	38(5)
C(59)	-817(3)	-2009(3)	6571(3)	58(2)
C(60)	-1097(4)	-1697(4)	5908(3)	97(2)
C(61)	-1760(3)	-2219(3)	5579(3)	65(2)
C(62)	-1637(3)	-3042(3)	5945(2)	61(2)
C(63)	-441(3)	-2306(3)	8530(3)	72(2)
C(64)	-903(3)	-1574(4)	8571(3)	89(2)
C(65)	-1643(3)	-1745(4)	8178(3)	111(3)
C(66)	-1633(3)	-2582(3)	7850(3)	64(2)
CS1	-1047(10)	-9501(12)	11608(7)	141(8)
CS2	-1559(11)	-9630(11)	10940(6)	171(9)
CS3	-1531(12)	-8934(9)	10488(7)	186(10)
CS4	-1487(10)	-9375(11)	9884(7)	162(9)
CS5	-985(10)	-8821(9)	9652(7)	133(7)
CS6	-869(10)	-9210(11)	9073(7)	101(6)
CS7	-1453(8)	-9418(8)	11591(5)	78(4)

CS8	-1594(11)	-8991(11)	10953(6)	183(9)
CS9	-1171(12)	-9407(12)	10573(7)	209(11)
CS10	-1302(11)	-8890(10)	9962(7)	153(7)
CS11	-982(12)	-9398(9)	9540(7)	200(10)
CS12	-1003(11)	-8864(11)	8967(7)	149(9)

U_{eq} is defined as one third of the trace of the orthogonalized U_{ij} tensor.

Table B.14. Anisotropic Displacement Parameters [$A^2 \times 10^3$] for **57**.

	U11	U22	U33	U23	U13	U12
Yb(1)	31(1)	34(1)	31(1)	-1(1)	13(1)	-1(1)
O(1)	44(2)	42(2)	47(2)	9(2)	14(2)	2(2)
O(2)	39(2)	45(2)	45(2)	-6(2)	14(2)	5(2)
C(1)	30(3)	30(2)	27(2)	-5(2)	12(2)	-6(2)
C(2)	34(3)	41(3)	33(3)	-10(2)	20(2)	-4(2)
C(3)	38(3)	48(3)	29(3)	-5(2)	16(2)	-9(2)
C(4)	29(3)	47(3)	29(3)	3(2)	11(2)	0(2)
C(5)	25(2)	40(2)	28(3)	-2(2)	10(2)	-5(2)
C(6)	28(3)	43(3)	28(3)	2(2)	13(2)	-2(2)
C(7)	33(3)	48(3)	33(3)	8(2)	15(2)	2(2)
C(8)	35(3)	44(3)	45(3)	8(2)	19(3)	8(2)
C(9)	44(3)	61(3)	54(3)	19(3)	26(3)	22(3)
C(10)	39(3)	98(4)	83(5)	12(4)	17(3)	20(3)
C(11)	64(4)	109(5)	75(4)	23(4)	47(4)	51(3)
C(12)	83(5)	64(4)	133(6)	39(4)	73(5)	40(3)
C(13)	38(3)	51(3)	38(3)	1(2)	25(2)	4(2)
C(14)	35(3)	45(3)	34(3)	0(2)	20(2)	1(2)
C(15)	45(3)	49(3)	27(3)	0(2)	18(2)	1(2)
C(16)	41(3)	48(3)	26(2)	7(2)	14(2)	1(2)
C(17)	37(3)	39(3)	30(3)	0(2)	11(2)	6(2)
C(18)	37(3)	44(3)	31(3)	9(2)	7(2)	6(2)
C(19)	34(3)	30(2)	46(3)	2(2)	14(2)	2(2)
C(20)	36(3)	55(3)	60(4)	11(3)	18(3)	13(2)
C(21)	70(4)	45(3)	91(5)	3(3)	46(4)	20(3)
C(22)	33(3)	70(4)	116(5)	18(4)	22(3)	8(3)
C(23)	60(4)	111(5)	80(5)	31(4)	21(4)	52(4)
C(24)	32(3)	35(2)	35(3)	0(2)	19(2)	-3(2)
C(25)	32(2)	26(2)	26(2)	-5(2)	13(2)	-3(2)
C(261)	16(7)	40(8)	26(7)	-2(6)	7(5)	-4(6)
C(271)	32(9)	36(7)	43(7)	-3(6)	19(7)	-12(6)
C(281)	25(7)	37(8)	9(6)	-4(5)	3(5)	-4(6)
C(291)	30(8)	27(6)	38(7)	-5(5)	10(6)	-1(5)
C(262)	26(7)	51(8)	27(6)	-2(5)	13(5)	2(5)
C(272)	48(7)	36(6)	39(6)	-4(4)	18(5)	-12(5)
C(282)	21(6)	48(8)	23(6)	-5(5)	9(5)	-1(5)
C(292)	38(7)	48(7)	40(6)	-12(5)	12(6)	-7(6)
C(30)	29(2)	28(2)	31(3)	-3(2)	17(2)	-6(2)
C(31)	33(3)	32(2)	34(3)	-5(2)	16(2)	-3(2)
C(32)	36(3)	49(3)	26(2)	-3(2)	13(2)	-6(2)
C(33)	32(3)	35(2)	33(3)	5(2)	18(2)	0(2)

C(34)	23(2)	35(2)	27(2)	-1(2)	11(2)	-2(2)
C(35)	24(2)	34(2)	28(3)	2(2)	11(2)	-2(2)
C(36)	32(3)	33(2)	31(3)	9(2)	15(2)	2(2)
C(37)	39(3)	31(3)	40(3)	-4(2)	23(2)	-1(2)
C(38)	55(3)	27(2)	47(3)	-1(2)	29(3)	-1(2)
C(39)	127(6)	36(3)	73(4)	-7(3)	27(4)	-11(3)
C(40)	84(5)	50(3)	150(7)	25(4)	57(5)	19(3)
C(41)	134(6)	33(3)	90(5)	6(3)	69(5)	-1(3)
C(42)	52(3)	35(3)	44(3)	-9(2)	29(3)	-2(2)
C(43)	46(3)	34(2)	36(3)	-4(2)	24(2)	0(2)
C(44)	55(3)	41(3)	32(3)	-7(2)	24(2)	-4(2)
C(45)	53(3)	43(3)	32(3)	6(2)	25(3)	-1(2)
C(46)	43(3)	35(2)	31(3)	4(2)	20(2)	-3(2)
C(47)	45(3)	35(3)	40(3)	8(2)	22(2)	0(2)
C(48)	34(3)	33(2)	42(3)	1(2)	19(2)	0(2)
C(49)	56(3)	29(2)	57(4)	6(2)	33(3)	-1(2)
C(50)	81(4)	42(3)	113(5)	15(3)	56(4)	14(3)
C(51)	89(5)	43(3)	78(4)	-10(3)	29(4)	-21(3)
C(52)	119(5)	28(3)	78(4)	13(3)	57(4)	3(3)
C(53)	40(3)	32(2)	33(3)	-2(2)	19(2)	0(2)
C(54)	35(3)	29(2)	35(3)	-3(2)	20(2)	-3(2)
C(551)	27(6)	24(5)	19(6)	-1(4)	5(5)	-6(4)
C(561)	27(5)	26(5)	38(5)	-6(5)	13(4)	-1(5)
C(571)	29(6)	24(5)	27(5)	-10(4)	14(5)	-11(5)
C(581)	40(5)	28(5)	33(5)	6(4)	14(4)	3(5)
C(552)	46(12)	29(7)	21(9)	-8(6)	6(9)	-2(8)
C(562)	26(7)	58(12)	24(7)	11(7)	3(6)	5(8)
C(572)	49(13)	36(9)	29(10)	-3(7)	27(10)	-13(9)
C(582)	11(7)	59(12)	46(9)	-8(10)	10(6)	0(9)
C(59)	56(4)	48(3)	73(4)	10(3)	24(3)	4(3)
C(60)	126(6)	72(4)	80(5)	28(4)	16(5)	-11(4)
C(61)	66(4)	75(4)	52(4)	15(3)	20(3)	19(3)
C(62)	52(3)	64(3)	52(4)	8(3)	-1(3)	-3(3)
C(63)	58(4)	82(4)	72(4)	-35(3)	16(3)	1(3)
C(64)	83(5)	67(4)	110(6)	-39(4)	23(5)	10(4)
C(65)	68(5)	113(5)	123(6)	-67(5)	-8(4)	38(4)
C(66)	41(3)	57(3)	92(5)	-11(3)	20(3)	5(3)

The anisotropic displacement factor exponent takes the form:

$-2\pi^2[h^2 a^{*2} U11 + \ldots + 2 h k a^* U12]$

Table B.15. Hydrogen Coordinates (x 10^4) and Isotropic Displacement Parameters (A^2 x 10^3) for **57**.

	x	y	z	U(eq)
H(2A)	-366	-5879	7026	41
H(3A)	-1344	-5070	6197	44
H(4A)	-2219	-4435	6696	41
H(7A)	-2820	-4252	7543	44
H(10A)	-4330	-4930	7931	111
H(10B)	-4125	-4452	7386	111
H(10C)	-4723	-4059	7654	111
H(11A)	-3972	-4298	9024	116
H(11B)	-4362	-3432	8731	116
H(11C)	-3527	-3429	9175	116
H(12A)	-3405	-3054	7635	127
H(12B)	-3180	-2673	8330	127
H(12C)	-4018	-2680	7894	127
H(13A)	-2802	-4673	9331	47
H(15A)	-1830	-5626	10043	46
H(16A)	-774	-6474	10233	45
H(18A)	250	-7052	9891	46
H(21A)	784	-7898	8251	96
H(21B)	597	-8498	8749	96
H(21C)	1418	-8429	8745	96
H(22A)	1512	-6525	8631	110
H(22B)	2140	-7098	9093	110
H(22C)	1812	-6319	9367	110
H(23A)	1487	-7305	10143	126
H(23B)	1841	-8069	9879	126
H(23C)	1022	-8141	9887	126
H(24A)	271	-6548	8116	38
H(27A)	-1927	-6902	8695	53
H(27B)	-1392	-7265	8345	53
H(27C)	-2002	-6584	8002	53
H(29A)	-599	-4569	9445	48
H(29B)	-1123	-3899	8980	48
H(29C)	-544	-4422	8760	48
H(27D)	-586	-4376	8702	60
H(27E)	73	-4824	9231	60
H(27F)	-642	-4540	9385	60
H(29D)	-1868	-6880	8710	63
H(29E)	-1889	-6680	8008	63
H(29F)	-2569	-6434	8227	63

H(31A)	849	-2469	7974	38
H(32A)	883	-3703	8702	44
H(33A)	933	-5069	8131	38
H(36A)	1093	-5993	7248	37
H(39A)	831	-7401	5450	120
H(39B)	217	-7428	5781	120
H(39C)	745	-8220	5835	120
H(40A)	2392	-7295	6880	135
H(40B)	2170	-7351	6132	135
H(40C)	2054	-8149	6524	135
H(41A)	1377	-7351	7382	116
H(41B)	1066	-8185	6983	116
H(41C)	545	-7386	6934	116
H(42A)	1398	-6160	5545	48
H(44A)	1503	-4818	4964	48
H(45A)	1418	-3328	4864	48
H(47A)	1334	-1890	5319	46
H(50A)	651	348	6273	109
H(50B)	538	-472	6646	109
H(50C)	175	-427	5899	109
H(51A)	2029	196	6758	104
H(51B)	2416	-673	6688	104
H(51C)	1922	-625	7133	104
H(52A)	1440	293	5596	103
H(52B)	965	-474	5209	103
H(52C)	1831	-567	5512	103
H(53A)	1046	-1733	7032	40
H(56A)	2447	-3064	6778	45
H(56B)	2420	-3963	6447	45
H(56C)	2286	-3900	7109	45
H(58A)	-114	-4848	5799	50
H(58B)	44	-4011	5467	50
H(58C)	-93	-3949	6128	50
H(56D)	-178	-3250	5667	56
H(56E)	-93	-4057	6113	56
H(56F)	50	-4142	5455	56
H(58D)	2503	-4635	6892	58
H(58E)	2270	-3747	7108	58
H(58F)	2430	-3819	6457	58
H(59A)	-279	-1958	6742	70
H(59B)	-1032	-1682	6841	70
H(60A)	-722	-1766	5702	117
H(60B)	-1228	-1092	5898	117
H(61A)	-1800	-2319	5135	77
H(61B)	-2210	-1936	5591	77
H(62A)	-2088	-3212	6028	73

H(62B)	-1503	-3496	5701	73
H(63A)	14	-2108	8467	86
H(63B)	-311	-2642	8922	86
H(64A)	-884	-1489	9011	107
H(64B)	-722	-1054	8427	107
H(65A)	-1822	-1290	7864	133
H(65B)	-1968	-1781	8436	133
H(66A)	-1897	-3019	8006	76
H(66B)	-1871	-2522	7391	76
HS1A	-999	-10031	11842	211
HS1B	-1244	-9063	11814	211
HS1C	-566	-9326	11598	211
HS2A	-1437	-10172	10780	206
HS2B	-2065	-9676	10949	206
HS3A	-1098	-8572	10675	223
HS3B	-1974	-8578	10388	223
HS4A	-1284	-9951	9981	195
HS4B	-1977	-9413	9563	195
HS5A	-1203	-8253	9547	160
HS5B	-509	-8759	9990	160
HS6A	-498	-8886	8963	151
HS6B	-1329	-9198	8722	151
HS6C	-705	-9796	9164	151
HS7A	-1804	-9210	11785	117
HS7B	-956	-9288	11863	117
HS7C	-1507	-10031	11532	117
HS8A	-2122	-9017	10713	219
HS8B	-1453	-8389	11019	219
HS9A	-1339	-9995	10470	251
HS9B	-644	-9417	10818	251
HS1D	-1831	-8799	9751	184
HS1E	-1060	-8333	10059	184
HS1F	-1268	-9921	9401	240
HS1G	-473	-9557	9776	240
HS1H	-677	-9113	8762	223
HS1I	-842	-8288	9103	223
HS1J	-1502	-8850	8671	223

Current data set:
NAME =avcg2039EXPNO =1PROCNO = 1
USER =KAyubDU =D:/Bruker/TOPSPIN

Number	Integrated Region		Integral
1	7.440	7.352	12.92380
2	7.352	7.290	8.58820
3	7.281	7.219	9.74061
4	7.219	7.175	3.96074
5	4.202	4.087	6.37154
6	3.804	3.680	19.39141
7	1.442	1.380	9.60041
8	1.009	0.938	29.42328